University of Bath

PHD

Effects of drug crystal polymorphism on the drug carrier interactions in dry powder mixes for inhalation

Carvajal-Pinal, M. Teresa

Award date:
2001

Awarding institution:
University of Bath

Link to publication

Alternative formats
If you require this document in an alternative format, please contact:
openaccess@bath.ac.uk

Copyright of this thesis rests with the author. Access is subject to the above licence, if given. If no licence is specified above, original content in this thesis is licensed under the terms of the Creative Commons Attribution-NonCommercial 4.0 International (CC BY-NC-ND 4.0) Licence (https://creativecommons.org/licenses/by-nc-nd/4.0/). Any third-party copyright material present remains the property of its respective owner(s) and is licensed under its existing terms.

Take down policy
If you consider content within Bath's Research Portal to be in breach of UK law, please contact: openaccess@bath.ac.uk with the details. Your claim will be investigated and, where appropriate, the item will be removed from public view as soon as possible.

Download date: 05. May. 2023

Effects of drug crystal polymorphism on the drug carrier interactions in dry powder mixes for inhalation.

Submitted by
M. Teresa Carvajal-Pinal B.Sc., M.Sc.
for the degree of Doctor of Philosophy
of the University of Bath
2001

COPYRIGHT

Attention is drawn to the fact that copyright this thesis rests with its author. This copy of the thesis has been supplied on condition that anyone who consults it is understood to recognise that its copyright rests with its author and that no one quotation from this thesis and no information derived from it may be published without prior written consent of the author.

This thesis may be made available for consultation within the University Library and may be photocopied or lent for the purposes of consultation.

UMI Number: U135466

All rights reserved

INFORMATION TO ALL USERS
The quality of this reproduction is dependent upon the quality of the copy submitted.

In the unlikely event that the author did not send a complete manuscript
and there are missing pages, these will be noted. Also, if material had to be removed,
a note will indicate the deletion.

UMI U135466
Published by ProQuest LLC 2013. Copyright in the Dissertation held by the Author.
Microform Edition © ProQuest LLC.
All rights reserved. This work is protected against
unauthorized copying under Title 17, United States Code.

ProQuest LLC
789 East Eisenhower Parkway
P.O. Box 1346
Ann Arbor, MI 48106-1346

UNIVERSITY OF BATH
LIBRARY
40 - 2 JUL 2001
Ph.D.

Acknowledgements

I would like to take this opportunity to express that I am deeply grateful to Professor John N. Staniforth for first believing in me, for his encouragement, support and patience. Also to Brian Meakin for his guidance, positive remarks, constructive criticism and interest in my advancement. I would also like to add my profuse appreciation and respect for John and Brian as scientists and as friends.

I feel in debt with and deep gratitude to Hashim Ahmed, Elaine Phillips, Tarik Roshdy and Sam Del Terzo. Hashim was the key person, he introduced me to John Staniforth. Working with Elaine, research was even more beautiful, enjoyable and with lots of satisfaction in the world of aerosols. Elaine made possible the use of the drug in this study. Tarik lent me his laboratory, and Sam supported and encouraged me all the time with my research. My appreciation is extended to more members of Hoffmann-LaRoche: Maurice Munroe (PARD), Louis Todaro (PChem), Ray Ducoat and Ed Guzzo (Machine Shop).

I also wish to thank staff and postgrads members of the School of Pharmacy & Pharmacology and Centre of Electronic Optics at the University of Bath for their help in one way or another.

A very special thanks goes to Margarida Dolan and Sue Johnson for their friendship and invaluable help throughout these years. Everything they have done for me cannot be expressed with words.

I am immensely grateful for the support, encouragement, patience and love of Rodolfo Pinal throughout my Ph.D.

To my Rodo.

He captured my eye in College

and has held my heart ever since.

He is the most wonderful husband

God ever gave a woman.

To my miracle: Monica Elizabeth

ABSTRACT

The physical and physicochemical properties of drug particles were studied in terms of their observable effects on the nature and strength of the interactive forces between the drug particles and lactose, in dry powder mixes. The relationship between physico-chemical properties and particle interactions was studied from two different perspectives and scales, each requiring different instrumentation and techniques. At a microscopic level, the surface energy characteristics of the drug were determined and then related to the macroscopic properties of the mix such as ease of metering and dispersing.

The drug used in this study exists in two well-characterised polymorphic forms. This type of system was chosen in order to investigate the interactive properties of two different surfaces of the same chemical composition. The basic hypothesis of this study was that two polymorphs of the same drug, will exhibit measurable differences in their interparticle cohesive/adhesive interactions. The differences in interparticle interactions between the two polymorphs, which manifest themselves macroscopically as processing performance qualities of the mix, should in turn, at a molecular level, be the result of differences between the surface energetics of the two polymorphs.

The choice of crystal polymorph was found to have a significant effect on the detachment and deposition characteristics of the resulting blend when actuated from a dry powder inhaler (DPI) device. The differences between the two polymorphs were found to be significant enough as to be directly

observable by different experimental techniques used to study drug-lactose blends. Such experimental techniques include detachment measurements by the centrifuge method, static and dynamic electrostatic measurements, and deposition form from the actual DPI device. In addition, the sorption and calorimetric methods were used to study the particle surface characteristics, and to differentiate between the two crystal forms. Polymorph A was found to exert stronger cohesive and adhesive interactions. In addition to being consistent with the device deposition results, data form the centrifuge method and electrostatic measurements are also capable of differentiating between the two crystal forms. Study of the surface energy properties of the two polymorphs revealed that polymorph A exhibits the energetic equivalent of surface fuzziness: a greater number of weaker interactive sites. The net result being greater cohesion and/or adhesion energy for the particle as a whole in the case of polymorph A.

Despite efforts to eliminate the effects of surface geometry, the results suggest that the shape of the drug particles continues to play a significant, although not necessarily dominant role in the aerosol deposition properties of powder mixes. Nevertheless, a major purpose of this study was to explore the relationship between the energetics of interaction of dry powder inhaler particles and deposition in a realistic pharmaceutical situation. The system chosen for this study is a true pharmaceutical new chemical entity for pulmonary delivery, tested in the clinic, and the results of the present study should provide a pharmaceutically relevant, representative picture of the power and limitations of the type of analysis employed.

TABLE OF CONTENTS

LIST OF TABLES

LIST OF FIGURES

1. INTRODUCTION

The interaction among particles is one of the fundamental properties of dry powder mixes that influence many processing properties including: homogeneity, flow, metering, dispersion, compression and dissolution. The interaction forces between drug and carrier particles are critical factors to be considered for the optimal formulation of powders for inhalation. Formulations of powders for inhalation are often made of binary blends consisting of micronised drug and usually coarser α-lactose monohydrate. For such drug-α-lactose monohydrate systems to be therapeutically effective, a significant number of drug particles must detach from α-lactose monohydrate carrier particles upon the application of a removal force. However, the drug-carrier adhesion forces must also be strong enough to prevent disruption under processing conditions, storage and transport. Staniforth [1987] studied in detail the powder properties relevant in the formation of stable homogeneous powder blends. A controlled modification of these properties may result in optimal interactive forces for powders for inhalation. The adjustment of these properties on formulation of dry powders for inhalation have been studied by several workers [Ganderton and Kassem, 1992; Ganderton, 1992; Timsina *et al.*, 1994; Martin *et al.*, 1994; Podczeck, 1998].

The interactive forces responsible for the adhesion of particles have been characterised in a number of studies. The interactions involved in drug-carrier blends are affected by environmental factors and by carrier properties. Some studies have aimed exclusively at studying the role of

carrier α-lactose monohydrate morphology as a general factor influencing the aerosol drug deposition behaviour of dry powders for inhalation [Wong and Pilpel, 1988 and 1990a; Ganderton and Kassem, 1992; Chawla *et al.*, 1994; Robertson, 1997; Steckel and Müller, 1997; Kawashima *et al.*, 1998; Podczeck, 1998; Zeng *et al.*, 2000a and b]. Others were general studies that investigated those factors that affect adhesion between particles and substrates such as the size, shape and texture of particles [Corn, 1961; Zimon, 1982; Otsuka *et al.*, 1988; Schaefer *et al.*, 1995]. The forces of adhesion involved among particles of different size, shape and texture have been usually assessed by determining the force required for detachment by centrifugation [Staniforth *et al.*, 1982b; Kulvanich and Stewart, 1987c; Staniforth, 1987; Lord, 1993; Podczeck *et al.*, 1995; Kawashima, 1998; Boerefijn *et al.*, 1998]. Other investigators have considered the effects that environmental conditions such as humidity and temperature have on the electrostatic behaviour of powders and the formation of capillary forces [Zimon, 1963; Stephenson and Thiel, 1980; van den Berj, 1981, Kulvanich and Stewart, 1988; Balachandran *et al.*, 1991; Hickey and Martonen, 1993; Hashish *et al.*, 1994; Peart, 1996]. Some authors have studied combinations of dry powder formulation properties, device characteristics and in vitro testing conditions [Gerrity, 1990; Meakin *et al.*, 1995; O'Byrne, 1995; Marple *et al.*, 1995; Hindle *et al.*, 1996].

The variety of parameters and techniques for studying the behaviour of powders and their performance in the formulation during aerosolisation is almost as wide as the variety of studies conducted. Clark and Hollingworth [1993] studied the implications of in-vitro testing in the relationship between

powder inhaler resistance and peak inspiratory conditions in healthy volunteers. Timsina *et al.* [1994] studied drug delivery to the respiratory tract using dry powder inhalers under different experimental approaches and concluded, as others before, that for efficient lung deposition, particle size is an important parameter. Olsson *et al.*, [1996b] studied the effect of inlet throat on fine particle dose; Niven [1993] explored aerodynamic particle size using a time-of-flight aerosol beam spectrometer whereas Hindle *et al.* [1996] used cascade impaction methods. One feature common to all methods, techniques and studies is that they all had the objective of producing efficient dry powders for inhalation in terms of the extent and reproducibility of drug delivery. The level of success was assessed by focusing on patients' response, device performance and formulation carrier characteristics. To this effect, much of the earlier work focused on α-lactose monohydrate and part of it focused on a few studies used model drug compounds. Although significant progress has been achieved in this area, the relationship of drug physicochemical properties, such as surface characteristics, affecting drug interactions with α-lactose monohydrate for powders for inhalation, has only been sparingly evaluated.

The interactive forces responsible for adhesion between drug particles and other surfaces (including α-lactose monohydrate) could in principle be associated with the compound's physical properties at different scales: at the molecular level, at the particulate level or at the bulk level. Each of these scales provides different characterisation parameters that in turn should allow optimum parametisation, depending on the process/property under scrutiny.

The characterisation of the interactive forces responsible for adhesion of particles has been addressed by analysing properties at the particulate scale such as particle morphology and particle size distribution [Wong and Pilpel, 1990a,b]. At the powder bulk scale, Gonda and Chan [1989]; Ganderton [1992] and Hickey *et al.* [1994] have analysed the effect of surface area on powder flow and dispersion characteristics. At present, work characterising behaviour at the molecular scale is lacking in the literature. The few studies reported thus far do not focus on drug surface characteristics, but rather on excipient surface characteristics [Ahmed, 1989; Ticehurst *et al.*, 1994; Ahfat *et al.*, 1997].

Adamson [1990] categorises the intermolecular forces in powders as:

a) structural and dynamic aspects related to the position and orientation of powder particles with respect to each other.

b) thermodynamic aspects related to:
   i) the powder surface energy with its surroundings
   ii) details of motions of particles and their contributions to the energy of the system

a) Structural aspects can be analysed by spectroscopic techniques such as infrared, Raman, X-ray powder diffraction, single crystal X-ray diffraction (to obtain information molecular position). Dynamic aspects include rotational and orientational contributions that can be measured by NMR. Spectroscopy and diffraction methods have been extensively used for the study of solid surfaces at the molecular level.

b) The thermodynamic aspects of surface phenomena can be related to forces between particles and to the imbalance of forces at an interface. In the study of the surface of a solid, the solid-vapour interface offers a system well suited

for the experimental assessment of surface energetics. The solid-vapour interface allows some direct energy measurements as well as other experimental determinations from which thermodynamic parameters can be derived.

1.1 Relevance of interactive forces in solid-solid mixes.

In powder mixes for pharmaceutical systems, drug fines adhere to surface asperities, irregularities and lattice defects of the carrier [Crooks and Ho, 1976; Staniforth, 1980]. The fine particles possess greater surface area per unit weight and present more sites for adherence [Lord and Staniforth, 1996]. Some regions of the coarse carrier surface are rich while some regions are poor in drug, despite efforts to produce a completely homogeneous mixture [Staniforth *et al.,* 1981b]. In fact, in all probability most fine particles exist on the surface of the carrier not as a single monolayer but rather in complete multilayers [Bryan *et al.,* 1979]. Free fine particles tend to form agglomerates in order to reduce the material's (excess) free energy by producing more stable, *i.e.* larger, units (particles) [Yip and Hersey, 1977]. The delivery of fine particles adhered to a carrier in a binary powder blend is at the core of pharmaceutical dry powder inhaler (DPI) development. In fact, the majority of the current commercially available pharmaceutical powders for inhalation consist of fine, cohesive micronised drug mixed with coarse α-lactose monohydrate as a carrier to form adhesive mixes [Zanen *et al.,* 1992].

The overall interactive force in powder blends, composed of micronised drug particles and coarse α-lactose monohydrate particles predominantly consists of van der Waals (vdW) and electrostatic interactions [Visser, 1989]. The strength of the interactive forces is crucial to the performance of the final product. The interactive forces in a powder blend intended for inhalation need to be strong enough to hold particles together during handling, yet weak enough to fall apart and allow the fine particles to separate into a fine powder and disperse in the airstream produced upon actuation of the aerosol device.

The dispersion of micronised drug particles in the inspired air depends on the energy required to overcome the strength of the cohesive forces between drug particles and adhesive forces between carrier and drug particles [Byron 1986]. Hickey *et al.* [1994] and Martin *et al.* [1994] described some of the factors that are likely to influence the relative strength of the interparticulate bonds, and consequently, affect the dispersion of dry powders.

Dispersion of powders in a DPI is controlled by the interaction energy between the drug particles, *i.e.*, by the adhesion of fine drug particles onto the surface of larger particle substrates. The method for assessing the aerodynamic properties of pharmaceutical aerosols generally consists in measuring the extent of powder dispersion in terms of the fine respirable dose, which in turn is quantifiable by an *in vitro* impaction technique [Hindle and Byron, 1995; Hindle *et al.,* 1996; Olsson *et al.,* 1996a].

1.2 Interaction forces.

The interactive forces between powders, either of the same (cohesion) or different materials (adhesion) play an important role during the handling, processing, packaging and stability of pharmaceutical materials [Byron, 1986]. Interactions between components in pharmaceutical powder blends are both unavoidable and necessary. The key lies on controlling such interactions by means of a process that produces a physically stable, homogeneous powder mix. The behaviour of pharmaceutical powder blends often depends on the quality of the powder mixing, which is a reflection of the interactive forces involved, and their manipulation [Staniforth, 1987].

In a pharmaceutical dry powder blend, particles of different materials must interact to an appreciable extent in order to form a homogeneous mixture. This interaction is essentially of an attractive nature [Visser, 1989]. Attraction forces are caused by differences in physicochemical properties of powders at their surfaces. Formulations of dry powders intended for inhalation often consist of mixtures of powders of different size: micronised drug particles combined with coarse carrier α-lactose monohydrate particles. In such drug-carrier systems, the acting attraction forces are both adhesion and cohesion. Particle interaction occurs when the attractive forces between particle components are greater than the detachment forces exerted on the particles [Stewart, 1986].

Interactive forces responsible for particle adhesion and cohesion can be broadly classified into two categories, long and short range interactions [Krupp, 1967; Zimon, 1982], depending on their macroscopic effects. Long-range

interaction forces contribute to the formation of particle agglomerates. The particles come close enough to establish interaction without actually making interfacial contact. Examples of these interactions include gravitational forces, Coulombic forces or electrostatic interaction and magnetism. Conversely, short-range interaction forces only exist when the particles have actual interfacial contact. This set of forces includes van der Waals forces (vdW, repulsive or attractive, dipole forces), electrical double layer, dipole forces, hydrogen bonding and surface tensional/capillary forces.

The adhesion of solid particles is the result of a combination of the various interactive forces present in a particular system. The relative contributions of different types of interaction forces in the overall adhesion will be affected by material properties, as well as environmental and processing conditions [Staniforth, 1993]. Drug particles must interact to an appreciable extent with the carrier excipient to form adhesive mixes. Staniforth [1987] has considered some practical examples of the interactive forces involved in the formation of these adhesive mixes.

Interactive forces affect the physical adsorption and magnitude of adhesion of drug particles on excipient carrier particles in a powder blend. Physical adsorption and adhesion phenomena are also known to influence physical and mechanical properties of powders including blend stability, flowability, dispersibility, compressibility and dissolution characteristics. The physical properties of powders are also affected by crystalline form of a drug entity. For instance, crystals may show preferred orientation during compression [York, 1983]. Some crystals also have the tendency to orient themselves parallel to the upper flat punch face, causing tablets to laminate

[York, 1983], which results in variable dissolution rates [Tuladhar *et al.*, 1983; Shah *et al.*, 1994; Mosharraf and Nystrom, 1995]. Staniforth *et al.*, [1981b] investigated the use of excipients prepared with different crystal habits. The use of different crystal habits resulted in variations in tablet compression and non-segregating properties in low dose mixes with small-sized drug particles.

Particle interactions in pharmaceutical systems are the combination of various interactive forces that can result from a number of discrete mechanisms, the total adhesion force (F) will consist of the sum of component forces present in a given system [Stewart, 1986]:

$$F = F_{vdW} + F_e + F_{im} + F_s \qquad (1)$$

where F_{vdW} are vdW forces, F_e are the contact potential forces, F_{im} are the Coulombic interactions and F_s are the surface tensional forces. The relative contribution of these forces to the overall adhesion in a particular system will depend on the material properties and the environmental and processing factors.

The interparticle forces acting between small drug particles and large carrier particles in an ordered mix include London van der Waals [Staniforth *et. al.*, 1982b; Miller, 1988], electrostatic forces [Staniforth *et. al.*, 1982a] and surface tensional or capillary forces [Stephenson and Thiel, 1980]. Because of the particle size scale typically found in drug-carrier systems, vdW interactions and electrostatic forces play important roles.

1.2.1 van der Waals interactions

Intermolecular forces are usually visualised as pairwise interactions between any two molecules where at least one of the entities is either ionic or polar, *e.g.*, ion-ion, ion-dipole, dipole-dipole, ion-induced dipole, hydrogen bonding, donor-acceptor. Although often overlooked, intermolecular forces do exist between neutral or non-polar molecules, the reason being that the electrons are in constant random movement that causes the formation of transient dipoles [Hendricks, 1973]. The instantaneous dipole moment of one molecule induces a dipole in the neighbouring molecule (A induces a dipole in B, and B induces a dipole in A): the interaction between the two induced dipole moments accounts for the attractive forces between non-polar molecules. The magnitude of the energy E of this interaction is given by:

$$E = -\frac{3}{4} h \nu_0 \frac{\alpha^2}{d^6} \qquad (2)$$

where α represents the polarisability of the two molecules, h Planck's constant, ν_0 frequency and d the separation distance. These forces are known as London-van der Waals, dispersion or induced dipole-induce dipole forces [Vemulapalli, 1993].

vdW forces operate at very short ranges and are the major cause of particle-particle adhesion, strength of solids, surface tension, wetting and physical adsorption. This type of forces is always present in all the molecules when two particles are in contact [Israelachvili, 1992].

vdW forces have bond energies that vary with the specific type of interaction and depend on temperature, but are typically in the range of 1-10 Kcal mol^{-1}. vdW forces are in turn divided into three categories [Martin, 1993]: 1) Dipole-dipole interaction or orientation forces, molecules must have permanent dipole moments. The opposite poles attract even though random molecular motion keeps the attraction weak. The magnitude of the interaction energy depends on the mutual alignment of the dipoles; 2) Induction forces may exist when a dipole is induced on a nonpolar molecule. The magnitude of these forces depends on the polarisability of the nonpolar molecule; 3) Dispersion forces or London forces, this type of forces is present in all molecules and result from instantaneous configurations produced by perturbations of the electronic clouds of neighbouring atoms. In all three types of vdW forces, the potential energy of attraction varies inversely with the distance of separation, r, raised to the sixth power, r^6.

Because of the difference in size between drug and carrier, assuming that the powder blend consists of spherical particles adhered to a plane surface is an adequate approximation for purposes theoretical study. In their theoretical treatment of vdW attractive forces, Hamaker and Visser [1989] defined the force between a sphere and a plane as:

$$F_{vdW} = \frac{A_H \, r_r}{6z^2} \qquad (3)$$

where A_H is the Hamaker coefficient, z distance between two bodies and r_r is the radius of the particle. The interactive energy for the vdW attraction is of

the order of 0.1 eV, and these forces have a diminishing effect as the particle size increases. In addition to van der Waals forces of attraction, electrostatic and capillary forces operate between particles. Pharmaceutical compounds behave as insulators and electrostatic charges therefore play an important role in particle interactions [Hickey *et. al.,* 1994].

1.2.2 Electrostatic interactions

Electrostatic properties of pharmaceutical powders are considered important because of the presence of charges, either moving or stationary may influence the behaviour and consequent performance of these powders.

Electrostatic charges present in a powder can be of different nature: electric double layer and Coulombic interactions. Coulombic interactions result from the contact of charged particles with uncharged surfaces. Electric double layers are the result of the formation upon particle contact, of a shell of oppositely charged electronic layers located at the interface. The two types of electrostatic interactions may be involved in the adhesion of ordered powder mixes.

1.2.2.1 Electrical double layer

The formation of an electric double layer at a contact point of two particles depends on the properties of the contacting surfaces, *e.g.*, on the chemical nature of the surface of the materials involved. The chemical

properties of the material affect the forces at the interface depending on whether the material acts as an electron donor or electron acceptor [Zimon, 1982]. Specific functional groups confer electron donor/acceptor characteristics on a given material [Derjaguin *et al.*, 1978]:

Donor: $-NH_4$ > -OH > -OR > -COOR > $-CH_3$ > -Ph > -X > -COOH > =CO > CN **Acceptor**

Considering particle charges on detachment from a carrier surface, the magnitude of the contact force, F_e, is calculated from the particle charge on detachment from the carrier, q, and the contact area, A, between the particle and the carrier surface [Stewart, 1986].

$$F_e = \frac{2\pi q}{A} \qquad (4)$$

1.2.2.2 Coulombic forces

Coulombic forces sometimes are also called electrostatic forces. Electrostatic attraction forces can be generated from charges on the surface and their effects are subject to environmental conditions such as humidity.

Coulombic interactions between solid materials occur when a charged particle induces an equal but opposite charge on an uncharged surface [Stewart, 1986]. Coulomb's law embodies this adhesive type of interaction:

$$F_{im} = k\frac{q_1 q_2}{r^2} \qquad (5)$$

Coulomb's equation (5) shows that the repulsive or attractive force F_{im} between the two charges q_1 and q_2 falls off as a function of the square of the distance, r^2, between them; k is a proportionality constant, and since the SI unit of charge is defined in relation to current, 1 coulomb (C) = 1 ampere second (A·s). With this definition, the proportionality constant becomes:

$$k = \frac{1}{4}\pi\varepsilon_o \qquad (6)$$

where ε_o is the permittivity of free space.

In general, for powders that are not artificially charged by a high voltage field, the electrical interactive force due to contact (F_e) is much greater than the Coulombic image force (F_{im}).

Pharmaceutical powders are generally organic materials that behave as electrical insulators under ambient conditions. Their surfaces can acquire electric charge by contact and frictional electrification (often termed triboelectrification), mechanical fracture in some materials, corona charging, spray drying, induction charging of sprayed liquids, ion and electron beam charging, photoelectric charging, thermionic and field emission [Hendricks, 1973]. These processes contribute greatly to the electric charge on the particle surfaces that often remain charged even after separation [Kulvanich and Stewart, 1987a]. Tribocharging occurs due to differences in work

functions [Krupp, 1967; Stewart, 1986] between the two dissimilar surfaces. Work function (φ, energy potential difference) is equal to the energy given to an electron in order for the electron energy to be freed and able to transfer from one material to the other [Hendricks, 1973].

All materials, whether conductors or insulators, have electrons available at their surfaces which take part in contact charging. This is true especially for insulators. In order for an electron to go from one energy level to another, the electron has to acquire sufficient energy to bring the electron to an excited state higher than its resting or ground state. The transfer of electrons between the materials results in a potential difference that develops until the potentials of the materials are aligned the corresponding Fermi levels. The Fermi level is the energy in a solid at which the average number of particles per quantum state is ½; *i.e.*, one half of the quantum states are occupied [Holden, 1992].

1.2.3 Hydrogen bonding (polar groups), surface tension forces, hydrophobic and hydrophilic interactions.

vdW and electrostatic forces predominate in low humidity environments, but at high humidities (≥ 65%) surface tensional effects become increasingly important. Surface tension and the force of the liquid bridge between particle and surfaces are related by:

$$F_s = 2\pi \gamma \; r_r \cos\theta \qquad (7)$$

where r_r is the radius of the particle, γ is the surface tension and θ is the contact angle.

Hydrogen bond and hydrophobic interactions are particularly relevant to interactions in materials containing water. Hydrogen bonds are strongly orientation-dependent, water tends to adopt a highly directional tetrahedral co-ordination rather than a higher packing density configuration (*i.e.*, close-packed van der Waals interactions where the bonds are non-directional). Hydrogen bonding is not a phenomenon unique to water; it exists in varying degrees between electronegative atoms (*e.g.*, O, N, F, Cl) and hydrogen atoms that are covalently bound to similar electronegative atoms [Israelachvili, 1992]. The presence of polar groups such as $-NH_2$, -NH, -OH, -COOH and $-CONH_2$ confer molecules the capability for hydrogen bonding. Hydrogen bonds have the intermolecular distance of the O---H bond in the order of 1.7 Å. The distance for H-bonds of the N---H type typically ranges between 2.4 and 3.2 Å. The bond energy of most hydrogen bonds lies between 5-20 kJ mol^{-1}. Their bond energy places hydrogen bonds as somewhat stronger than typical van der Waals bonds (~1 kJ mol^{-1}) but significantly weaker than covalent or ionic bonds (~500 kJ mol^{-1}). However, hydrogen bonding forces are strongly temperature-dependent [Vemulapalli, 1993]. Hydrogen bonds occur both intermolecularly and intramolecularly, and can even exist in a non-polar environment [Pixton and Warburton, 1976]. They are important for instance in macromolecular and biological assemblies such as carbohydrates and proteins [Rizvi and Benado, 1984].

Hydrophobic interaction describes the unusually strong interaction between hydrophobic molecules and surfaces in water or other polar chemistries. These interactions are usually stronger than the vdW attraction and are associated with rearrangements of H-bond configurations as two hydrophobic species come together [Israelachvili, 1992]. Up to date, few direct measurements of pure hydrophobic interactions between non-polar molecules exist, mainly because they are so insoluble. At present, a satisfactory theory of hydrophobic interaction does not yet exist because of the inherent problem of making a summation over numerous pair potentials.

The hydrophobic interaction plays a central role in many surface phenomena, such as molecular self-assembly, micelle formation, biological membrane structure, and in determining the conformations of proteins [Kauzman, 1959; Tanford, 1980].

In the case of a solid, unlike that of a liquid, surface tension is difficult to determine. There is a rather limited number of methods for obtaining experimental surface energy and free energy values for solid materials, and many of such methods are peculiar to special solids or situations [Adamson, 1990]. For example, the particular case of the direct manifestation of surface tensional forces in NaCl crystals measured by the work of cleaving the crystal with mica [Adamson, 1990]. There are just a few methods suitable for indirect estimation of surface tension like a) calorimetry to determine heats of adsorption (small differences exist between coarse and fine crystalline material); b) gas adsorption studies (surface area by BET); c) contact angle measurements; d) fractal surfaces analysis for the determination of surface area (using a specific mathematical geometry) [Meakin, 1988].

For purposes of studying the dependence of physical properties on surface energy, the solid-liquid interfacial tensions can be estimated from solubility measurements, nucleation studies and change in lattice parameters by compression followed by its dissolution characteristics. Methods for estimating surface energy differences at solid-liquid interfaces have focused on contact angle measurements and solubility changes [Egawa *et al.*, 1992].

The interfacial free energy at a solid-vapour interface can be obtained by gas adsorption studies [Adamson, 1990]. Adsorption experiments are usually conducted at constant temperature and the amount adsorbed is represented as a function of the equilibrium gas pressure, followed by a thermodynamic treatment, which provides some indication of the energy of adsorbate-adsorbent interaction [Hiemenz, 1986]. At solid-solid interfaces, adhesive forces exist between powder particles in contact, however, little information is available to quantify these interaction forces.

1.3 The interactive behaviour of powders

The interactive behaviour of powders in a formulation is associated with the forces acting between particles. The formation of interactive powder systems, *i.e.*, drug-drug and drug-excipient interactions, depends primarily on the balance between the attractive forces (adhesion and cohesion) involved. Adhesive forces in powders develop as a result of the contact of particles having dissimilar surfaces and their separation distance [Stewart, 1986]. The resulting force depends on the properties of the

contacting bodies, mainly size and chemical surface properties. Interactive forces among particles will be affected by factors such as the physicochemical characteristics of the individual components as well as environmental and processing conditions [Staniforth, 1993].

1.3.1 Factors affecting particle interaction.

The factors that contribute to particle interaction include: humidity/moisture content, morphological characteristics of drug and carrier particles, particle size, drug/carrier mass ratio, crystallinity of blend components, the use of ternary components, process conditions, such as time and scale of mixing [Staniforth *et al.,* 1982b; Hickey *et al.,* 1994; Peart, 1996; Louey and Stewart, 1999]. These factors have to be considered fully in order to advance in DPI formulation development. The overall performance of a dry powder inhaler, as far as device filling, emptying and powder lung penetration is concerned, relies on the formulation characteristics and its interactions with the device. The formulation characteristics depend on bulk powder properties such as mixing, flow/packing, entrainment and separation. In addition, individual particle properties including morphology and particle surface effects, electrostatics, and surface tension, further modulate powder blend properties. Staniforth [1994] summarised the published work on the study of the factors influencing the adhesion, cohesion and separation of interacting particles. It is interesting to note, the majority of the published studies have focused on investigating properties of the carrier, namely α-lactose monohydrate, while little work has

been devoted to studying the influence of the physicochemical properties of the drug.

The evaluation of the surface properties of drug and excipients has been largely carried out indirectly by measuring powder characteristics *e.g.*, batch uniformity of well characterised materials such as griseofulvin [Zografi and Tam, 1976; Hansford *et al.*, 1980]. α-Lactose monohydrate was characterised by contact angle measurements [Buckton and Newton, 1986a]; and salbutamol sulphate characterised by inverse gas chromatography (IGC) [Ticehurst *et al*,. 1994; Feeley *et al.*, 1998]. Some studies evaluate the degree of crystallinity in solids by IGC [Ticehurst *et al.*, 1996] and isothermal microcalorimetry [Berlin *et al.*, 1971; Bystrom, 1990; Angberg *et al.*, 1992; Sebhatu *et al.*, 1994] and water sorption by microbalance [Hendrisken *et al.*, 1995, Stubberud *et al.*, 1995]. Similarly, drug surface properties and degree of dispersion have been investigated indirectly by assessing drug dissolution characteristics [De Villiers *et al.*, 1994; Shah *et al.*, 1994]. Some studies addressed interactions in drug-excipient systems (Griseofulvin with cyclodextrins in solid binary systems by solubility and dissolution studies [Veiga *et al.*, 1998]) or interactions between gases and solid materials [Bakri, 1997].

1.4 Theoretical considerations of the gas-solid sorption process.

Sorption is the general term applied to the interaction between gas molecules (probe vapour) and a solid surface [Adamson 1990]. In any solid, the atoms at the surface are subject to out-of-balance forces of attraction

normal to the surface plane due to the severe distortion of their interatomic spacing and charges. The balance of these forces can be partially restored by the adsorption of gas molecules [Brunauer, 1943 in Shaw, 1992].

In adsorption, most of the gas molecules remain held at the surface of the solid without any intimate mixing between the molecules of the gas phase and those of the solid phase. Although gas may enter the cracks or fissures of the solid, it is not incorporated into the solid surface itself. The process by which bulky gas atoms or molecules penetrate into the structure of the solid by a process of diffusion is referred to as absorption. Sorption is a rather general term comprising either adsorption or absorption and the combination of both. When the gas molecules are freed from the solid into the gaseous phase, the phenomenon is known as desorption. In the sorption process, the terms of adsorbent and adsorbate correspond to the solid and the gas, respectively.

Sorption processes can be classified according to the strength and nature of the interaction between the adsorbate molecules and the surface of the adsorbent. The term chemisorption refers to adsorption systems in which the energy of interaction between the adsorbate and adsorbent is large, approaching that of a covalent bond [Adamson, 1990]. Chemical sorption involves transfer of electrons between the solid and the gas. Actual chemical bonds may be formed at the surface of the adsorbent, and the heats of adsorption may be as high as 100 kcal per mole [Purnell, 1962]. The term physisorption refers to adsorption systems in which the energy of interaction between the adsorbate and adsorbent is relatively small. These interactions are based on weak van de Waals interactions, such as

dispersion interactions, dipole-dipole interactions, and hydrogen bonding. Physical sorption results from molecular interaction forces. The formation of a physically sorbed layer is similar to the condensation of vapour to form a liquid provided that the conditions of temperature and pressure are suitable. The heat of physical sorption is of the same order of magnitude as that of condensation of the adsorbate ($\leq$ 15 kcal mol^{-1}). The heat of adsorption reflects the binding energy between the molecules of a vapour and the surface of the adsorbent. Under suitable conditions of temperature and pressure, multilayers of physically sorbed molecules are usually formed [Brunauer *et al.*, 1938 in Shaw, 1992]. Physical sorption is reversible in the sense that equilibrium is attained, and that upon desorption, the adsorbate is recovered unchanged [Adamson, 1990].

The adsorption system in the present study consists of pharmaceutical organic drug as the adsorbent and organic probe vapours as the adsorbates. The interaction between the drug and organic probes are relatively weak; therefore, the system used here is a physisorption system.

1.4.1 Sorption Forces and Energy

With the working conditions of temperature and pressure of 20 to 45 °C and pressure of 1 atmosphere (atm), respectively, the sorption of organic probes and water vapours by drug compounds is of a physical type. In physical sorption, the forces between probe vapour molecules and the surface of the adsorbent are usually of van der Waals character [Adamson,

1990]. The predominant interactions at the surface of particles forming dry powder mixes of drug and carrier are of the van der Waals, H-bonding and electrostatic types.

The energy associated with electrostatic forces is much greater than that of vdW dipolar forces or hydrogen bonds. However, the dominant interaction force between particles in organic powders is the vdW force of attraction. The vdW forces are noticeable when the interfacial distance between particles is 0.2 to 1 nm [Visser, 1989].

The interaction of a gas with a solid is the sum of the individual interactions of the gas molecules with the molecules of the solid [Gregg and Sing, 1982]. If van der Waals forces alone are effective between the gas molecule and the surface of a solid, the potential energy of interaction (sorption energy) is a function of the distance between adsorbent and adsorbate molecules [Hill, 1950]. The curve for the general shape of the potential energy between two isolated atoms is the Lennard-Jones potential, or '6-12 potential', expressed by [Gregg and Singh, 1982]:

$$U(r) = -Cr^{-6} + Br^{-12} \qquad (8)$$

where $U(r)$ is the total potential energy between two atoms, B is an empirical constant, C is a dispersion constant and r the distance between the centres of the two atoms. In the first term, the inverse sixth power corresponds to the attraction term. Attraction is due to dispersion forces, van der Waals, and conventionally the negative sign implies this contribution, whereas the second term indicates repulsive forces arising from the interpenetration of the electron

clouds of the two atoms. Attraction of the atoms occurs when $r > r_e$ and repel for $r < r_e$, where r_e is the distance of closest approach. For the total potential energy $U(r)$ of sorption of a gas onto the surface of a solid has a minimum at $r = r_e$, and $U(r) = 0$ at $r = \infty$(Hill, 1950).

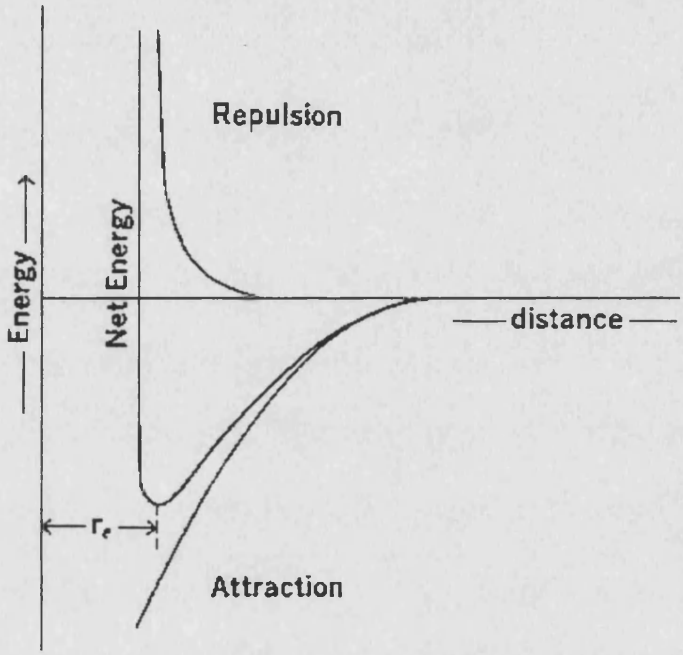

Figure 1. Graphical representation of the intermolecular Lennard-Jones potential energy. Repulsive and attractive energies and net energy as a function of the distance between molecules [Martin, 1993].

In physical sorption, the energy of interaction between the surface of a solid and a gas of different polarity has three components: orientation forces, induction forces and dispersion forces.

The potential energy varies irregularly from point to point on a solid surface. The points corresponding to the maximum potential energy are considered active sites [Hiemenz, 1986]. The surface of a real solid is bound to contain various kinds of imperfections like cleavage steps, dislocations,

defects (Gregg and Singh, 1982; Adamson, 1990). The presence of imperfections inevitably produces energetic heterogeneity of the surface and sorption takes place on the most energetic (active) sites first.

In the sorption of solvent vapours, the amount of probe solvent sorbed is a function of solvent and surface polarities, as well as the number and accessibility of polar and non-polar sites on the surface of the drug powder. In the case of sorption of polar solvents, the polar groups of the drug organise and orient the adsorbate molecules in order to form hydrogen bonds. The sorption behaviour of solvent vapours on solid drug surfaces will have different interactions depending on the type hydrophilic or hydrophobic groups prevalent at the powder's surface.

In sorption phenomena, solvent molecules attracted by the solid surface will remain bound for a time period, a residence time. Sorption residence time depends on the binding energy, on the kinetic energy of the solvent molecules and on temperature. Dynamic equilibrium in sorption is attained when the balance between the adsorbate-adsorbent collision frequency and resident time is such that no net gain or loss of adsorbate molecules at the surface takes place over time [De Boer, 1968].

Sorption isotherms where the amount of solvent sorbed (X) is a function of solvent vapour pressure (p) and the temperature (T), is given by:

$X = F(p,T)$ or for an isothermal process: $X = F_T(p)$

Brunauer, Emmet and Teller [1940 in Shaw, 1992] considered five principal forms of vapour sorption for the experimental isotherms. These five

types of sorption isotherms are known as BET isotherms and are illustrated in Figure 2. Type I corresponds to Langmuir's monolayer formation. Type II is sigmoidal in shape and corresponds to multilayer formation. Type III is characterised by heat of adsorption equal to or less than the heat of condensation. Type IV and V are considered to reflect capillary condensation phenomena in that sorption levels off before the saturation pressure is reached.

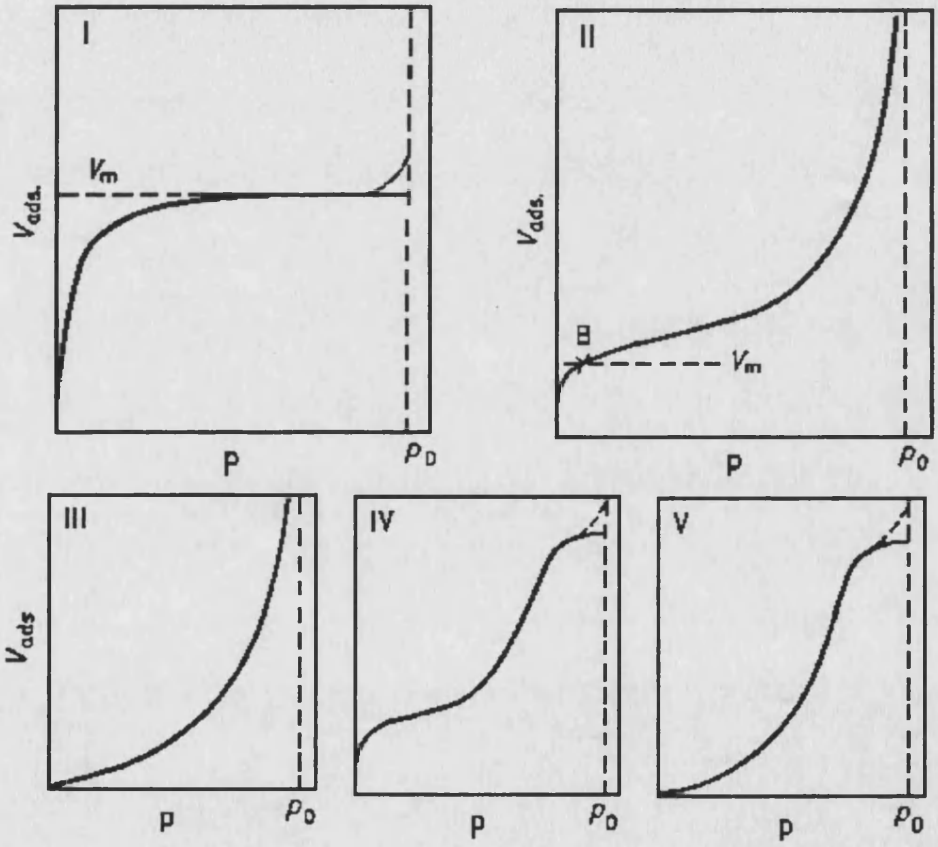

Figure 2. The five types of BET adsorption isotherms. p_o= saturation vapour pressure [Shaw, 1992].

The procedures for obtaining sorption isotherms or for studying the interaction of water with organic materials include thermometric, dew point, gravimetric, hygrometric, etc [Gal, 1975; Prixton and Warburton, 1976; Troller and Christian, 1978], and inverse gas chromatography [Coelho *et al.*, 1978; Smith *et al.*, 1981]. Inverse gas chromatography (IGC) in the pharmaceutical field has been used for the determination of adsorption properties of solvent probes on the surface of powders. Ahmed [1989] and Ticehurst *et al.*, [1994] have described in detail the use of this technique in the study of excipients. The authors analysed the adsorption properties by evaluating the surface free energy (γ) of the dispersive component.

1.5 Thermodynamic aspects of sorption.

The thermodynamic parameters of the adsorption of gas molecules onto a solid can be determined by using IGC and isothermal microcalorimetry. The analysis of these parameters provides information about the vdW forces at play in the physical adsorption vapour at the solid/gas interface. The forces of attraction between adsorbent and adsorbate reflect in turn the surface chemistry and charge of the powders.

1.5.1 Free energy of sorption.

The free energy required to transfer a solvent molecule from the vapour phase onto a solid surface is a measure of the affinity of the solvent for the

solid [Bull, 1944]. This is a key thermodynamic parameter for evaluating the interaction propensity of a solvent for a solid.

Adsorption of a gas on a solid is a spontaneous process and is therefore characterised by a decrease in the free energy of the system, *i.e.*, a negative free energy change, the more negative the quantity, the stronger the tendency toward sorption. Consequently, the free energy of sorption ΔG_s is an indicator of the propensity of sorption. It is related to the enthalpy ΔH_s and entropy ΔS_s, of sorption through the Gibbs equation:

$$\Delta G_s = \Delta H_s - T\Delta S_s \tag{9}$$

Both ΔG_s and ΔS_s are negative, therefore ΔH_s must also be negative. Accordingly, the adsorption process should be exothermic and this is true irrespective of the nature of the forces involved [Adamson, 1990]. The decrease in the heat content of the system is called the heat of adsorption.

A system is in equilibrium when its entropy is at maximum or its free energy at a minimum. In terms of the Gibbs free energy, at constant temperature (T) and pressure (P), the condition of equilibrium is: $(dG)_{T,P} = 0$

The change in Gibbs free energy with temperature and pressure is given by:

$$dG = -sdT + vdP + \sum \mu dn_i \tag{10}$$

$$\mu_i = \left(\frac{\partial G}{\partial n_i}\right)_{T,P,n_j} \tag{11}$$

where μ_i is the chemical potential. The chemical potential is an intensive quantity, while G is an extensive property.

The thermodynamic equilibrium between molecules in the gas phase and the solid surface is defined by the chemical potential and expressed by:

$$d\mu(gas) = d\mu(surface) \tag{12}$$

The chemical potential of the gas depends on pressure and temperature, and the chemical potential of the surface molecules depends on temperature. From the thermodynamic point of view, isothermal sorption equilibrium is reached when the chemical potential of the solvent on the solid is equal to that of the solvent vapour above the solid.

$$\mu^{\circ}{}_s = \mu^{\circ}{}_v + RT \ln\left(\frac{P}{P_o}\right) \tag{13}$$

the subscripts s and v denote solid (sorbed) and vapour phases respectively, P is the partial pressure of solvent vapour at given temperature (T); P_o is the pressure of the solvent vapour in a saturated atmosphere at T, R is the gas constant.

If the vapour is considered to behave ideally, and if Raoult's law is introduced for the solvent probe $P = P^{\circ} x_1$, where x_1 is the (mole fraction)

concentration of the probe vapour, the chemical potential can be written in the form:

$$\mu_1 = \mu^o + RT \ln x_1 \tag{14}$$

At equilibrium, the Gibbs free energy (ΔG_s^o) at any temperature can be further calculated by taking into account the relationship between the equilibrium constant and the free energy change:

$$\Delta G_s^o = -RT \ln \frac{x_s}{x_v} \tag{15}$$

or

$$\Delta G_s^o = -RT \ln K_{eq} \tag{15a}$$

where x is expressed in mole fraction, and K_{eq} is the equilibrium constant. Thus, sorption is accompanied by a decrease in the free energy of the system, the more negative ΔG_s the stronger the tendency towards sorption, when the system is in equilibrium ΔG_s is zero (Noggle, 1985).

From a thermodynamic or statistical mechanics point of view, the internal energy and entropy of a molecule should be different in the adsorbed state from that in the gaseous state [Vemulapalli, 1993]. It is clear that the adsorbed molecule may lose part or all of its freedom to rotate. The average molar energy for the system E_m can be written:

$$E_m = RT^2 \frac{\partial \ln Q}{\partial T} \tag{16}$$

The free energy of sorption is related to the partition function Q that relates the probability of finding a molecule at some particular point on the surface according to the Boltzmann principle [Adamson, 1990]. From the definition of Helmholtz free energy:

$$A_F = E_m - TS \tag{17}$$

where A_F is the Helmholtz free energy, then:

$$A_F = -RT \ln Q \tag{18}$$

where Q could be essentially Q_{rot} for the evaluation of rotational energy contribution to the energy and entropy change occurring during the adsorption of gas molecules on surfaces.

1.5.2 Enthalpy and Entropy of sorption.

Heat is given off upon the sorption of vapour on the solid, *i.e.*, sorption is an exothermic process. Upon desorption, heat is absorbed by the system, *i.e.*, it is an endothermic process. The enthalpy of adsorption (ΔH_s) at constant surface coverage is called isosteric enthalpy, which is the quantity of heat

released or absorbed during the sorption process. The heat of sorption is a measure of the interaction between the vapour and the solid. Rearranging equation (13):

$$\Delta G_s^o = \mu^o{}_s - \mu^o{}_v \tag{19}$$

$$\Delta G_s^o = -RT\ln\left(\frac{P}{P_o}\right) \tag{19a}$$

$$R\ \ln\left(\frac{P}{P_o}\right) = \frac{\mu_s^o}{T} - \frac{\mu_v^o}{T} \tag{20}$$

$$R\ \ln\left(\frac{P}{P_o}\right) = \frac{-\Delta G_s^o}{T} \tag{20a}$$

ΔG_s^o is the standard free energy of change for the sorption of one mole of the vapour. Where P is the partial pressure of solvent vapour at given temperature (T); P_o is the pressure of the solvent vapour in a saturated atmosphere at absolute temperature T, and R is the gas constant. For the derivative since P_o is a constant, $d(\ln P_o)/d(1/T)$ gives the Clausius-Clapeyron equation:

$$\left[\frac{d\ln P}{dT}\right]=\left[\frac{\Delta H_s}{RT^2}\right] \tag{21}$$

or

$$\left[\frac{d\ln P}{d(1/T)}\right]=-\left[\frac{\Delta H_s}{R}\right] \tag{22}$$

Even though enthalpy is a function of temperature, it can be treated as a constant over a small temperature range (for example, the enthalpy of vaporisation of water changes only by 1% for a 10°C change in temperature). The value of the isosteric heat of sorption is usually obtained from the Clausius-Clapeyron equation using vapour pressure of the solvent at a minimum of two temperatures: more temperatures will give a better estimate [Labuza *et al.*, 1985]. The Clausius-Clapeyron equation is derived by considering two different equilibrium states, at slightly separated temperatures and pressures [Noggle, 1985]. Enthalpy is a state function, a differential molar quantity that varies with the amount sorbed. The Clausius-Clapeyron equation (22) can also be integrated into the following working expression:

$$\ln P=-\left(\frac{\Delta H_s}{R}\right)\left(\frac{1}{T}\right)+C \tag{23}$$

where C is the integration constant. Thus, the enthalpy of sorption can be obtained by plotting $\ln P$ *vs.* $1/T$ under isosteric conditions, which results in a straight line with negative slope equal to $-\Delta H_s/R$. The enthalpy change is a measure of the energy changes occurring upon sorption of solvent molecules onto powder surfaces. The enthalpy changes can be related to the binding or repulsive forces of the system. Negative values denote the existence of binding whereas positive values denote repulsion [Apostolopoulos and Gilbert, 1990]. In the case of sorption, negative values denote sorption whereas positive values denote desorption.

The effect of temperature on equilibrium constant is obtained from equation (15):

$$\ln K_{Eq} = -\frac{\Delta G}{RT} \tag{24}$$

$$\frac{d \ln K_{Eq}}{d T} = \frac{\Delta H}{R T^2} \tag{25}$$

known as the van't Hoff equation. This may be integrated, assuming ΔH_s to be constant over the temperature range considered.

The sorption process involves the loss of degrees of freedom for the adsorbate molecules when passing from the free gas phase to the adsorbed layer, hence a decrease of entropy occurs. The entropy of adsorption can be interpreted in solid surface behaviour in the same manner as it is interpreted in solution thermodynamics. For instance, the degree of

'disorder' of an organic surface is related to the number of possible configurations which that surface can have under specified conditions [Rizvi and Benado, 1984]. Namely to the number of different states with the same average internal energy the system can adopt. In sorption of water, entropy decreases from localisation of water at specific randomly distributed 'active sites' of high ΔH_s, while an increase in entropy results from solubilisation and swelling [Bryan, 1980].

Once ΔG_s and ΔH_s are obtained by means of the Clausius-Clapeyron and van't Hoff equations, respectively, the entropy of sorption can be calculated by rearranging equation (9):

$$\Delta S_s = \frac{\Delta H_s - \Delta G_s}{T} \tag{26}$$

Entropy changes can be used to characterise the degree of 'order or disorder' existing in the system and to the interpretation of processes like crystallisation, dissolution, and swelling [Iglesias *et al.*, 1976]. Negative ΔS_s values denote a change toward more ordered systems whereas positive ΔS_s values identify more random systems.

Bryan [1980] reported that water sorption on proteins consists of two entropic contributions: positive ΔS_s value for the incipient solution formation and negative ΔS_s for the localisation of water molecules. Similarly, Betthelheim *et al.*, [1970] working with polymer-water systems reported that the entropy is positive for the water molecules but could be either negative or positive for the polymer, depending on the particular polymer. Polymer matrix swelling due to

water molecules resulted in a positive entropy change for polymers undergoing such a conformational change.

1.6 Thermodynamic approach to surface energy for the evaluation of particle interactions.

Surface energy properties can be weighed by thermodynamic parameters. Thermodynamic properties have been used to understand the behaviour of liquids, *e.g.*, water at the surface and in the interior of solid compounds. For solids, thermodynamic functions can be obtained to provide theoretical interpretations to the physical phenomena occurring in powder surfaces.

The surface tension (γ, surface free energy) of solids are invariably more difficult if not impossible to measure than those of liquids. The surface of a solid is very seldom homogeneous as that of liquid interfaces. Several investigators [Zografi and Tam, 1976; Kawashima *et al.*, 1981] based their work on measurements of contact angles on compressed solids to study surface energetics. Buckton and Newton [1986b] studied the effect of particle size on wetting of pharmaceutical powders using contact angle measurements.

The contact angle technique has been widely used although its application to powders in the pharmaceutical area has decreased due to the problem associated with compressing the powder in order to make the measurement, and the resulting uncertainty about the faces making the interface at the time of measurement. For instance, crystals may show

preferred orientation planes during compression due to the tendency of the crystals to orient themselves parallel to the upper flat punch face [Chan and Doelker, 1985].

There are alternative or complementary techniques to contact angle measurements for the examination of thermodynamic parameters. The most recent techniques for the study of water sorption on solid pharmaceutical systems are gravimetric or microbalance, inverse gas chromatography and isothermal microcalorimetry. Sorption isotherms can be obtained by varying the relative humidity surrounding the powder sample, isotherms are useful especially for studying the surface integrity of powders in terms of crystallinity/amorphous content for stability purposes.

The vacuum microbalance was used by Otsuka *et al.* [1988] and Saleki-Gehardt *et al.* [1994] to detect small changes in surface energetics of materials including α-lactose monohydrate. They observed that the face of a crystal has a greater tendency to wet than has the bulk powder, due to the differences in energetics of crystal defects and edges compared to the energetics of flat surfaces.

Inverse gas chromatography (IGC) is a technique that was first used in the field of Food science [Gilbert, 1984], shortly after the technique found wide use in Soil sciences [Rhue and Rao, 1990]. IGC probe analysis has been widely used to study the sorption of water and volatile organic chemicals on materials such as soil [Pennell *et al.*, 1992]. In Food science, Apostopoulus and Gilbert [1990] determined moisture sorption of a series of coffee components, and Lin [1993] studied the sorption properties of corn meal extrudates. The thermodynamic functions obtained by IGC have been

successfully applied to investigate the structure changes in biopolymers [Carrillo *et al.*,1988] and to predict biopolymers mucoadhesion and biocompatibility [Esposito *et al.*, 1994]. In the pharmaceutical field, IGC has been used for drugs and excipients [Ahmed, 1989; York, 1994].

Microcalorimetry has a number of applications in physical pharmacy. Bakri [1993] designed an isothermal microcalorimeter flow cell for the Thermal Activity Monitoring (TAM). Bakri [1988a, b, 1997] has carried out extensive work using TAM for the study of surface thermodynamic properties of powders relevant to pharmaceutical systems. Sheridan *et al.*, [1993] used α-lactose monohydrate for the microcalorimetric determination of the heat adsorption of water.

1.6.1 Inverse Gas Chromatography (IGC).

In the pharmaceutical field, Ahmed [1989] used IGC for the determination of the solubility parameter of sodium starch glycolate (Explotab™, Penwest) with other powders in complex quinary mixtures and Ticehurst *et al.* [1994] studied the surface properties of salbutamol sulphate.

IGC is a high-resolution technique frequently used in pharmaceutical research for investigating the thermodynamic properties of powdered materials. IGC involves packing the powder of interest into a standard glass GC column and individually injecting small amounts of solvents of varying polarity used as probes (*e.g.*, non-polar alkanes and polar volatile organic solvents). The selection of different organic probes is based on the molecular reactivity [Gilbert, 1984].

The different column retention of a given probe reflects the difference in surface energetics between the solid materials used for packing the column. From the retention data, the obtained capacity factors are in turn used to estimate thermodynamic parameters such as heats of sorption, Gibbs free energy, entropy and enthalpy of Sorption.

Examination of the solid state properties (structural and thermodynamic) by IGC, allows the estimation of other solid properties like dissolution, flow and/or compaction [Esposito *et al.*, 1994].

Studies utilising IGC for pharmaceutical systems [Ticehurst *et al.*, 1994, 1996; Huu-Phouc *et al.*, 1986, 1987] demonstrated that this technique is suitable for surface analysis of powders before and after a processing operation. Several investigators have used IGC to measure and compare the solubility parameters of test materials before and after subjecting the materials to a given process. Ahmed [1989] determined the solubility parameters of sodium starch glycolate (Explotab) to calculate the interaction parameter (ϕ) and relative intensities of the cohesive and adhesive interactions in ternary and quinary systems. The author concluded that the relative intensities of interactions rather than the values themselves appeared to predict particle interaction behaviour in a given powder system. Egawa *et al.*, [1992] showed that the solubility parameters increased after cefalexin powder was milled or lyophilised, indicating that the energy of cohesive interactions between molecules had increased. Milling was proven to be a high-energy mechanical treatment that increases cohesive energy of the materials as measured by IGC. Ticehurst *et al.*, [1994, 1996]; York *et al.*, [1998] and Feeley *et al.*, [1998] studied the effect of communition on the solubility parameters of several

pharmaceutical powders including aspirin, carbamazepine, α-lactose monohydrate, *d-l* propranolol hydrochloride and salbutamol. It was determined that the solubility parameters of aspirin and carbamazepine were not significantly affected by milling whereas those of α-lactose monohydrate, *d-l* propranolol hydrochloride and salbutamol were affected.

1.6.2 Isothermal Microcalorimetry by Thermal Activity Monitor (TAM).

Microcalorimetry under isothermal conditions using TAM is well established for compatibility and stability studies during drug development. [Bakri, 1993 and 1997]. The recorded heat flux (P) can be related to the reaction rate and reaction enthalpy of the process under study [Bakri *et al.*, 1988a, 1988b and Bakri, 1990]. The sample is usually loaded into a sealed ampoule and is then placed in the measuring position of the TAM. This closed system does not allow any control or change of the environmental factors such as water or solvent vapour pressure within the sample during the measurement. It is important to be able to cover the entire range, 0%-100%, of relative humidity (RH), or vapour pressure change at ambient temperature when studying the thermodynamics and kinetics of the sample/vapour interaction. For this purpose, a gas pressure controller device was developed to allow very accurate control of solvent vapour pressure (*e.g.*, humidity) of a continuously flowing gas phase to which the sample is exposed [Bakri, 1992]. Bakri [1997] studied powder surface energy using sorption isotherms determined by TAM during vapour induced

phase transitions, the study explored the effect of water activity on amorphous powders.

Microcalorimetry is a technique where the heat of adsorption of water onto the surface of powder is measured. This method provides a direct measurement of energy changes in a process by monitoring the heat change in an isothermal system. Two different experimental set-ups can be used in microcalorimetry, the closed ampoule and the open flow systems. The closed ampoule system is often used to measure heat of mixing. The flow cell configuration is used to measure the heat of adsorption of solvent vapours flowing through powder samples in the instrument's cell. The technique contains sample and reference cells held at constant temperature by a large heat sink. The technique has the sensitivity to measure very small heat changes of the order of $\mu J\ s^{-1}$. Rowe *et al.* [1993] determined the heats of adsorption of water on different grades of microcrystalline cellulose. Landin *et al.*, [1993] investigated how heats of adsorption correlate with the amorphous content of the adsorbent. Microcalorimetry has also been used to study the amorphous content of α-lactose monohydrate following processing, by conducting heat of crystallisation measurements that enabled the characterisation of amorphous content down to 1% [Briggner *et al.*, 1994, Sebbatu *et al.*, 1994]. This technique allows the presence of surface amorphous material to be detected which is not possible with other techniques like X-ray diffraction (XRD).

Atomic force microscopy (AFM) and molecular modelling are techniques that have been used in pharmaceutical systems as complement to IGC [York, 1998], and TAM [Carvajal and Staniforth, 1998]. The combined use of

instrumental techniques allows a better understanding of the physical properties of powders. Only a few studies using AFM [Louey *et al.*, 1999] or molecular modelling in combination with other techniques have been reported to date because of the high degree of experimental care required, especially with AFM, and also due to the elusiveness of reliable computational interaction parameters required with these techniques.

1.7 Objective.

This study focuses on the impact that the physicochemical properties of a drug have on the drug's bulk properties, specifically in terms of the drug's behaviour as a powder and its interactions with other powders. The importance that powder properties and powder interactions have in the pharmaceutical industry cannot be overemphasised. And this study explores the extent to which the physicochemical properties of a drug, particularly its surface properties, manifest themselves at a macroscopic level in the bulk drug destined for pharmaceutical manufacturing. The experimental design for an investigation such as the present one requires the surface properties of the drug as one of the control variables. The observer can then fix the type of surface and determine how different sets of surface properties respond to the same perturbation. To this effect, the investigation reported here used as test materials two crystal polymorphs of the same drug. The choice of crystal polymorphs as test materials for this study offers a unique lens through which, it is hoped, some molecular attributes of the crystal

surface can be viewed in a common frame with the bulk properties of the corresponding powder.

Crystal polymorphs are different materials with the same chemical composition. Differences in physicochemical properties between polymorphs stem from the different configuration and packing arrangements of the same molecular entity. A critically important point is that the above statement applies to all physicochemical differences between polymorphs, including their reactive and interactive properties. The basic hypothesis of the present study was that if two polymorphs of the same drug exhibit, as powders, measurable differences in their cohesive/adhesive interactions, the two materials should exhibit corresponding physicochemical differences at the microscopic level of their surfaces' molecules. By studying the interactions of the two types of surfaces with a common molecular probe, the observed differences in surface properties of the two materials can be linked to the macroscopic cohesive/adhesive behaviour of the corresponding bulk powders.

The investigational drug Ro 24-5913, a LTD_4 antagonist, was chosen for the present study. The chosen drug meets two criteria critical for purposes of the present study. First, the drug is intended for respiratory delivery, so the drug choice will produce results that are reflective of, and consequently of immediate relevance to, a true clinical trials situation. Second, the selected drug exists as two well characterised crystal polymorphs, making a material suitable for testing the above stated hypothesis.

The idealised conception of the experimental design for this study has the pharmaceutical processing scientist confronted with two choices, A and B. The choices A and B are lots of bulk drug substance made of polymorph A and B, respectively. The two lots of drug substance are equally suited for pharmaceutical manufacturing in terms of critical processing properties such as particle size distribution and powder bulk density. In this scenario, the choice of polymorph does not affect product shelf-life, *in vivo* activity nor patent protection. The processing scientist has to make her choice based on the differences that the two materials exhibit during pharmaceutical manufacturing, and the consequent differences in final product performance the choice of polymorph brings.

1.8 Drug polymorphism and polymorphic drug behaviour.

Many organic molecules are known to crystallise into several modifications known as polymorphs. Polymorphism is the ability of any compound to crystallise as more than one distinct thermodynamic phase, *i.e.,* it exhibits more than one three-dimensional molecular packing and orientation in its crystal lattice. Crystal polymorphism is an extremely common occurrence among organic molecules, particularly drugs. Polymorphs exhibit among themselves differences in crystal energy contents associated with different molecular structures. The typical free energy differences between polymorphs are small (lattice energy differences of a few tenths of kcal mol^{-1}) [Burger and Ramberger, 1979].

The different behaviour of organic polymorphs is of fundamental importance to some industries, particularly the pharmaceutical, painting pigments, explosives, agrochemical and photography industries [Leusen, 1994]. It is well established that crystal polymorphs have considerable effects certain physicochemical properties such as solubility and dissolution rate, such effects in turn reflect differences in the free energy at the polymorphs' core and at their surfaces, respectively. In the solid state, polymorphic drugs affect products during formulation development and on-stream processing [Chan and Doelker, 1985; Brittain, 1994] with downstream effects on bioavailability and therapeutic efficacy. Polymorphism influences the powder properties of the drug such as vapour pressure, apparent solubility, density, surface tension, hygroscopicity and rates of reaction [Fairbrother and Grant, 1978; Marshall and York, 1989; Giron, 1990].

Polymorphic drugs present variations in surface free energy, affecting particle and bulk properties of the powdered solid, thus affecting interactions with carrier's and overall performance in a formulation. Changes in one physical attribute of the active, such as particle size or crystal habit, can have important consequences pharmaceutical processing parameters like dissolution, flow and/or compression, as well as on dosage form performance (efficiency of drug delivery and bioavailability).

In dry powder inhaler formulation, particle powder properties are crucial for efficient drug delivery into the lower airways of the lung. Given the critical requisite for delivering the drug's fine particles from drug-α-lactose monohydrate powder blends with DPIs, analytical methods are necessary for quantifying the interparticle forces during powder mixing, deaggregation and

fluidisation processes in dry powder formulations. Examination of powder adhesion, surface charge and thermodynamic properties are likely to aid in the optimisation of DPI formulations.

The use of thermodynamic parameters as practical indicators for the detection of differences in the surface energies of different materials provides an opportunity to explore how intermolecular interactions ultimately manifest themselves at the macroscopic level of the bulk powder.

York [1994], Hancock *et al.* [1997] and Feeley *et al.* [1998] have examined the surface energy properties of several batches of powdered raw materials used in pharmaceutical manufacturing. The authors showed that subtle differences in the powder properties among batches could be detected using inverse gas chromatography (IGC). Bakri [1997] used a novel calorimetric approach to study the interactions between powdered materials and water vapour.

Polymorphism brings about changes in several physicochemical and physico-mechanical properties of organic compounds. As a result, other factors related to the functionality and/or processability of pharmaceutical products can be affected.

The behaviour of powders, in terms their mixing and the resulting physical stability of their blends, dispersion and deposition properties, may be explained in terms of the surface energetics responsible for the interaction of the drug with the carrier excipient. Linden *et al.* [1994] pointed out that the interaction energy should be "controlled" by exploiting interfacial properties of the powders in order to enhance powder properties.

1.9 Physicochemical properties of the two polymorphs of Ro 24-5913.

The drug Ro 24-5913 was specifically selected in the present study because of its therapeutic potential for pulmonary delivery and because it exhibited two distinct polymorphic forms. This type of system was chosen in order to investigate the interactive properties of two different surfaces of the same chemical composition.

This pharmaceutical new chemical entity Ro 24-5913 {(E)-4-[[3-[2-(4-Cyclobutyl-2-thiazolyl) ethenyl] phenyl] = amino]-2,2-diethyl-4-oxobutanoic acid}, is a leukotriene D_4 antagonist. It is somewhat sensitive to light and very hydrophobic, practically insoluble in water (equilibrium solubility < 2 µg/ml) and buffer at physiological pH. The two different polymorphs of Ro 24-5913, A and B, can inter-convert A to B via solvent-mediated transformation [Kulkarni and Robinson, 1994]. The chemical structure and some physicochemical properties of this compound are given in Figure 3.

Molecular weight	412.6
Aqueous Solubility	< 2 µg/ml
Log $P_{o/w}$	4.14

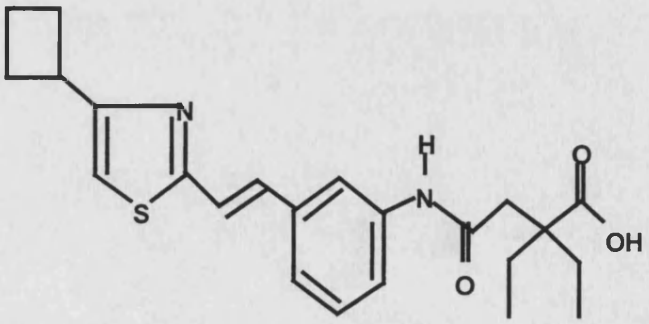

Figure 3 Chemical structure of Ro 24-5913 and physicochemical properties.

Polymorph B is the thermodynamically stable crystal modification. However, the two polymorphs are sufficiently stable as to remain without change for indefinite periods of time under ambient conditions. The two polymorphs are also stable under processing conditions such as milling. The two crystal forms of the drug used in this study can be clearly distinguished by different techniques.

The single crystal X-ray diffraction structures of the two crystal modifications have been solved by Blount *et al.*, [1993]. The unit cell parameters of for both phases are summarised in Table 1. Figure 4 shows the graphical representations of the data in Table 1. The two crystal phases are monoclinic, but they have evident differences in molecular conformation and packing, clearly shown in Table 1 and Figure 4.

Table 1 Unit cell parameters for polymorphs A and B of Ro 24-5913 [Blount *et al.*, 1993].

Crystal Form	Z	a (Å)	b (Å)	c (Å)	β	Volume ($Å^3$)	Volume per Molecule ($Å^3$ molec $^{-1}$)	Space group
A	4	18.018	6.916	18.182	92.15	2264	566	$P2_1/a$
B	4	6.930	23.059	13.606	96.55	2160	540	$P2_1/n$

Polymorph A

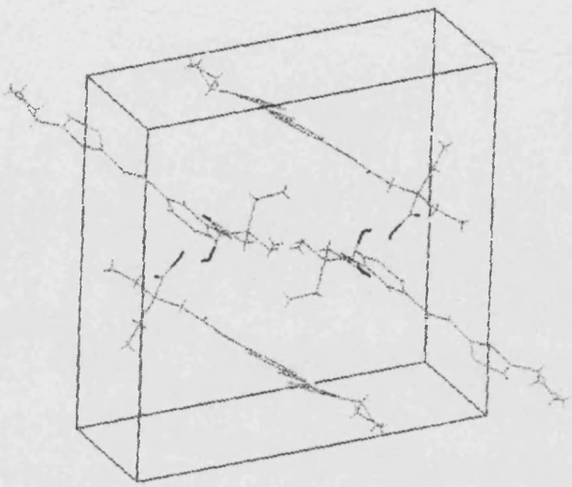

Polymorph B

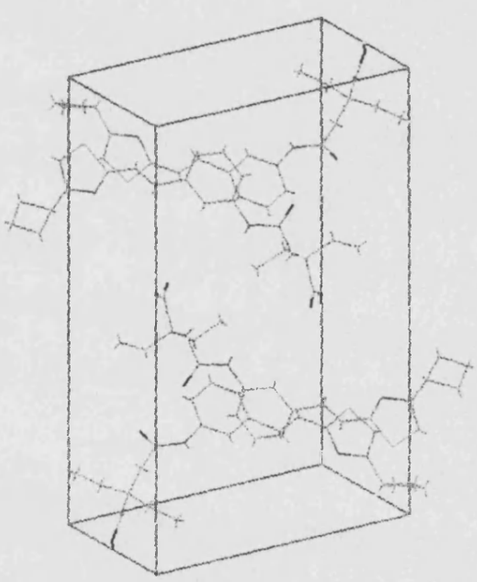

Figure 4 Differences between polymorphs A and B. Unit cells are presented in their corresponding spatial representation [after Blount *et al.*, 1993].

Intrinsic dissolution is a test frequently performed when studying crystal polymorphs. This parameter corresponds to the dissolution rate at constant surface area. Therefore, differences in intrinsic dissolution between polymorphs provide the first quantitative measure of the differences between the polymorphs' surfaces. Figure 5 shows the different intrinsic dissolution of polymorphs A and B [Phuapradit *et al.*, 1993]. The slower dissolution of form B is consistent with it being the more stable form.

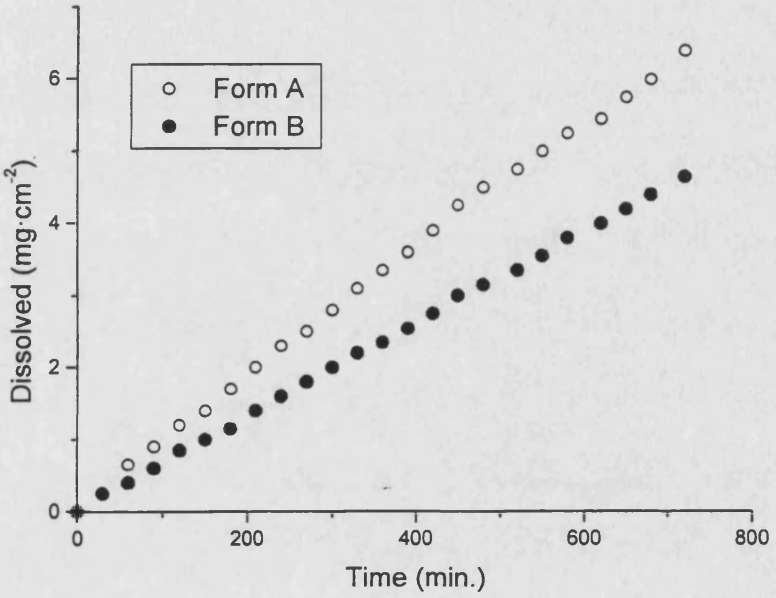

Figure 5 Intrinsic Dissolution profiles of Ro 24-5913 polymorphic forms [Phuapradit *et al.*, 1993].

The choice of polymorph for tablet manufacturing has a measurable influence in the dissolution properties of the dosage form. Figure 6 shows that the extent of dissolution of Ro 24-5913 tablets after 45 minutes was

greater for polymorph A than B, 96% *vs.* 85%, respectively [Phuapradit *et al.*, 1993].

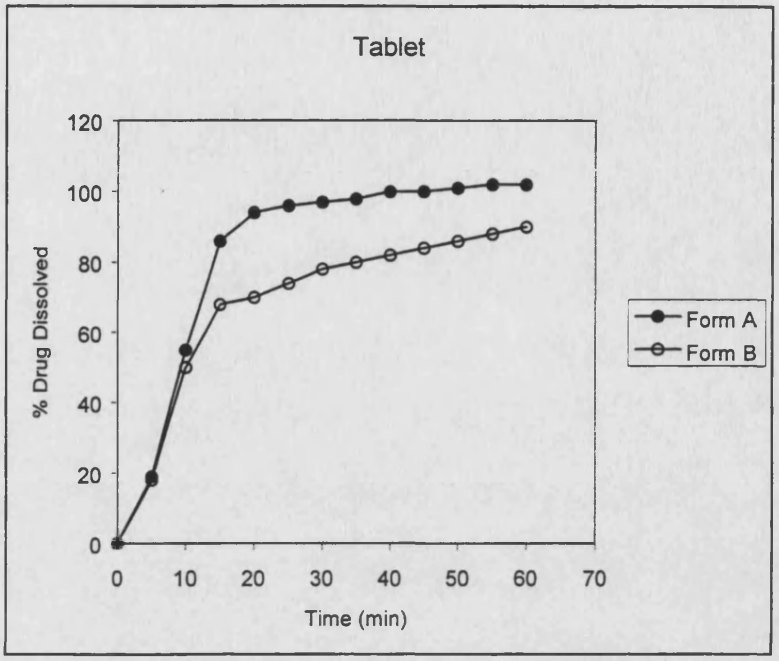

Figure 6 In-vitro dissolution profile of polymorphs A and B of Ro 24-5913 in a suspension and a tablet [Phuapradit *et al.*, 1993].

The effect of polymorphism on dissolution is one of the most widely known and best documented aspects of polymorphism in pharmaceuticals. But polymorphism has other important effects, especially during pharmaceutical processing. Polymorphs often have significantly different mechanical properties, making it necessary to use different to attain a similar end point during manufacturing. Figure 7 shows the difference in compactability between Polymorphs A and B [Phuapradit *et al.*, 1993].

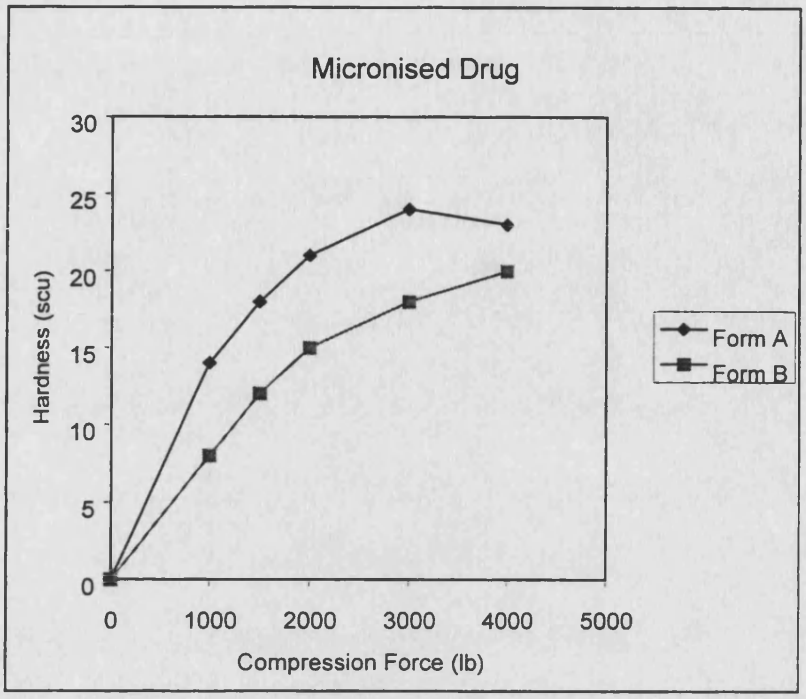

Figure 7 Intrinsic compaction force profiles of polymorphic polymorphs A and B of Ro 24-5913 [Phuapradit *et al.*, 1993].

Table 2 provides a summary of comparative information on some of the physicochemical properties of polymorphs A and B. Form B exhibits greater solubility and intrinsic dissolution, consistent with form B being the thermodynamically stable form. Form B also exhibits the higher absolute density, a frequent occurrence in the case of thermodynamically stable polymorphs. The information of Tables 1 and 2, together with Figures 4 through 7 clearly shows that polymorphs A and B are two different materials. The two crystal forms have different molecular arrangements (Table 1 and Figure 4), as well as different physicochemical (Figures 5 and 6) and different physicomechanical (Figure 7) properties. The present study

investigates how the physicochemical differences between polymorphs A and B are manifested at the surface of the crystals' particles, and how such differences relate in turn to the interactive behaviour of the corresponding bulk powders.

Table 2 Physico-Chemical Properties for Ro 24-5913 polymorphs A and B

Physico-chemical Property	Polymorph			
	A		B	
Crystal Habit	unmicronised	needle-like	unmicronised	equadrant-like
(See SEMs)	micronised	elongated	micronised	rounded
Bulk Density g ml^{-1}	unmicronised	0.155	unmicronised	0.384
	micronised	0.170	micronised	0.168
Absolute Density[1] g ml^{-1} (unmicronised form)	1.157		1.239	
Absolute Density[1] g ml^{-1} (micronised form)	1.260		1.290	
Melting Point °C (Hot stage microscopy)	162-167°C		162-172°C	
ΔH_f J g^{-1} (unmicronised)	254.2		275.8	
ΔH_f J g^{-1} (micronised)	275.0		300.0	
Water Solubility[2] µg ml^{-1}	1.23		0.86	
Intrinsic Dissolution[3] mg cm^{-2} min^{-1} (Fig. 5)	0.0090		0.0062	
In-vitro Dissolution[3] % at 45 min (Fig. 6).	96		85	
Compaction[4]	Fig 7			

[1] Gas Pycnometry (Porous Material Inc.).

[2] Equilibrium solubility at 25 °C determination by HPLC (Sethachutkul *et al.*, 1990).

[3&4] Phuapradit *et al.*, 1993.

2. MATERIALS, METHODS AND PHYSICAL CHARACTERISATION

Dry powder formulations were prepared as binary blends consisting of α-lactose monohydrate as the carrier and polymorph A or B of the drug. The drug substance, irrespective of polymorph, was milled in order to bring its particle size to a range suitable for processing and use in a DPI formulation. In addition, for purposes of the present study, the particle size distribution of the two crystal forms of the drug substance had to be made the same in order to eliminate, as much as possible, the effect of particle size differences on the interactive properties of the powders.

All organic solvents and reagents used for HPLC analysis were UV grade; water was freshly distilled and the gases for IGC and TAM were of high (chromatography grade) purity.

2.1 Characterisation of Carrier α-Lactose Monohydrate

α-Lactose monohydrate (Sheffield Products, Plainfield, NJ, USA) was sieved in order to obtain a size fraction between 45 - 106 µm (including fines, *i.e.* size < 45 µm), using a vibratory sieve shaker (Model Analysette 3, type Fritsch GmbH, Manufacturers Inc., Germany) operated at an amplitude setting of 4 for 20 minutes.

2.1.1 Particle Size Analysis

Sieve analysis. In order to verify the particle size range of α-lactose monohydrate obtained, sieving analysis was carried out using an ATM sonic sifter (ATM Corporation, Milwaukee, WI, USA) at 7 sift amplitude for one minute. The sieve apertures used were 45, 53, 75, 90, 106 and 125 μm. About 2 g. of powder were used for each test. After the sieving test, the powder from each stage (sieve fraction) was carefully collected and weighed on an analytical balance (Mettler PM480 DeltaRange, Mettler Instruments Group, NJ, USA). The sieving analysis was done in triplicate.

Laser Diffraction Analysis. The particle size distribution of the powdered material was measured by laser light diffraction analysis with a Mastersizer X (Malvern Instruments Ltd., Malvern, UK). The technique involves the measurement of the angle of diffraction of the light scattered by the particles traversing a laser beam. The angle of diffraction, which is a function of the particle size, allows the calculation of the particle size distribution. A 20 ml volume stirring cell was chosen as the sample presentation unit, circulating at medium speed (1800 – 2200 RPM). α-Lactose monohydrate was dispersed in 2-propanol (Fisher Scientific), the sample was sonicated for 5 minutes in order to disperse agglomerates. The suspension was then added dropwise until an obscuration of 10-30% was attained in the instrument. Once the obscuration reading had stabilised for approximately 1 min., the particle size measurement was carried out in triplicate using a 100 mm lens. Particle distribution by

volume, using Fraunhofer analysis was obtained and reported throughout this work.

The particle size distribution of the sieved α-lactose monohydrate is shown in Figure 8. The 10^{th} (dv_{10}), 50^{th} (dv_{50}) and 90^{th} (dv_{90}) percentiles of the sample size population correspond to 35.4 µm, 72.2 µm and 114 µm for dv_{10}, dv_{50} and dv_{90}, respectively, with a mean diameter of 78 µm. The surface area of α-lactose monohydrate, measured by the BET method using a gas adsorption/desorption apparatus (PMI, Porous Materials Inc. Automated BET Sorptometer) was 0.70 $m^2 g^{-1}$.

Lord [1993] reported that a lactose sieve fraction in the range from 90 to 125 µm produced reproducible fluidisation, entrainment and removal of powder from the Rotahaler™ DPI device. In the present study, the use of a sieve fraction of α-lactose monohydrate in the range of 45 – 106 µm resulted in good powder properties in terms of fluidisation, entrainment and removal of powder with both the Rotahaler™ and the Dryhaler™ DPI devices.

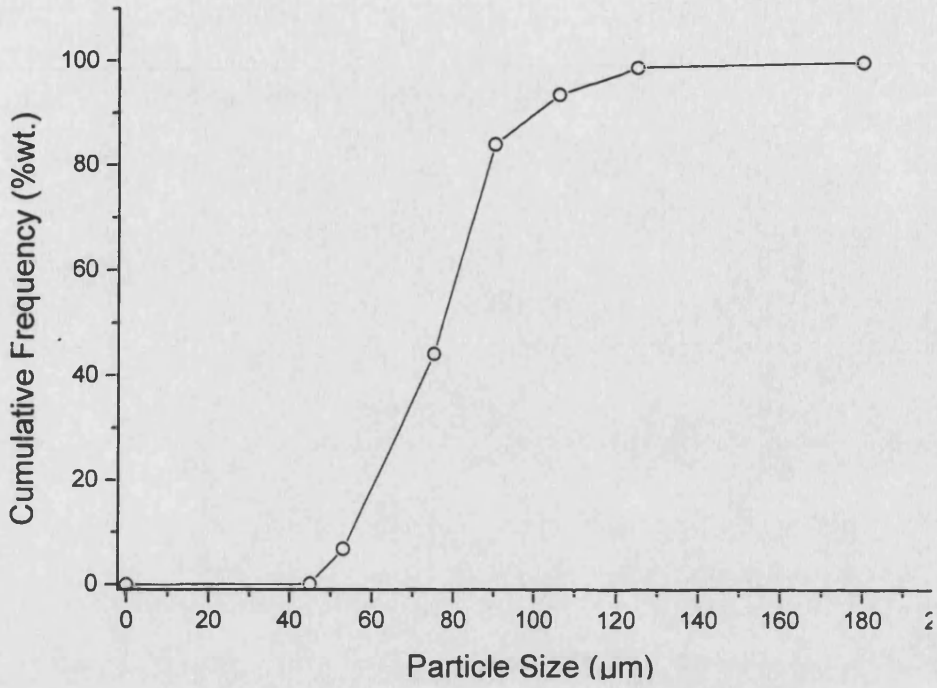

Figure 8 Particle size distribution of sieved α-lactose monohydrate (sieve fraction 45-106 µm).

The mechanically sieved α-lactose monohydrate contained 'fines' (particles < 45 µm). Fines were determined by removing them with an air jet sieving (Alpine air jet) and found to be present at the level of about 12% by weight. The presence of fines has been shown to improve DPI performance [Lord 1993; Ahmed 1994]. Based on these practical and functional reasons, it was decided not to remove the fines from the sieved fraction used in the present study.

2.1.2 Scanning Electron Microscopy (SEM)

The particle characteristics of α-lactose monohydrate were examined using scanning electron microscopy (JEOL 6310, Japan Electron Optics, Ltd., Tokyo, Japan). For the sample preparation, α-lactose monohydrate powder was carefully sprinkled on double adhesive carbon fixers mounted on aluminium planchettes. A thin conductive layer of gold was sprayed on the sample surface using a sputter coater (Model S150B, Edwards High Vacuum, Sussex, U.K.).

Figure 9 shows the SEM for α-lactose monohydrate crystals with their typical 'tomahawk' shape. Lactose fines are also observable in the picture.

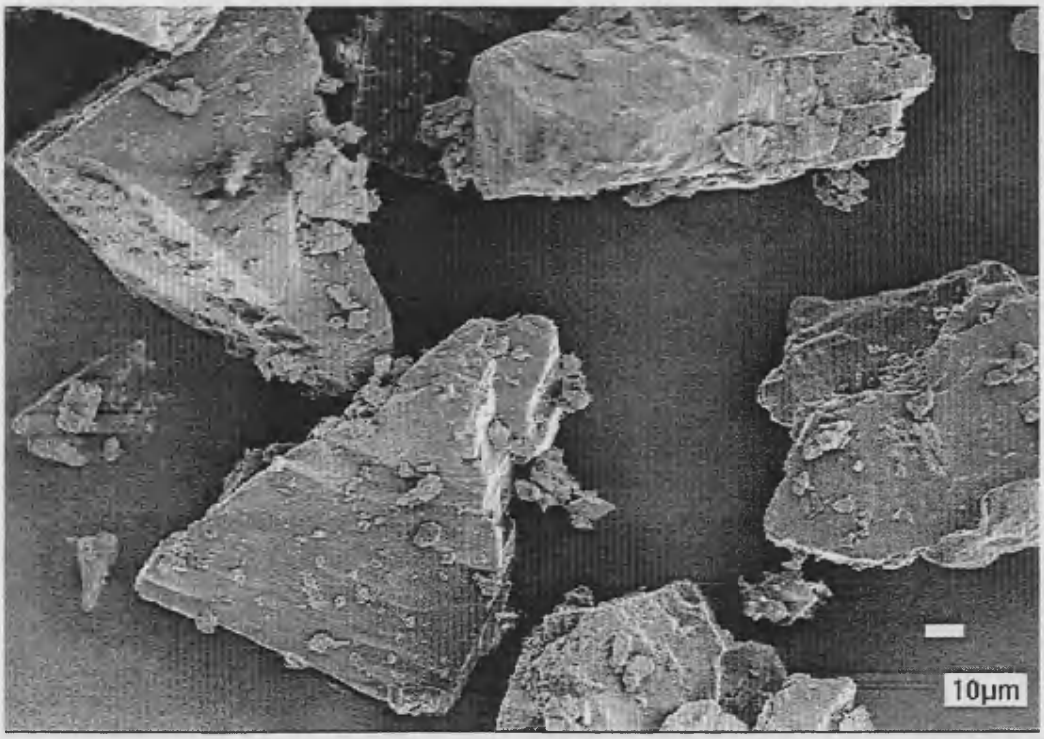

Figure 9 SEM for α-lactose monohydrate, size 45-106 µm (including fines).

2.2 Characterisation of Bulk Drug Substance

2.2.1 Drug micronisation technique

All formulation work was carried out using micronised drug in order to reduce the particle size to the desired range of less than 6 μm, for inhalation use. For the micronisation process, the bulk drug was first screened through 6 and 12 mesh sieves. The screened material was then placed in the mill's feeder, and passed through a fluid energy mill (4" Sturtevant Micronizer) where the micronisation took place. The conditions used for the operation of the mill were: feeder # 250 (1.5") at flow rate of 17-20 g min^{-1}, air volume of 1.42 m^3 min^{-1}, injection jet (feed) pressure 45.5 Kg and a grinding pressure of 40.9 Kg. In the air micronising reduction mill, grinding is achieved by continuously projecting the drug particles in high speed air jets against a rapidly circulating stream of the still unmilled particles. The velocity of the particles in the jet is of the order of 300 m s^{-1}, thus producing the high-energy impact responsible for particle size reduction.

2.2.2 Methods for solid state characterisation of Ro 24-5913

Polymorphism can have a significant impact on the bioavailability of the drug and on the *in vivo* performance of a drug product. One aspect of crystal polymorphism that generates much interest in pharmaceuticals is precisely that of its effect in bioavailabilty. The focus of the present study, as stated in Chapter 1, is rather to use the phenomenon of polymorphism as a

means to have one chemical entity, namely the active ingredient, in two distinct surface configurations. The drug used in the present study was subjected to analysis by a variety of techniques commonly used in the characterisation of solids state materials. The series of analyses described below provide the baseline differentiation between the two polymorphs used, and most importantly, point toward the analytical techniques of choice for purposes of comparing the materials' surfaces and the corresponding powders' interactive properties.

2.2.2.1 *X-Ray Powder Diffraction (XRD)*

Powder XRD measurements were conducted on a Scintag XDS 2000 X-ray diffractometer, equipped with a Copper X-ray source and a Peltier-cooled solid state detector.

Sample Preparation. The samples were run using a zero background plate made out of quartz. The zero background plate was covered with a thin layer of petrolatum to hold the powder sample and then placed on a stainless steel analysis cup. The sample powder was then sprinkled on top of the plate. The plate was gently tilted in order to let the powder flow downward, a portion of the powder would stick to the plate, while the excess powder would fall off onto a sheet of weighing paper. In this way the powder particles stick to the plate in a random manner; at least, no orientation of the particles is forced by the operator. The excess powder was reapplied in the

same fashion in order to get a uniform and complete coverage of drug particles on the plate.

Operating Conditions. On each day powder XRD experiments were conducted, the instrument's alignment was verified prior to running the samples. A Curundum standard shaped plate (NIST SRM 1976 Curundum Plate Standard) was placed on the sample holder and the standard diffraction pattern between the 2-θ. range of 34.8° and 35.5°, changing the 2-θ angle at steps of 0.02° and 2.5 sec. of duration, was obtained.

Sample Analysis. Samples were run under the same conditions as the Curundum standard with the exception of the 2-θ angle, which covered the range of 1° to 40° for the samples. The detector scatter slit had a width of 0.3 mm for the samples. A change of the detector slit from 0.5 to 0.3 mm resulted in a decrease in the peak intensities measured, but it allowed a better resolution capability between peaks.

Results. Samples of micronised polymorphs exhibited the same powder XRD patterns as unmicronised material (not shown), indicating that no solid-phase transitions occurred during micronisation (Figure 10), at least not detectable by XRD.

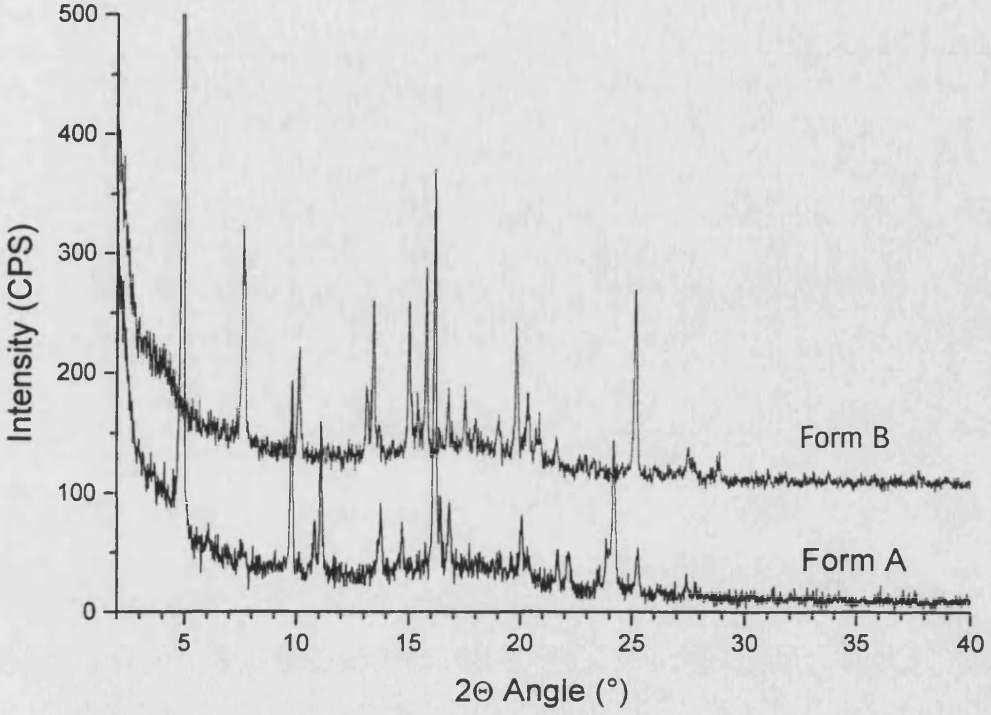

Figure 10 Powder XRD patterns for micronised Ro 24-5913 polymorphs A and B.

2.2.2.2 FT-IR and FT-Raman spectra

FT-IR and FT-Raman spectra are also widely used techniques to differentiate polymorphs. The FT-Raman procedure consisted of placing powder on a sample holder in the Raman accessory of Bio-Rad Digilab FTS-60A FT-Raman spectrophotometer. FT-Raman spectra were obtained under the following conditions: Excitation laser type, Nd-YAG near-IR laser operating at 1.064 μm or 9395 wavenumbers; the laser power at the sample was 710 mW, with a typical scan time of two minutes. The instrument was

equipped with a liquid nitrogen-cooled Germanium detector. The resolution was 8 cm^{-1} at a typical range of 3500-200 cm^{-1}.

The bulk drug substance was analysed by FT-IR and FT-Raman in order to determine if such spectroscopic techniques can differentiate the two polymorphs. The IR and Raman spectra are presented in Figures 11 and 12, respectively. The IR analyses were run at with a resolution of 4 cm^{-1} using twenty co-added interferograms over the frequency range 4000-400 cm^{-1} [Lanyi, 1993]. The FT-IR results indicated that polymorph A and polymorph B are distinguishable but complicated, namely, that their spectral differences are not readily discernible. In other words, the IR patterns are so closed to each other that differences between the two polymorphs could be missed. Although these results do not necessarily preclude the ability of FT-IR as a technique to differentiate between the two polymorphs, the results indicate that FT-IR is not one of the most suitable techniques for purposes of the present study.

The obtained FT-Raman spectra are much simpler and readily useful for identification of the two polymorphs. The analytical peaks chosen were the two at 1626 and 1608 ±2 cm^{-1} delta shift. The ratio used can be defined as I_{1626}/I_{1608} where I_ν is the peak height intensity at the frequency ν. These two peaks were chosen because they correspond to peaks present in the spectrum of polymorph A but absent in the spectrum of polymorph B. The ratios of I_{1626}/I_{1608} for the pure polymorphs are 1.34 and 2.72 for polymorphs A and B, respectively.

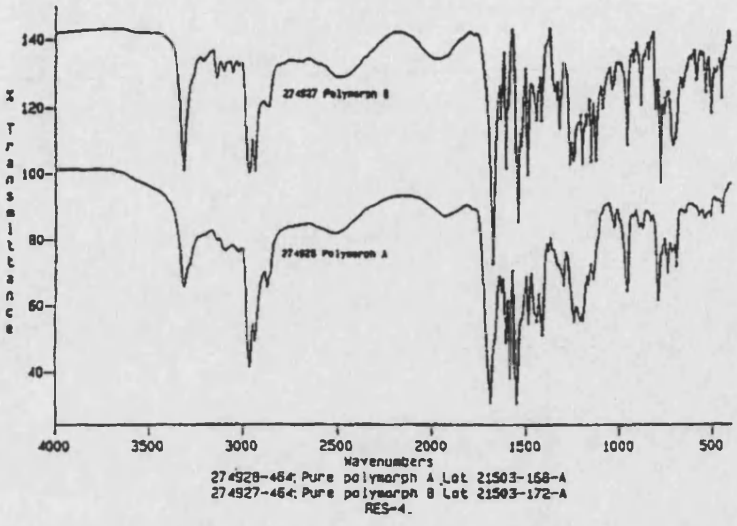

Figure 11 IR patterns for Ro 24-5913 Polymorphs A and B.

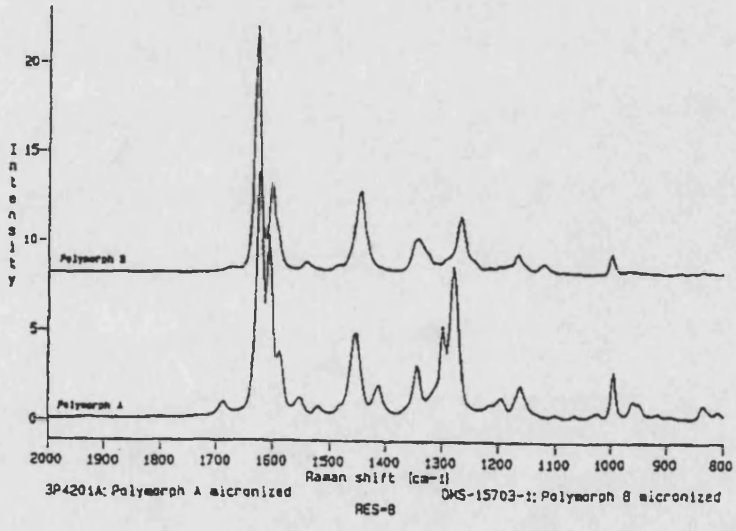

Figure 12 Raman patterns for Ro 24-5913 Polymorphs A and B.

2.2.2.3 Microscopic Analysis.

Three microscopy techniques were used for the analysis of the two polymorphs of the drug substance. The techniques used were optical microscopy, Scanning Electron Microscopy (SEM) and atomic force microscopy (AFM). Drug particle and surface characteristics (crystal habit and texture) were examined using scanning SEM and AFM, respectively. It is worth mentioning at this point that the powder blends of the formulations were also examined by SEM.

2.2.2.3.1 Methods

Optical Microscopy. The unmicronised samples were suspended in USP grade mineral oil and observed under the microscope (Leitz Aristomet, Leitz Wetzlar, Germany) at 500X magnification.

SEM. A sample of drug powder or powder blend with α-lactose monohydrate was sprinkled on to double adhesive carbon fixers mounted on aluminium planchetttes. In some instances, the pure drug was suspended in an organic solvent such as cyclohexane in order to obtain an acceptable dispersion of individual particles. With this treatment, the electrostatic charging of the particles was reduced, thus facilitating sample preparation for SEM analysis. Following the same technique for sample examination as that described above for the SEM analysis of α-lactose monohydrate, a thin conductive layer of gold was sprayed on the sample surface using a sputter

coater. The prepared samples were then examined using the JEOL 6310 SEM instrument.

AFM. Powder particles were mounted on smooth sheets of mica. The powdered samples were prepared using Tempfix™ (Agar Scientific LTD, U.K.), which was melted at a temperature of 120°C on top of a steel thin disk plate and allowed to cool before the sample powder was sprinkled on it. In order to avoid agglomerates, the coated steel plate was scantly sprinkled with the powder sample, either α-lactose monohydrate or drug. The steel plate was then re-warmed on a hot plate to a temperature of 50°C, at which the resin becomes very adhesive for about 20 minutes. After cooling to room temperature, the resin sets quickly trapping some particles and the excess powder was blown off. The surface of the α-lactose monohydrate and drug particles were examined using atomic force microscope (MultiMode SPM and Nanoscope III control system, Digital Instruments, Santa Barbara, CA, USA) operating in tapping mode, with a silicon V-shaped cantilever at a frequency of 2-5 Hz. A 125-µm x-y scanner was used. More than 20 individual measurements were performed at randomised sites for each sample.

2.2.2.3.2 Results

Optical Microscopy. Figure 13 shows the microscope images for unmicronised polymorphs A and B. The two micrographs shown in the figure were obtained at the same magnification. The morphological differences

between polymorph A and polymorph B are clearly distinguishable on the photographs. Unmicronised Ro 24-5913 drug polymorph A exhibits needle-like crystals, whereas polymorph B exhibits rod-like crystals. In addition, the differences in size of the two polymorph drug crystals are readily noticeable.

SEM. After micronisation, polymorph A looks elongated and B looks rounded (Figure 14). The photographs of the material showed that projected particle size obtained after milling was less than 5 μm.

AFM. The AFM images obtained here can only be used in a qualitative manner in the assessment the surface of the micronised (3 – 5 μm) drug particles. This is so because the AFM analysis of the micronised drug presented a series of problems. Similar difficulties were reported by Robertson [1997], who reported the difficulties encountered trying to obtain good AFM representations of surface morphology when working with particles smaller than 10 μm. The problems associated with the AFM analysis of micronised materials have to do with the risk of tip contamination with minute particles. The AFM analysis in the present study was mostly restricted to flat exposed areas of the crystal, where the cantilever was able to scan freely without being impeded to move by tapping as the tip approached the crystal surface.

The AFM examination of drug surfaces indicated that the surface of polymorph A is smooth and somewhat flat (Figure 15). In contrast, surface of polymorph B presents more asperities and clefts, evident as 'hills' and 'valleys' of Figure 16.

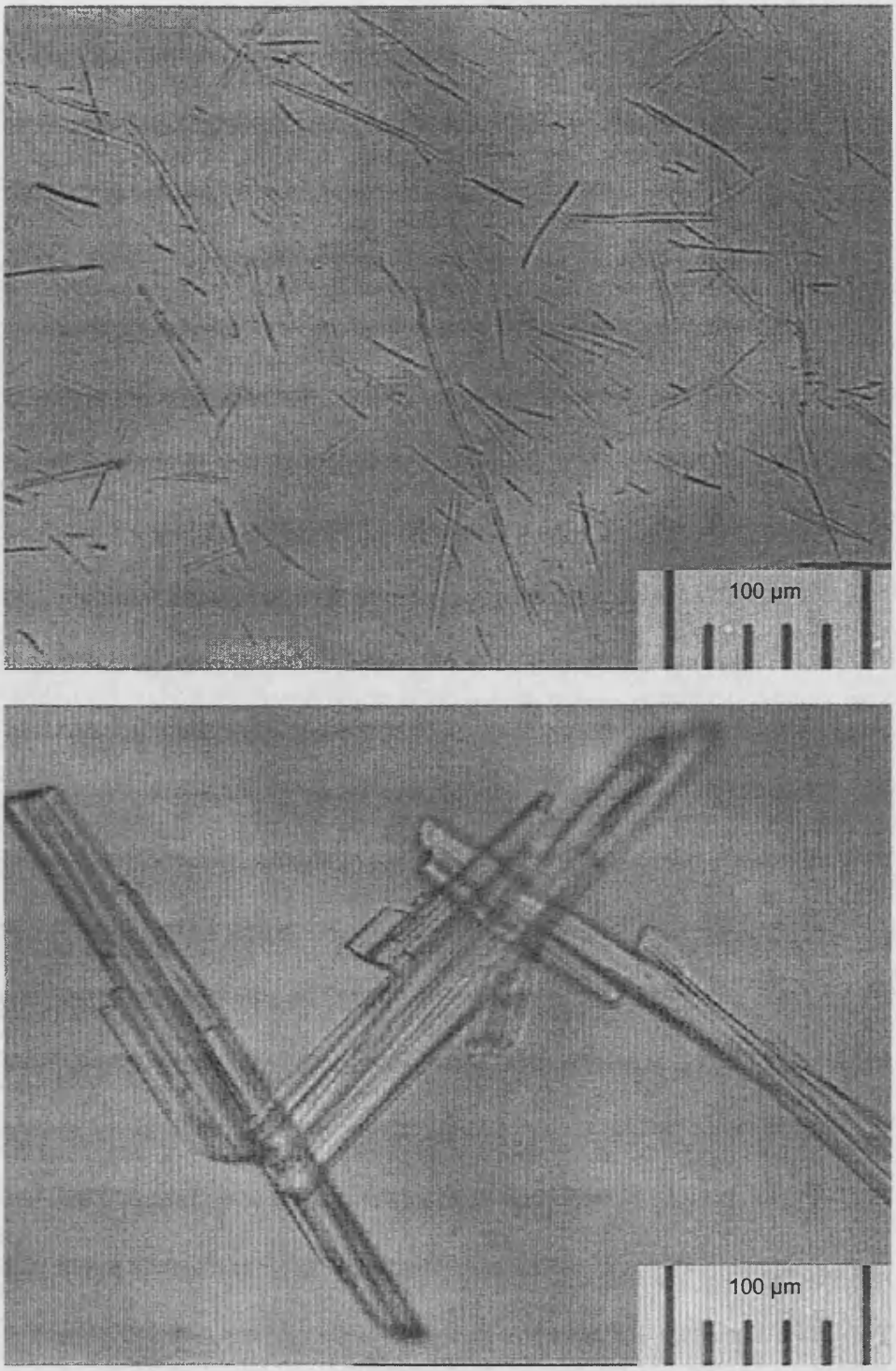

Figure 13 Microscope images of unmicronised drug polymorphs A (top) and B (bottom). Notice that the two images are taken at the same magnification.

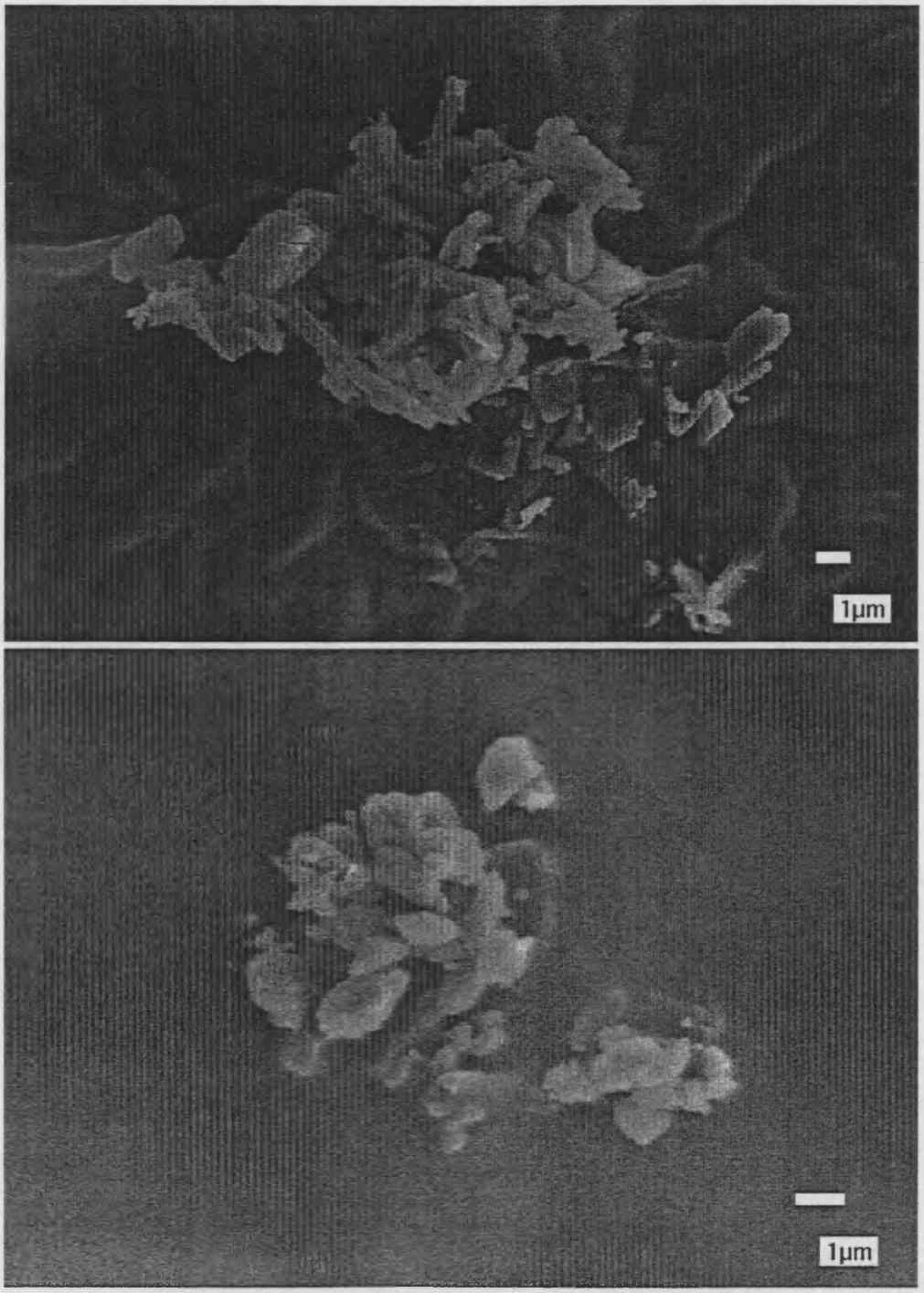

Figure 14 Scanning electron photomicrographs of micronised drug, top: polymorph A , bottom: polymorph B.

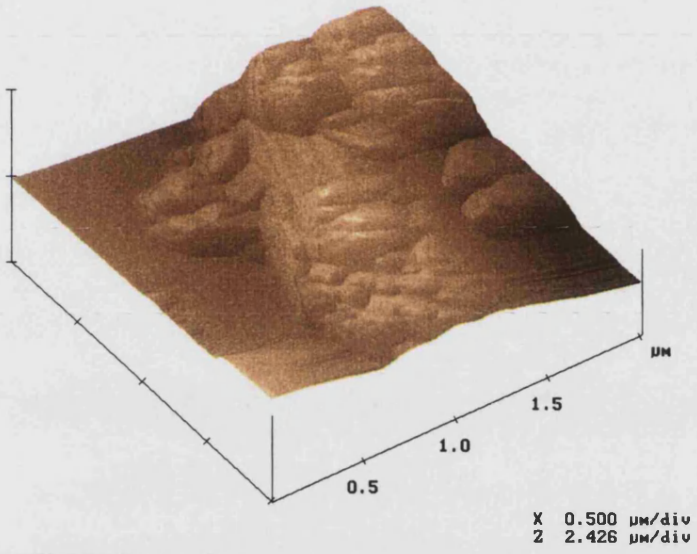

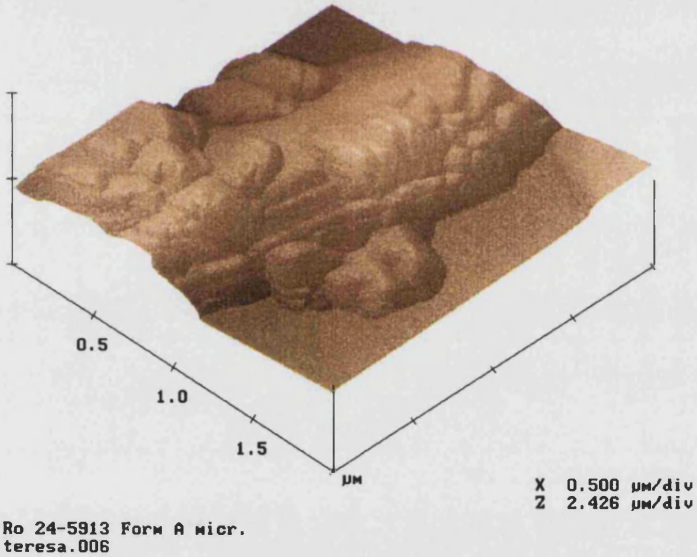

Figure 15 AFM images of drug micronised polymorph A (n>20, individual measurements were performed at randomised sites for each sample).

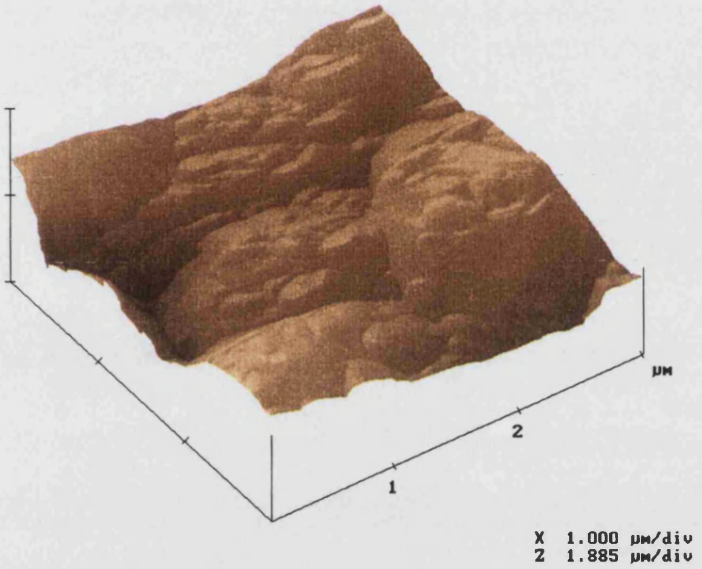

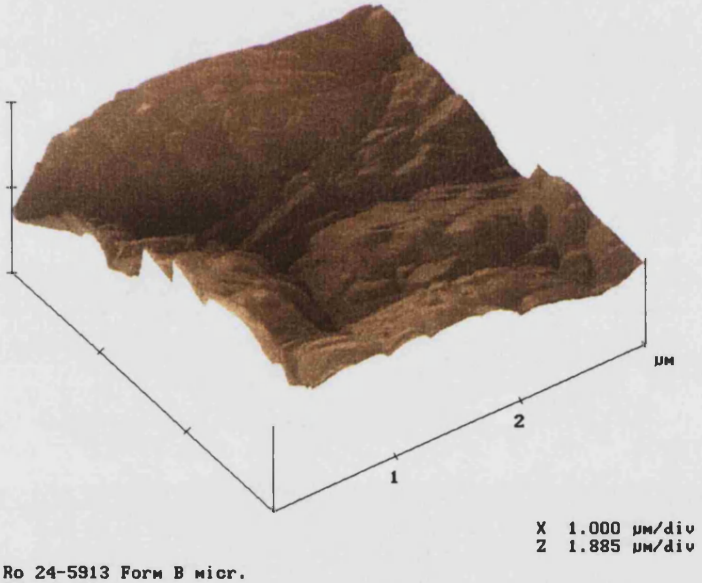

Figure 16 AFM images of drug micronised polymorph B (n>20, individual measurements were performed at randomised sites for each sample).

2.2.2.4 Particle size analysis and surface area.

Particle size analysis of the drug was performed using a Malvern Mastesizer X laser light diffraction instrument, in the same manner as described above for α-lactose monohydrate. However, the sample preparation for the drug was slightly different from that of α-lactose monohydrate. It is noteworthy to mention at this point that the instrument was checked for reliability with monodisperse polystyrene beads of different sizes, traceable by the NIST (National Institute of Standards and Technology). In addition, to ensure reproducibility and validation of the method two experimental practices were carried out: a) possible formation of undesired agglomerates or aggregates in the dispersed particle phase were looked for using a light microscope; b) obscuration was monitored with time, as no change was necessary. The drug was dispersed in hexane (Fisher Scientific), and sonicated for one minute to disperse agglomerates. The hexane-drug suspension was then added dropwise until an obscuration of 20-30% was obtained. The 45 mm lens was chosen for the detection of particles in the range of 0.1 – 80 µm. Three runs were conducted for each drug sample. Fraunhofer analysis was used for the calculation of the particle size data, and the frequency distribution by volume.

A gas adsorption/desorption apparatus (PMI, Porous Materials Inc. Automated BET Sorptometer) was used for the determination of the surface area of both polymorphs of the drug by the BET method. About 2 g of sample was placed into the glass loop then this loop was submerged into liquid nitrogen. Vacuum was applied to the sample for about 24 hrs. prior to

the measurement. Depending on the magnitude of the sample's surface area, either nitrogen or krypton can be used as penetrating gas. Nitrogen is generally used for measuring large surface areas, whereas krypton is used for measuring smaller surface areas. Both gases were used for the determination of the micronised drug surface area.

As discussed in Chapter 1, the experimental design of the present study requires that the particle size distributions of the two polymorphic materials of Ro 24-5913 to be as close as possible to each other. Table 3 shows the particle size distributions of micronised Ro 24-5913, polymorphs A and B. A comparison of the particle size distributions for both polymorphs are shown in Figure 17. Results of surface area analysis are also presented in Table 3.

Table 3 Particle size[a] distributions and surface area[b] for micronised Ro 24-5913, polymorphs A and B.

Ro 24-5913	Lot No.	Surface Area $m^2 g^{-1}$	Particle Size Distribution (μm)		
			dv_{90}	dv_{50}	dv_{10}
Polymorph A	DS 21687-44	8.18	5.8	2.4	0.9
Polymorph B	3P-4223	7.38	4.7	2.2	0.8

[a] Particle size distribution by Malvern Mastersizer X Laser Diffraction.
[b] Surface area by BET.

The particle size of the drug for both polymorphs was reduced in the present study in order to make the materials suitable for processing. Size reduction also results in an increase of both surface forces and surface free energy [Staniforth 1982b], which promote inter-particle interactions.

The particle size of α-lactose monohydrate, as previously mentioned, was kept in the range of 45-106 µm (including fines) for use as carrier with similarly-sized micronised drug of two polymorphs. Thus, any change in the performance of the powder system could be considered to be primarily the result of properties other than the particle size of the drug.

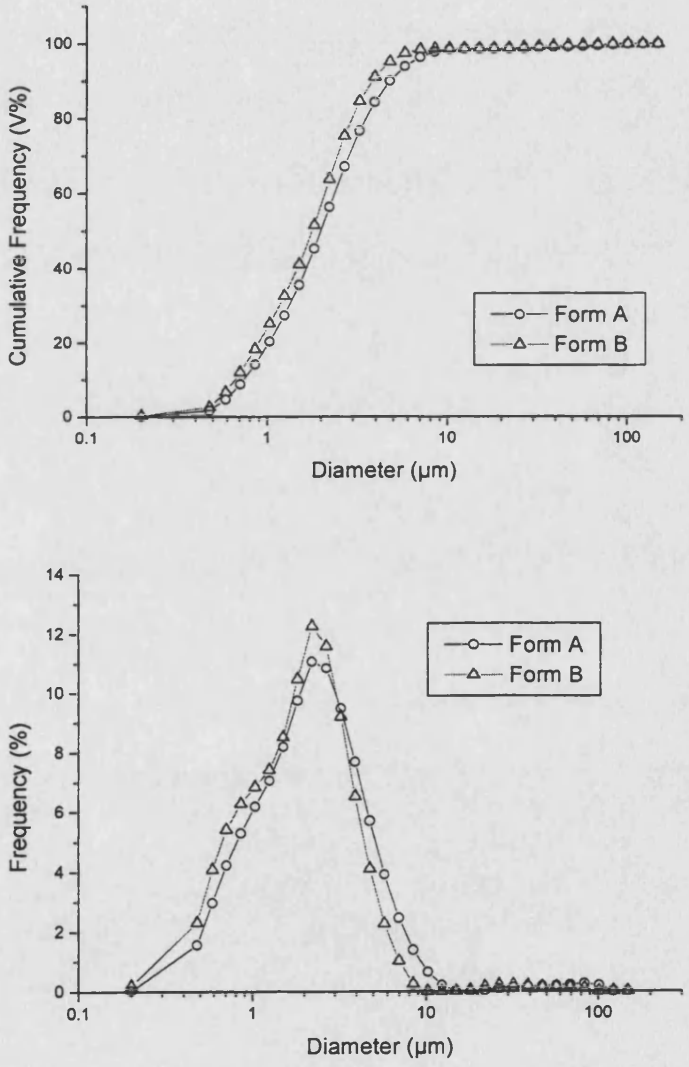

Figure 17 Particle size distribution for both polymorphs of the micronised drug (n=3).

The micronised powders of polymorphs A and B showed to have very similar particle size distributions, as shown in Figure 17.

2.2.2.5 Thermal analysis – Differential Scanning Calorimetry (DSC) and Heat capacity.

The DSC technique is commonly used to differentiate and to study the thermodynamic relationship between polymorphs. Samples of both polymorphs of Ro 24-5913 were analysed using DSC. A sample of about 2 - 3 mg was placed into an aluminium pan and hermetically sealed. The sample was placed in the DSC apparatus (DSC-7 Perkin Elmer, Connecticut, USA). Two different heating rates were used, 5 and 10°C min^{-1}. Table 4 shows the DSC data obtained.

Table 4 DSC Ro 24-5913

Compound	Heating Rate (°C min^{-1})	Mass (mg)	ΔH_f (mJ mg^{-1})	Onset Temp. of the endothermic event (°C)
Indium (Calibration)	10.0	7.350	28.6	156.5
Ro 24-5913 Polymorph A unmicronised	5.0	2.740	254.2	172.7
micronised	5.0	3.124	275.0	172.1
	10.0	2.792	279.7	174.3
Ro 24-5913 Polymorph B unmicronised	5.0	3.665	275.8	173.6
micronised	5.0	3.080	300.1	171.9
	10.0	3.237	282.4	174.7

The DSC was used to determine the onset temperatures of the endothermic melting event and the heats of fusion of both polymorphs. Typical DSC thermograms for Ro 24-5913 are shown in Figure 18. These thermograms remained similar at the two heating rates used. Variations in DSC thermograms produced by changing heating rates are indicative of non-thermodynamic (*i.e.*, kinetic) events accompanying the event under study. Such kinetic events are in turn the manifestation of imperfections in the crystal phase due to impurities for example, or brought about by external factors such as the mechanical stress exerted on the on the crystal during milling. The DSC thermograms in Figure 18 show that the indications of changes to the crystallinity of the micronised drug were not observable by DSC.

Heat Capacity is another thermodynamic quantity that can be readily measured by DSC. Heat capacity corresponds to the second derivative of free energy with respect to temperature, thus making it a more sensitive parameter in differentiating solid phases, particularly of the same material. Polymorph B has lower heat capacity than polymorph A (Figure 19). Heat capacity is perhaps the one thermal property that depends entirely on how the molecules are assembled, *i.e.*, it depends on an ensemble of molecules, on how they pack together, and on how far and how fast the molecules can move from their equilibrium positions while still maintaining the crystal phase. Other thermal properties depend on the chemistry of individual molecules, or on groups of molecules, but at the precise point where the thermodynamic phase they form is being disrupted (*i.e.*, on how the molecular ensemble is disassembled).

Table 5 and Figure 19 represent the average values of two runs for each polymorph. Two runs were sufficient for reliability in the results, since the instrument is checked daily for calibration prior to use with a sample. Table 5 gives the heat capacity measurements for the two polymorphs of Ro 24-5913 . Figure 19 shows that the heat capacity of polymorph A was higher than that of polymorph B for the entire temperature range studied. This result is consistent with polymorph A being the less thermodynamically stable of the two polymorphs [Burger and Ramberger, 1979; Brittain, 1994].

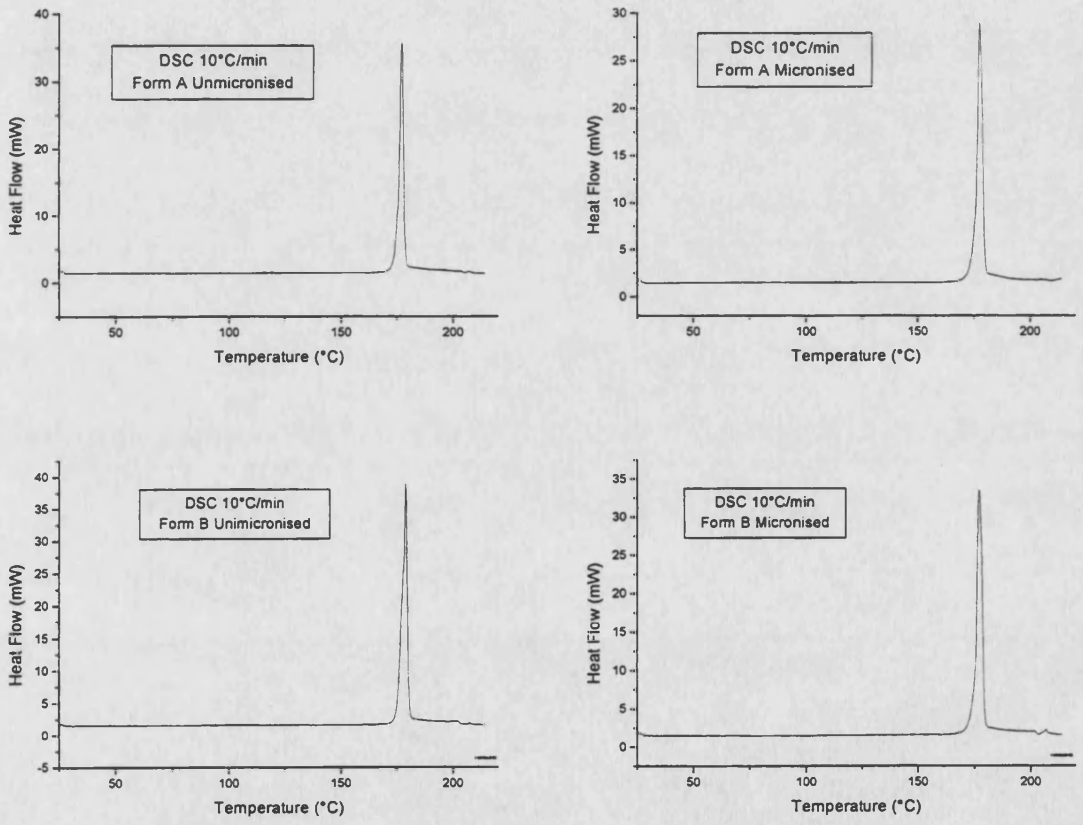

Figure 18 DSC thermogram for Ro 24-5913 polymorphs.

Table 5 Heat Capacity for Ro 24-5913 polymorphs A and B
Note: Universal Gas Constant , R = 8.31 J mol^{-1} $°K^{-1}$
Ro 24-5913 M.W. = 412.55 g mol^{-1} Temp. °K = 273 + °C

Temperature °C	Polymorph A Average (n=2) J g^{-1} $°C^{-1}$	Polymorph B	Polymorph A Cp Relative to R Dimensionless	Polymorph B
30	1.2993	1.2815	0.2129	0.2319
40	1.3351	1.3292	0.2118	0.2405
50	1.3787	1.3517	0.2119	0.2446
60	1.4228	1.3924	0.2121	0.2519
70	1.4617	1.4284	0.2116	0.2584
80	1.4976	1.4651	0.2106	0.2650
90	1.5416	1.4995	0.2108	0.2711
100	1.5843	1.5428	0.2109	0.2789

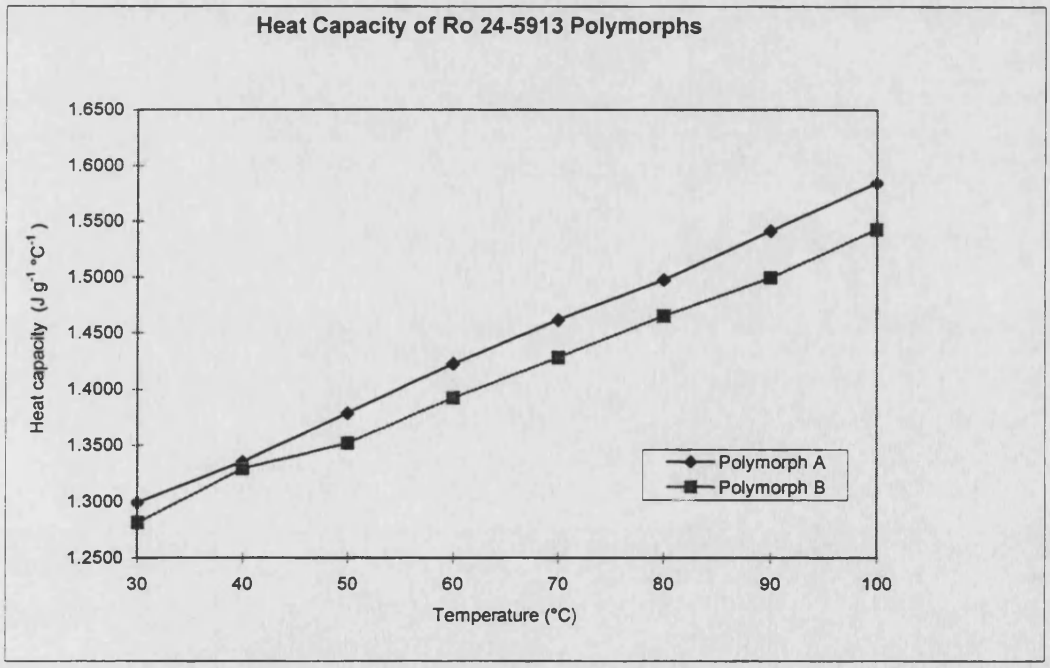

Figure 19. Graphical representation of heat capacity for both drug polymorphs.

2.2.2.6 Water vapour sorption

The two polymorphs of the experimental drug in the present study have shown differences in their physical characterisation by a number of the techniques reported above. Vapour sorption is also a technique often used to characterise polymorphs. Water uptake by a powder may have different effects on the powder's interactive properties, for example, increasing agglomeration via surface tension forces, and reducing electrostatic charges. These effects may depend on how the amount of water sorbed alters the functionality of the drug in systems such as DPI formulations.

Samples of both polymorphs were placed in a microbalance water vapour adsorption/desorption apparatus (VTI Corporation, Hialeah, FL, USA). Two different instrumental variants are available for the determination of sorption isotherms: a vacuum system and a flow system. The vacuum system uses pressure to control the relative humidity, the pressure is varied from a zero-point value to the saturation pressure of water at the temperature of interest. In the vacuum system, the atmosphere surrounding the sample consists exclusively of water vapour, and samples have to be dried prior to the analysis. The flow system uses wet/dry gas and uses the dew point feedback mechanism to control the relative humidity. In the flow system, the sample is always under 1 atm. of pressure in an environment made of a mixture of nitrogen and water vapour. Samples do not have to be dried prior to starting an analysis with the flow system. The vacuum and flow systems are equivalent in principle, although in practice they are rather complementary. The vacuum system is very valuable in the

study of the properties and qualities of the material, *e.g.*, during chemical synthesis optimisation, whereas the flow system is very useful for studying the behaviour of powder materials under conditions pertinent to pharmaceutical processing.

The amount of sample used for an analysis depends on the sample's tendency to pick up water. If the sample is highly hygroscopic, about 2-5 mg are sufficient for the test, but if the sample is non hygroscopic, a larger mass is needed, about 25 mg or more. For this study, water sorption isotherms for both polymorphs were carried out using the flow system and a sample size of about 50 mg.

2.3 Preparation of drug Lactose blends

2.3.1 Blending technique.

Mixing of powders is one of the most important unit operations during production of pharmaceutical dosage forms, whether solids for oral delivery or powders for inhalation. α-Lactose monohydrate is the most widely used carrier in DPI formulations, and was chosen for the formulations of the present study. Homogeneous binary powder blends of drug and α-lactose monohydrate were prepared. The blends contained different concentrations of micronised Ro 24-5913, either as polymorph A or B. α-Lactose monohydrate (Sheffield Products, Plainfield, NJ, U.S.A.), sieved fraction of 45-106 μm (including fines), was used as the carrier. The powder blend

formulations prepared had drug loads of 1, 5, 25, 50 % w/w. The powders were mixed in a glass container using a Turbula mixer (Willy A. Bachofen Maschinenfabrik, Switzerland) for 15 minutes using a 100 g batch size. A mixing time between 10 and 20 minutes is usually sufficient to obtain powder mixes with homogeneous characteristics. A shorter mixing time might result in an inhomogeneous system and longer times may cause segregation [Ahmed 2000]. After mixing, samples were removed and assayed for drug homogeneity by HPLC.

2.3.2 Content uniformity studies.

Homogeneity of the powder blends was assessed for each polymorph/lactose mixture by randomly withdrawing with a spatula, 10 samples, each weighing 20 ± 1.0 mg, from different parts of the powder blend. The powder samples were placed individually in 10 ml amber volumetric flasks. The diluent system used throughout the analysis consisted of a solvent mixture of acetonitrile:water:tetrahydrofuran at a ratio of 50:30:20. Diluent was added to each flask containing the powder sample, and the resulting mixture was then sonicated for 10 min. After sonication, the volumetric flasks were filled to volume with the diluent and thoroughly mixed. The resulting solutions were filtered through a Millex HV 0.45 µm filter. All work was conducted under subdued light and using low-actinic glassware. Samples were assayed by HPLC, using the method of reported by Aggarwal *et al.,* [1993].

2.3.3 HPLC analysis.

The HPLC method used is outlined in Table 6. Linearity of the HPLC method was confirmed by preparing standards of Ro 24-5913 at different concentrations for both polymorphs within the range of concentrations used.

Table 6 HPLC Method for Ro 24-5913:

Instrument	Waters HPLC
Pump	Model 600E Multisovent Delivery System
Injector	WISP Model 712
Column	Nova-Pak C_{18}, 15 cm x 3.9 mm i.d., 4 mm
Mobile Phase	Buffer pH 5.5:Acetonitrile:Tetrahydrofuran (52:43:5)
Flow Rate	1.0 ml min^{-1}
Detector/Setting	Applied Biosciences/240 nm.
Injection Volume	25 µl
Approx. Ro 24-5913 Retn. Time	4.8 min
Approx. Run Time	10.0 min

Calibration curves with each polymorph of Ro 24-5913 (Figure 20) were prepared to verify concentration range linearity and performance of the HPLC instrument. A series of standard solutions were prepared from stock solution of 1 mg ml^{-1} to cover the concentration range of 1 – 250 µg ml^{-1}. This concentration range was sufficient to encompass the concentrations of all unknown samples analysed. Each standard solution for the calibration curve was injected in duplicate.

For each analysis session, fresh standard solutions were prepared in duplicate, each from separate weighs, at high and low concentrations within the range of linearity for both polymorphs. For the determination of the concentration of Ro 24-5913 in the samples, standard solutions were

injected along with the samples to be tested before and after the unknown samples. Standards were injected five times and unknown samples twice. The response factor (*R.F.*) was calculated for each standard according to equation:

$$R.F. = \frac{C_{Std}}{AUC_{Std}} \qquad (27)$$

the concentration of drug Ro 24-5913 in the sample was determined using the mean response factor and the peak area of the unknown sample.

Tables 7 and Figure 20 show the linear regression obtained for the calibration curves for Ro 24-5913 polymorph A and B, respectively. Calibration plots were linear over the range 1-250 µg ml^{-1}, and passed through the origin.

Table 7 Linear regression data for HPLC analysis of Ro 24-5913 polymorphs A and B.

Ro 24-5913	Slope (counts)*	Intercept (counts)*	R^2
Polymorph A	29241	3636	0.9999
Polymorph B	30363	16120	0.9997

A typical chromatogram for Ro 24-5913 is shown in Figure 21 (data information obtained from PE Nelson Access Chrom Integration Package validated and used at Roche).

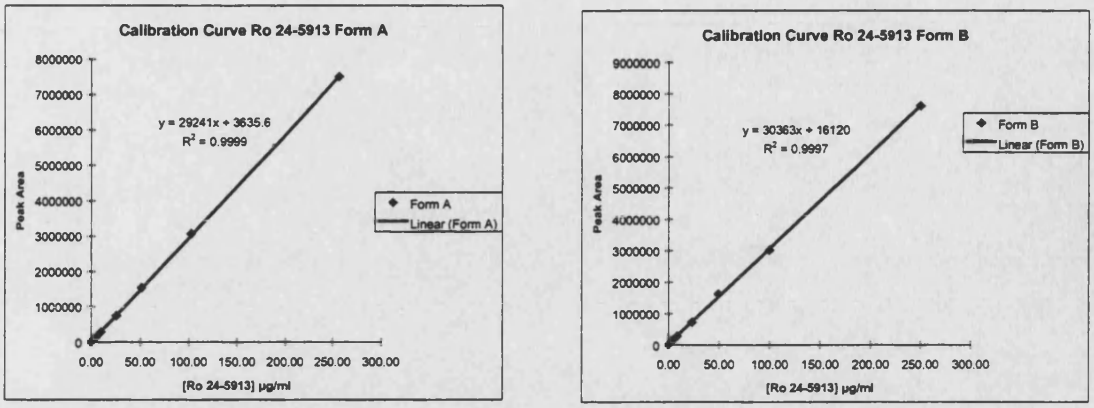

Figure 20 HPLC calibration curves for Ro 24-5913 polymorphs A and B.

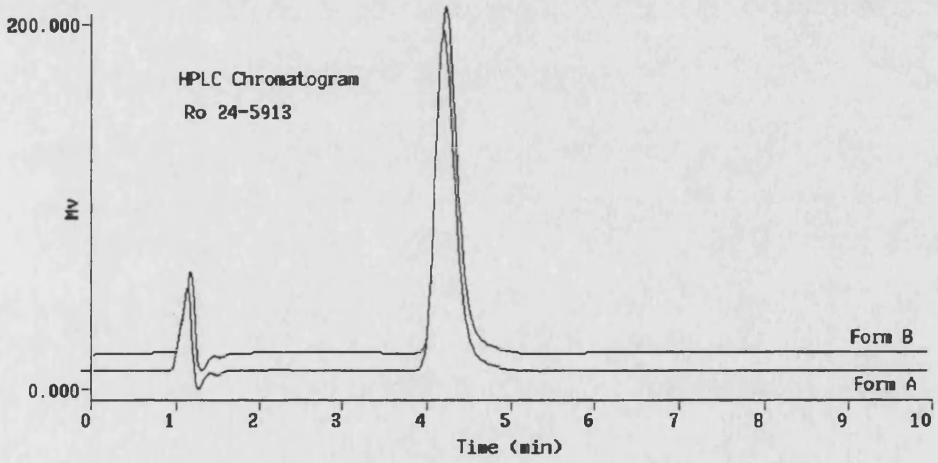

Figure 21 HPLC Chromatogram of Ro 24-5913.

2.3.4 Content uniformity testing.

The average values of content uniformity for Ro 24-5913/α-lactose monohydrate blends are shown below in Table 8. The coefficient of variation was found to range from 3 to 5.7% indicating acceptable homogeneity of the powder blends. The range value for content uniformity

of the active ingredient is within the acceptable criterion given for dry powder inhalers to ensure uniformity of dosage units [U.S. Pharmacopeia XXIII, 1995].

Table 8 Content uniformity analysis for different Ro 24-5913 formulations. Mean and standard deviation for n= 10.

Polymorph A				
% w/w	1%	5%	25%	50%
Mean	1.03	4.80	24.06	49.41
SD	0.03	0.26	1.06	1.34
CV	3.08	5.68	4.62	2.71
% Recovery	103.00	96.00	96.24	98.82
Polymorph B				
% w/w	1.0 %	5%	25%	50%
Mean	1.02	4.87	24.59	49.70
SD	0.04	0.15	1.19	1.80
CV	3.57	3.32	5.29	3.63
% Recovery	102.00	97.40	98.36	99.40

2.4 Characterisation of Powder Blends.

2.4.1 Infrared and Raman Spectroscopy

These techniques involve examination of the twisting, bending, rotating and vibrational motions of the atoms in the molecule. IR detects a change in the dipole moment whereas Raman detects changes in the polarisability of the molecule during vibration. Raman spectroscopy can provide important information that is often not available from IR. When an incident beam of laser light hits upon the sample, some of the light may be absorbed, but much of it will be scattered by the material. The spectrum of

a compound is essentially the superposition of absorption bands of the specific functional groups of pure materials. In the case of mixtures, the lack of absorption in specific frequency regions can be correlated with restrictions on specific vibrational modes in the molecule. The loss or shift of vibrational modes in a molecule is, in turn, indicative of an intermolecular interaction involving the corresponding functional group. Consequently, when comparing the IR or Raman spectrum of a pure material with that of a blend, it is possible, at least in principle, to gather information about the type of interactions taking place between the materials in the blend. Hindrance in the powder blend to a particular molecular vibration would be indication the interaction between the drug and α-lactose monohydrate, for example.

The Raman spectra for the neat polymorphs A and B are shown in Figures 22 and 24, respectively. For comparison, each of these two figures also shows the Raman spectra of neat α-lactose monohydrate. Figures 23 and 25 show the Raman spectra obtained from the 5% drug-lactose mix for polymorphs A and B, respectively. Figures 23 and 25 show the blends' spectra originally obtained, as well as those resulting after subtracting the spectrum of α-lactose monohydrate.

It was found that the lower limit of detection by Raman of Ro 24-5913 polymorph A is of the order of 1%. The band at 1626 cm^{-1} is clearly not due to α-lactose monohydrate, but to polymorph A. At higher concentrations, more details of the spectrum become apparent. On the other hand, polymorph B is a very strong Raman scattering material. This substance is detectable even at 0.5% w/w.

Functional groups manifest themselves at different frequency regions of the FT-IR or FT-Raman spectrum. The OH and NH groups, which are likely to form hydrogen bonds, are noticeable a wavenumber values greater than 3000 cm^{-1}. Functional groups containing aromatic CH groups are in the region below than 3000 cm^{-1}. Double bonds such as C=C, C=O and C=N are located in the region below 1600 cm^{-1}.

The top spectra in Figures 22 and 24 correspond to drug form A and drug form B respectively. Both showed a peak close to 3000 cm^{-1}, which is typical for aromatic CH groups. This peak disappeared after mixing either of the drug polymorphs with α-lactose monohydrate and subtracting the α-lactose monohydrate pattern from the drug (Figures 23 and 25 bottom spectra). These results can be interpreted as an indication of van der Waals interactions between the drug and α-lactose monohydrate. No evidence of hydrogen bonding between the drug and α-lactose monohydrate was detected, and the rest of the drug spectrum after subtracting α-lactose monohydrate was identical to that of the pure component.

The IR technique did not reveal the spectral changes observed by Raman when comparing neat materials and powder blends. Even though the drug and α-lactose monohydrate both possess dipoles and hydrogen bonding groups (prerequisites for Raman and IR detection), interactions between the drug and α-lactose monohydrate in the binary powder blends used in this experiment were not detected by IR.

The interactions taking place at the surface of dry powders for inhalation are mainly due to van der Waals forces and electrostatic

interactions [Visser 1989]. The Raman spectra in Figures 23 and 25 show interactions involving the aromatic moieties of the drug. Since the carrier lacks aromatic groups, the drug-carrier interactions detected by Raman are of the van der Waals type, specifically dispersion interactions involving a dipole and an induced dipole.

The interactions in the powder blends may be too weak to produce a change in a permanent dipole or functional group in the molecule, capable of producing a noticeable shift in the IR spectra. These results do not necessarily mean that the IR spectra are devoid of any information regarding hydrogen bonding or other dipole interactions between the drug and the carrier. It is possible that a more in depth analysis of the IR spectra will reveal not readily observable drug-carrier interactions. However, the purpose of the present study is not to investigate whether IR, or any other technique whose measurements produce practically imperceptible differences between polymorphs A and B, can be made to differentiate between them. The variety of instrumental characterisation techniques explored in this study was included with the purpose of identifying those techniques that most clearly and readily differentiate between polymorphs A and B, in terms of their interactive behaviour as powders.

2.4.2 SEMs of the drug blends

Characterisation of powder formulation blends of drug-lactose at different drug concentrations was conducted by scanning electron microscopy. SEM photographs showed how micronised drug particles

physically adhere on coarse α-lactose monohydrate. SEM could also show, in a rough manner, the drug load necessary to cover α-lactose monohydrate particles in a "monolayer".

SEM photographs of 1, 5 and 25% w/w drug polymorphs A and B in α-lactose monohydrate blends are presented in Figures 26, 27 and 28 respectively.

The photomicrographs clearly show that a drug load of 1% is not sufficient to completely cover the crystals of α-lactose monohydrate, whereas photomicrographs of 25% drug load shows an "overload". Among the different drug concentrations used in this study, the 5% w/w drug load seems to be the closer percentage needed for covering the α-lactose monohydrate in a "monolayer". A more detailed discussion in regards to the degree of drug coverage of α-lactose monohydrate will be presented in Chapter 5.

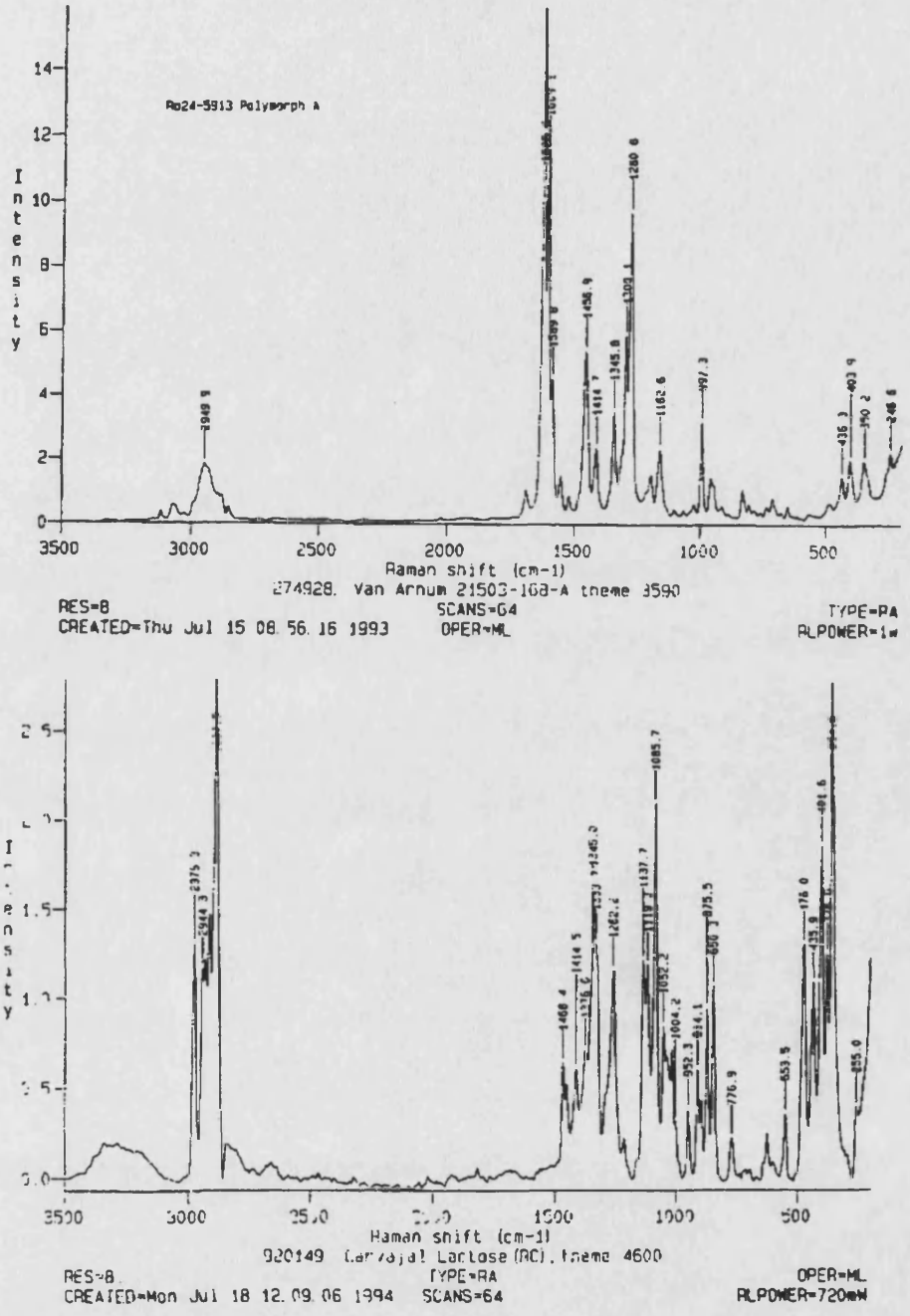

Figure 22 Raman spectrum for pure Ro 24-5913 polymorph A (top) and α-lactose monohydrate (bottom).

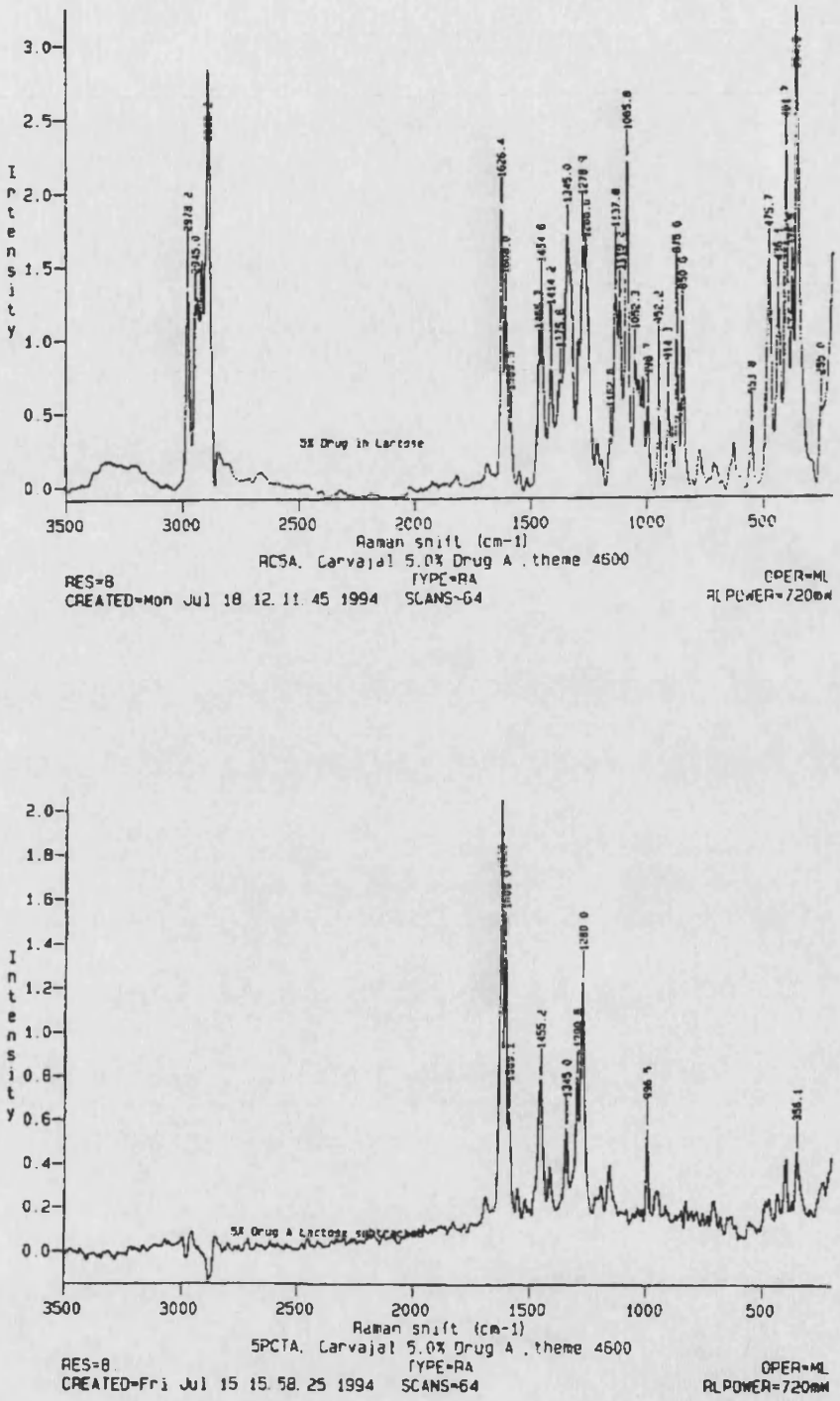

Figure 23 Raman spectrum for the mix 5% of drug polymorph A in-α-lactose monohydrate (top); and the spectrum of the 5% drug polymorph A, with α-lactose monohydrate subtracted out.

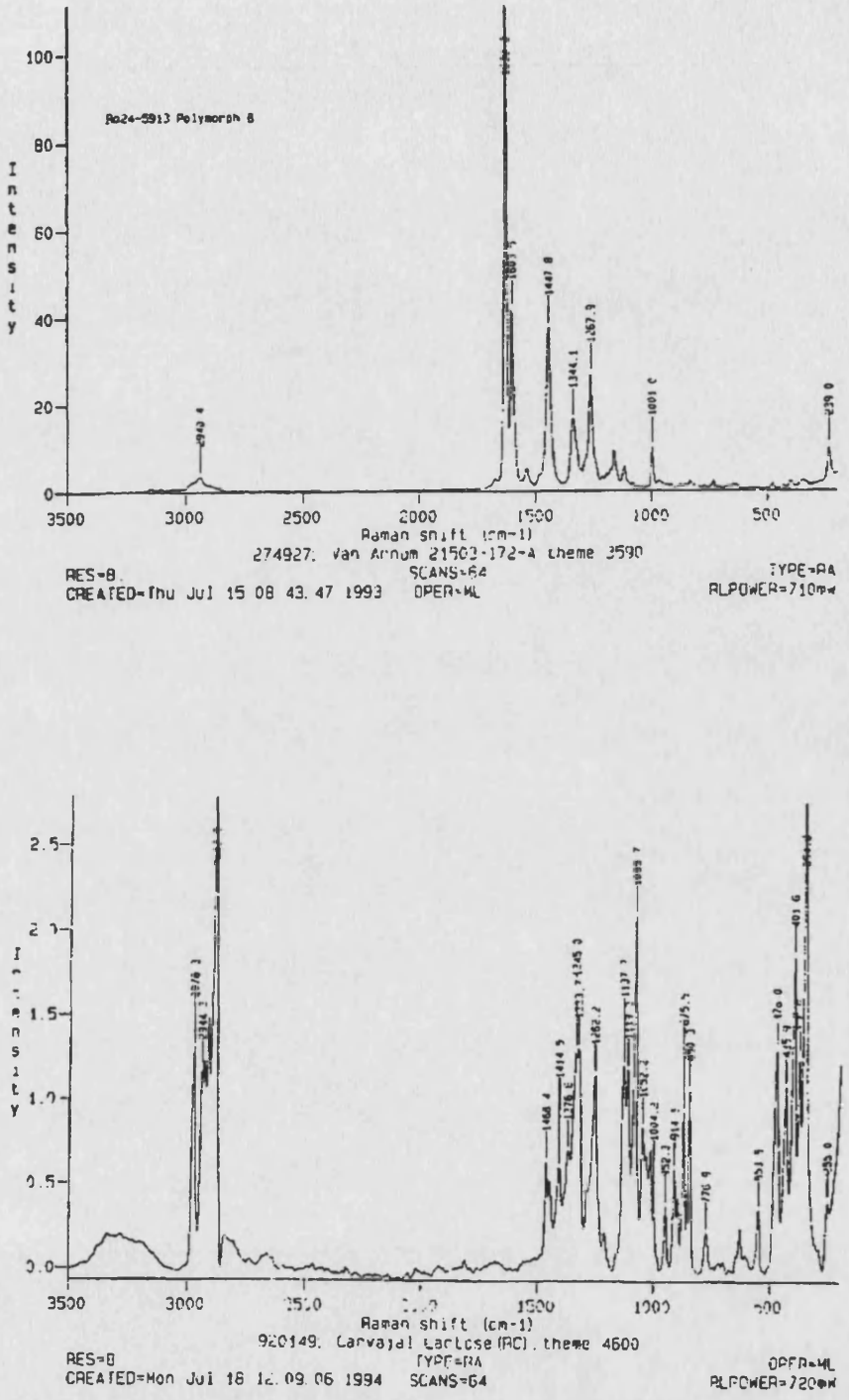

Figure 24 Raman spectrum for pure Ro 24-5913 polymorph B (top) and α-lactose monohydrate (bottom).

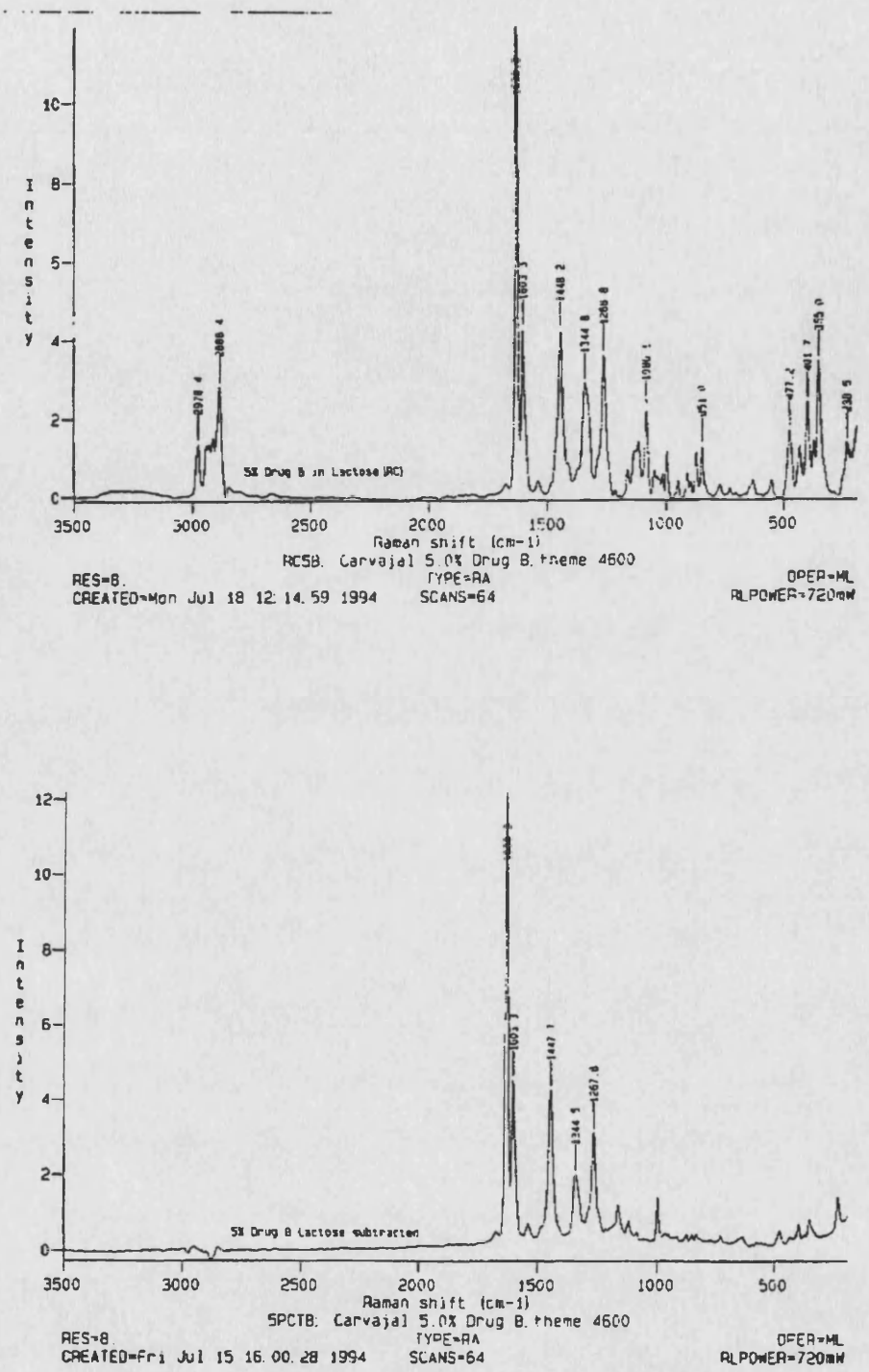

Figure 25 Raman spectrum for the mix 5% of drug polymorph B in α-lactose monohydrate (top); and the spectrum of the 5% drug polymorph B, with α-lactose monohydrate subtracted out.

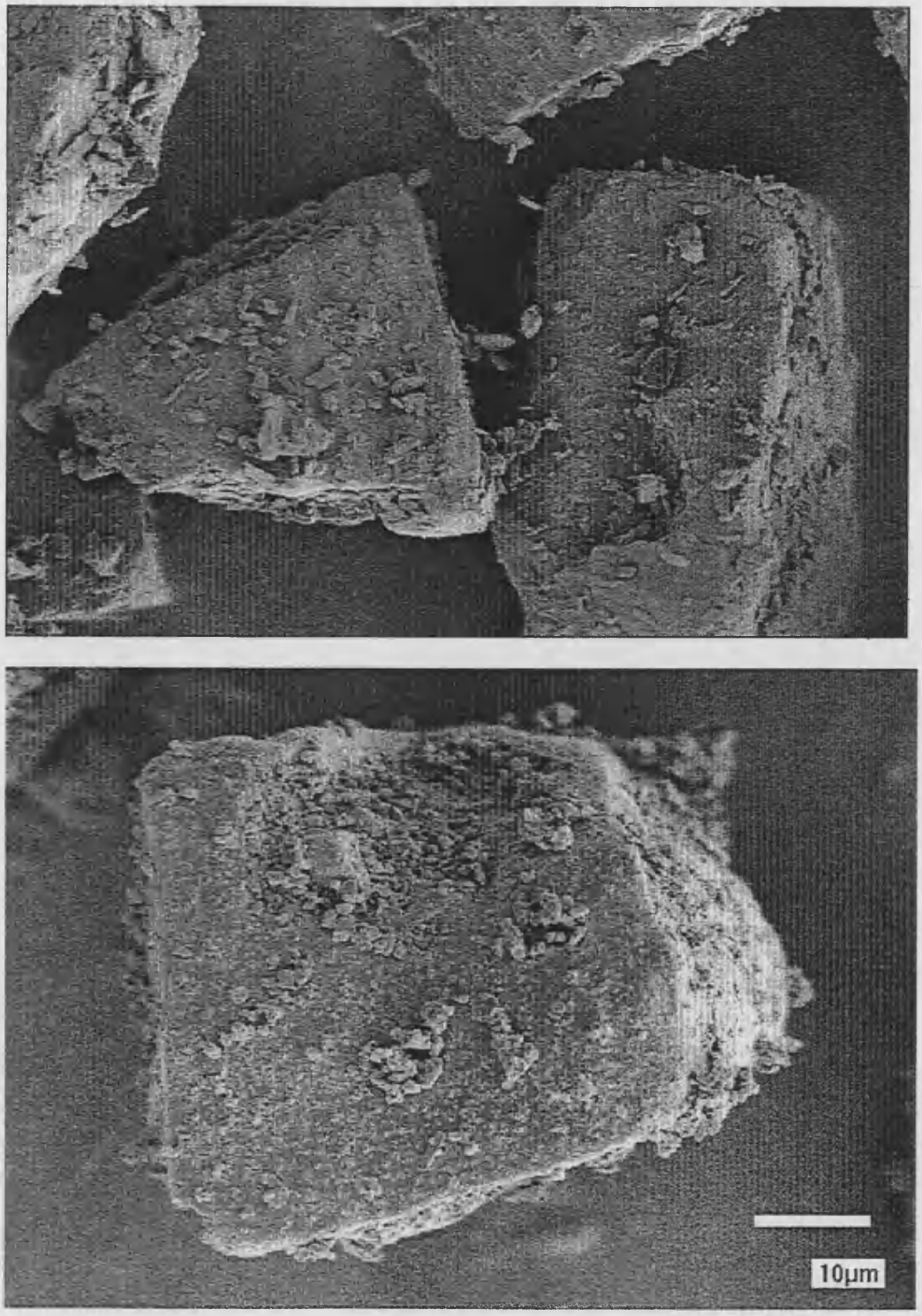

Figure 26 1% micronised polymorphs A (top) and B (bottom) in α-lactose monohydrate (45-106 µm).

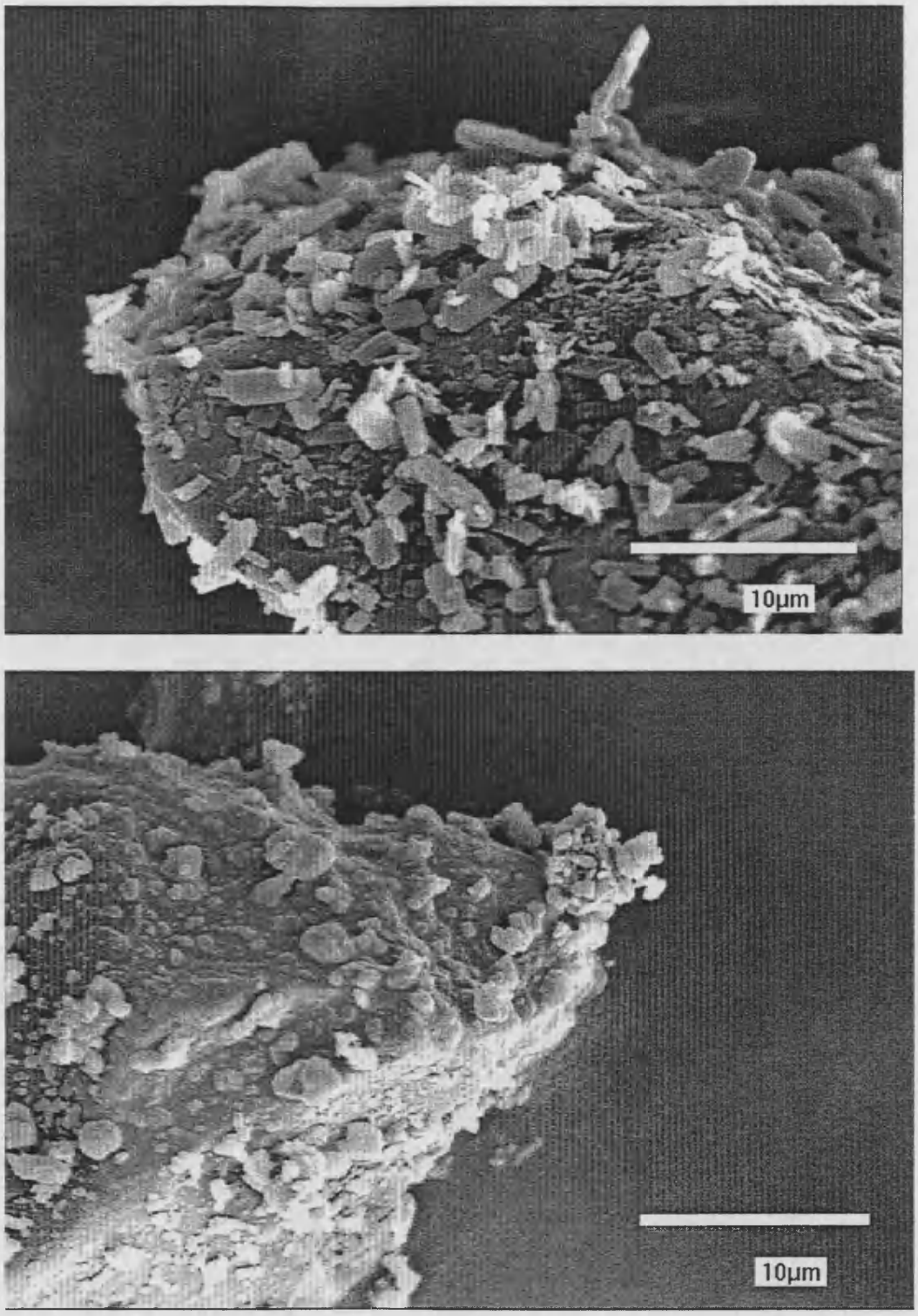

Figure 27 5% micronised polymorphs A (top) and B (bottom) in α-lactose monohydrate (45-106 µm).

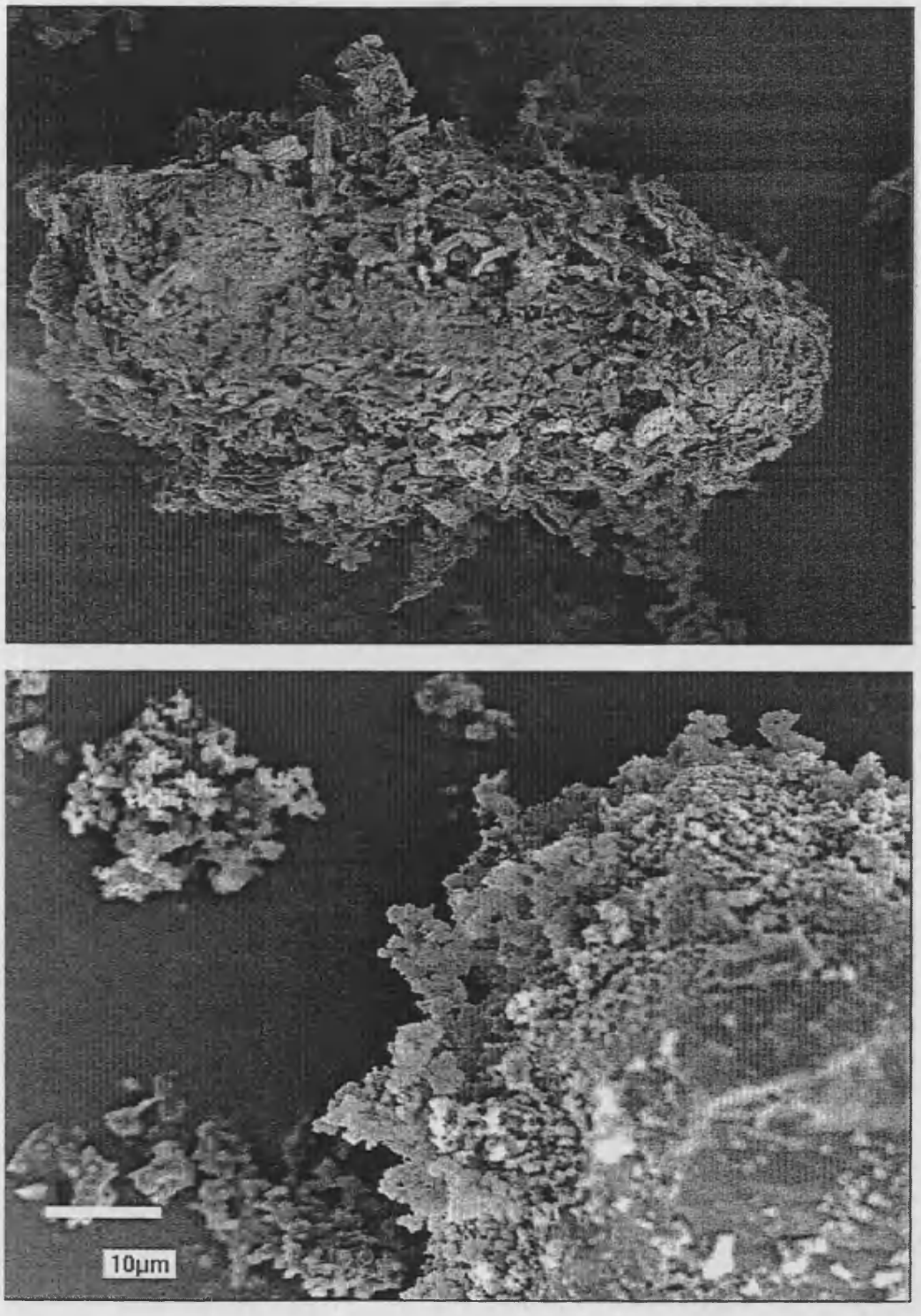

Figure 28 25% micronised polymorphs A (top) and B (bottom) in α-lactose monohydrate (45-106µm).

3. STUDY OF PARTICLE INTERACTIONS: ADHESION AND ELECTROSTATIC FORCES.

3.1 Adhesion Force Measurements

The forces of adhesion of solid particles onto surfaces have been measured in a number of reported studies, using variations of a centrifuge method. The results of such studies have been reported by Donald [1969], Staniforth [1981a and 1982b], Laycock and Staniforth [1984], Booth and Newton [1987], Kulvanich and Stewart [1987c]. All reported methods are variations of a technique originally devised by Krupp [1967], which consists on placing a powder sample in a modified centrifuge tube. The adhesive forces are indirectly measured by overcoming them through the application of a known centrifugal force that causes the detachment of adherent powders from substrate surface.

Kulvanich and Stewart [1987c] developed a compartmental centrifuge cell that effectively separated small particles from large ones. The centrifuge method assesses the extent of particle detachment by assaying the total amount of material detached, the centrifuge method provides no information on the number or the size of the particles detached from the carrier. The centrifuge method is nevertheless capable of reflecting differences in processing conditions used in the manufacture of DPI's. In order to apply forces of magnitude similar to those undergone by powders during aerosolisation in DPI formulations, Lord [1993] reported modified conditions of centrifugation. Blends made from different combinations of

powder materials have been used in investigations intended to characterise and differentiate between mixes of unstable or weakly bound, and stable or strongly bound particles. Staniforth *et al.* [1981a] found that using a spin rate of 4000 rev min^{-1} (RPM), a 'break' point existed between relative stable and unstable adhesive mixes. Similarly, Lord and Staniforth [1996] later reported that the 'break' point occurred at a relative centrifugal force of 2000 g using a maximum centrifuge velocity of 4000 RPM.

In the present study, the centrifuge method was used to carry out adhesion force measurements. Powder blends were subjected to spin rates of 1000, 3000 and a maximum of 5000 RPM (3000 g). The extent of drug detachment from drug-lactose blends was investigated under the above centrifugation conditions, using also different drug load concentrations. The results are expressed as percentages of drug removed from the carrier.

3.1.1 Materials and Methods

Centrifugation studies were carried out on the binary powder blends of the drug (Ro 24-5913) and α-lactose monohydrate. The drug load concentrations used were 1, 5, 25 and 50% (w/w), for each of the two crystal forms of the drug. The centrifugation technique used was the same as that described by Lord [1993]. Figure 29 shows a diagram of the centrifuge cell used in the adhesion studies. The centrifuge cell consists of a sample and collection compartments separated by a 45 μm mesh screen. The size of the screen mesh was chosen based on the lactose size range of 45-106 μm . The

purpose of the mesh was to trap the large α-lactose monohydrate particles in the sample compartment of the cell, while allowing the small drug particles to pass to the collection compartment of the cell. In this way, the assay of the drug in the collection compartment is a measure of the amount of drug detached from the carrier.

It is pertinent at this point to discuss the effect of α-lactose monohydrate fines in these experiments. As discussed in Chapter 2, the α-lactose monohydrate carrier used in this study contained a fraction fines, *i.e.*, particles smaller than 45 µm. The presence of fines was an intentional attribute of the carrier, included for purposes of product performance. One consequence of having α-lactose monohydrate fines in the blends is that the amount of drug assayed in the collection compartment of the cell is a composite quantity. The assay of drug in the collection compartment after centrifugation is the combined measurement of drug coming from two sources. One is the drug coming as particles detached from the carrier. The other is the drug still attached to, and carried over by, the α-lactose monohydrate fines that passed into the collection compartment. The amount of carrier fines is exactly the same in all powder blends irrespective of the drug polymorph used; the same α-lactose monohydrate material was mixed with both polymorphs. One cannot overemphasise that the present work is in essence a comparative study of the effects that the choice crystal form of the drug (namely, polymorph A or B) has on a set of otherwise invariant conditions, and the reader is referred to Section 1.7 of this report. Throughout this work, any individual measurement is a necessary means to

an end, namely, a comparison. In the context of the present investigation, a result is the comparison between polymorphs A and B, and an individual measurement can be considered as half the minimum information needed for a comparison. Therefore, given the spin rate and drug load of centrifuge experiments described here, the differences observed in the extent of drug detachment between blends of polymorphs A and B (as measured by the composite drug assay in the cell's collection compartment), are attributable to the choice of polymorph used to present the drug.

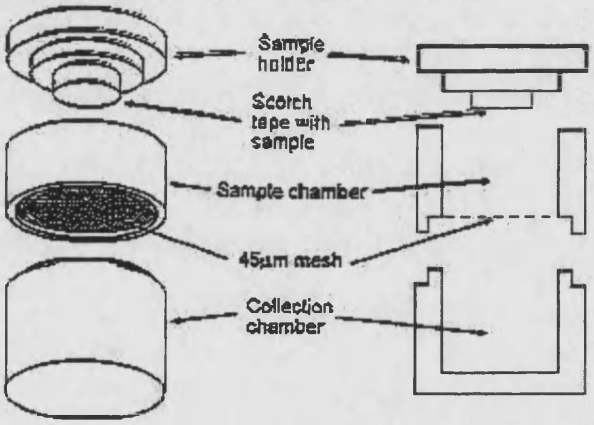

Figure 29. Schematic of the centrifuge cell [Lord 1993].

A double-sided adhesive carbon conductive stub (12 mm) was attached to the sample compartment. An aliquot of powder blend was placed on the carbon stub. The loaded sample compartment was assembled in a centrifuge cell without the mesh screen. The cell was placed on a jolting volumeter (Vankel, Edison, NJ USA) to dislodge the excess of weakly adhered powder,

where two taps were sufficient to remove the excess of powder in a reproducible manner. The screen mesh was then placed in position and the sample was centrifuged at 1000, 3000 or 5000 RPM for 1 minute.

Samples from the donor compartment, the collection compartment and the mesh were analysed by HPLC. The content of drug still adhered to or detached from lactose was analysed by HPLC (as described in Chapter 2), by ultraviolet (UV) or by fluorescence spectrophotometry. UV Absorption spectrophotometry was used to analyse the amount of drug retained on the carrier at the 5, 25, and 50% w/w levels of drug concentration. Fluorescence was used in the case of 1 % w/w drug.

Ultraviolet (UV) and Fluorescence Analyses: Standard curves of each polymorph, A and B, were prepared. A stock solution of 1 µg/ml of the drug was prepared in 100% methanol, aliquots were withdrawn from the stock solution and further diluted in a mixture of methanol: water (50:50). The drug-lactose samples were dissolved in this solvent mixture directly. The standard concentrations used were 0 (blank), 50, 100, 250, 500, 750 ng/ml. A Hewlett Packard photodiode ,array spectrophotometer model 8452A UV/VIS (Hewlett Packard Co., Paramus, NJ) and 1-cm quartz cuvettes were used for the analyses. Each determination was carried out using a wavelength scan, and readings of absorbance at two different wavelengths, 238 and 336 nm, were taken to construct the standard curve. The standard curve obtained was linear for the range of concentration chosen, and the concentrations of the unknown samples all fell within the range of the linearity of the curve. Fluorescence spectrometry was used to measure drug concentrations in cases where the drug content was low, as in the case

of blends with 1 % w/w drug load. A standard curve was prepared using solutions with drug concentrations ranging from 5 ng/ml to 250 ng/ml. The emission intensity of the solutions was measured in a Shimadzu RF-551 spectrofluorometer (Shimadzu Corporation, Kyoto, Japan), using 1 cm. quartz cells and wavelengths of 340 nm and 405 nm for excitation and emission, respectively.

The amounts of drug present after centrifugation in the cell's sample and collection compartments, as well as the mesh were determined by chemical assay as described above. The assay values were then used to account for mass balance. Table 9 summarises the drug mass balance of for drug detachment at different drug concentrations (1, 5, 25 and 50% w/w of drug in α-lactose monohydrate) by centrifugation at 5000 RPM (3000 g) for 1 min. The highest spin rate was chosen for purposes of confirming that mass balance is maintained through these experiments. It should be noted that 5000 RPM was the only spin rate for which detachment was observed at all drug concentrations.

Table 9 Summary of the drug detached from lactose using the centrifuge technique – Data represent the mean and standard deviation (n = 4).

Powder Blend % w/w Drug Polymorph	Percentage of drug content found					
	Removed		Adhered		Mesh	
	Mean	s.d.	Mean	s.d.	Mean	s.d.
1% A	1.91	0.48	98.09	2.56	1.43	0.75
1% B	4.88	1.03	95.12	1.33	3.66	2.36
5% A	14.87	2.69	78.89	3.79	6.24	2.04
5% B	18.40	0.42	77.49	5.56	4.11	1.41
25% A	17.48	0.52	72.78	4.18	9.74	3.24
25% B	21.41	1.29	73.54	2.97	5.05	0.84

The data in Table 9 show that the methodology used for analysis of the centrifuged samples provides quantification of the amount of drug in the different sections of the centrifuge cell used in this study.

3.1.2 Results and Discussion

The forces of separation measured using the centrifuge method can be considered as a measure of the drug-carrier adhesion forces overcome during centrifugation at that particular spin rate. Each spin rate results in a different detachment force applied to the drug-lactose-blend. The spin rate can therefore be viewed as a force probe applied to determine the amount of drug with the corresponding attachment force in the blend.

The force of adhesion between a fine adherent particle and a carrier substrate surface resisting removal by spinning in the centrifuge until it finally detaches, can be calculated from Newton's second law of gravity:

$$F = m\,(a + g) \qquad (28)$$

where F is the force acting on the particle, m is the mass of the particle, a is the centrifugal acceleration and g is the acceleration due to gravity. The centrifugal acceleration (a) can be calculated from:

$$a = \omega^2 l \qquad (29)$$

where ω is the angular velocity and l is the distance between the centre of the particle and the axis of rotation:

$$\omega = \frac{\pi}{30\, S_\omega} \qquad (30)$$

S_ω is the centrifugal speed in rev min^{-1} (RPM).

For $\omega^2 l >> g$, the following approximation applies:

$$F_{det} = m\, \omega^2\, l \qquad (31)$$

where F_{det} is the detachment force from the carrier applied to the drug particle. The force acting on the particle during centrifugation is related to the particle mass, the angular velocity and the distance between the centre of the particle and the axis of rotation. For spherical particles, the detachment force from equation 28 can be rewritten in terms of the material's density and the particle size:

$$F_{det} = \frac{\rho\, \pi\, d^3\, \omega^2\, l}{6} \qquad (32)$$

where d is the diameter of the drug particle and ρ is the particle density.

The relative centrifugal force (R.C.F.) is defined as:

$$R.C.F. = \frac{F_{det}}{F_g} \qquad (33)$$

where $F_g = mg$, and g = 980 cm sec^{-2}

Table 10 gives the relative centrifugal forces applied in this experiment for the different spin rates and the calculated force of separation for the 50-percentile-diameter size of 2.4 and 2.2 μm for polymorph A and B, respectively (equations 25-30).

Table 10 Relative centrifugal force. Centrifuge distance between the centre of the particle and the axis of rotation l = 10.8 cm.

centrifuge spin rate RPM	ω rad·sec^{-1}	$\omega^2 l$ cm·sec^{-2}	R.C.F. g	F_{det} Dynes·particle^{-1}	
0				A	B
0	0.00	0	1.000	0.00	0.00
1000	104.72	118436	120.853	1.08	0.85
3000	314.16	1065922	1087.676	9.72	7.67
5000	523.60	2960895	3021.322	27.00	21.30

In cases where a system is composed of monosize adherent particles, the adhesion and detachment forces are the same but with opposite sign [Krupp, 1967; Zimon, 1982]. Thus, the detachment force of all particles leaving the substrate can be calculated by multiplying particle mass and the R.C.F (equation 33). However, the calculation of the detachment force of the two systems in the present (real situation) study is more complicated because

the particle size is not a single value, but a distribution. Each polymorph of the drug has a particle size distribution that is difficult to define without resorting to assumptions regarding particle geometry. Consequently, particle masses in systems consisting of distributions of irregularly shaped particles are always indirect estimates. For any particle shape, an increase in size is projected as a square power in surface area and a cubic power in its volume, hence its mass. Since the surface area, which provides the particle's "anchor" for attachment onto the carrier, increases more slowly than the mass as the particle size increases, it follows that the coarser particles will be removed with greater ease than the fine adherents at a given detachment force. The estimation of the true adhesive (or detachment) force between drug particles and carrier is not entirely possible because particles' masses are not exactly known, and available methods for particle size measurement assume spherical particle shape, thus giving always underestimates for particle surface area.

The magnitude of the error involved by the assumption of spherical geometry can be assessed by comparing the specific surface area calculated from the particle size distribution and absolute density data, with the specific surface area measured directly by BET isotherm. Figure 17 (Chapter 2) shows the raw particle size distribution for polymorphs A and B of the drug, determined by laser diffraction. The ordinate represents the frequency P (in percent volume), for each particle size, (diameter) D, of the corresponding (assumed) spherical particles. Consider a volume V of the material under investigation, for each particle diameter, D_i, there is a volume $\frac{P_i V}{100}$ occupied by particles of that size. Thus there are

$$n_i = \frac{P_i V}{100 \cdot \frac{4}{3}\pi\left(\frac{D_i}{2}\right)^3} \qquad (34)$$

particles of diameter D_i in a volume element $\frac{P_i V}{100}$. It follows that the particles in each fraction of the sample have a collective surface area of

$$n_i \cdot 4\pi\left(\frac{D_i}{2}\right)^2 \qquad (35)$$

The specific surface area, A_s, is thus given by:

$$A_s = \frac{\sum_i n_i 4\pi\left(\frac{D_i}{2}\right)^2}{\rho V} \qquad (36)$$

where ρ is the absolute density of the material determined by gas pycnometry.

Equation 36 gives estimates of specific surface area of 2.81 $m^2 \cdot g^{-1}$ and 3.11 $m^2 \cdot g^{-1}$, for polymorph A and B, respectively. In contrast, the experimentally determined specific surface areas for polymorph A and B are 8.18 $m^2\ g^{-1}$ and 7.38 $m^2\ g^{-1}$, respectively. The discrepancy in surface area calculated from particle size data and measured by BET isotherm is a clear indication of the complexities that the irregular geometries of powders bring into

their study. There are two major sources of discrepancy between the calculated and measured specific surface areas. The laser diffraction analysis of particle size underestimates surface area by assuming spherical shape. In addition, the yardstick scales between laser diffraction and BET isotherms are totally different. Reliable laser diffraction analysis is applicable at scales approaching 1 μm or greater (nanometer-sized particles are more reliably measured by dynamic light scattering). In contrast, BET measurements are made at the scale of the Helium atom. Consequently, while BET surface area measurements encompass particle shape, rugosity and porosity at the atomic scale, laser diffraction measurements represent spherical particles with smooth surface at the near-micron scale.

It is pertinent at this point to digress on what is meant by a smooth surface in laser diffraction, and the difference between the yardstick scales of laser diffraction and BET pycnometry. The definition of a smooth surface is actually quite objective, and is dependent on the wavelength of the light used for inspection. A surface of optical flat grade is smooth to a scale of $\lambda/20$, where λ is the wavelength of the incident light. The laser diffraction measurements reported here use a beam of red light, placing λ in the order of 800 nm. This means that any irregularities such as bumps, kinks, fissures and the like, with dimensions in the order of 40 nm (the yardstick for diffraction) or less, will have no discernible effect on the diffraction pattern of the particle. However, the 40 nm scale is sufficiently large to fit a few hundred of the Helium atoms used in BET pycnometry. Depending on the scale, particle topology characteristics clearly reflected in BET measurements can be undiscernible in the corresponding light diffraction pattern. The tendency of diffraction

measurements leading to underestimates of surface area is accentuated by the fact the mathematical treatment of diffraction data restricts particle geometry to that of spheres, thus to the minimum surface area.

The surface area of interest to this study corresponds to that available for particle attachment, in all likelihood, this surface area is underestimated by laser diffraction and overestimated by BET.

Figure 17 shows that the particle size distributions for both polymorphs are nonetheless very similar. Suggesting that the error produced by assuming spherical shape is a systematic one, thus allowing meaningful comparisons among data from the two materials. The force of detachment was calculated taken into account the size at 50-percentile for both polymorphs (Table 10). The values obtained for the force of detachment indicated that polymorph B required lower force than polymorph A for the separation from lactose (Figure 30). This means that the percent of form A still adhered to lactose is higher than that of form B for all R.C.F.'s investigated.

Figure 30 also shows that the different types of detachment profiles observed seem to be more a function of drug load than of the crystal form. Polymorph B detaches more easily than polymorph A at all drug loads. However, the patterns of each polymorph at different drug loads have very similar shapes. This is a very significant result, because it indicates that the difference in particle shape between the two polymorphs (Figure 14) is not the determining factor in their attachment to lactose particles. Different drug loads result in different detachment profiles, but for a given drug load, the two polymorphs exhibit similar detachment profiles, and at all drug loads, polymorph B is more easily detached than polymorph A. The differences in

particle geometry between polymorphs A and B are not significant enough to result in different detachment profiles, but polymorphs A and B are differently enough to consistently exhibit different attachment forces.

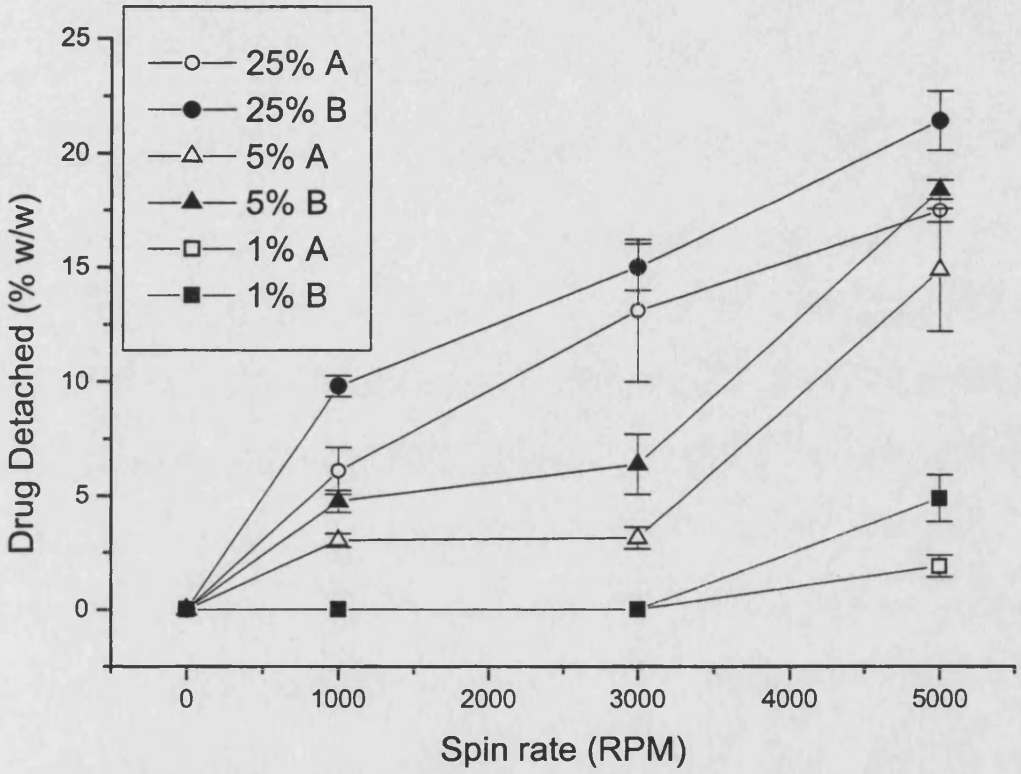

Figure 30. Effect of centrifugation spin rate and drug load concentration on the percent detached from the stub in the donor compartment.

Table 11 presents the percentage of drug detached from the carrier as function of the spin rate for the two polymorphs, at different drug load concentrations. A graphical representation is shown in Figure 30. The figure shows that percentage of drug detached increased with the spin rate applied and with drug load. Detachment of the drug from the carrier was different for the two polymorphic forms. The extent of drug detachment for form B was

Table 11 Percentage of drug Ro 24-5913 detached from the carrier lactose monohydrate as function of the spin rate for the two polymorphs.

Ro 24-5913 load		Spin Rate (RPM) 1000	3000	5000
		Percentage of drug content removed		
1% A	Mean	ND	ND	1.91
	s.d			0.48
1% B	Mean	ND	ND	4.88
	s.d			1.03
5% A	Mean	3.03	3.14	14.87
	s.d	0.30	0.48	2.69
5% B	Mean	4.74	6.37	18.40
	s.d	0.49	1.31	0.42
25% A	Mean	6.08	13.09	17.48
	s.d	1.03	3.11	0.52
25% B	Mean	9.79	15.00	21.41
	s.d	0.46	1.02	1.29

TABLE 12 Analysis of variance for comparing centrifuge results for both polymorphs A and B.

25%	**F-value**	**p**
5000 rpm	103.2852	< 0.01
3000 rpm	22.74579	< 0.01
1000 rpm	43.36239	< 0.001
5%	**F-value**	**p**
5000 rpm	6.715087	< 0.025
3000 rpm	21.36375	< 0.01
1000 rpm	36.17267	< 0.01
1%		
5000 rpm	**F-value**	**p**
	27.70178	< 0.01

greater than for form A at all spin rates and drug concentrations, except at the lowest concentration and spin rates, where detachment for both crystal forms was negligible. One way analysis of variance indicated a significant difference in the detachment profiles for both polymorphs of the drug concentrations in the blend (Table 12).

The detachment profiles in Figure 30 show what could be called a 'break' point (Staniforth [1981]) at 3000 RPM. This is observed here for the low drug loads of 1% and 5%. The data suggest that there is no weakly bound drug at 1% drug load for either form A or B. At 5% drug load, a low spin rate of 1000 RPM removed a portion of the drug, but the remaining portion could not be detached at 3000 RPM. These results, combined with the absence of a break point at 25% drug load, suggest that if sufficient attachment sites are available on the surface of the lactose particles (*i.e.*, a sufficiently large carrier surface area available per drug particle), the drug-lactose interaction is considerably stronger than when the attachment sites on the carrier become scarce. This in turn suggests that adhesion forces are measurably stronger than cohesion forces for Ro 24-5913.

Adhesion and cohesion are both present at all drug load concentrations, and one would expect cohesion to become more significant the higher the drug load, while adhesion playing a major role at lower drug concentrations. The presence of a break point in Figure 30 supports this notion, especially because the detachment profiles are flat before the break. A perfectly flat detachment profile before the break point would be highly indicative of adhesion as the primary source of particle interaction. The only requirement for such a profile is a drug-carrier interaction strong enough as to require a threshold force to be

overcome. Conversely, in the case of cohesion, a break point threshold following a flat detachment profile could only be explained by an extremely uniform particle size or agglomerate size of the drug, which is not the case.

The detachment profile at 5% drug load is particularly illustrative, because it combines the attributes of the profiles obtained at 1% and 25% drug load. The profile at 5% drug load is clearly a composite one, showing the detachment of drug from the lactose surface above 3000 RPM as well as from drug agglomerates at 1000 RPM.

Spin rates in the range of 1000 to 3000 RPM have been used in the past in the study of DPI's [Lord 1993]. These spin rates were insufficient for complete separation in the present situation, since there was a further increase in drug detachment at a spin speed of 5000 RPM. Travers [1975] reported that at low spin rates, the removal force is not enough to cause detachment, and particles will only rearrange to stronger adhesion sites. This explanation, however, is not consistent with the higher detachment values found here for form B over form A because the profiles for both forms are almost parallel in the presence and absence of the break. Travers [1975] explanation is consistent with a set of detachment profiles that includes both obtained here for 1% and 25% drug load, but precludes the patterns obtained for 5% load. At 5% drug load, Figure 30 shows detachment at the lowest (1000 RPM) spin rate applied, followed by no additional detachment at the intermediate (3000 RPM) spin rate. Lord and Staniforth [1996] have indicated that a relative centrifugal force of 2000 g corresponds to the low removal forces of magnitude similar to that drug-carrier agglomerates in DPI devices are likely to

experience during aerosolisation. The 'break' point in this study occurs at about half that limit, placing it well within the range of low removal forces.

The results obtained indicate that there is a consistent difference between polymorphs A and B in terms of their interaction with lactose. And this difference is more the result of different physicochemical properties than of different geometries of the two crystal forms.

The adhesion ability of a particle is predominantly a surface property, whereas the counteracting detachment force is determined by the particle mass. Detachment of adhered particles by the centrifuge method consists in breaking the balance between the force of particle attachment and the separation force imposed by the spin rate, *i.e.*, the balance between a surface and a bulk property. The nature of particle interactions makes the nature of the surfaces of the interacting materials a determining factor in their behaviour. Kulvanich and Stewart [1987c] made surface modifications to the materials of their study and found that the physicochemical properties of the surfaces brought into contact are the primary factors determining the degree of the interactions produced. The particle interaction system chosen for the present study was used without any modifications to the materials' surfaces. This situation represents the true case of the clinical development programme in a pharmaceutical setting. However, crystal polymorphism is a very common pharmaceutical occurrence, and the inclusion of two polymorphs in this study corresponds precisely to introducing two very well controlled surface modifications of Ro 24-5913.

Polymorph B, which consistently shows greater detachment than polymorph A, has also higher absolute density. It follows that for a given

particle diameter, form B particles will be subjected to a greater detachment force than particles of form A, when subjected to the same spin rate. If the particle size distributions for the two polymorphs were identical, detachment forces on polymorph B should be consistently greater than those acting on the particles of polymorph A, by a factor of 1.29/1.26, the ratio of their absolute densities. This factor, however, corresponds to an excess detachment force on polymorph B of about 2.5%, too small to be measurable considering the experimental variation (Table 9).

If we take this analysis a bit further and consider the particle size distribution of the two polymorphs (Figure 17), it is evident that although very similar, the two distributions are not identical. Figure 31 provides an alternative presentation of the particle size distributions shown in Figure 17. The alternative presentation helps establishing whether the greater detachment observed for polymorph B is simply the result of denser particles than those of polymorph A of the same size. Figure 31 corresponds to the cumulative frequency of the distributions shown in Figure 17. The volume percent of Figure 17, however, is expressed in its numerical mass equivalent in Figure 31. Presented this way, the 100% percent volume allows the graphical representation of the different absolute densities of the two crystal forms. The figure is also cumulative in a reverse fashion: the frequency summation is done starting with the largest particle size and the smallest at the end. The reverse integration was done in order to facilitate data presentation for this discussion.

The application of an increasing centrifugal acceleration can be visualised as a threshold detachment force that sweeps from left to right in Figure 31. For either polymorph, the largest (having higher mass) particles will

detach first, with increasing detachment forces being needed in order to detach the finer particles. The vertical line in Figure 31 corresponds to the 45 µm cut off diameter imposed by the mesh used in the centrifuge cell. Only particles smaller than 45 µm can pass to the receiver chamber of the cell. The 45 µm line is therefore the starting point for detachment.

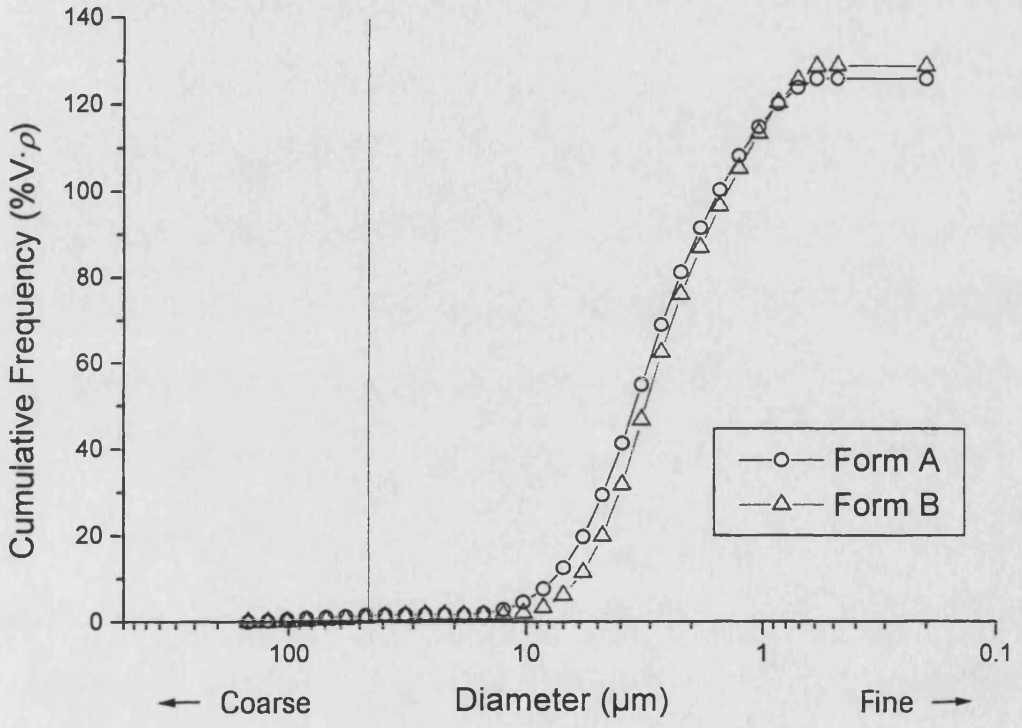

Figure 31 Particle size distribution of polymorphs A and B. The cumulative frequency is expressed in its mass equivalent.

Figure 31 clearly shows that even though polymorph B has the higher density, polymorph A has slightly more of the larger particles. Figure 31 also shows that the effect of the higher density of form B resulting in stronger detachment forces would not be observable for particles larger than ~0.86 µm,

the point where the two profiles cross. The mass distribution among the particles of the two polymorphs thus favours greater detachment of polymorph A, contrary to the obtained results.

Microscopic analysis was conducted after centrifugation of the powder in order to observe the lodging position of the particles on the mesh. In addition, SEM analysis was performed on the particles still adhered to the carbon conductive stub.

The foregoing discussion indicates that neither the differences in particle geometry between the two polymorphs, nor their difference in density or particle size distributions, can account for the differences observed in their detachment behaviour. Polymorph A is better retained in the sample chamber of the centrifuge cell than polymorph B. Whether this is solely due to a stronger interaction with lactose (adhesion), or also to an ability on the part of polymorph A to form stronger aggregates (cohesion), which must also be larger than 45 μm, cannot be conclusively established from the present analysis. In either case, however, the explanation must reside on a difference between the intrinsic properties of interaction of the two polymorphs.

3.2 Electrostatic charge measurements of drug-carrier dry powder mixtures.

Several investigators [Staniforth and Rees, 1982a; Ahmed, 1989; Hughes, 1989, Ahmed *et al.,* 1992; Lord 1993; Peart, 1996] have used different modifications of experimental methods designed to measure electrostatic charges in powders. Electrostatic forces in DPI formulations can be expected to play part in the attraction between drug and carrier particles, considering the mass to charge ratios obtained for respirable sized particles [Staniforth, 1994]. Electrostatic measurements on powders can be classified into two types, depending on the experimental setting: static or dynamic. Both types of experimental methods provide information on the charges generated upon powder movement. The static method is considered useful for information during mixing, pouring and filling, whereas the dynamic method gives useful information during fluidisation or aerosolisation of powders.

The static method for evaluating the electrostatic characteristics of dry DPI formulations is the shallow Faraday well static charge detector (SFC). The dynamic methods are variations of the Faraday cage dynamic charge detectors, these are the air stream (ASFC) and the capacitor interchangeable mesh (CIMFC).

The shallow Faraday well has been used to measure the electrostatic charge induced on powders poured from containers made of different materials [Staniforth and Rees 1982a], and the effect of these charges on the content uniformity of a binary powder system [Ahmed *et al.*, 1992].

Kulvanich and Stewart [1987a] adopted the "blow-off" approach used in xerography [Donald and Watson, 1970; Schein and Cranch, 1975] for the measurements of electrostatic charges in pharmaceutical systems under dynamic conditions. In this type of experiments, the detector registers the electrostatic charges generated as the result of movement of the particles in an air stream.

Peart [1996] modified the dynamic cage charge system of Hughes [1989] for use for the first time in dynamic measurements for pharmaceutical aerosols. The method consisted of an inner cage cylinder with mesh on both ends. The net charge was measured for α-lactose monohydrate and lactose-salbutamol systems. Peart [1996] found that the electrostatic interactions influenced the *in-vitro* characteristics of dry powder formulations for inhalation.

The aerosolisation of powder formulations produced upon the actuation of DPI devices produces electrostatic charges. The electrical fields produced by the aerosol clouds of formulation-device systems have been measured using two different apparatuses: the electrostatic fieldmeter (EFM) and the transient charge monitor (TCM). These two apparatuses, which monitor the bipolar charging characteristics of aerosols, have been used and described in detail by Peart [1996].

The TCM method was specifically designed to detect bipolar charging characteristics of pharmaceutical powder aerosols [Balachandran *et al.*, 1991]. Drug detachment produced upon actuation of DPI devices can result in the development of both positive and negative charges on the same particle [Balachandran *et al.*, 1991]. Such bipolarity can, in turn, have effects on the overall performance of powder systems, especially if aggregation of

charged particles occurs. Particle aggregation presents the risk of the drug not being able to reach the parts of the airways targeted for pulmonary drug delivery.

The development of pharmaceutical powder formulations for inhalation requires the well controlled mixing of powder materials for complete homogeneity. Well controlled mixing is particularly critical, considering that small drug particles are mixed with larger particles of the carrier. The challenges involved in achieving the homogeneous mixing of powder materials with particle size distributions separated by more than one order of magnitude, cannot be overestimated in the development of DPI formulations.

Table 13 shows the different experimental techniques that have been used by various investigators to characterise electrostatic interactions in dry powder mixes. The present study investigates the contribution of electrostatic charges to the interparticulate forces between the micronised drug, Ro 24-5913, in its two polymorphic forms, and α-lactose monohydrate. The electrostatic characterisation was carried out on the pure components as well as on powder blends. The static method was used for the characterisation of pure materials, whereas two different dynamic methods were used for the characterisation of powder blends.

Table 13 Apparatuses used for the electrostatic characterisation of poured and fluidised powders, and aerosolised powders from DPI.

Apparatus	Investigators
1). "Static" Method: Faraday Wells for poured powders	
• Shallow well	Staniforth and Rees, 1982a Ahmed, 1989; Ahmed *et al.*, 1993
• Deep well	Lord, 1993; Staniforth, 1994
2). "Dynamic" Method: Faraday Cages for fluidised powders	
• Air stream (ASFC)	Kulvanich and Stewart, 1987a; Peart 1996.
• Capacitor Interchangeable Mesh (CIM).	Hughes, 1989; Peart, 1996
3). "Dynamic" Method for powder aerosol generated from a DPI	
• Electrostatic fieldmeter (EFM)	Peart, 1996
• Transient Charge Monitor (TCM)	Peart, 1996; Machowski, 1996

3.2.1 Materials and experimental conditions.

Micronised drug Ro 24-5913, polymorphs A and B and coarse carrier α-lactose monohydrate were subjected to electrostatic characterisation as pure components and as drug-carrier powder binary blends (described in Chapter 2). Experiments were conducted under controlled conditions of temperature (T) and relative humidity (RH). Temperature of the room varied between 20°C and 22°C and the relative humidity between 24% to 30% (Honeywell T and RH room controller; RH was also continuously monitored with a hygrometer), unless otherwise stated. Six replicate determinations were carried out for each powder sample.

3.2.1.1 Electrostatic properties from poured and fluidised powders: Measurement of Electrostatic Forces

Among the different apparatuses used in the present study for the measurement of electrostatic charges, the SFC, ASFC and CIMFC are all essentially capacitors, in which two plates of a conductor material are separated from one another by a dielectric. In this study, the conducting material in the apparatus is brass and the dielectric materials used were PTFE (with the SFC and CIMFC) and PVC (with the ASFC). For all three capacitor devices, the inner container was connected by a shielded co-axial cable to an electrometer (Type 610C, Keithley Instruments, Cleveland, OH, USA) where charge measurements were performed. When a charged material is introduced into the apparatus' well, an equal and opposite charge is induced on the inner walls of the well. The induced charge is then measured by the electrometer.

The charge measured by the electrometer is based on the following equation:

$$\left[C = \frac{Q}{V_E}\right] \qquad (37)$$

where C is the capacitance, Q is the charge and V_E is the applied voltage.

The electrostatic charge measurements of powders from the different Faraday wells were used to obtain the average charge-to-mass ratio generated on the drug particles detached from the carrier. The following equation was used for this determination:

$$\left[Q_{sp} = \frac{Q}{m}\right] \qquad (38)$$

where the mean specific charge, Q_{sp}, is obtained from the charge magnitude, Q, and the mass, m, of the powder. The specific charge was determined for SFC and ASFC. For the CIMFC, the total charge was measured rather than the specific charge, after Peart [1996].

Static Method: Shallow Faraday well charge detector (SFC). These studies were conducted by making the powders flow off chutes made from different materials. The chutes used were made of stainless steel, brass and perspex (polymethyl-methacrylate). A powder sample of approximately 0.5 g was placed on the chute. Flow of the powder was effected by vibration of the chute. The chute's vibrating frequency was adjusted such that a powder flow rate of 0.2 g sec^{-1} off the chute was attained. The flowing powder was poured into the brass Faraday well (Figure 32). At least five determinations were made for each powder and charge reported as mean specific charge (equation 38). After each determination, the chute surface was cleaned thoroughly in order to avoid surface contamination that could affect the subsequent measurements. Proper cleaning in electrostatic measurements is particularly critical because trace contamination can result in totally misleading measurements.

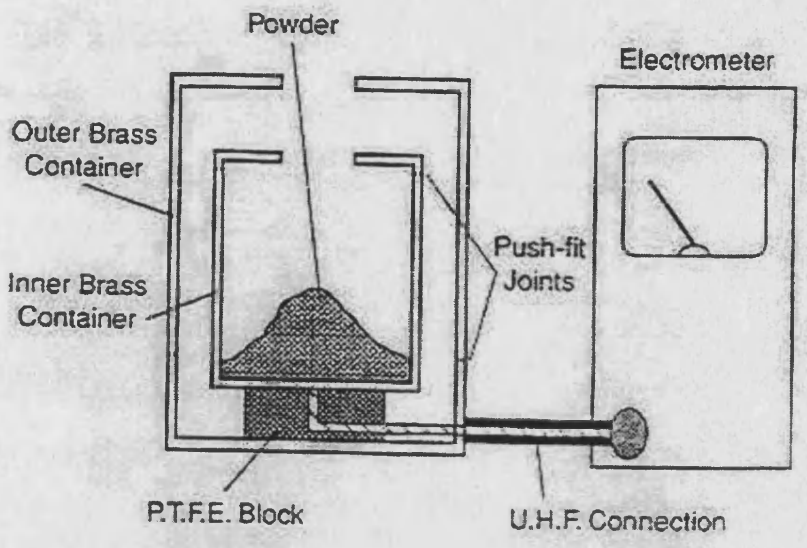

Figure 32 Diagram of the Faraday cage static charge detector (after Staniforth, 1994).

Dynamic Methods: ASFC and CIMFC are dynamic methods that involve fluidisation of the powders inside the electrostatic cage; these methods measure the electrostatic charges generated as the result of the movement of particles in an air stream [Kulvanich and Stewart, 1987a; Staniforth, 1994*]*.

Air stream Faraday Cage (ASFC). The apparatus used in the present work was similar to that used by Peart [1996], which was in turn an adaptation of the apparatus described by Kulvanich and Stewart [1987a]. In the configuration used here, the Faraday cage consists of an open brass cylinder equipped with a 45 µm mesh screen placed over each end. A mesh of this size allows the drug particles, which are smaller than 10 µm, to

leave the cage, whereas α-lactose monohydrate particles (45 – 106 μm) remain within the cage. The screens are mounted on PVC o-rings, which insulate the cylinder from the mesh (Figure 33). Compressed air was taken from an air line supply filtered through of 0.2 μm (PTFE Acro 50, Gelman) membrane. The in-line filter was placed in order to prevent potential particulate impurities present in the air from entering the cage. The airflow rate was adjusted to 60 l min^{-1} after the filter with a float-type flow meter (Gilmont No. 15, Reichert-Jung). The air flow meter was calibrated with a high-bubble generator flow calibrator for the airflow range from 2 to 80 l min^{-1} (The Gilbrator, Gilian Instruments Corporation, USA).

Peart [1996] studied the effect of sample size and airflow rate on the electrostatic charges developed upon detachment, and found no significant difference when using different sample size. However, a flow rate of 60 l min^{-1} gave a maximal removal for drug adhered.

The sample size used in the present study was 0.5 g and the airflow rate used was 60 l min^{-1}. Validation of the 45 μm mesh was carried out by allowing air alone to go through the mesh, this resulted in no spurious charge generation. The charges generated were thus due only to the aerosolization of the powder sample. Charge measurements were performed by placing an accurately weighed amount of sample powder mixture in the apparatus' mesh. The sample was placed on the lower mesh of the ASFC and fluidised for 30 seconds. Under fluidisation, some powder left the cage, and the powder remaining on the mesh inside the chamber was weighed. The specific charge was calculated using equation 38.

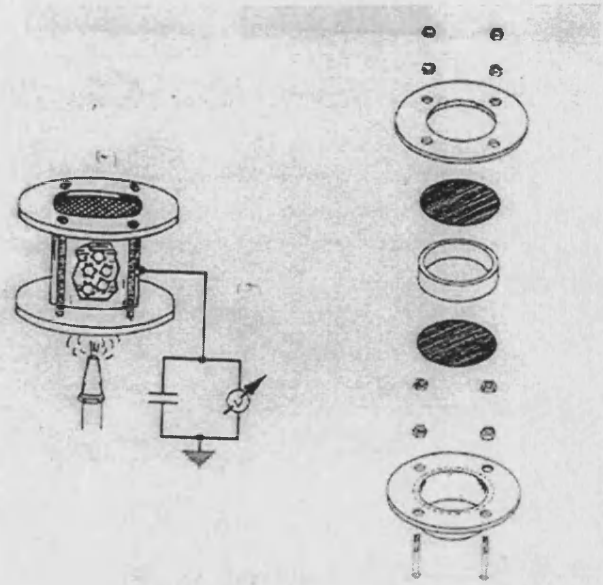

Figure 33 Air Stream Faraday Cage (ASFC) for measuring electrostatic charge of powders by "blow-off" from the bottom [After Kulvanich , 1986].

Capacitor Interchangeable Mesh (CIMFC). The arrangement of this cage is horizontal, giving a greater opportunity for particle-cage wall collisions. Peart [1996] used a modified version of the apparatus described by Hughes [1989] for testing binary, ternary and quaternary powder systems.

The CIMFC consists of an inner brass well with interchangeable end caps of different mesh sizes. In this experiment, mesh screens of 45 μm in both ends were used for the same reason given above, namely, to entrap the coarse α-lactose monohydrate particles while allowing the carrier fines and drug particles leave the cage. Figure 34 shows a photograph of the CIMFC

set up. The inner container is enclosed by the larger, grounded brass container (or outer well). PTFE was used to insulate the inner from the outer wells. A powder sample of 0.5 g was placed in the inner well. Two air jets were then applied, one at each end of the cage, in order to simultaneously blow the powder from both ends of the inner well. The compressed air was directed in such a manner as to provide a total airflow of 60 l min^{-1}. These settings produced optimal aerosolisation and particle removal from the well. The inner well was connected to an electrometer, which registered the resulting net charge.

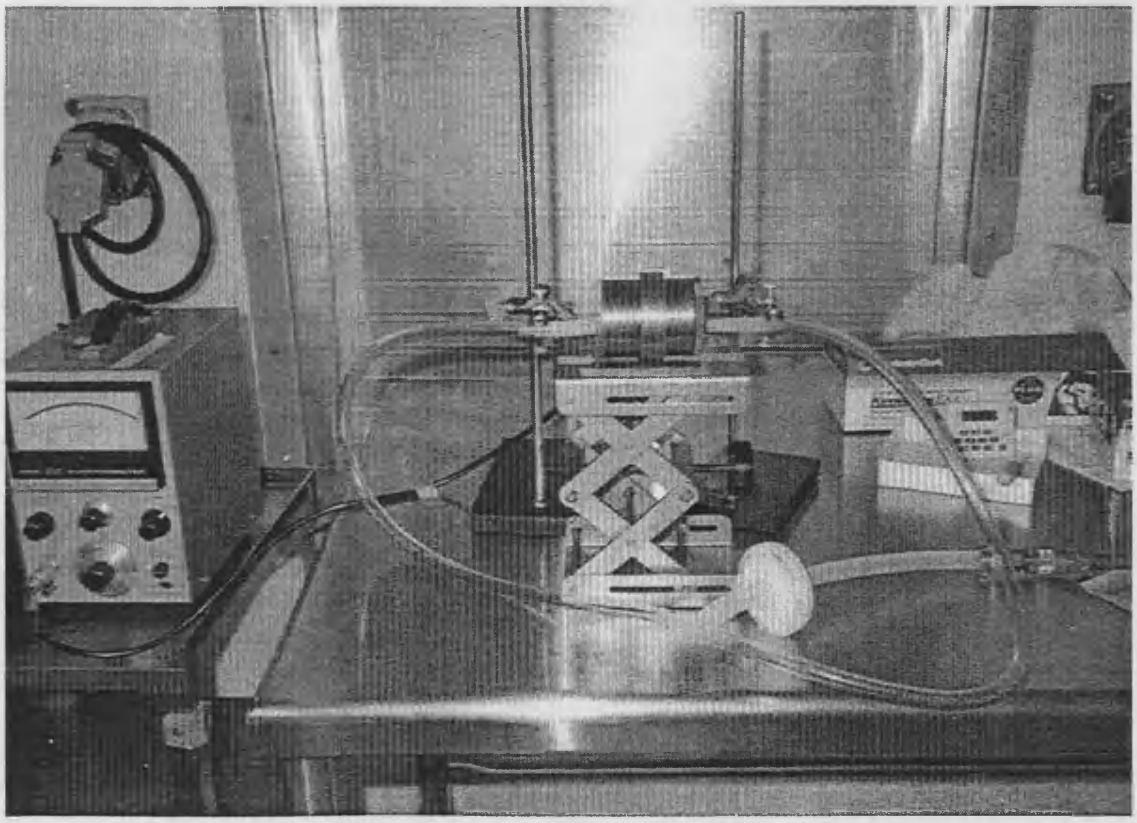

Figure 34 Photograph of the CIMFC system used for measuring charges during fluidisation.

3.2.1.2 Electrostatic properties of aerosol generated from DPI devices containing drug-lactose monohydrate powder mixtures.

The direct dosing dry powders by means of inhalation devices involves problems of powder fluidisation, flow, and dispersion [Fuchs, 1964]. During powder aerosolisation within the DPI device, the movement of particles and their collisions with the device surfaces result in the development of electrostatic charges. Such electrostatic charges affect, in turn, inter-particle interactions.

In this study, the electrostatic properties of aerosol clouds generated upon actuation of a DPI device have been characterised using the electrostatic fieldmeter (EFM) and the transient charge monitor (TCM).

Transient Charge Monitor (TCM). The TCM [Machowski, 1996] is an instrument designed to detect both positive and negative charges on powders. This is done through a number of electrodes configured in series, meant to "mimic" the airways of the respiratory tract [Machowski, 1996]. In the present study, TCM was used to explore the charging phenomena of the two polymorph powder systems aerosolised from two different DPI devices. The DPI devices selected for the delivery of the polymorph powder systems were the Rotahaler™ (Glaxo) and the Dryhaler™ (Dura Pharmaceuticals). The Rotahaler was chosen for its simplicity and availability. The Dryhaler was chosen for its purported de-aggregation efficiency [Hill, 1994].

The Rotahaler requires the powder to be filled into capsules, the filled capsules are lodged into the device prior to actuation. Hard gelatine

capsules, size 3, were filled with 25 mg ± 0.625 mg of the 1, 5 and 25% w/w drug blend, and stored for a week under room ambient conditions in order to allow equilibration of electrostatic charges. For each run, the air supply was operated until a steady background signal was attained, the Rotahaler was then actuated, opening the capsule. Ten empty capsules were first discharged from the inhaler into the TCM in order to detect any possible signal coming from the capsule opening step. Subsequently, ten filled capsules of each blend were discharged from the device.

For the Dryhaler, the powder was filled directly into the device. Samples of 10 – 15 mg of each the blends containing 1, 5 and 25% w/w drug of each polymorph were filled into the device, followed by dispersion of the powders by the device into the TCM.

Experiments were conducted in an environment of temperature of 20 to 25°C and relative humidity ranging from 55 to 60 %. Compressed air was generated from the exhaust outlet of a vacuum pump adjusted to a flow rate of 60 l min^{-1} (Model 1423, Gast Manufacturing Inc., Michigan, USA). A vacuum cleaner (Vax 2000, Droitwich, U.K.) was used as the air supply for aerosolisation of the inhalation powder. When the powder is discharged from the device, a charged aerosol cloud of particles is formed producing an electrical signal as it travels along the TCM tube. The electric signal detected by the electrodes was simultaneously captured and stored on a P.C. in Excel™ (Microsoft) spreadsheet format. The experiments were conducted in triplicate for each powder blend.

3.2.2 Results and Discussion

3.2.2.1 Electrostatic properties from poured and fluidised powders

The triboelectrical charges developed by the pure powder components following flow over chutes made of different materials is attributed to the samples' crystal and chemical properties [Inculet in Moore, 1973]. The tendency of a molecule to develop a partial charge is determined by its functional groups' electronegativity. And the ability of that molecule's crystal to develop a surface charge is determined by the type of functional groups exposed on the crystal surface. A number of functional groups have been ranked in a donor-acceptor series (Derjaguin, *et al.*, 1978, see Chapter 1).

Table 14 shows the mean specific electrostatic charge determined by the static (SFC) method for the two polymorphs, and α-lactose monohydrate particles following flow over the stainless steel, brass and perspex chutes. The tabulated results show that the two drug polymorphs and α-lactose monohydrate all developed negative charges following flow-off from chutes of all three materials tested. Lactose monohydrate being a sugar is very rich in one functional group: hydroxyl, the location of the single ether group in the lactose molecule makes it virtually inaccessible for surface to surface contact with other materials at the macroscopic level. The abundance of oxygen atoms throughout the lactose molecule provides a highly electronegative surface for this material, at any scale. The molecular structure of Ro 24-5913

(Figure 5, Chapter 1) possesses carboxyl and amide functional groups that could also make the drug behave as an electron acceptor.

Since the two polymorphs have the same chemical structure, they will have exactly the same molecular electronegativity. Whether the two different molecular arrangements in the crystal translate into a difference in their macroscopic electrostatic properties, will depend on how effectively the same set of electronegative groups in one molecular ensemble *versus* another, can distribute a change within the ensemble. The electrostatic properties of the two crystal forms will also be greatly influenced by whether the electronegative groups of the molecule are exposed or inaccessible on one type of surface *versus* the other. Table 14 shows that the two polymorphs develop very similar charges. This result suggests that the two crystal modifications have surfaces with similar average, *i.e.*, macroscopic, electronegativities. The fact that drug and carrier, *i.e.*, the two individual components of the DPI blend formulation, both develop negative charges, suggests that the drug-lactose attraction will include a weakening element of repulsion to allow subsequent detachment in the blend. The larger the difference in magnitude of electropositive and electronegative charges of two powders, the greater the attraction [Ahmed, 1991]. In addition, the polarisability of the drug molecule, whose signs were observed in the Raman spectra of drug-lactose monohydrate blends, can promote particle attraction by facilitating the redistribution of charges on a particle.

The large surface area of the two micronised polymorphs compared with that of α-lactose monohydrate offers greater opportunity for particles to develop charges. The charge values registered following flow on the metal

surfaces were about ten-fold greater for the micronised drug than for the α-lactose monohydrate powder. This ratio is of the same order of magnitude as the ratio of specific surface areas. However, the charge values after moving through the perspex chute was only slightly higher for the micronised drug than for α-lactose monohydrate. This result is quite possibly explained by the fact that perspex is itself a material rich in electronegative (ester) groups; tribocharging by means of the interaction two electronegative materials is hindered by the inability of one of the materials to develop a stable positive charge.

Static measurements of the pure materials following flow on a chute are useful to determine the type and magnitude of charge the different materials are likely to develop. But the technique is somewhat limited in terms of its ability to highlight differences between polymoprhs A and B, since the magnitude and polarity determined for the two polymorphs was similar.

Table 14 Mean specific charge for drug Ro 24-5913 and carrier α-lactose monohydrate powders following contact with metal and PMMA surfaces (n=5). Static method (SFC)

Material	Polymorph	Perspex (PMMA)		Stainless Steel		Brass	
		Polarity	Mean Specific Charge $C \times 10^9 g^{-1} \pm SD$	Polarity	Mean Specific Charge $C \times 10^9 g^{-1} \pm SD$	Polarity	Mean Specific Charge $C \times 10^9 g^{-1} \pm SD$
α-Lactose monohydrate (45-106 μm)		-	2.721 (0.179)	-	0.343 (0.101)	-	0.627 (0.048)
Ro 24-5913 (micronised)	A	-	3.860 (0.112)	-	4.020 (0.320)	-	6.447 (0.318)
	B	-	3.676 (0.139)	-	4.141 (0.278)	-	6.676 (0.235)

For the dynamic methods, Figures 35 and 36 show the electrostatic profiles obtained for each polymorph with the ASFC and CIMFC apparatuses, respectively. In each case, there is a significant difference between the two polymorphs. It is also apparent that the charge profiles obtained with these two dynamic methods are qualitatively very similar but with reversed polarity, even though the magnitude of charges evolved in the two apparatus are quite different. One immediately apparent difference between the two polymorphs is that in both the ASFC and CIMFC methods, blends containing polymorph A exhibit a change in polarity when the drug load is increased from 1% to 5%. Such a change of polarity does not occur in the case of polymorph B. Peart [1996] reported the bipolar behaviour of powder blends during investigations with the CIMFC and ASFC apparatuses. The reversal in charge polarity observed for polymorph A with the two apparatuses, indicates the bipolar behaviour of the selected powder blends.

The dielectric nature of organic materials allows the displacement of charges within them without flow (*i.e.*, conduction) of charge. Organic materials are bipolar because the development of a net absolute charge would require them to be conductors, and this in turn, would produce extreme repulsion among the particles. Consequently, charge measurements on powder blends correspond to the imbalance between the positive and negative charges within the sample, *i.e.*, the algebraic sum of the charges. Faraday cages produce a net charge by the friction of particles colliding in a confined space. Therefore, the cage's geometry as well as the disposition of the powder within will affect the net charge that develops.

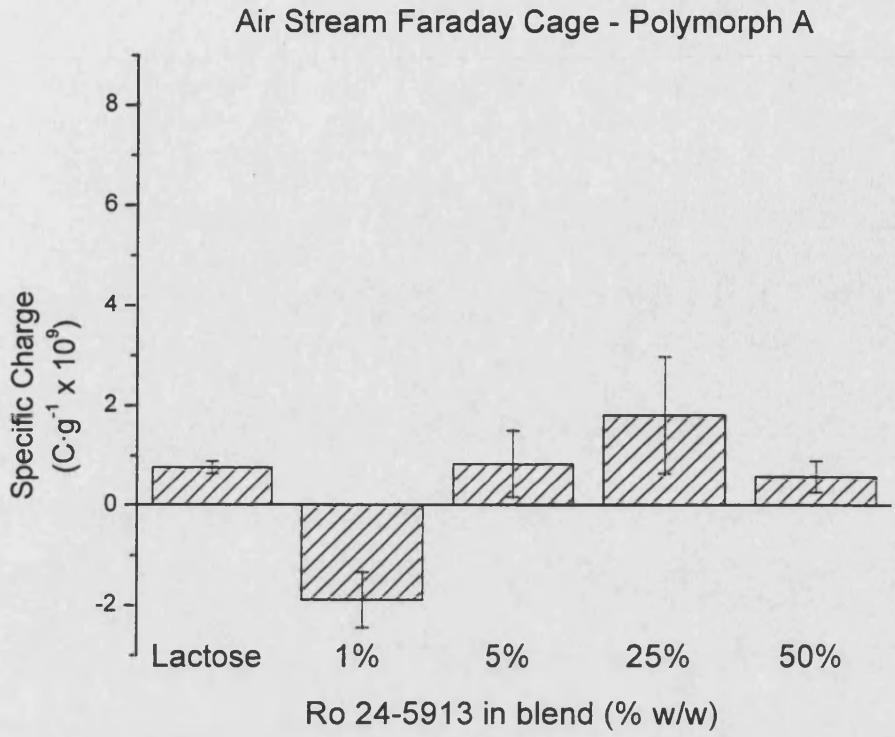

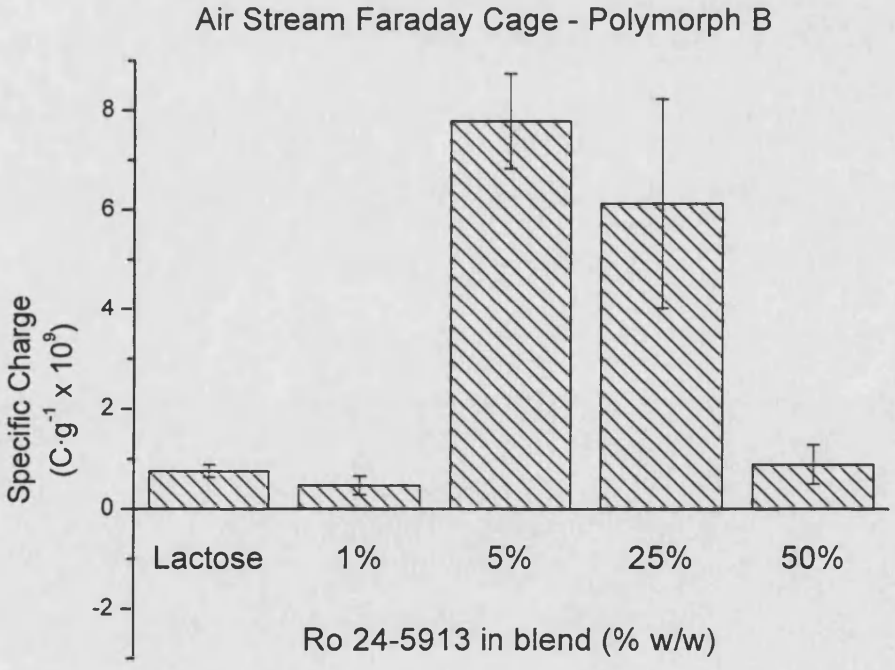

Figure 35 Effect of drug load on the electrostatic charge developed upon detachment of micronised Ro 24-5913 from coarse α-lactose monohydrate at 60 l min^{-1} (n= 6).

Kulvanich and Stewart [1987a] proposed several possible mechanisms by which spurious charges associated with the environment surrounding the apparatus for electrostatic measurements. Factors such as charge accumulation in the compressed air or charge accumulation through carrier interactions have been proposed. For purposes of the present discussion, the difference in the electrostatic behaviour between the two crystal polymorphs within the same apparatus is far more significant than the difference observed from one apparatus to another. One difference worth mentioning between the CIMFC and ASFC apparatuses is that of sample mass integrity. The geometry and sample disposition in the CIMFC make it very difficult for drug particles to leave the cage, whereas the monodirectional air flow in the ASFC favours the expulsion of micronised drug particles through the 45-μm mesh. This difference may be partially responsible for the net charge reversal observed between the two devices. Schein and Cranch [1975] reported that the electrostatic charge produced upon drug detachment from the carrier substrate could be modified during the charge measurement within the "blow-off" cage.

Independently of the polarity of the charge that develops, the increase in net charge in a dynamic measurement is an indication of drug detachment. Figures 35 and 36 show that with both the ASFC and CIMFC methods, polymorph B tends to produce greater charges than polymorph A. This result is consistent with the higher detachment of polymorph B observed in the centrifugation studies reported in Section 3.1.

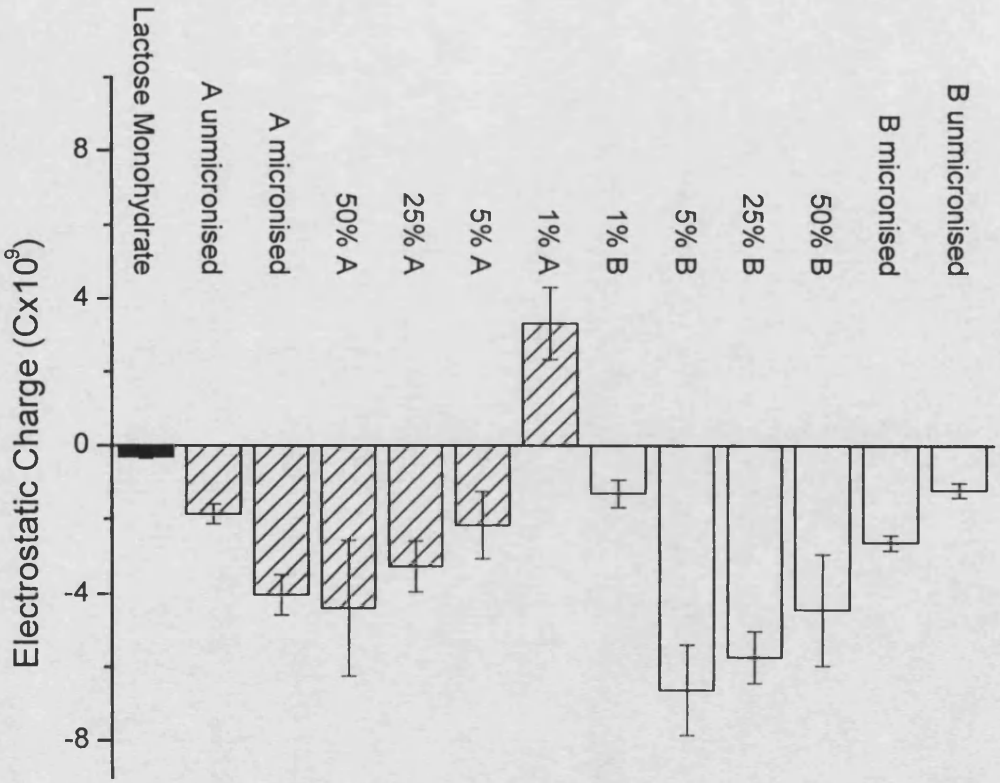

Figure 36 Graphic representation of the electrostatic measurements by capacitor interchangeable mesh (CIMFC). Mesh used 45-µm (n=7)

Centrifugation studies showed that for both polymorphs, drug detachment increased with drug load. Those studies also showed that for the two polymorphs, the extent of detachment is negligible at the 1% drug load level. Therefore, the polarities observed at the 1% drug load using the ASFC and CIMFC methods, most likely reflect the adhesion of drug particles that become very much immobilised upon attachment.

The electrostatic properties of powder blends containing 1% drug show a dramatic difference between polymorphs A and B. However, it is worth pointing out that when the two polymorphs are studied individually, *i.e.*, under non-interactive conditions, the two crystal forms exhibit virtually identical electrostatic behaviour under static conditions (SFC, Table 14), and not very different behaviour under dynamic conditions (CIMFC, Figure 36).

Figures 35 and 36 reveal other differences in electrostatic behaviour between blends containing polymorphs A and B. For drug concentrations of greater than 1%, blends of polymorph B tend toward electroneutrality with increasing drug concentration, whereas the opposite trend is observed for polymorph A. A possible explanation for these differences can be given terms of the rearrangement of drug particles. Drug loads of 5% or higher are likely to give place to powder blends in which drug particles have an ability to move not encountered at 1% drug load. The SEM analysis presented in Chapter 2 showed that a drug concentration of 5% is of the order of the amount needed, at least compared to the 1% or 25% concentrations, to attain full ('monolayer') coverage of the α-lactose monohydrate particles. Drug loads in the order of 25% or more correspond to more than monolayer

coverage. The higher the drug load, the higher the drug detachment for either polymorph, and consequently, the higher the frequency of inter-particle collisions during dynamic measurements. In the case of polymorph B, the downward trend in charge with increasing concentration is suggestive of inter-particle collisions producing a cohesive rearrangement of drug particles that leads toward electroneutrality. Cohesion rearrangement will be minimal at low drug concentrations because the very low detachment levels will prevent a high frequency of drug particle collisions. Higher drug concentrations, which produce higher drug detachment, will be accompanied by an increase in drug-drug particle collisions. Higher frequency of drug-drug particle collisions will have a very pronounced effect on charge when drug cohesion is a major factor. It appears that in the case of polymorph B, the higher detachment accompanying higher drug concentrations is somewhat offset by cohesion rearrangement, thus resulting in lower charges as the drug concentration is increased.

Polymorph A exhibits a trend that is the opposite of that of polymorph B. The charges generated with powder blends of polymorph A increase with drug concentration. In this case, the corresponding increase in drug detachment and the concomitant increase in inter-particle collision frequency result in a system with increased electrostatic imbalance. These results could be explained by a system in which adhesion plays an important role in particle rearrangement, thus disfavouring efficient charge neutralisation. However, it should be pointed out that for both the ASFC and the CIMF methods, the charge produced by polymorph B is higher than the charge produced by polymorph A at the same drug load, for all drug concentrations

investigated. It is therefore possible that upon detachment, the particles of polymorph A undergo rearrangement that involves both adhesion and cohesion interactions.

Table 15 Analysis of variance for ASFC. Two polymorphs

Polymorph system	F-value	p
1%	58.508	< 0.001
5%	273.129	< 0.001
25%	158.888	< 0.001
50%	3.118	< 0.12

Tables 15 and 16 show the statistical comparison between the two polymorphs for the ASFC and CIMFC results, respectively. In both systems the two polymorphs exhibited significantly different charges ($p<0.001$). This was true at all drug concentrations investigated, with the exception, with both apparatuses, of the 50% drug load. It seems that when the α-lactose monohydrate carrier is overloaded with drug particles, as in the case of 50% drug load, the drug particles begin to act as a screen, masking the carrier particles. Under these circumstances, the differences in charge produced by the powders begin to reflect a combination of the differences between the pure polymorphs and the binary blends.

Table 16 shows that significant differences were observed between samples ($p<0.001$), pure components and blends at all concentrations except 50%.

Table 16 Analysis of variance for CIMFC. Two polymorphs

Pure components	F-value	p
Unmicronised	25.943	< 0.001
Micronised	40.103	< 0.001
Blends (drug with α-lactose monohydrate)		
1%	30.492	< 0.001
5%	83.384	< 0.001
25%	62.696	< 0.001
50%	0.056	0.816

3.2.2.2 Production of aerosol from a DPI device.

The electrostatic properties of aerosols generated upon actuation from two dry powder inhaler devices, the Rotahaler and the Dryhaler, were measured using two different apparatuses: the Electric Fieldmeter (EFM) and the Transient Charge Monitoring (TCM) apparatus. The objective of this part of the study was to investigate if the differences in electrostatic behaviour observed between the two drug polymorphs have a significant bearing on the electrostatics evolved in actual pharmaceutical DPI devices.

The EFM technique has the potential to give a highly accurate quantification of aerosol cloud charge behaviour [Peart 1996]. However, the EFM measurements obtained in this investigation could not be used to differentiate between the electrostatic behaviour of different polymorph blends

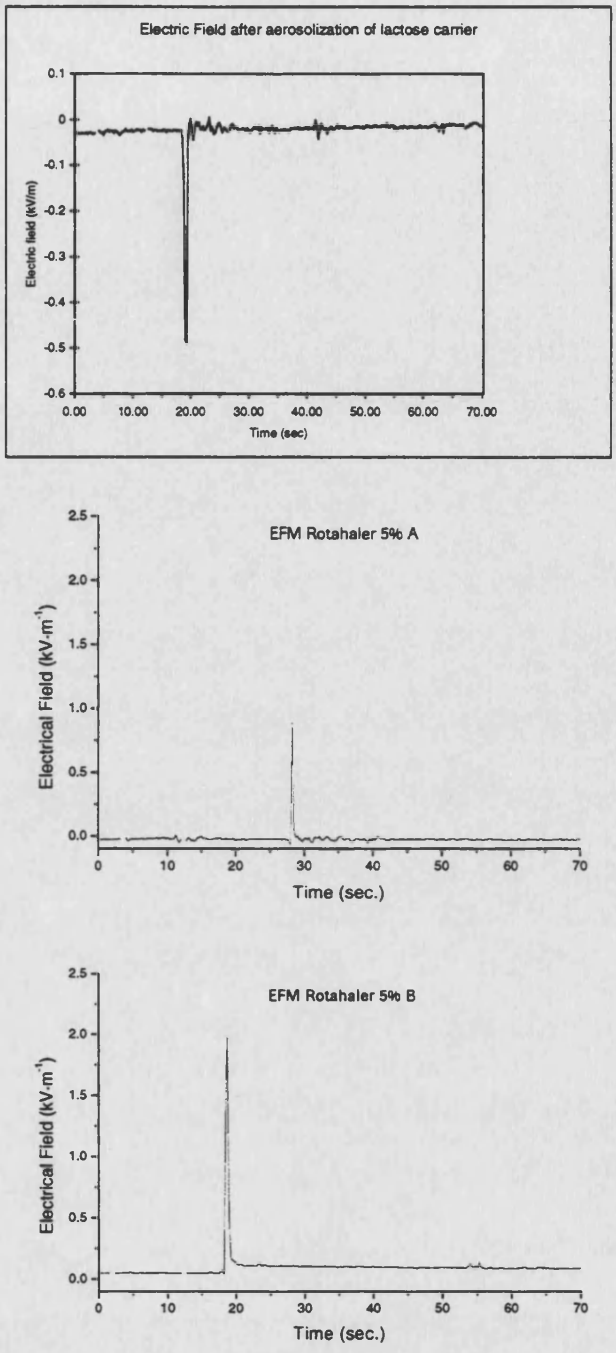

Figure 37 Electric field detected after aerosolisation from the Rotahaler™ of 25 mg of α-lactose monohydrate, and binary blends with 5% Ro 24-5913, polymorphs A and B, in α-lactose monohydrate (n=15).

or of pure α-lactose monohydrate. Measurements with drug-lactose monohydrate blends turned out to be difficult to perform due to a high tendency of particles to contaminate the field meter. An example of the results obtained from this technique is shown in Figure 37. Measurements with the pure drug, regardless of crystal form, were not possible, because of the more intense field meter contamination. It was concluded that the EFM technique was not suitable for use with the powder systems chosen for this study, and its use was not considered further.

The Transient Charge Monitoring (TCM) apparatus consists of a series of circular electrodes capable of detecting either positive or negative charges. The apparatus is equipped with a tube where the electrodes are located along the tube's length. The positions of the electrodes are arranged in a manner intended to roughly model the airways of the respiratory tract (Machowski, 1996). The electrodes in the apparatus tube are numbered such that the lower the electrode number, the closer the electrode to the aerosol device.

Pure α-lactose monohydrate carrier showed exclusively electropositive properties when tested with the TCM apparatus following aerosolisation from the Rotahaler device (Figure 38). The magnitude of the actuation-evolved charge decreased as the actuated sample moved along the apparatus. Since TCM is modelled after the human respiratory tract, deposition within the upper respiratory tract is associated with low-number electrodes in the TCM apparatus. Figure 38 shows that the carrier charge is completely neutralised by the time the sample exits the apparatus. Such a result is consistent with the

deposition within the upper respiratory tract expected for the coarse α-lactose monohydrate particles.

Figures 39 and 40 show the TCM results obtained with the Rotahaler and Dura devices, respectively. In contrast to the behaviour observed for pure α-lactose monohydrate, the presence of drug in the mix produces an increase in the electrostatic charges developed upon actuation. This is true for both crystal forms of the drug. The TCM apparatus can provide a more detailed characterisation of the electrostatic behaviour of powders than other methods because it provides a direct observation of the bipolar behaviour of the sample under dynamic conditions. This type of information can be quite revealing. Consider for example the data obtained when polymorph B at 5% is actuated from the Dura device (Figure 40). The initial net charge in this case is the lowest observed (*i.e.*, the closest to electroneutrality). However, the amount-of-charge, the distance between the positive and negative charge components, is the highest.

The TCM apparatus readily shows how the bipolar behaviour of the powder mix can bring about a net change in polarity. A change form net positive to net negative charge is observed in Figures 39 and 40 except in the case of polymorph B from the Dura device. Moreover, the change in net charge in all three cases was produced by a decrease in the positive component, accompanied by an increase in the negative one. Polymorph B actuated from the Dura device also produced a decrease in positive charge. In this case however, there was a gradual decrease in the negative component, but the net charge remained negative at all times. The gradual nature of this

shift in charge is again (see CIMFC and ASFC results above) suggestive of charges sufficiently weak to allow them a prolonged decay.

One consistent difference between polymorphs A and B is that TCM profiles show polymorph B as having a greater amount-of-charge than polymorph A. This could be interpreted as an indication that polymorph B is more electrostatic than polymorph A. However, the CIMFC (previous section) and Centrifuge experiments (Section 3.1) show that polymorph A is more effective than polymorph B in neutralising its charges by forming agglomerates. Therefore, a more plausible explanation seems to be that polymorph B exhibits a greater amount-of-charge because its charge is less unstable (weaker) than that of polymorph A. A highly electrostatic material will generate stronger, highly unstable charges. If sufficiently strong, these charges can produce an immediate particle rearrangement toward neutralisation, and the resultant decay may have a time scale that is shorter than a TCM measurement.

Analysis of variance is presented in Table 17, p-values demonstrated significant differences in charge development between the two polymorph powder blends.

The TCM apparatus shows a general difference between the electrostatic behaviour of drug-lactose monohydrate blends containing two different polymorphs. The observed differences, however, are not detailed enough to provide direct information about the differences in dynamic behaviour between polymorphs. When comparing different materials, some of the instrumental techniques employed provide measurements that directly reflect a particular difference between the samples. But not all instrumental techniques provide the same level of differentiation, and finding which

methodologies are more informative than others becomes part of the investigation. For the system studied here, the TCM method can be useful in providing information that is valuable but of a secondary nature. The TCM technique shows clear differences between the two polymorphs studied here. But the information obtained, although quite revealing, would have its greatest use helping in the understanding or interpretation of results form other (primary) techniques.

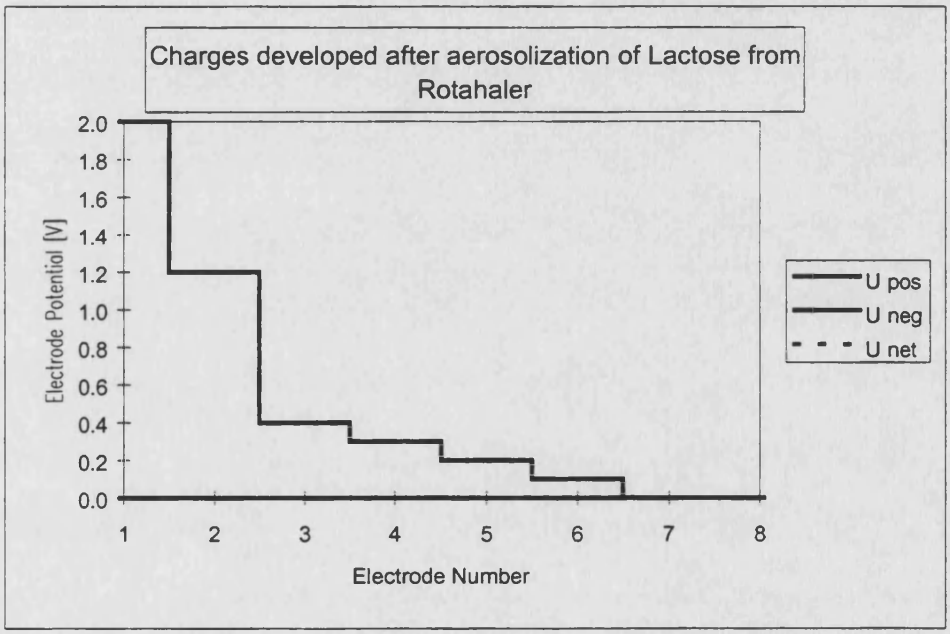

Figure 38 Charges developed after aerosolisation of α-lactose monohydrate from Rotahaler™ (n=3).

Table 17 Analysis of variance for the bipolar charges generated by the two polymorphs of Ro 24-5913 A and B (**5% w/w**) when discharging the powder from two devices: Rotahaler™ or Dryhaler™ as detected by TCM. Data shows the **p** value for the different levels (electrodes) for positive, negative and net charges.

Summary of the ANOVA analysis for the charges												
Electrode	Positive				Negative				Net			
	Rotahaler		**Dura**		**Rotahaler**		**Dura**		**Rotahaler**		**Dura**	
LEVEL 1	F-value	p	F-value	p	F-value	p	F-value	p	F-value	p	F-value	p
	2.218	0.25	121	< 0.001	21.274	< 0.01	29.822	< 0.01	0.7313	0.50	52.071	< 0.001
LEVEL 2	F-value	p	F-value	p	F-value	p	F-value	p	F-value	p	F-value	p
	5.563	< 0.05	0.198	0.50	12.982	< 0.01	23.242	< 0.001	0.0036	0.953	5.054	< 0.05
LEVEL 3	F-value	p	F-value	p	F-value	p	F-value	p	F-value	p	F-value	p
	4.961	< 0.05	0.198	0.50	28.722	< 0.001	20.028	< 0.01	6.490	< 0.05	23.198	< 0.001
LEVEL 4	F-value	p	F-value	p	F-value	p	F-value	p	F-value	p	F-value	p
	3.119	0.25	0.063	0.806	32.399	< 0.001	17.679	< 0.01	127.872	< 0.001	26.150	< 0.001
LEVEL 5	F-value	p	F-value	p	F-value	p	F-value	p	F-value	p	F-value	p
	1.864	0.25	0.412	0.50	28.122	< 0.001	18.819	< 0.01	69.187	< 0.001	20.938	< 0.001
LEVEL 6	F-value	p	F-value	p	F-value	p	F-value	p	F-value	p	F-value	p
	0.742	0.50	1.689	0.25	25.776	< 0.001	11.691	< 0.01	59.201	< 0.001	15.357	< 0.01
LEVEL 7	F-value	p	F-value	p	F-value	p	F-value	p	F-value	p	F-value	p
	0.328	0.50	4.807	0.1	30.675	< 0.001	7.0609	< 0.025	63.096	< 0.001	9.8256	< 0.025
LEVEL 8	F-value	p	F-value	p	F-value	p	F-value	p	F-value	p	F-value	p
	0.373	0.50	4.764	0.1	30.412	< 0.001	7.131	< 0.025	63.496	< 0.001	9.533	< 0.025

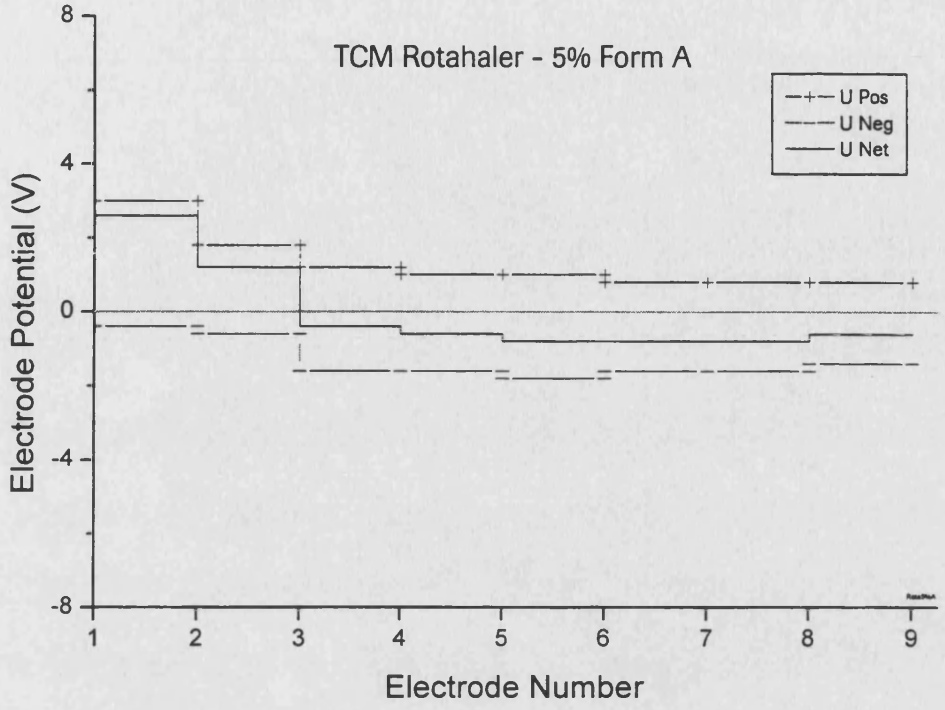

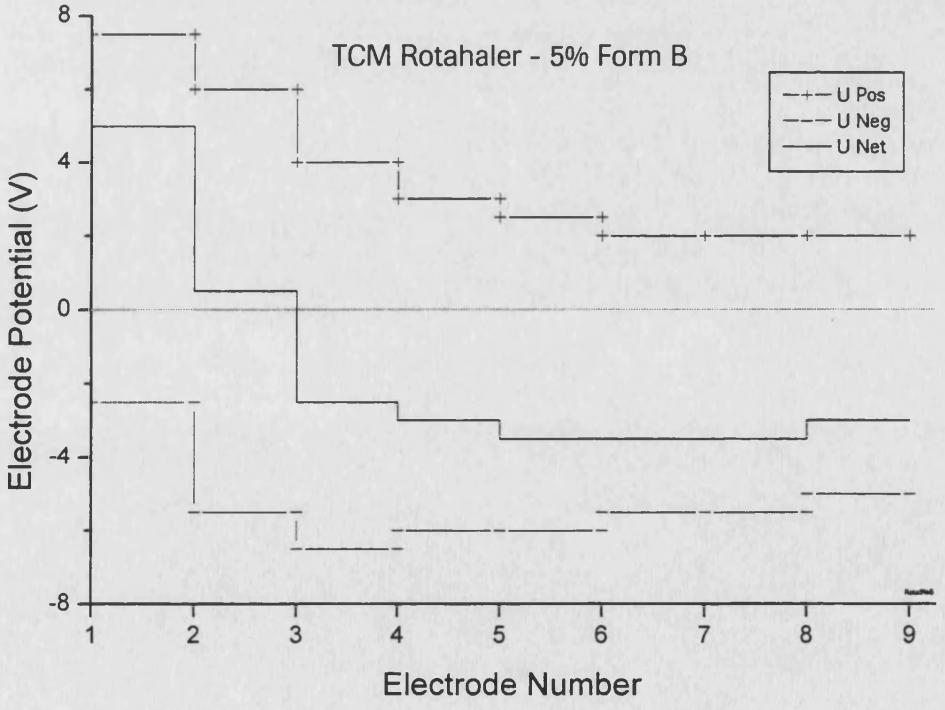

Figure 39 Bipolar charges developed after aerosolisation of blend 5% polymorphs A and B from Rotahaler™ (n=3).

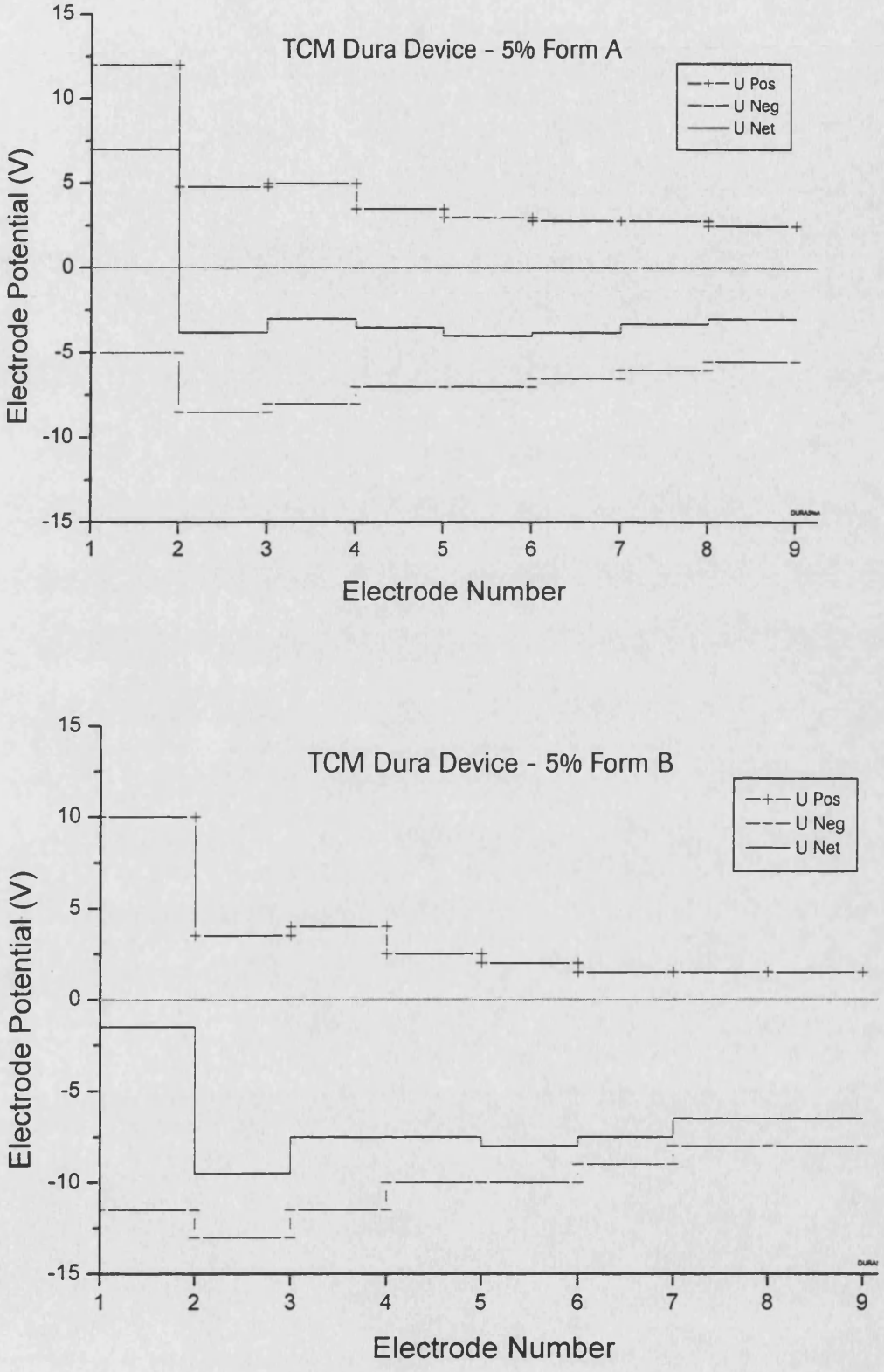

Figure 40 Bipolar charges developed after aerosolisation of blend 5% polymorphs A and B from Dryhaler™ (n=3).

4. ENERGETIC PROPERTIES OF POWDER SURFACES

Variations in the surface properties of materials are in general more difficult to detect and measure than the corresponding differences in bulk properties. Surface properties, however, can be as influential on product's functionality, if not more, as the bulk properties of powders.

A number of methods are currently available for the analysis of surface properties. Among these are interfacial contact angle measurements, inert gas adsorption, microcalorimetry, solvent sorption isotherms, inverse gas chromatography (IGC), atomic force microscopy (AFM) and molecular modelling. Each method has specific advantages and limitations in terms of methodology, complexity and applicability, all of which may affect the usefulness of individual measurements. The above listed techniques are nonetheless often complementary in terms of the information they provide, and in combination, analysis techniques can assist in providing a more viable total description of the behaviour of pharmaceutical powder surfaces, than any individual technique could.

In this section of the present study, TAM, water uptake and IGC are explored in their use for the analysis of surface energetic properties of the polymorphic drug. With the results from these analyses, it should be possible to examine the interactions of the drug with lactose in a dry powder formulation for inhalation, in a light that permits relating the physical properties of the drug's surface to its behaviour and impact on the "product's" functionality.

Polymorphism corresponds to differences in the crystal lattice, which are likely to alter the surface of the material and consequently its surface energy. Physico-chemical characterisation measurements performed on the two polymorphs (Chapter 2), established that the two crystal forms of the drug exhibit those physicochemical differences frequently observed between crystal polymorphs. However, the analysis of such differences has not been directed toward the surface of these materials, namely, toward the surface energetics of the two polymorphs and the differences between them.

To such an effect, the working hypothesis is that the surface energetics of the two polymorphs can be distinguished through the study of their interactions with a common probe. A suitable probe consists of the vapour of a solvent, chosen as the adsorbate in the interaction with two (polymorphic) surfaces. By measuring heats of adsorption, quantitative comparisons between the two crystal surfaces should be possible. In addition to the direct quantitative comparisons made possible with the use of a common probe with two surfaces, the results of experiments involving different probes and a common surface can provide an additional angle for comparison between surfaces. For instance, by comparing hexane and pentanol, which are geometrically similar but different in their interactive properties (one is non-hydrogen bonding and the other is both donor and acceptor), it is possible to study the contributions of hydrogen bonding and non polar interactions to the adsorption on a given surface. The information thus obtained can, in turn, help in better assessing the nature of the drug surface for purposes of formulation optimisation.

Surface analysis. Physical adsorption at the solid/gas interface is essentially the result of VdW forces. The adsorption characteristics of powders depend to a large extent on the surface chemistry and surface charge of the particles. The adsorption properties are evaluated by means of thermodynamic parameters: free energy of sorption (ΔG^{o}_{s}), enthalpy of sorption (ΔH^{o}_{s}), and entropy of sorption (ΔS^{o}_{s}). These parameters can be obtained from adsorption isotherm experiments by TAM and from IGC retention data under nearly ideal (*i.e.*, infinite dilution) conditions. TAM and IGC are techniques used here to study the surface energy of the polymorphs and to assess the impact that the surface could have on the interactive forces of these polymorphs with lactose carrier. This drug-carrier interaction is what ultimately determines the performance of the dispersion powders for inhalation.

4.1 Isothermal Microcalorimetry (TAM)

Microcalorimetry can be used as a method for monitoring chemical, physical or biochemical changes. In particular, the TAM technique has been used for studying the rate and extent of degradation reactions (stability), interactions between drugs and microorganisms, as well as interactions between drugs and excipients (compatibility). Microcalorimetry is a very sensitive technique that permits measurement of the heat evolved by virtually any physicochemical event such as phase transitions, physisorption, chemisorption, etc. The output from the microcalorimeter, heat flow, provides quantitative information about the enthalpy and the rate of the

process. In addition, microcalorimetry can be used to characterise the solid state properties of powders when exposed to different processing stresses (*i.e.*, milling, crystallisation, freeze and spray drying, compression, coating, etc).

Recent calorimetric measurements for the analysis of solid surfaces in pharmaceutical systems have resulted in the increased application of highly sensitive microcalorimeters. Bakri [1993] reported the application of heat conduction microcalorimetry to study the adsorption of water vapour onto solid pharmaceuticals. Other authors have reported the potential of the technique on precipitation [Puppedi *et al.,* 1995] and desorption [Duddu *et al.,* 1995] processes.

In the present work, the heat of adsorption of probes of different vapour pressures onto the surface of Ro 24-5913 solid drug of both polymorphs was measured using a heat conduction microcalorimeter (TAM). The effect of vapour pressure on the powder is studied by means of the accurate sorption isotherms of probe vapour on the polymorph obtained with this technique.

4.1.1 Methodology

Micronised Ro 24-5913 polymorphs and (solvent vapour) probes of different polarity were used for these experiments.

Microcalorimetry: The integral heats of adsorption were measured using a heat conduction microcalorimeter (Thermal Activity

Monitor, TAM, Thermometric AB Sweden) with a Thermometric RH perfusion ampoule (accessory Model 2255) adapted with Kalrez O-rings. The control of the vapour pressure above a solid sample was similar to the one originally designed by Bakri [1993], which is now commercially available as an accessory to the TAM. A schematic of the RH perfusion accessory as used for the TAM set up, shown in Figure 41.

The system creates and accurately maintains (within 0.1%) a user-selected value of relative humidity, or vapour pressure, in the sample chamber by mixing dry nitrogen and nitrogen pre-saturated with probe vapour. The instrument is equipped with Gas Pressure Controller device (GPCD) that accurately controls the relative humidity/vapour pressure. The GPCD delivers the set relative vapour pressure of the gas phase to which the sample is exposed. The relative humidity (*RH*) can be controlled from 0% to 100% *RH* within about ± 0.1%. During the calorimetric experiments, a flow controller connected to a switching valve delivers the dry nitrogen gas. The high purity Nitrogen used here was further dried by passing it through a drying tube containing Drierite™ (anhydrous $CaSO_4$), prior to feeding it into the TAM. The flow controller has a valve that continuously alternates between two positions. In one position, the valve delivers dry gas directly to the sample ampoule. In the other position, dry gas is passed over two humidifier reservoirs in thermal contact with the calorimetric bath. The gas delivered from the valve in the second position is thus saturated with the solvent vapour before reaching the measuring ampoule. Both dry and solvent saturated gas pass separately through heat exchanges for thermal equilibration prior to entering the measuring cell of the instrument. The

incoming *RH* to the sample can be controlled from a valve and varied from 0 to 100% by mixing appropriate ratios of dry and wet gas [Bakri 1997]. The RH accessory's software permits the use of any predefined *RH*. The *RH* delivered via switch valve of the TAM was verified using 100% *RH* and temperature probes by placing pure water in the humidity chamber. A humidity probe was then connected at the gas outlet and to a Rotronic Hygrometer. The HT125 Humidity-Temperature transmitter (Rotronic Instrument Corp. NY) produced a signal reading the generated humidity. In addition, standard %*RH* solutions (25, 50, 80 and 95%) were placed into the ampoule and checked in similar manner in order to verify the relative humidity that the microcalorimeter (TAM) delivered. When setting a specific %*RH* value to be delivered by the microcalorimeter, it gave a precise match to the corresponding *RH* standard solutions. A humidity calibration curve at 25°C for the TAM was also performed using the Rotronic Hygrometer. The data are presented in Table 18 and Figure 42. The variation of about 2% was due to the difference in temperature between the measuring cell within the instrument and the room where the instrument was located. The instrument cell was set at 25°C whereas the thermocouple/probe was exposed at the room's temperature, 21°C.

The gas pressure delivered from the cylinder to the instrument's inlet was set to 2 atm with a gas gauge controlling the flow rate of the dry gas system. In addition, a gas flow controller for gas chromatography was used to control the gas flow into the measuring cell. The total flow rate of the gases (dry and wet) was kept constant at 1 ml min^{-1}.

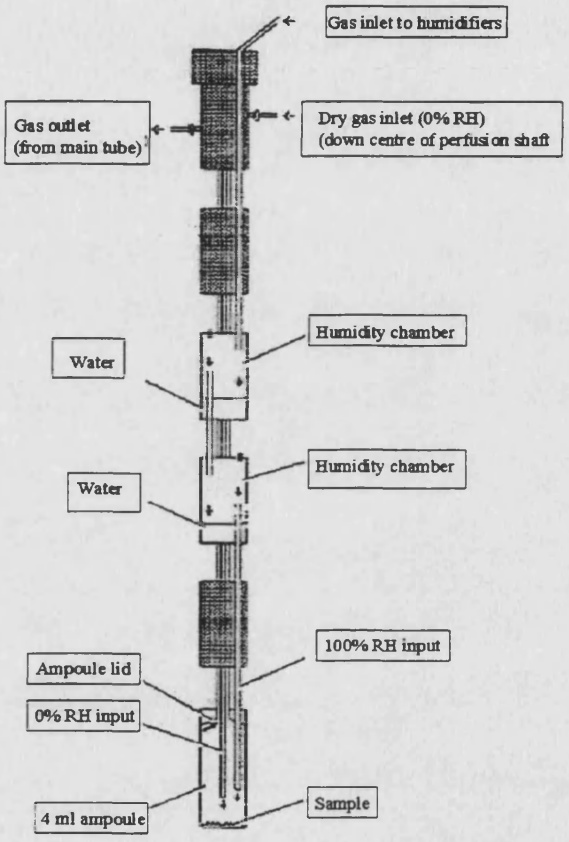

Figure 41. A schematic of the RH perfusion cell.

Table 18. Calibration %*RH* set in TAM monitored by the Rotronic Hygrometer Room Temp. = 21.3 ° C

	% *RH*		Temperature °C	
TAM Set	***Rotronic*** Measured Mean (n=7)	s.d.	Measured Mean (n=7)	s.d.
0	2.474	0.092	21.166	0.199
10	12.613	1.973	21.170	0.201
20	23.139	1.398	21.424	0.244
30	32.816	1.493	21.444	0.173
40	42.281	1.382	21.477	0.300
50	51.423	2.095	21.474	0.291
60	61.593	2.110	21.601	0.176
70	71.456	2.611	21.497	0.243
80	79.940	2.368	21.233	0.142
90	85.577	0.628	21.294	0.167
100	96.079	0.313	21.384	0.222

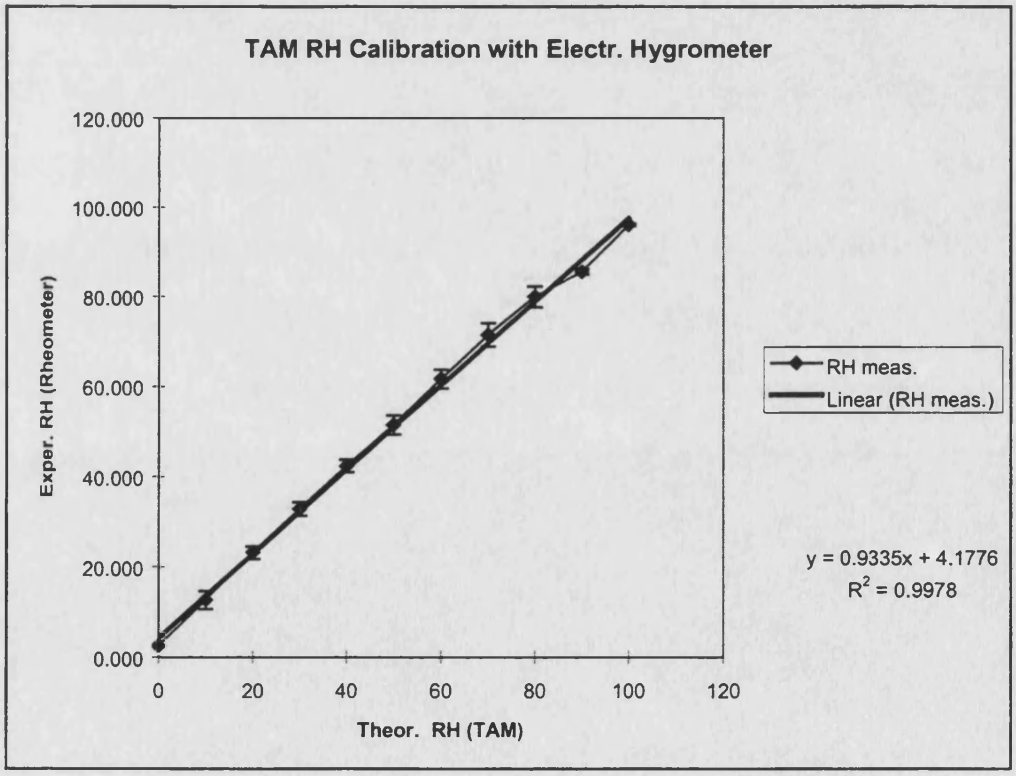

Figure 42. Humidity calibration curve for the TAM at 25°C.

Sorption experiments: An accurately weighed sample of approximately 30 mg of each polymorphic drug was placed in a 4 ml stainless steel sealed ampoule. The ampoule, which is a component of the TAM instrumentation, was then attached to the RH perfusion unit (Figure 41), and slowly lowered into the calorimeter's measuring position of the. Prior to calorimetric analysis, the sample was dried overnight under dry nitrogen flow (0% *RH*) until a signal of zero heat flow was attained. For each solvent probe and temperature, a blank experiment was conducted in an identical manner with no sample in the ampoule. The calorimetric adsorption experiments were conducted at four temperatures (20, 25, 35 and 45 °C).

The incoming vapour pressure was set to increase in 10% steps up to 100%, a positive response was recorded until equilibrium was reached, *i.e.* no heat flow (P_μ=0). The time integral of the recorded heat flow (P_μ) gives the enthalpy of the process under study. The area under curve of each adsorption peak was calculated using the baseline fitting programs in Origin™ 5.0 (Microcal, MA).

4.1.2 Results

Figure 43 shows a typical calorimetric response to the adsorption of MEK (methyl ethyl ketone) vapour on a sample of drug polymorph A. The reproducibility of the response was good (CV typically less than 2% with different solvent probes).

View Results Report Wednesday, November 18, 1998 11:34:55 AM
Pin[1] = ""
Pin[2] = ""
Pin[3] = "A:\59 Ass1 0-100MEK1-20C.xpt",RAW,NA,NI,F1+676,E1-105328
Sample information
Sample name: Ro 24-5913 Form A Id: DS-44
Sample amount: 33.000 mg
Sample date: 4 - Nov. - 98
Additional info
Micronised form A exposed to MEK vapors from 0 - 100% "*RH*" (P/P^o) at 20°C; N_2 P = 2 psi; FR = 1 ml/min. Ref. empty SS ampoule.

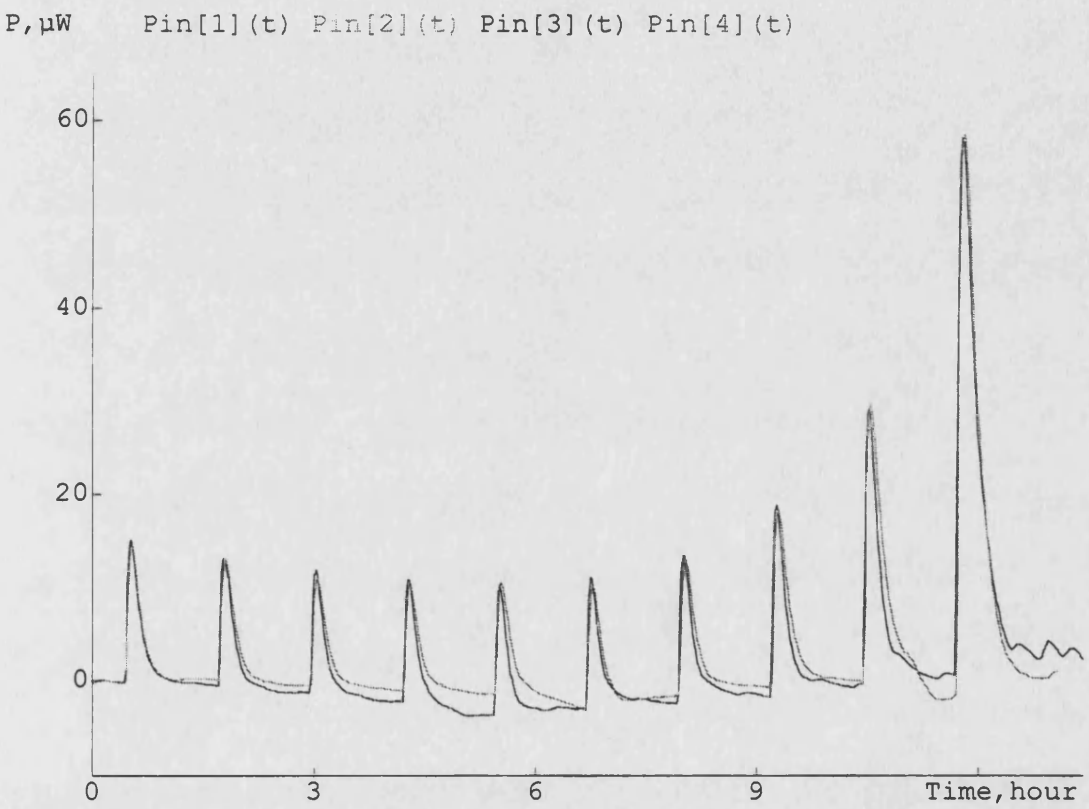

Figure 43 Typical calorimetric power/time curves and reproducibility.

The high sensitivity of the calorimeter permits detection, even at low humidities, of heat flow due to interaction of solvent vapour with the solid. Results of the integration of calorimetric power/time curves are the heat of

adsorption (Q_{ads}) of the various organic probe vapours (an example is presented in Figure 43). The heat flow (P_μ) can be described by:

$$P_\mu = \frac{dQ_{ads}}{dt} = \Delta H_{ads} \frac{dn}{dt} \qquad (39)$$

where: dQ_{ads}/dt and ΔH_{ads} are the rate and enthalpy of adsorption, respectively, and n denotes the number of moles adsorbed. This equation is related to two aspects of the process having place during interactions, a thermodynamic aspect (what interactions will occur, extent of adsorption) and kinetic aspect (how fast, rate of adsorption).

Values of Q_{ads} are presented in Figures 44-45 as a function of vapour pressure at three experimental temperatures. For a given polymorphic drug quantity, Q_{ads}, is given by [Bakri 1997]:

$$Q_{ads} = \Delta H_{ads}\, n \qquad (40)$$

where ΔH_{ads} is the adsorption enthalpy of the organic probe vapour on the polymorphic drug, and n is the quantity of sorbed water.

ΔH_{ads} can be obtained directly from the calorimetric data at the four temperatures investigated. Adsorption is considered a reversible process, and desorption experiments were conducted at the end of the adsorption experiments by making decrements of vapour pressure of 10% until reaching 0%. It was observed that the area under the curve of the adsorption peak was equal in magnitude, but opposite in sign, to the area under the corresponding

desorption peak, thus indicating the reversibility of the process. Since the adsorption process is a reversible one, van't Hoff law is applicable:

$$\frac{d(\ln K)}{d(1/T)} = \frac{\Delta H_{ads}}{R} \qquad (41)$$

where K is the equilibrium constant. ΔH_{ads} may vary with the vapour pressure since the adsorption sites may be different. It is also important to recall that van't Hoff's equation is a general one and does not require ΔH_{ads} to be constant with respect to temperature.

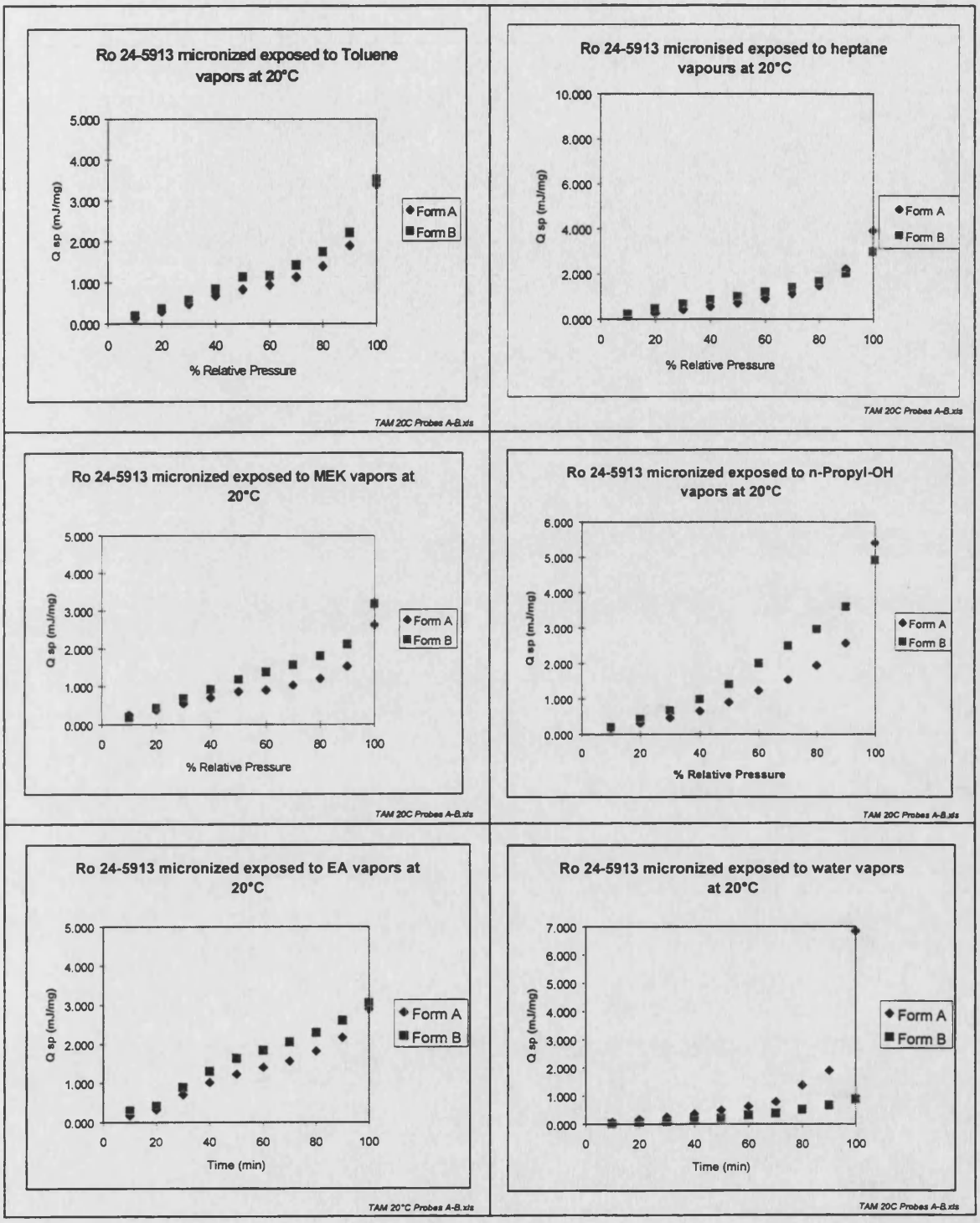

Figure 44 Micronised drug exposed to different solvent vapours at 20°C

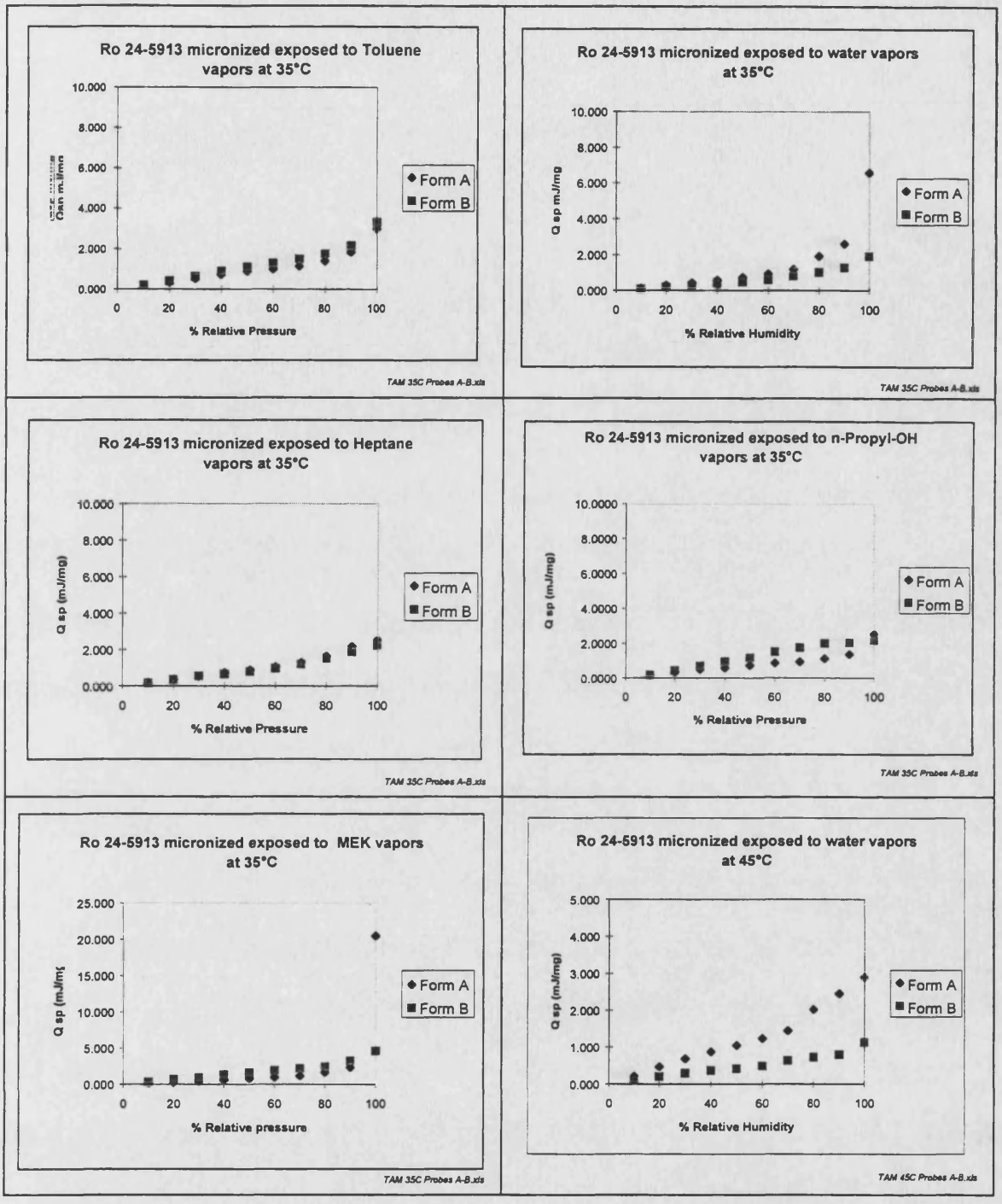

Figure 45 Micronised drug exposed to different solvent vapours at 35° and 45°C.

4.1.3 Discussion

4.1.3.1 Surface Energetics

Polymorphs are distinctly different materials with identical chemical composition. All bulk physicochemical and physicomechanical differences between crystal polymorphs arise from the different physical arrangement of the same molecule. Consequently, the crystal forms' interactive properties can be expected to be reflected in the polymorphs interaction with a probe molecule. Crystal parameters can describe the exact physical structure of the surface in a perfect crystal. And the excess free energy inherent to surfaces is bound to produce variations on the crystal surfaces beyond the unit cell parameters for the two polymorphs of study. Such surface variations play a significant role in the sorption properties of surfaces; excess free energy at a surface site translates into a higher thermodynamic activity for that site. The nature and resulting interactive properties of a non-perfect (real) crystal are thus a composite of the physical nature of and the type and number of defects on the surface. One of the premises of the present study is that the crystalline structure of the materials selected is reflected on their surface properties. Consequently, the differences between the polymorphs' surfaces can in turn be used to explain differences in the polymorphs' behaviour during processing.

The interaction of the two crystal forms with different probe molecules was investigated. The probe molecules selected for the study can be divided into three categories: Hydrogen bond donors, hydrogen bond acceptors and non-hydrogen bonding.

Figures 44 and 45 show that in the case of non-hydrogen bonding probes such as toluene and heptane, the heat of adsorption is the most similar between the two polymorphs. This result indicates that the type and nature of non-hydrogen bonding adsorption sites are similar on the two surfaces studied, making the two polymorphs energetically equivalent in terms of their hydrophobic interactive properties.

Figures 44 and 45 also show that the two polymorphic surfaces are not quite equivalent when the adsorption of the probes involves interactions of more specific nature. The heat of adsorption obtained with all hydrogen bonding probes shows more differences between the two polymorphs than those obtained with the non hydrogen bonding solvents.

It is noteworthy that in all cases, solvent adsorption on polymorph B involved higher energy of the interaction. The only, and quite prominent exception is water. The heat of water sorption was greater for polymorph A than for B, at all temperatures studied. Among the different solvent probes selected for this study, water occupies a central role, not only because its singular observed behaviour, but also because its ubiquitous nature and common use in pharmaceutical processing.

4.1.3.2 Water Uptake

The water uptake of the two polymorphs of Ro 24-5913 was determined as a function of relative humidity (*RH*) at different temperatures. Figure 46 shows

the sorption isotherms obtained for the two polymorphs at 20°C, 25°C, 35°C and 45°C.

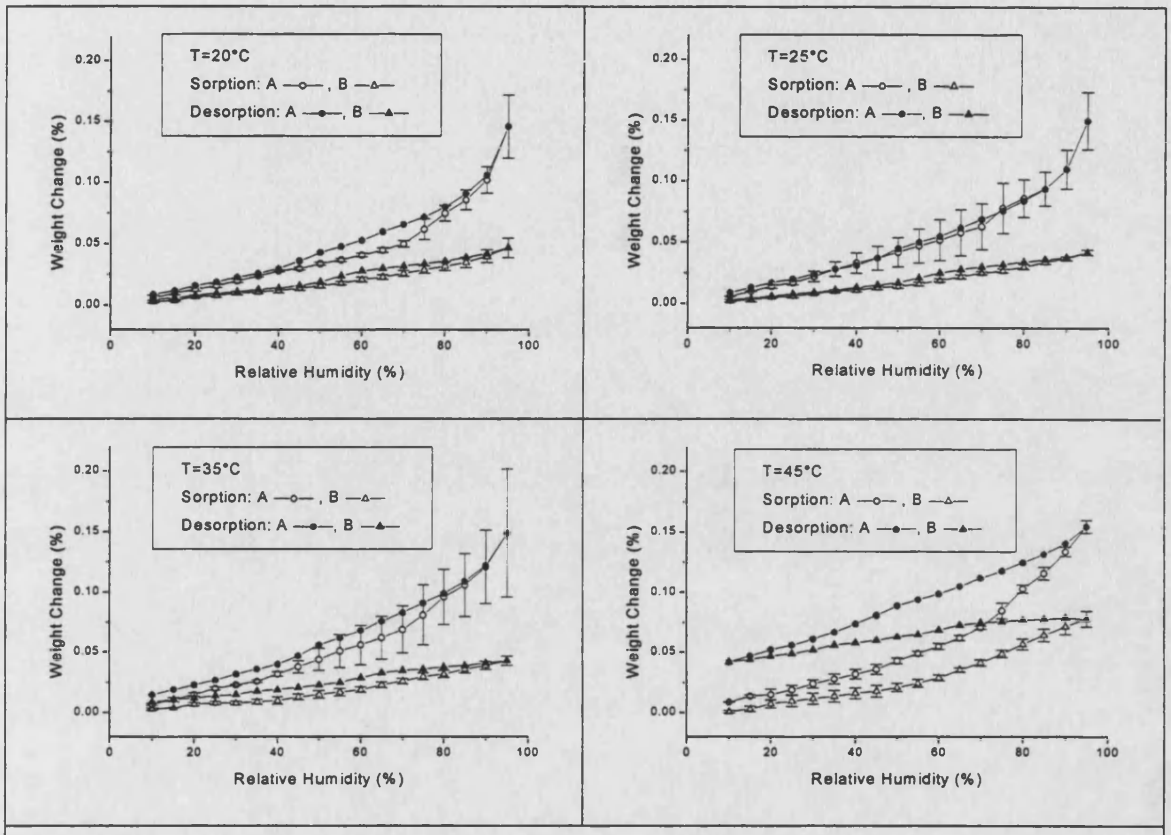

Figure 46. Comparison of the water sorption isotherms obtained for Polymorph A and B at different temperatures.

The isotherms in Figure 46 show that polymorph A sorbs greater quantities of water vapour than polymorph B at the different temperatures investigated. It is noteworthy that Figure 46 also shows that the isotherms of form B gave substantially less variability than those of form A, particularly at 25°C and 35°C. Water uptake measurements were done under the exact same conditions for the two polymorphs. Therefore, the difference in uncertainties about the isotherm points between the two polymorphs is

attributed to the inherent differences between the materials studied and not to experimental variation *per se*. Polymorph A produces water sorption isotherms with wider variability about points, suggesting that polymorph A has a more heterogeneous surface than polymorph B. These results is are at first glance consistent with form A being thermodynamically metastable in the temperature range selected. A less stable crystal is expected to have greater number of energetic sites which favour water sorption [Zografi and Tam, 1976].

Figure 46 also shows that hysteresis is particularly significant at 45°C for both polymorphs. In fact, the profiles obtained at 45°C can be interpreted as suggestive of condensation taking place at such temperature.

Although all the information relative to the water uptake of the two crystal forms is contained in Figure 46, data presentation as isotherms may not be the optimal for purposes of comparison. In this situation, isobars offer a more intuitive means of data presentation. Figure 47 shows the sorption portion of data of Figure 46 as isobars, specifically as *relative* isobars, *i.e.*, as lines of constant relative humidity.

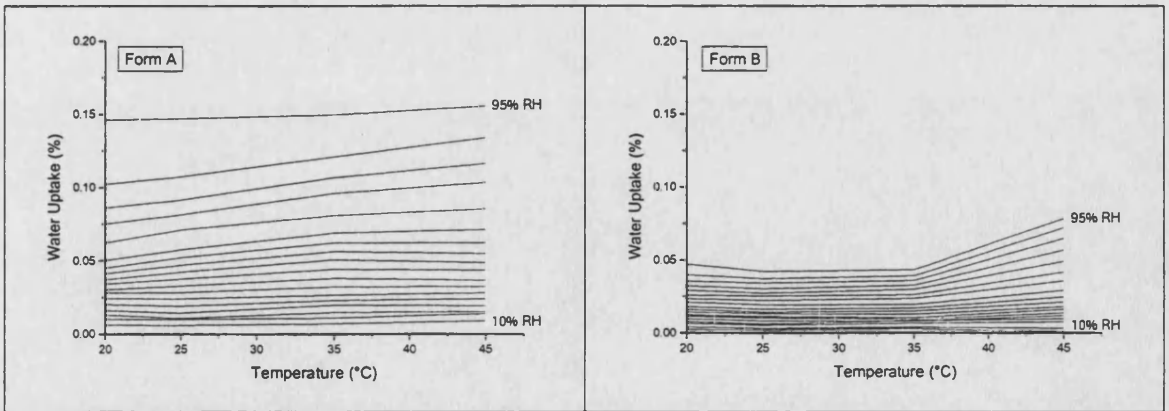

Figure 47. Comparison of the water sorption relative isobars obtained for Polymorph A and B as a function of temperature.

Data presentation as relative isobars makes it an easier task to separate the effects of temperature and those of relative humidity on the sorption behaviour of water vapour on the surfaces of two different polymorphs.

Each line in Figure 47 corresponds to a constant level of *RH*, the lines are termed relative isobars because each line corresponds to a constant value of water vapour pressure *relative* to the water saturation pressure at the same temperature. The relative isobars presented in the figure correspond to *RH* ranging from 10% (bottom) to 95% (top), with increments of 5%. Thus, moving upward in the figure at constant temperature corresponds to a *linear* increase in water concentration in the vapour phase. In addition to being linear, such an increase in vapour phase water concentration represents also a degree of freedom in terms of Gibbs phase rule; it is controlled directly by the experimenter. Moving along a relative isobar with increasing temperature also corresponds to an increase in the vapour phase water concentration, with the ratio of the water vapour concentration to its saturation concentration remaining constant. But unlike moving along the ordinate, the change in water vapour concentration along an isobar is non-linear and does not represent a degree of freedom; it is fixed by the temperature. The increase in vapour phase water concentration along the relative isobars follows from the fact that the water saturation pressure ($P°$) increases with temperature. An increase of 10°C in temperature along a relative isobar corresponds to an increase of 70% to 80% in water concentration in the vapour phase [Martin, 1999].

Figure 47 shows that polymorph A not only sorbs a greater amount of water than polymorph B, but also that sorption by form A exhibits greater

variability as a function of both temperature and relative humidity. The relative isobars of polymorph A are almost isosteric, whereas the isobars of polymorph B show a definite increase in sorption between 35°C and 45°C. At a given temperature, sorption by polymorph B tends to increase in a fashion that is more or less proportional to the increase in *RH*. Polymorph A on the other hand, exhibits increases in sorption that are not proportional to the increase of *RH* for *RH* values greater than 70%, particularly at the lower temperatures. It should be noted that individual isotherms showed a slight but consistent jump in sorption at 70% *RH*, especially at 20°C and 25°C. Such a jump is not directly appreciable in Figure 47, although its effect still appears as a change in the general curvature of the isotherms. It appears that around 70% *RH*, the water adsorption of polymorph A presents some sort of threshold that triggers or enhances a different mode in the sorption of water vapour. Investigations in the semiconductor field [Vilan *et al.*, 1998] have produced evidence of two-site adsorption mechanism for organic molecules. Form A possibly has a threshold *RH* value at which a second type of sorption sites start becoming occupied.

It is important to note that at a given *RH*, increasing temperature produces two counteracting effects on water sorption. On the one hand, because water sorption is an exothermic process, it is disfavoured the higher the temperature. On the other hand, as discussed, the increase in P° produced by higher temperatures increases the water concentration in the vapour phase, which could favour sorption if the adsorbing surface is energetically heterogeneous. Increased sorption produced by increasing temperature at constant *RH* can also result if condensation of the adsorbate takes place. It

should be pointed out that sorption-induced condensation need not be condensation of the bulk liquid, as it is apparently the case at 45°C in this study. Water sorption on activated carbons results in the formation of water clusters at fairly low *RH*. In these cases, surface phenomena control the sorption process at relative humidities of 30% or less. Surface heterogeneity results in different sorption sites, some of them acting as primary adsorption centres. Population of the primary sites then initiate the process of cluster formation [Salame *et al.*, 1999].

The interplay between the two counteracting effects described above is more clearly observable if data are presented as the distribution of water between the two phases. Consider a system consisting of water vapour molecules distributed in equilibrium between the vapour phase and the surface of the adsorbant. The distribution coefficient, K_D, for this system is given by:

$$K_D = \frac{C_s}{C_v} \qquad (42)$$

where C_s and C_v are the water concentrations in the sorbed and vapour phases, respectively. Figure 48 shows the distribution coefficients obtained from Equation 42. The C_s values used are in moles of water per square meter of adsorbant, and the C_v values used are given in moles of water per cubic meter. Water concentrations in the vapour phase were calculated as follows:

$$C_v = \frac{P^o \, RH}{100 \, R \, T} \qquad (43)$$

where $P°$ is the saturation pressure at the absolute temperature T, and RH is the relative humidity selected by the experimenter, and R is the ideal gas constant. The values of $P°$ (in torr) were in turn calculated as follows [Martin, 1999]:

$$\log P^o = \frac{2939}{T} - 4.987 \quad \log(T) + 23.573 \qquad (44)$$

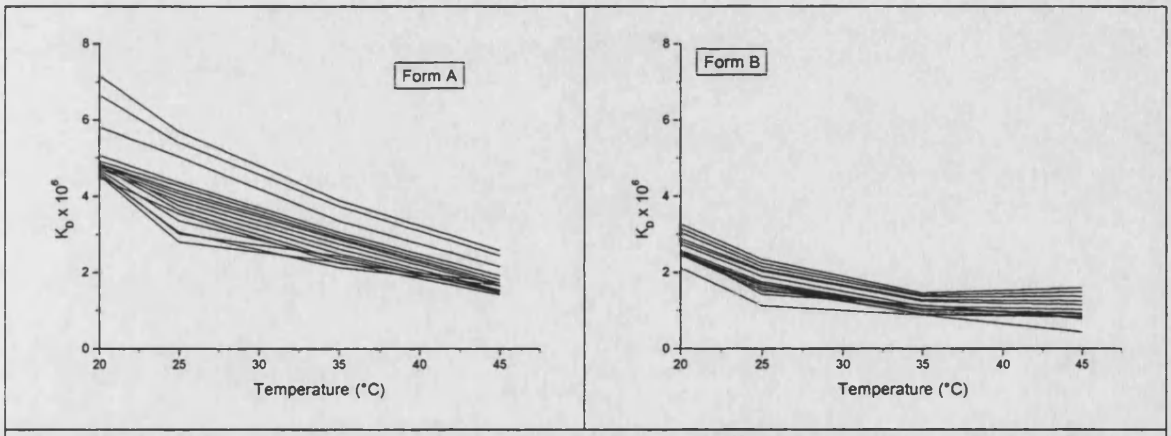

Figure 48. Comparison of water distribution coefficient relative isobars for Polymorphs A and B as a function of temperature.

Figure 48 shows the distribution coefficient of water for the two polymorphs as a function of temperature. The two polymorphs exhibit a net decrease in the distribution coefficient with increasing temperature. Figure 58 also reveals that the increase in sorption by polymorph B observed from 35°C to 45°C (Figure 48), can be accounted for, simply by the corresponding

increase in P^o with temperature. This is an important result, because it means that no new process of water uptake is triggered at 45°C, even though this corresponds to the only temperature for which significant hysteresis was observed (Figure 46).

Figure 48 shows that the distribution coefficient profile of polymorph B is consistent with that expected from a system in which the sorption sites on the surface are for the most part energetically equivalent. In such case, the distribution coefficient is expected to increase in proportion to an increase in RH at a given temperature. Such a system is also expected to exhibit an exponential decrease in equilibrium sorption with increasing temperature, as predicted by the van't Hoff equation. Figure 48 shows that for polymorph A, the span of K_D values is the widest at 20°C and becomes more narrow as the temperature increases. This result is indicative of a surface on which the sorption sites are not energetically equivalent. The span of K_D values in Figure 48 is not only wider for polymorph A, it also varies more with temperature than for polymorph B. Water sorption results for polymorph B can be considered as being closer to an ideal behaviour than the results for polymorph A. This is apparent by considering both the change in water uptake as a function of RH at a given temperature (Figure 47) as well as by the change of the sorption coefficient as a function of temperature at constant RH (Figure 48).

The existence of sorption sites of different nature on inorganic crystal surfaces has been established in the past. In fact, work on catalysis research has shown that the surface of zirconium dioxide crystals contains adsorption sites of different nature: acidic, basic, oxidising and reducing. Moreover, zirconia polymorphs exhibit different adsorptive properties due to different

nature and density of adsorption sites on their surface, which in turn is the direct result of their different crystal structures [Bachiller-Baeza *et al.*, 1998].

The foregoing discussion establishes that the surface of polymorph A crystals is more heterogeneous than the surface of polymorph B. The statements concerning the energetics of sorption are based on the effects that temperature have on the distribution coefficient. The common format for analysing the energy of sorption would be to plot the data on a van't Hoff type plot. The slope of such a plot corresponds to the enthalpy of the process (normalised to the ideal gas constant). However, van't Hoff plots are well suited for ideal or nearly ideal systems, *i.e.,* homogeneous surfaces giving place to an enthalpy of the process that is invariant with temperature. This is not the case for either polymorph in this study.

4.1.3.3 Heat of Adsorption

In the present study, the analysis of the energetics of water sorption was taken one step further by directly measuring the heat evolved by the water uptake for each polymorph under different relative humidities, and at the same temperatures as the sorption measurements. The heat of adsorption was measured by microcalorimetry using the TAM instrument equipped with the flow cell system to control relative humidity. Figure 49 shows the heat of adsorption, presented as relative isobars, for each polymorph.

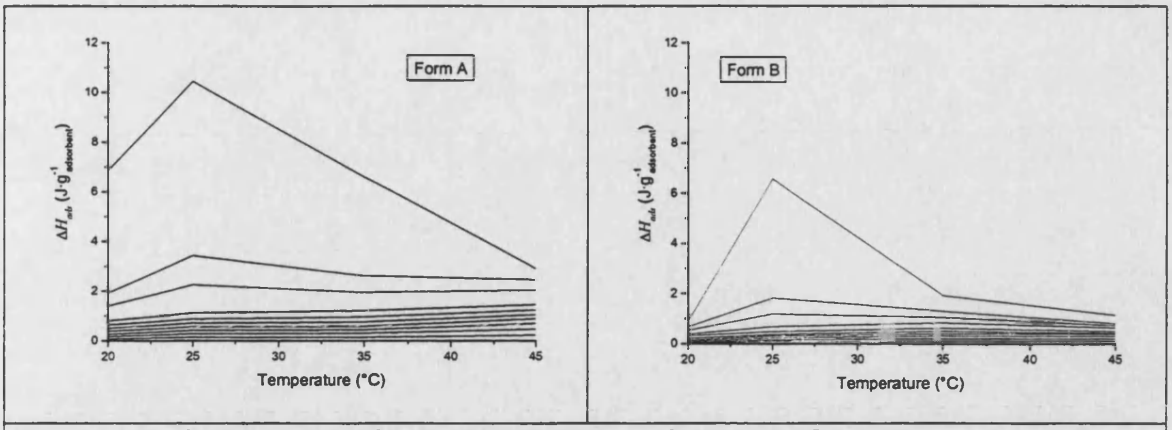

Figure 49. Comparison of heat of adsorption of water for Polymorphs A and B as a function of temperature. Data presented as relative isobars.

From bottom to top, the relative isobars in Figure 49 correspond to 20% to 90% *RH*, with 10% increments. The figure shows that the two polymorphs show more similarity in terms of the energy profile obtained than in terms of their water distribution coefficients. The heat of adsorption for polymorph A is significantly higher at all relative humidities and temperatures investigated. However, the two polymorphs qualitatively follow similarly shaped profiles. Most notably, there is a significant increase in the heat evolved upon adsorption at 25°C and high relative humidity.

The sharp increase in heat of adsorption seen in Figure 49 indicates that the two polymorphs have heterogeneous surfaces. Both crystal forms appear to have a portion of their surface covered with less energetic, less specific sites which get occupied at 25°C, as a result of the increase in vapour phase water concentration produced by increasing temperature at constant *RH*. This effect could be the result of partially crystalline or even amorphous regions produced by the milling process. But the lower heat of sorption observed at 20°C compared to that at 25°C is difficult to explain in terms of

amorphous regions. Because such an explanation would require a liquid-liquid (super cooled liquid in the case of the amorphous drug) hydrogen bond interaction that is stronger at 25°C than at 20°C. A more plausible, albeit speculative explanation would be a scenario similar to the sorption of water vapour on activated carbons. Sorption at secondary (weaker) sites which allows mobility to the adsorbed molecules, and consequently water-water (exothermic) interactions. At 35°C, the temperature is too high for sorption at these weaker sites, and net decreases in both energy of sorption and water distribution coefficients are observed.

Figures 48 and 49 are greatly informative in differentiating between the two polymorphs in terms of their interaction with water vapour. However, the information in these figures is still somewhat limited because both water uptake and energy of adsorption are given relative to the amount of adsorbant present. In order to establish the inherent differences in surface energetics between the two polymorphs, it would be more informative to look into the energy evolved when a water molecule "lands" on one type of surface or the other. Figure 50 combines the information in Figures 47 and 49. This figure shows the specific heat of adsorption, *i.e.*, the heat of adsorption relative the amount of water sorbed instead of to the amount of crystalline adsorbate present. The specific heat of adsorption is more informative about the energetics of sorption. It centres on the water and the energy that such water evolves upon sorption, without the confounding effects of whether a unit mass of from A is equivalent to a unit mass of form B in terms of surface area or of any other suitable criterion.

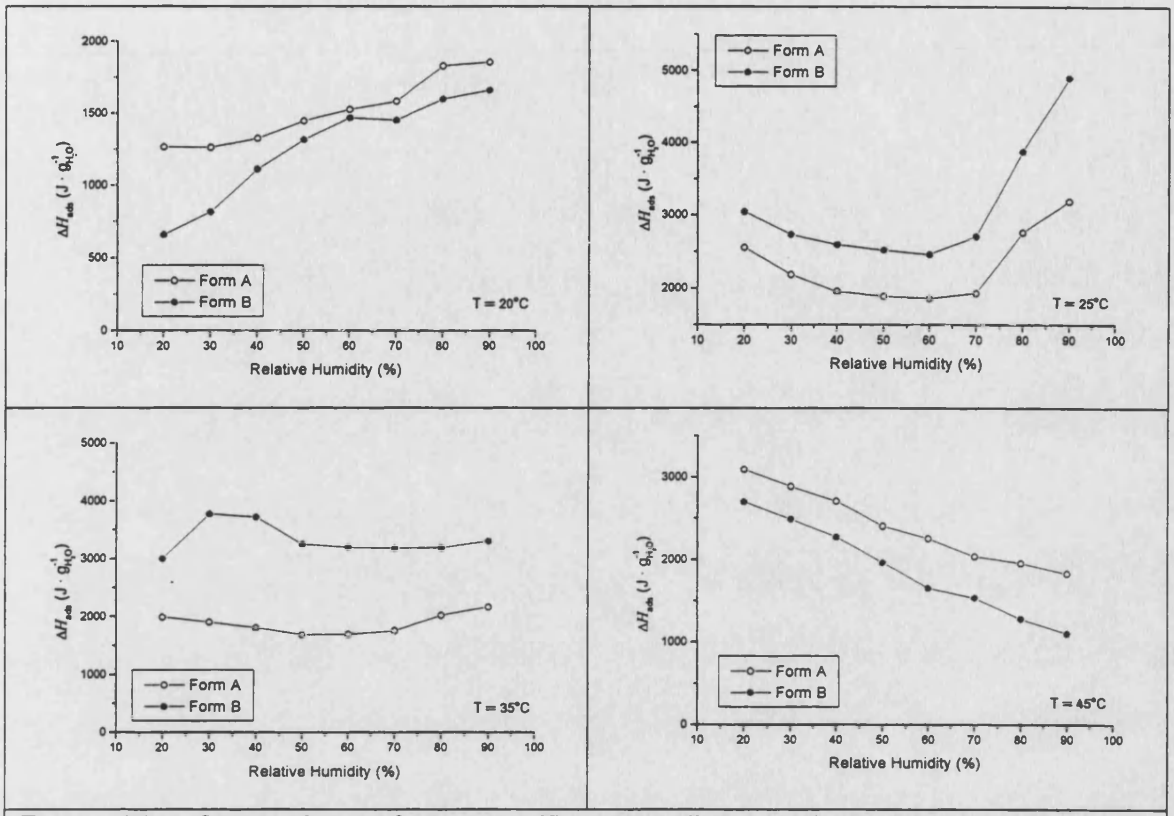

Figure 50. Comparison of the specific (normalised to the amount of water sorbed) heat of adsorption of water for polymorphs A and B. Heat of adsorption.

Figure 50 shows that the energetic differences water molecules will encounter when lodging on one polymorph surface or the other. The differences between polymorphs in terms of their surface energetics are observable on the specific heat of adsorption at different RH values, as well as on its variation with temperature for each polymorph. The specific heat of adsorption is very similar for the two polymorphs at 20°C and somewhat greater for polymorph A at 45°C. Between 25°C and 35°C however, the specific heat of adsorption of water on polymorph B is considerably higher than for polymorph A.

The data in Figure 50 point toward a fundamental difference between polymorph A and polymorph B. At 25°C, both the total heat of adsorption and the amount of water sorbed are greater for form A than for form B. However, the specific heat of adsorption is greater for form B. This result is strong indication of a very different type of interactive surface in each case. More water can sorb onto form A than on form B by occupying a greater number of sites on the crystal surface of A that are *weaker* than the sites on the surface of form B, in terms of their interaction with water. Weaker, less specific sorption sites on the surface of form A can also account for the much wider variation in water uptake and distribution coefficients observed for this polymorph at 20°C and 25°C, as a function of *RH*. Water sorption at the weaker sites is overcome at sufficiently high temperatures, as observed at 35°C for polymorph A. The significance of these findings rests on the fact that they present different pictures of the surfaces of the two polymorphs. Polymorph A exhibits an "excess" sorption at lower temperatures. Such excess is evidenced in the sorption profile shown in Figure 58 and is the result of water adsorbing on sites which are weaker than those mostly occupied at 35°C. Polymorph B also shows evidence of excess sorption, but it is not directly observable as with polymorph A. Evidence of weaker active sites on the surface of form B is given in the energy profile of Figure 49. It is important to point out that the peak in heat of adsorption observed at 25°C for the two polymorphs is most likely due to a similar effect. And that because the mechanism of water adsorption is hydrogen bonding (which is significantly weakened the higher the temperature), the excess sorption with temperature has to be the result of the increased collision frequency of the water vapour

molecules onto the crystal's surface and other water molecules. It follows that the "excess" sorbed molecules should have greater mobility over the surface, than the molecules adsorbed at the primary (stronger) sites.

In the range of temperatures typical of pharmaceutical processing, polymorph A thus offers a greater ability to interact through a *greater* number of *weaker* active sites on its surface than those present on polymorph B. This situation translates into the energetic equivalent of surface "fuzziness" in the case of polymorph A. A crude but useful analogy on these lines would be to consider the surface of particles of polymorph A as consisting of a material such as Velcro®. In contrast, the surface of polymorph B would consist of a material covered with snap press buttons. Site by site, the interactions of the fuzzy surface are weaker, but they are more numerous and less restrictive in terms of orientation. The net effect is that an energetically fuzzy surface will result in a greater cohesion and/or adhesion energy for the particle as a whole. This explanation is also consistent with the greater detachment from drug-lactose blends, observed for form B (Chapter 3, section 1), as well as with the greater tendency of polymorph A to form particle aggregates determined by electrostatic measurements (Chapter 3, section 2).

Recent Atomic Force Microscopy studies with cimetidine have shown that the surfaces of the polymorphs of this drug are distinctly different. The differences in crystal polymorph surfaces are significant enough as to allow their differentiation by AFM even in polymorph mixtures. [Danesh *et al.*, 2000]. But form the present discussion's standpoint, a very significant development is that Danesh *et al.*, [2000] found that for one of the polymorphs, adsorbed water on the crystal surface actually produced changes in the AFM surface image

obtained. For one of the two polymorphs studied, the surface properties observed by AFM were in fact dependent on the relative humidity under which the AFM analysis was conducted.

The surfaces of the two polymorphs of the present study are energetically different to sufficient degree, as to allow direct and reliable measurements in terms of their interaction with a common probe such as water. These differences can in turn be related to the differences in behaviour between the two crystal forms observed in the study of drug-lactose blends studied by the centrifuge method and by electrostatic measurements. Furthermore, the discussion presented here about the differences in surface energetics between the two polymorphs could also help to support the explanation given in Chapter 5 for the different deposition behaviour these materials exhibit when studying their detachment from lactose upon actuation from DPI devices.

4.2 Inverse gas chromatography (IGC).

The need to predict the behaviour of powders in terms of their dispersive characteristics during aerosolisation has resulted in a resurgence of research on vapour-phase sorption. The use of gas chromatography (GC) as a tool to investigate material interactions and compatibilities offers the potential advantages of control over the chemical and physical environments in the powders under study. Gas chromatography provides accurate control over a wide temperature range encompassing the conditions under which the solid of interest undergoes interactions in pharmaceutical development. In addition, the ability to introduce immediate and precise temperature changes, from sub-ambient to above ambient, makes GC techniques very useful in gathering information about the interactive properties and energy of interaction of powder surfaces.

IGC probe analysis has proven to be successful as a tool in studying structure changes in biopolymers [Carrillo *et al.*, 1988; Gilbert and Roshdy 1989]. Ahmed [1989] determined the solubility parameters of sodium starch glycollate (Explotab) using IGC, in order to calculate the interaction parameter (ϕ) and relative intensities of the cohesive and adhesive interactions in ternary and quinary systems. The IGC technique has also been used in the determination of solubility parameters of pharmaceutical materials such as lactose, salbutamol, cefalexin [Ticehurst *et al.*, 1994 and 1996; Egawa *et al.*, 1992], in studies that characterised the surface properties of such materials before and after processing operations.

In the study reported here, IGC was used to explore the properties of the surfaces of the two crystal polymorphs of Ro 24-5913 and to study the binding energies of a common set of solvent vapour probes onto the two types of surfaces. Powder of the drug was packed as stationary phase into a gas chromatography column. A series of solvent vapour probes of different polarity were injected into the column under different temperature conditions. The resulting elution data were used to calculate the probes' sorption coefficients and other thermodynamic parameters including the enthalpy, entropy and free energy of sorption. The sorption properties of the probes used in IGC are used to examine and compare the hydrophilicity/hydrophobicity properties of the two polymorphs of the drug Ro 24-5913.

4.2.1 Experimental probe analysis of IGC

Selection and preparation of organic probes. The selection of different organic probes for the present study was based on a range of polar and non-polar reactivity. Table 19 provides a list of the different probes used in this study.

Table 19 Reactivity of the probes.

Solvent	Reactivity
Methane	non-interacting probe
2-Propanol (2-POH)	H-Bond donor/acceptor
Methyl Ethyl Ketone (MEK)	Carbonyl H-bonding
Ethyl Acetate (EA)	Carbonyl H-bonding
Toluene (TOL)	π-bond
Hexane, Heptane (alkanes, HX, HEP)	non-hydrogen bonding

Methane (Scott Speciality Gases) was used to determine the dead volume of the column in the probe analysis [Lipson and Guillet 1982]. All other probes were obtained from Fisher Scientific. The IGC technique requires probes to be injected at infinite dilution. In order to achieve this condition, the procedure described below was followed with all solvent probes used: Six separate vials of each probe were prepared, 100 µl of the selected organic solvent probe were placed each into 20-ml, 20-mm neck, head-space glass vials (Wheaton). The vials were capped with 20-mm Teflon® faced butyl septa (Supelco) and crimped with aluminium seals (Supelco). The sealed head-space analysis vials containing the solvent probes were then placed under -10°C conditions. At this temperature, the probe concentration in the overhead vapour phase is reduced, making it possible to withdraw considerably and consistently smaller masses of solvent than would be withdrawn at room temperature using standard GC sampling syringes,. This very practical procedure is remarkably effective in obtaining consistent, close to infinite dilution conditions without the need of specially designed accessories. Five different injection volumes, 5, 10, 25, 50 µl, of organic probe were used. Vapour samples for injection were withdrawn from the head-space of the glass vial containing the solvent probe, and injected into the GC. Using this technique, any possible concentration dependence of retention time could be resolved by extrapolation to zero concentration [Hatzidimitriu 1987]. For each injection volume, triplicate injections were made using gas-tight syringes with luer tip cemented conical needles of 10, 25 and 50 µl volume (Hamilton). A syringe Chaney adapter was also used (Hamilton) for better reproducibility.

The rubber septum at the injection port was changed every 20-25 injections in order to avoid leaking.

The amounts of probes injected into the GC were calculated using the ideal gas law:

$$PV = nRT \qquad (45)$$

where P is the pressure of the organic solvent vapour, V is the injection volume, n is the number of moles, R is the gas constant and T is the temperature (-10°C) expressed in °K.

From equation 45, the mass of vapour injected into the GC ranged from 1.13×10^{-7} to 7.32×10^{-6} g for the different solvent probes. Care was taken to ensure that the probe was introduced instantaneously as a "plug" into the column [McNair and Bonelli 1969]. It took about 15 minutes for the entire probe volume injected to elute from the column to the point at which a chromatogram baseline was re-attained, and this elution time covered all the probes used. Therefore, in order to ensure consistency and reproducibility for all data generated, a time interval of 15 minutes between injections was set.

IGC setting conditions. A Perkin Elmer AutoSystem gas chromatograph was used to measure retention volume. The GC was equipped with a Flame Ionisation Detector (FID) and a flow control system to set pressure and gas flow rate. A column oven was fitted to maintain the column temperature by circulating air. The temperature was maintained constant with a variation of ± 0.5 °C from the set temperatures.

High purity grade helium was used as the carrier gas. The gas carrier gas was further dried and purified before use by passing it through moisture and oxygen traps installed in the gas line feeding the GC. The flow rate for helium was set at 30 ml min^{-1}. A two-stage regulator located on the cylinder was used to set the inlet gas pressure to 80 psi.

The flow rate of the carrier gas was measured at room temperature (25°C) at the outlet of the detector using a soap bubble flow meter (HP Soap film flowmeter) and stop watch. The flow rate measurements were confirmed with an electronic flow meter AccuRate™ 1000, Intelligent Flow Meter (JHW Fison Scientific, Folsom, CA). The variation of the outlet column flow rate through experimentation was less than 0.5%.

The inlet carrier gas pressure was measured with a U-shaped mercury manometer (1 mm Hg precision) and verified with a Chromopack hand held pressure gauge (0.1 psi precision). The outlet carrier gas pressure was assumed to be at atmospheric conditions and measured using a mercury barometer.

The gases necessary for the detector were air and hydrogen (high purity grade). The flow rate for air was set at 450 ml min^{-1} and for hydrogen was 45 ml min^{-1}. The operating temperatures for IGC probe analysis are shown in Table 20.

Table 20. Operating temperatures for IGC probe analysis.

Column temperature:	25°C, 35°C and 45°C.
Injector temperature:	120°C
Detector temperature:	150°C.

Preparation of the Column. Varsano and Gilbert [1973] reported that the specific retention volume is not affected by operating variables such as column length and amount of stationary phase, but that specific retention depends exclusively on the thermodynamic variables of the system. Kontominas *et al.*, [1985] have shown that the effects of temperature and the nature of the stationary phase are considerably more critical than the effect of particle size of the stationary phase. The same authors have determined an optimum column length of 0.635 cm i.d., 11 cm long, particle size of about 75 µm and loading amount of hydrophilic/hydrophobic packing material. These parameters result in feasible conditions for differentiating the retention in the column of the inert agent (Methane) and the probes. Rhue and Rao [1990] used 10-cm long columns to measure retention times for several organic compounds injected into a column packed with 250 µm size fraction soil or aquifer materials.

Experiments in the present study used pre-cleaned instrument grade stainless steal tubing as the body for the columns, the length of the columns was 11 cm with a 0.639 cm o.d. A space of 0.5 cm. was left free at each end of the column in order to place silane-treated glass wool inserts (Supelco, Inc.). The amount of drug powder filled into the column as packing material was determined by weighing the column before and after packing. The column was held in a vertical position and, with the aid of a small funnel, the powder was poured, falling by gravity into the column. Vacuum between 0.5 – 1.0 mm Hg of pressure was then applied to the column outlet, at the same time a mechanical vibrator was used to shake the column while filling, in order to achieve uniform and tight column packing. Drug micronised in the range of

0.5 – 7.0 μm fraction size was filled into the column. Three columns were prepared for each of the drug polymorphs, A and B. Even though the flow properties and surface area of the two polymorphs are slightly different, the mass of powder filled was 0.43g for both forms, due to the fact that the bulk density of the micronised polymorphs is similar. The sample column was separated from the heated injector and detector by two 0.315 cm. o.d. x 20 cm length pieces of copper tubing connected by swage-lok™ fittings. Prior to any sample injections, the column was conditioned by passing dry helium at the experimental column temperature. Depending on the material of interest, 12 or 24 hours are typically necessary for equilibration and to remove possible water picked up during the packing process [Apostolopoulos, 1990]. In the experiments reported here, 12 hours were sufficient at the 25°C under helium flow to condition the column.

4.2.2 Data treatment.

In the gas-solid system, a series of assumptions have to be considered to calculate the thermodynamic parameters [Young 1968; Lipson and Guillet 1982; Hatzidimitriu 1987]:

a. The gas phase behaves as an ideal gas, *i.e.*, no interactions in the gas phase (solute-solute, carrier-carrier or solute-carrier) take place.
b. Henry's law is operative. This definition of ideality for the behaviour of the vapour can be satisfied with the injection of small amounts of solute or probe.
c. The molar volume of the probe does not vary greatly with pressure, *i.e.*, equation 45 is applicable.
d. The mobile and stationary phases are in continuous equilibrium. As the solute (adsorbate) vapour moves along the column, sorption equilibrium is attained instantaneously.

e. The retention volume, and consequently the equilibrium constant, are not affected by the concentration of the adsorbate.
f. The column is isothermal.
g. The adsorbate's adsorption coefficient is constant at the temperature of the experiment.

It is evident that there is some redundancy and overlap among the assumptions listed above. Some assumptions are a prerequisite for, or the direct consequence of another. The explicit long list is provided for convenience.

From IGC experiments, the retention time for a probe or solute on a given column at a given temperature is a property of the solute and its interactions with the stationary phase. The amount of time a solute spends on the column (stationary phase) is the retention time of the probe, t_r. A non-retained probe (*e.g.*, Methane) has a particular retention time, t_m. The value of t_m is a characteristic of each column, and corresponds to the physical travel of the gas from one end of the column to the other, under a given set of experimental conditions. The value of t_m contains no thermodynamic information *per se*; t_m is the direct result of the instrumental configuration used. However, t_m is a parameter that must be known in order to make the necessary corrections to obtain meaningful thermodynamic parameters from the IGC data. Gas chromatography experiments provide measurements of retention time. However, time has no direct application for purposes of the thermodynamic treatment of the data. For a given set of chromatographic conditions, each retention time (t_r) value has a corresponding retention volume, V_r. Retention volume is a thermodynamically meaningful quantity that measures the amount of mobile phase required for the probe sample to elute from the column. The net retention volume is given by:

$$V_n = V_r - V_m \qquad (46)$$

where V_n is the net retention volume, V_r is as defined above and V_m is the column's dead volume, *i.e.*, the retention volume of a non-retained probe (V_r=V_m when t_r =t_m).

Net retention volume is the fundamental parameter measured in IGC. Normalising V_n to the amount of stationary phase, results in the specific retention volume:

$$V_g = \frac{V_n}{W_s} \qquad (47)$$

where V_g is the specific retention volume and W_s is the weight of the stationary phase present in the column. There is no fundamental difference between V_n and V_g, the latter however, is the working parameter used in IGC because it allows for comparison of data obtained from more than one column.

The calculation of the thermodynamic parameters from IGC data can be performed from the V_n (or V_g) values obtained. An alternative treatment of the data consists in the use of the partition (sorption) coefficient, K_s:

$$K_s = \frac{V_n}{W_s\, A_{sp}} = \frac{V_g}{A_{sp}} \qquad (48)$$

where A_{sp} the specific surface area of the powder in the column. As stated, the values of K_s or V_g are obtained from IGC data and either parameter could be used for studying the properties and explaining the behaviour of the surfaces of powders. For instance, Carrillo *et al.,* [1988] related V_g to the degree of 'openness' of structures and to the number of exposed active sites of the sample. A higher value of V_g represented more accessible active sites. Some authors [York *et al.,* 1998] prefer to use K_s for explaining the surface properties and behaviour of powders such as α-lactose monohydrate and dl-propanolol hydrochloride, in terms of the binding energy of adsorption.

In order to make Henry's law operative, V_g and K_s are calculated at infinite dilution. The equilibrium constant in this sorption treatment corresponds to the probe's partition coefficient between the gas and adsorbed phases.

4.2.2.1 Adsorption thermodynamic parameters: Evaluation of Free Energy, Enthalpy and Entropy of Sorption.

The values of K_s obtained from equation 48 can be used to calculate various thermodynamic parameters such as the free energy, enthalpy and entropy of sorption. In the present study, the calculation of the standard free energy of adsorption, ΔG_s^o, is based on deBoer's [Meyer, 1980] arbitrary standard states for the adsorbed (π) and vapour (p) phases. For the standard vapour state of 1 atm, the value is 101 $kN \cdot m^{-2}$, and 0.338 $mN \cdot m^{-1}$ for the standard surface pressure:

$$\Delta G_s^o = -RT \ln\left(\frac{V_g\, p}{A_{sp}\, \pi}\right) \qquad (49)$$

or

$$\Delta G_s^o = -RT \ln\left(K_s \frac{p}{\pi}\right) \qquad (50)$$

The numerical value of ΔG_s^o will be dependent on the choice of standard states as well as on the units used to express p and π. The ratio of the standard states' pressures appears explicitly in equations 49 and 50 because the sorption process involves partitioning of the solute probe between a three-dimensional (volume) and a two-dimensional (surface) phases. The situation of equations 49 and 50 is analogous to that encountered when solubility is the equilibrium constant, which can be expressed in different concentration units.

Enthalpy is a quantity whose value is indicative of the overall balance between binding (exothermic) or repulsive (endothermic) forces prevailing in the system under study. The enthalpy of sorption can be obtained from the following equation:

$$\frac{d \ln K_s}{d(1/T)} = \frac{-\Delta H_s}{R} + C \qquad (51)$$

also

$$\frac{d \ln V_g}{d(1/T)} = \frac{-\Delta H_s^o}{R} + C \qquad (52)$$

where ΔH_s^o is the enthalpy of sorption and C is dependent on the chosen standard states.

The entropy of sorption reflects geometrical factors related to the possible energetically equivalent configurations of the probe on the stationary phase. During sorption, entropy usually decreases due to the localisation of probe molecules at specific active sites of the drug particles' surface. The entropy of sorption is not a directly measurable quantity; it is a calculated parameter whose value is also affected by the choice of standard states, much the same as the free energy:

$$\Delta S_s^o = \frac{\left(\Delta H_s^o - \Delta G_s^o\right)}{T} \qquad (53)$$

where ΔS_s^o is the entropy of sorption and its numerical value is consistent with that of ΔG_s^o (equations 49-50).

The thermodynamic treatment of GC data presented in equations 48 through 53 is the most commonly used and reported in the literature. Lin [1993] and Rhue and Rao [1990] showed that the free energy of sorption is sufficient to differentiate polar from non-polar interactions between vapour probes and solid surfaces. The spreadsheet created for the calculation of the parameters of equations 48 through 53 is given in the Appendix. Detailed discussions on the derivation of thermodynamic parameters from GC data can

be found in Meyer *et al.,* [1973], Meyer [1980], Lipson and Guillet [1982], Gilbert [1984], Rhue and Rao [1990], Lin [1993].

4.2.3 Results and Discussion

Retention time in chromatograms. For the range of concentrations used with the different solvent vapour probes, the peaks showed sharp front profile and diffuse tailing. Skewed peaks in IGC are fairly common, and the peak maximum provides a measure of the retention at infinite dilution. When the peaks show deviation from symmetrical (Gaussian) shape, several methods have been used for determining the retention time of the peak [Conder *et al.*, 1986]. One of these methods is peak maximum (PM), *i.e.*, retention time is measured at the maximum of the skewed IGC peak. The same methodology was used in this study to obtain the retention time.

Figure 51 shows how the sorption coefficient, K_s for both polymorphs changes as a function of probe polarity under isothermal conditions. Overall, polymorph B exhibited greater K_s values for the different probes at the different temperatures investigated. The only exception being 2-POH (a hydrogen bond donor) at 25°C. The figure also shows that at the lower temperatures (25°C and 35°C), the sorption coefficient of the non-hydrogen bonding probes was considerably higher for polymorph B. This difference between the two polymorphs prevails at 45°C, although not as pronounced. These results indicate that dispersion interactions are stronger on the surface of polymorph B than on polymorph A.

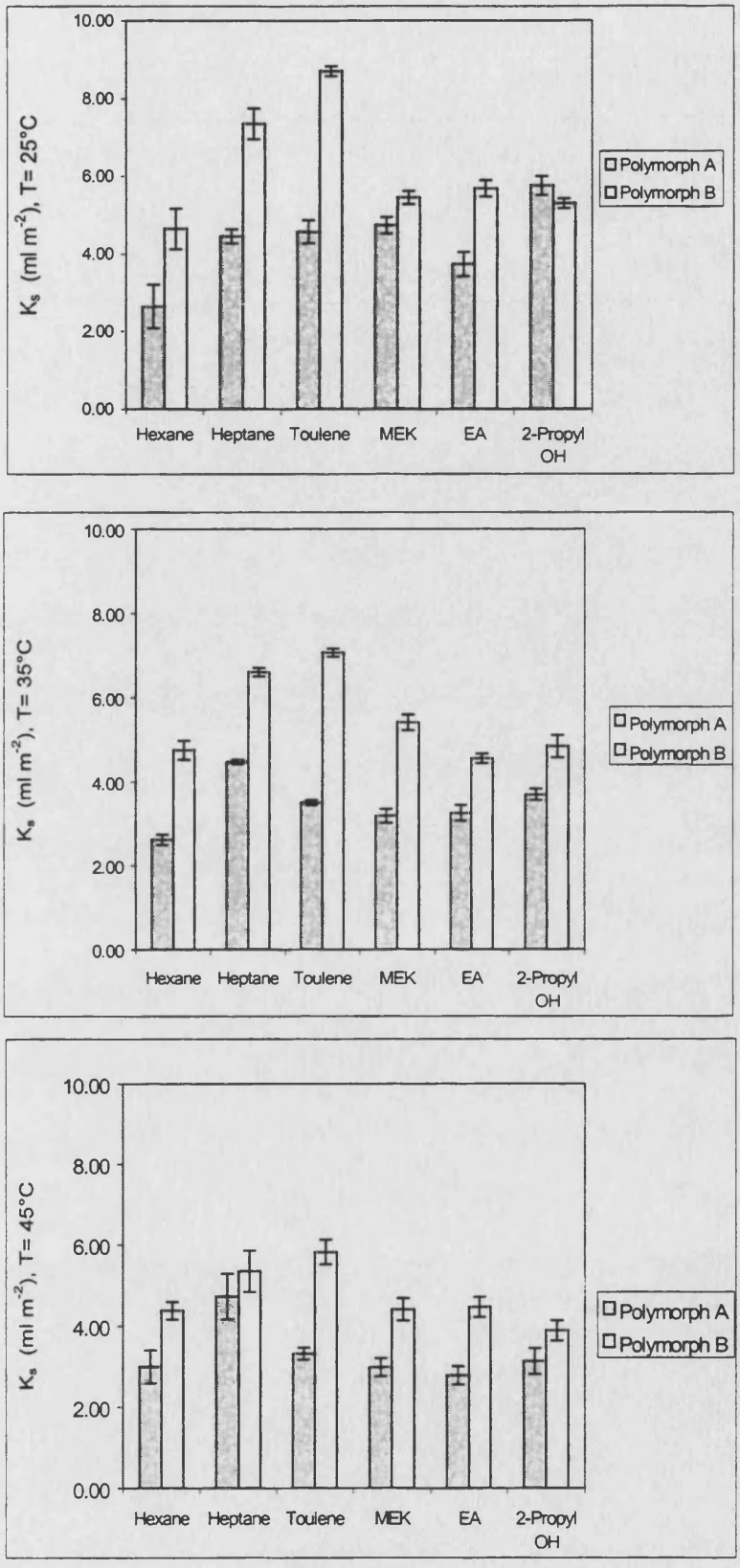

Figure 51 Sorption coefficient for various probes and temperatures for polymorphs A and B (n=18).

Another difference between the two polymorphs observable from Figure 51 is that for polymorph B, the K_s values obtained can be practically used to rank the probes into two groups, hydrogen bonding and non-hydrogen bonding, the latter giving the higher K_s values. A similar contrast cannot be made with the K_s values obtained from polymorph A.

It should be noted that the K_s values show that the surface polymorph B has a stronger affinity for non-polar probes than the surface of polymorph A. However, the higher affinity of polymorph B for non-polar probes is not accompanied by a greater affinity of polymorph A for the polar probes. Polymorph B also exhibits somewhat greater affinity for the polar probes. These results are a strong indication of a composite surface having separate polar and non-polar sites for adsorption.

Figures 52 and 53 show the change in K_s with temperature observed for polymorphs A and B. The data from non-polar and polar probes are shown in Figures 52 and 53, respectively. The figures show that for the majority of the solvent probes, K_s values were lower the higher the temperature. The two alkanes were the exceptions, the sorption coefficient for hexane remained constant with temperature for the two polymorphs. In the case of heptane the sorption coefficient decreased with temperature for polymorph B, while remaining constant with temperature for or polymorph A.

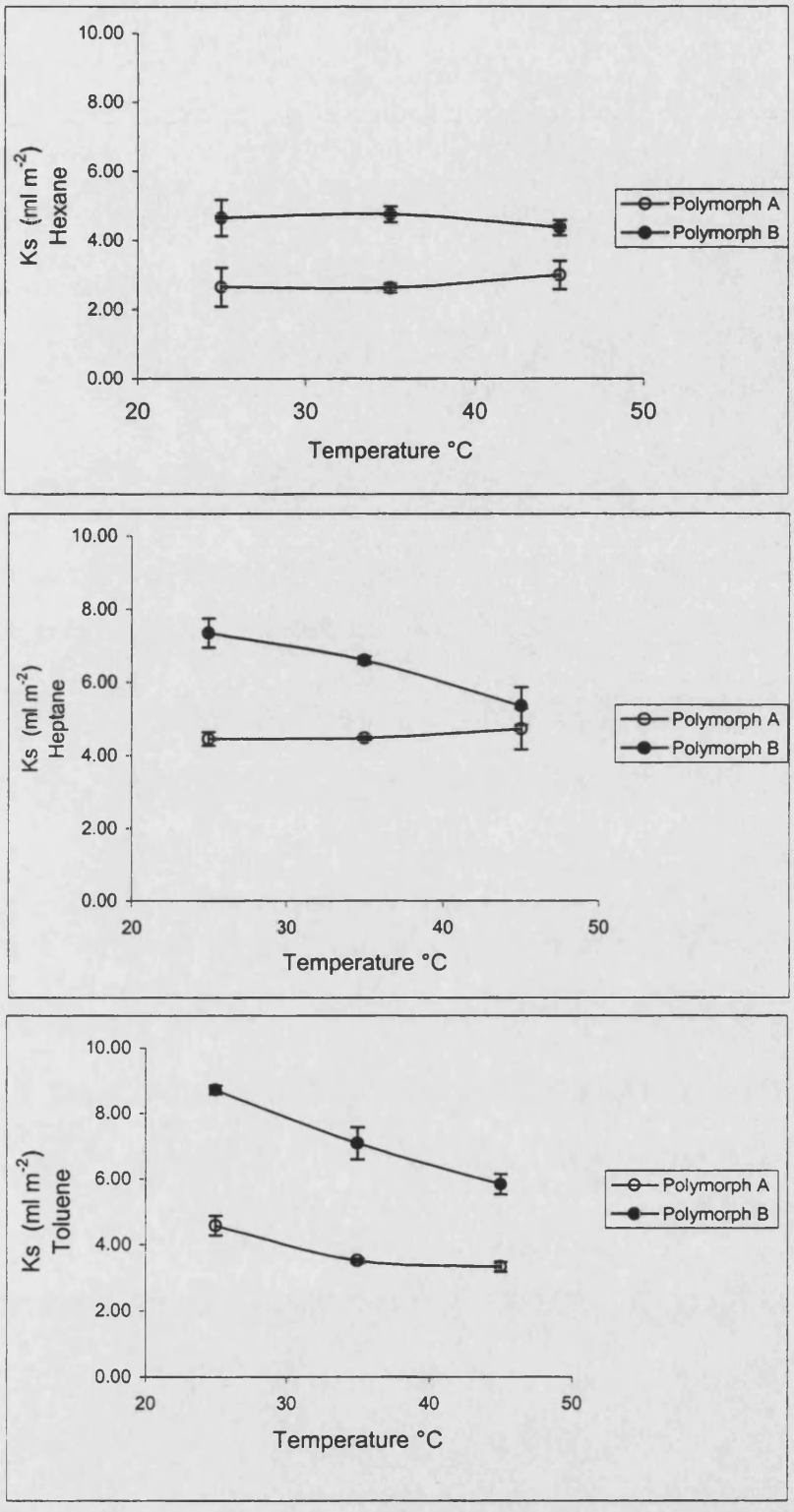

Figure 52. Sorption coefficient for non-polar probes for the two polymorphs as a function of temperature (n=18).

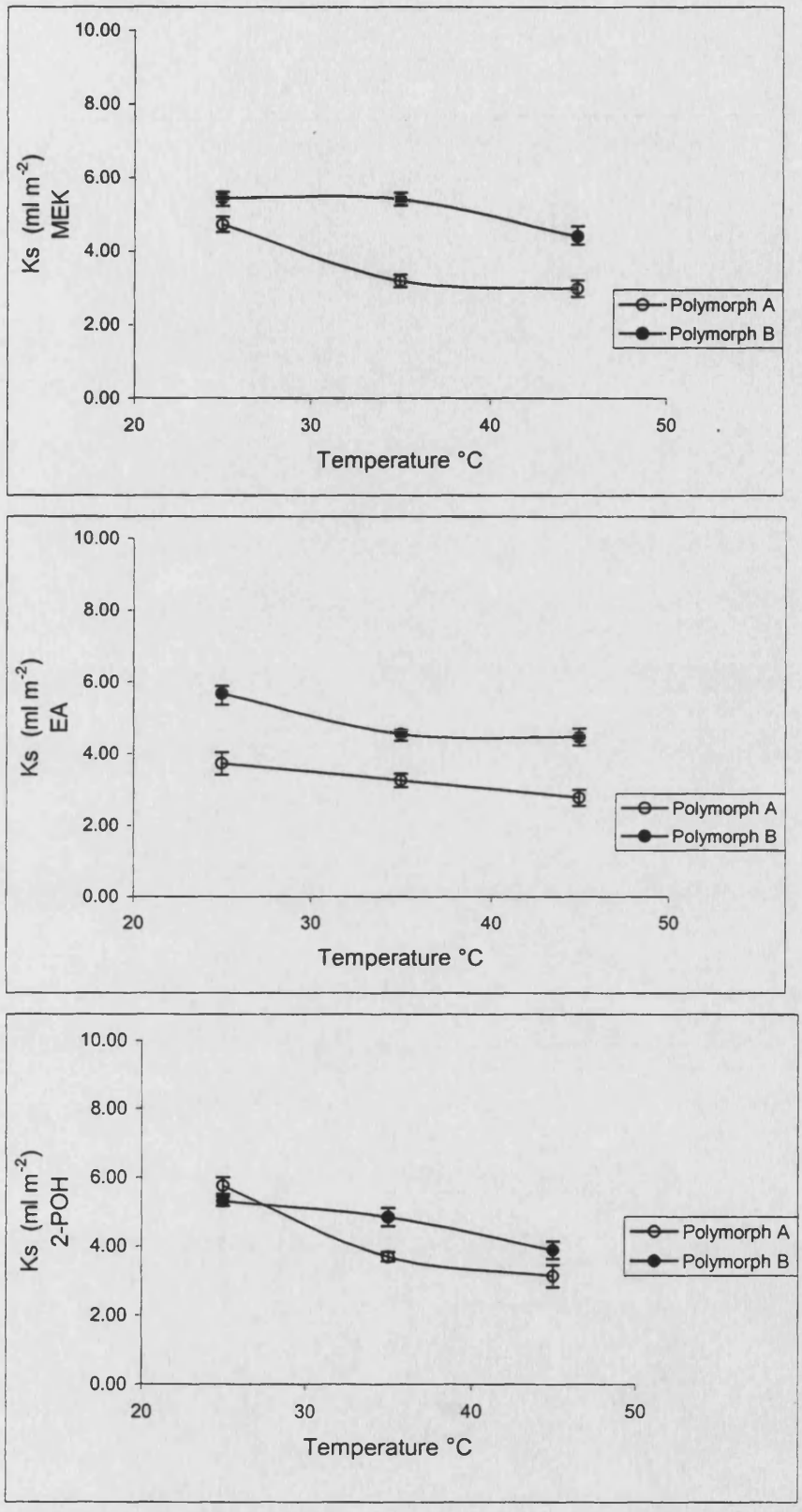

Figure 53 Sorption coefficient for polar probes for the two polymorphs as a function of temperature (n=18).

The values of the thermodynamic parameters of sorption, namely, ΔG_s^o, ΔH_s^o and ΔS_s^o obtained form the IGC data are provided in Tables 21, 22 and 23, respectively. Free energy values obtained form IGC data are more reliable than values obtained for enthalpy or entropy. This is so because in IGC, the free energy value is obtained in a very direct way from t_m (via V_g), the very measurement of IGC.

Table 21. Free energy of adsorption of solvent probes on Ro 24-5913, polymorphs A and B, at 25°C, 35°C and 45°C (n=18).

Probe	**Polymorph A**	**Polymorph B**
	ΔG_s^o (Equation 47) kJ mol^{-1}	
T=25°C		
Hexane	-5.398	-6.793
Heptane	-6.686	-7.929
Toluene	-6.751	-8.351
MEK	-6.839	-7.188
EA	-6.249	-7.292
2-POH	-7.323	-7.120
T=35°C		
Hexane	-5.376	-6.851
Heptane	-6.700	-7.665
Toluene	-6.097	-7.834
MEK	-5.862	-7.172
EA	-5.916	-6.744
2-POH	-6.225	-6.897
T=45°C		
Hexane	-5.707	-6.644
Heptane	-6.835	-7.142
Toluene	-5.958	-7.353
MEK	-5.693	-6.662
EA	-5.517	-6.693
2-POH	-5.816	-6.350

The enthalpy of sorption data listed in Table 22 show an important difference between polymorphs A and B. Toluene gives the highest enthalpy of sorption for polymorph B, whereas for polymorph A, it was the adsorption of 2-propanol what gave the highest enthalpy value. Interestingly, the values of ΔH_s^o for the adsorption of toluene on the surface of polymorph B and the adsorption of 2-POH on the surface of polymorph A, are of comparable magnitude. These results show an important difference between the surfaces of the two polymorphs: the most exothermic interaction for polymorph A is obtained from the adsorption of a hydrogen bond donor (and acceptor), whereas for polymorph B, the most exothermic interaction results from the adsorption of a non-hydrogen bonding probe.

Table 22 Enthalpy adsorption of solvent probes on Ro 24-5913, polymorphs A and B (n=18).

Probe	Polymorph A ΔH_s^o (Equation 48) kJ mol^{-1}	Polymorph B
Hexane	13.647	-10.486
Heptane	10.772	-78.524
Toluene	-49.659	-113.952
MEK	-69.559	-40.602
EA	-42.800	-48.546
2-POH	-103.967	-55.552

The IGC data obtained cannot be used to make reliable assessments of the enthalpy of adsorption of hexane with both polymorphs and hexane with polymorph A. The reason for this situation is visually apparent in Figure 52. Equation 51 calculates the enthalpy based on the change of sorption with

temperature (van't Hoff calculation), and as Figure 52 shows, the equilibrium constant was invariant with temperature in the case of hexane, as well as for heptane and polymorph A. But even if the enthalpy of sorption cannot be calculated in these cases, the constancy of K_s with temperature is in itself quite revealing.

The adsorption of a vapour onto a surface is an exothermic process, and in its simplest form, one manifestation of the exothermic nature of adsorption is a decrease in K_s with temperature (the fundamental relationship is given in Equation 51). Consider the K_s values obtained for hexane (see Figure 52), which remain constant with temperature for the two polymorphs. The practically flat profiles of K_s *vs.* T could be the result of very low heats of adsorption, not resolvable with the error inherent to the experimental methodology used. But such an explanation would not be convincing, because it must reconcile adsorption coefficients of similar scale as those obtained with other (measurably exothermic) adsorbates, but without the evolution of any heat. A more plausible explanation would be that there is an additional component to sorption on these surfaces. The additional sorption component would be necessarily athermal; excess sorption resulting of excess free energy at the adsorbent's surface. The excess free energy at the surface could in turn be explained in terms of imperfections or defects on the crystal surface, giving place to a predominantly athermal (less negative entropy change) excess sorption. Evidence of excess sorption was also observed with water as the probe under conditions far removed from infinite dilution (Chapter 4, section 1).

Table 23 lists the values of entropy of adsorption obtained from the IGC results. The limitations encountered when calculating the enthalpy change are carried over (through Equation 53) into the calculation of ΔS_s^o. This is particularly true for the adsorption of the alkane probes on polymorph A. The ΔS_s^o for hexane and heptane on polymorph A are obvious overestimates, since adsorption is accompanied with, thus disfavoured by, a negative entropy change.

Table 23 Entropy of adsorption of solvent probes on Ro 24-5913, polymorphs A and B (n=18).

Probe	Polymorph A ΔS_s^o (Equation 50) kJ mol^{-1} °K^{-1}	Polymorph B
T=25°C		
Hexane	0.069	-0.017
Heptane	0.063	-0.241
Toluene	-0.139	-0.360
MEK	-0.209	-0.113
EA	-0.168	-0.142
2-POH	-0.325	-0.162
T=35°C		
Hexane	0.067	-0.017
Heptane	0.060	-0.233
Toluene	-0.136	-0.350
MEK	-0.202	-0.113
EA	-0.161	-0.138
2-POH	-0.315	-0.160
T=45°C		
Hexane	0.064	-0.015
Heptane	0.056	-0.225
Toluene	-0.133	-0.339
MEK	-0.198	-0.110
EA	-0.156	-0.135
2-POH	-0.307	-0.156

One of the concluding remarks of Chapter 4 (section 1) reads as follows: "The surfaces of the two polymorphs of the present study are energetically different to sufficient degree, as to allow direct and reliable measurements in terms of their interaction with a common probe such as water." The same statement can be made about the results from IGC obtained here with all solvent probes investigated. It is important however, not to take the IGC data as simply another technique capable of showing differences between the two polymorphs of Ro 24-5913. Because the infinite dilution conditions used in IGC experiments, make the obtained results uniquely informative about the nature of the surfaces under investigation.

As discussed in Chapter 2 (section 2), the two polymorphic materials were subjected to a milling process in order to reduce the particle size of the crystals, from a few hundred microns (Figure 13) to the particle size distribution shown in Figure 17, which has a mean particle size smaller than 5 μm. Milling produces a significant increase in the surface area of the crystals. However, the exposure of the original crystals to the mechanical stress of the milling process, raises questions about whether or not the surface of the micronised crystals retains the crystalline character of the native (unmilled) material.

The existence of crystal defects, even at the core crystalline phases is well established, and to such a degree that the subject has been covered in some classical works [Kitaigorodskiy, 1967]. Because of the inherent excess free energy of surfaces and interfaces, crystal surfaces can be expected to have a higher incidence of defects than the core of the corresponding crystal. After all, the "carrier" of the excess free energy of a surface is the surface molecules themselves. Recall that an excess amount of free energy

corresponds to a gain in enthalpy of the molecule and/or a gain in entropy. A gain in enthalpy reflects a weaker interaction of the molecule with its neighbours, whereas a gain in entropy reflects a wider level of variation in the molecule's position or orientation relative those of a molecule in the core crystal.

It is widely accepted that the mechanical energy applied to the crystals during micronisation results in a reduction in the level of crystallinity of the surface, compared with the crystallinity of the un-milled crystal surface. The highly intuitive appeal of this concept, in addition to the experimental evidence in support of it, can easily lead to the presupposition that the crystalline nature of the surface of the two polymorphs used here, was obliterated during milling, such that the differences observed between the two (milled) materials no longer reflect the crystalline character of their surfaces. The IGC technique is particularly well suited for addressing such a question, as will be done next for Ro 24-5913.

The adsorption data of hexane in Figure 52 strongly support the concept of defects present at the surface of the two micronised polymorphic materials. As discussed, the apparently athermal adsorption of hexane onto both polymorphs can be explained as the result of some degree of molecular disorder at the crystal's surface. But the question at hand is not so much about the presence of molecular disorder on the crystals' surfaces, after all, even un-milled crystals are expected to exhibit some degree of molecular disorder at their surfaces. The question here is about the extent of molecular disorder on the surface of the micronised crystals, and its effects on surface interactions. It should be recalled that the crystalline character of a surface is

not an either/or attribute; surface molecules need not be either crystalline or amorphous. The crystalline character is a rather gradual attribute, determined by the free energy content of the molecules at the surface. Surface molecules can have the free energy of the (super-cooled liquid) amorphous or crystalline states, as the high and low extremes, respectively, and any value in between.

The presupposition that micronisation makes the surface of the resulting crystals lose its crystalline character bears implications worth examining under the light of the experimental evidence from IGC data. If milling produces changes on the particles' surface such that the surface no longer corresponds to either polymorph A or B, the crystalline structure would have to be totally disrupted at the surface, giving place to a predominantly amorphous surface. The amorphous content of a surface, being thermodynamically more energetic in relation to the crystal, results in more (energetically) active sites for adsorption. A factor critical to the present discussion is that IGC experiments are done under infinite dilution conditions. Since the most active adsorption sites of the adsorbent are the first to be populated [Vemulapalli, 1993], infinitely diluted vapour probes will adsorb onto the most active sites available at the surface. The IGC-derived adsorption coefficients (Figure 51) are thus measurements of vapour adsorption restricted to the most active sites available at the surfaces of the two polymorphs investigated. It follows that if the amorphous content of the polymorphic surfaces after milling were the determining factor in the powders' observed interactions, the infinite-dilution adsorption coefficients would have to be the same for polymorphs A and B, with all vapour probes, under all temperatures investigated. For if the two polymorphs produce the same amorphous phase, and their interactive

behaviour does not reflect their crystalline character, they should be indistinguishable as adsorbents under infinite dilution conditions. But the two polymorphs are clearly distinguishable as adsorbents, in fact, even for the adsorption of hexane, which shows clear evidence of the effects of molecular disorder at the surface (Figure 52), the adsorption coefficients for polymorphs A and B are still distinctly different.

Another finding from IGC relevant to the present discussion is the fact that one of the two surfaces investigated (polymorph B) showed stronger affinity for both polar and non-polar vapours. This result is also in conflict with the presupposition of crystal disruption, which attributes a disordered, non-crystalline character to the surface of the powder particles as the result of the micronisation process. An amorphous phase is in essence a super-cooled liquid, and a surface that exhibits stronger interactions with both polar and non-polar adsorbates than another surface of exactly the same chemical composition, requires a degree of structural order characteristic of crystals, not liquids.

Any physical model put forth to envisage a system under study starts based on a hypothesis or a presupposition. But in the end, the physical model must be backed up by, and consistent with experimental evidence. The presupposition that the milling process somehow masked the crystalline differences between polymorphs A and B, requires a non-crystalline surface. But the fact that that the infinite dilution adsorption coefficients obtained with the two polymorphs (for all vapours investigated) are different, requires in turn that upon milling, each polymorph gave place to a different non-crystalline phase. Two different amorphous phases of identical chemical composition

have been found to exist. But such a phenomenon, observed with a mixture of metal oxides, is extremely rare, and by no means easily achieved in the laboratory [Angell, 1995].

A physical model in which the particles of the two polymorphs retain their crystalline character at their surfaces, even after milling, is a more plausible explanation for the differences observed between the two crystal forms. It is very likely that the degree of molecular disorder at the surface of the micronised particles is greater than that of the original crystals. However, the results obtained indicate that the extent of molecular disorder produced upon milling is not sufficient to mask or obliterate the crystalline character of the surfaces under study. Adherence to the presupposition that the differences demonstrated between the powders are due to surface differences introduced during micronisation, rather than due to the surfaces' crystalline character, would require the scientist either to dismiss the collected experimental evidence in favour of the lack of experimental evidence supporting the applicability of the above-stated presupposition to the system under study, or to fit the obtained results to a border-line fantastic physical model that requires "poly-amorphism" of Ro 24-5913 in order to be consistent with the data. The fact remains that the surfaces of the two polymorphs are different when scrutinised under infinite dilution conditions and also under conditions far removed from ideality (Chapter 4, section 1). And, the experimental evidence indicates that the surfaces' behaviour predominantly reflects their crystalline character, even if the polymorphs are not (and they need not be, before nor after milling) perfect crystals at the surface.

5. *IN VITRO* DRUG DEPOSITION CHARACTERISTICS

An investigation of the *in vitro* drug deposition characteristics of the powders of the two polymorphs was conducted. The practical significance of the drug-drug and drug-carrier interactions, as determined in earlier chapters, is examined here within the framework of their functionality as dry powder formulations for inhalation, by investigating the *in vitro* drug deposition characteristics of the binary dry powder formulations of the two polymorphs. In this section of the study, the investigation will focus on how the differences observed between the two polymorphs would be expected to affect the powders' behaviour in dry powder formulations. An attempt is made to establish a connection between emitted fine particle dose and the interactive adhesion or electrostatic forces present among the particles in binary dry powders for inhalation.

5.1 Materials and Methods

Binary powders mixes of drug with α-lactose monohydrate of different drug concentrations, as described and characterised in Chapter 2, were used for each polymorph.

The fine particle and emitted doses of powder blend formulations were determined using a modified twin stage liquid impinger (TSI) described as apparatus A in the British (1988) and United States (1992) Pharmacopeias. Powder was aerosolised from a dry powder inhaler prototype Dryhaler ™(Dura

Pharmaceuticals) at a flow rate of 60 l min^{-1} and collected from each of the two stages of the TSI (Figure 54). At a flow rate of 60 l min^{-1}, stage II of the device is known from pre-calibration data, to collect fine particles with aerodynamic diameters smaller than 6.4 µm. Stage I collects particles having an aerodynamic diameter greater than 6.4 µm. Drug particles that penetrate into stage II are considered to be fine enough to have the potential to penetrate into the lung. The amount of drug collected in stage II was thus defined as the fine particle dose.

Replicate experiments of six measurements were conducted under controlled conditions of relative humidity (24% *RH*) and temperature (18°C). A load of 10 mg of the powder blend from each of the formulations was used for each measurement with either polymorphic form of the drug. Powder blends were weighed and then added directly into the sample compartment of the Dryhaler. The DPI was attached to the glassware mouthpiece inlet using a specially moulded PTFE mouthpiece adapter. The TSI Apparatus was set up using a volume of 5 ml of diluent solution (ACN:H_2O, 50:50) which was placed into the round bottom flask in stage I of the impinger apparatus. In order to ensure that the TSI was operating at 60 l min^{-1} with the DPI device in position, a custom-made airflow calibration glass housing (ACGH) was fitted as shown in Figure 55. After adjusting the flow rate to 60 l min^{-1} using a flowmeter (Gilmont), the ACGH was removed from the TSI set-up. The formulated powder was discharged from the DPI device over a four-second period using a three way solenoid-operated valve timer (ASCO Products, NJ. No. 8300D724) activated at a flow rate of 60 l min^{-1}, using an appropriately set vacuum pump. After the discharge period, the DPI device

was carefully removed from the mouthpiece adapter. The Dryhaler DPI was re-weighed and any weight loss was accurately recorded using an analytical balance (Mettler AE260, Delta Range. Mettler-Toledo Inc.). The TSI was disassembled and the powder samples collected in stages I and II were separately washed out with the diluent solution. Each wash-out sample was analysed by HPLC as described in Chapter 2.

The washing of the TSI apparatus is a critical part of the analytical procedure and was therefore performed with the required meticulous care. Stage I of the glassware (throat, neck tube and the upper impingement chamber) was rinsed with solvent and placed into a 50 ml amber volumetric flask. Stage II of the TSI glassware was also rinsed with the diluent solution and collected in a 25-ml amber volumetric flask. The collected washing solutions were then filled up to the mark with the same diluent solution and mixed thoroughly. The solution from each volumetric flask was filtered through a 0.45 µm membrane and transferred into HPLC amber glass vials with PTFE-lined caps. Samples were analysed using the HPLC methodology described in Chapter 2. The DPI device was thoroughly cleaned with a cotton swab dampened with Methanol, in readiness for the next set of experiments. Clean TSI glassware and terminal filter (glass fibre filter from Gelman Sciences type A/E 47 mm with stainless steel holder) set was assembled in readiness for the next set of experiments.

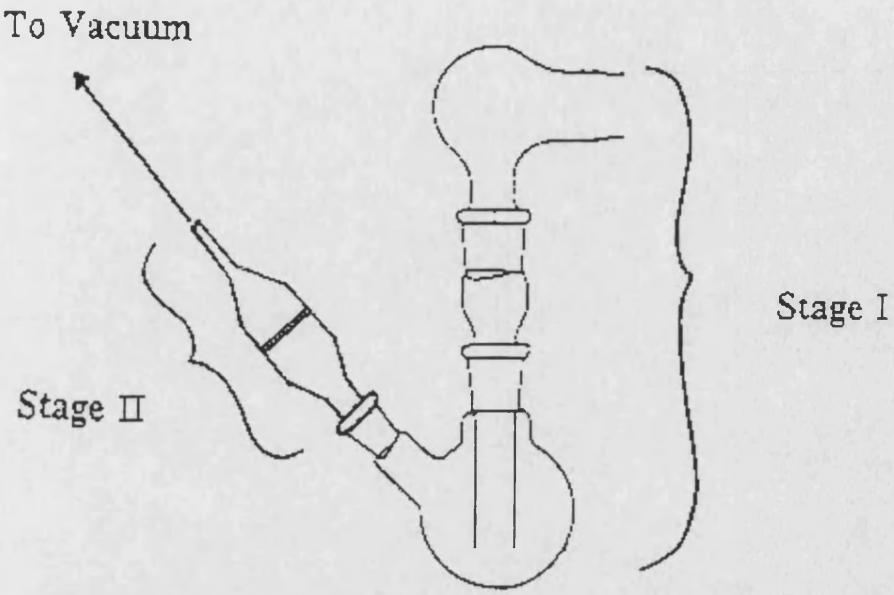

Figure 54 Modified Twin Stage Liquid Impinger.

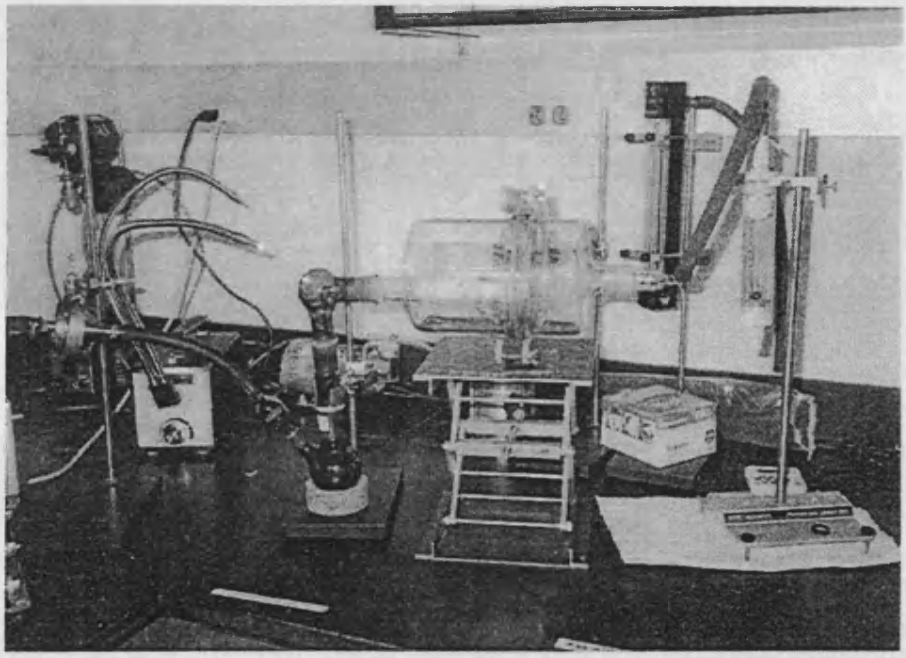

Figure 55 Photograph showing the air flow calibration housing set-up.

The powder blend formulations used for the in vitro evaluation of their performance cover a drug concentration between 1% and 50% (w/w) for each polymorph of Ro 24-5913. However, the information obtained from the evaluation of both polymorphic formulations, would be more useful if examined from a common reference framework for the two crystal forms. The monolayer coverage concentration can be used as a common concentration reference point for the two polymorphs, allowing objective comparisons between them. The monolayer coverage corresponds to the drug concentration in the blend, necessary to completely cover the carrier particles. The number of drug particles, N, needed to completely cover one α-lactose monohydrate particle is:

$$N = \frac{T_L}{A_D} \tag{54}$$

where T_L is the total surface area of an α-lactose monohydrate particle and A_D is the cross-sectional area of a drug particle:

$$T_L = 4\pi\left(\frac{d_L}{2}\right)^2 \tag{55}$$

and

$$A_D = \pi\left(\frac{d_D}{2}\right)^2 \tag{56}$$

where d_D and d_L are the diameters of the drug and α-lactose monohydrate particles, respectively. Each of the N drug particles is a circular "tile" used to

cover the surface of one particle of the carrier. The mass of a group of N drug particles, M_D, is given by:

$$M_D = N V_D \rho_D \qquad (57)$$

where ρ_D is the drug's absolute density and V_D is the volume of a drug particle:

$$V_D = \frac{4}{3}\pi\left(\frac{d_D}{2}\right)^3 \qquad (58)$$

In this calculation, an amount of drug weighing M_D is used to cover *one* particle of α-lactose monohydrate, which has a weight, M_L, as follows:

$$M_L = \frac{4}{3}\pi\left(\frac{d_L}{2}\right)^3 \rho_L \qquad (59)$$

where ρ_L is the absolute density of α-lactose monohydrate.

The weight percent drug needed for the complete coverage of a lactose particle, F_D, is thus given by:

$$F_D = \frac{M_D}{M_D + M_L} 100 \qquad (60)$$

An alternative treatment [Clark, 2001], gives the following expression:

$$drug\ mass\ fraction = \frac{1}{1+\frac{1}{4}\frac{d_L}{d_D}\frac{\rho_L}{\rho_D}} \qquad (61)$$

Table 24 gives the calculated drug concentration for monolayer coverage of α-lactose monohydrate as well as the parameter values used for the calculations (Equations 55-60). The monolayer coverage concentration values obtained are 9.4% w/w and 8.8% w/w for polymorphs A and B, respectively.

Table 24. Surface coverage calculations for Ro 24-5913 in α-lactose monohydrate (45-106 µm).

Material	Density ($g\ ml^{-1}$)	Diameter dv_{50} (µm)	Monolayer Coverage (% weight)
α-lactose monohydrate	1.52	75	----
Form A	1.21	2.4	9.37
Form B	1.27	2.2	8.84

5.2 Results and Discussion

The emitted and fine particle dose (ED and FPD) were determined for two polymorphs of the drug, A and B. The performance of each blend with the Dryhaler was measured in terms of three parameters: device emptying, fine particle fraction (FPF) and formulation/device performance. Device emptying

corresponds to the ratio of ED to the nominal dose (ND). The fine particle fraction (FPF = FPD/ED) is a parameter useful as a way to assess the "dispersion" ability of powders. The formulation/device performance is calculated as FPD/ND x 100.

Micronised drug Ro 24-5913. Since in formulating powders for inhalation there is the option to use 100% of the active ingredient, neat Ro 24-5913 was loaded into the DPI device. Table 25 shows the deposition characteristics, emitted, fine particle and dispersion percentages for the pure micronised Ro 24-5913 drug. When neat Ro 24-5913 was emitted from the DPI, it was observed that the device emptying was approximately 50%, of which, about 65% (32.5% of the total dose) was in the size range of less than 6.4 μm. Nevertheless, some practical problems were encountered resulting from the highly cohesive and electrostatic nature of the drug. A weight of 2 mg of drug proved to be a difficult sample size to weigh and handle, as the powder is light, bulky and easily charged. For these reasons, Ro 24-5913 was blended with a carrier (α-lactose monohydrate), in order to ensure accurate dosing.

Table 25 Deposition Characteristics for drug alone Ro 24-5913 emitted from Dura Dryhaler at 60 l min^{-1} and powder load in the DPI of 2 mg. Values in parentheses are standard deviations for n=3.

Batch	FPD/ED %	ED/ND%	FPD/ND%
Ro 24-5913 drug polymorph A	65.36 (4.96)	47.67 (2.14)	31.12 (2.29)

Note: FPD=fine particle dose; ED=emitted dose; ND=nominal dose

5.2.1 Blends of Ro 24-5913 polymorph A

Four blends of Ro 24-5913 polymorph A with α-lactose monohydrate were prepared, the concentrations of the blends were 1, 5, 25 and 50% w/w, as described in Chapter 2. Table 26 gives the fine particle and emitted dose data for the blends of Ro 24-5913 polymorph A with α-lactose monohydrate formulations emitted from the Dryhaler. At the low drug concentration of 1%, Ro 24-5913 was found to have a low fine particle fraction and high device emptying. At a drug concentration of 25% w/w in α-lactose monohydrate, Ro 24-5913 was found to have slightly higher fine particle fraction than at 1% w/w, but device emptying efficiency was considerably lower. At the high drug concentration of 50% w/w, intermediate values were obtained for both the percent of fine particles and device emptying. However, at this high drug concentration, the resulting powder blend was very cohesive and highly charged, presenting problems similar to those encountered when using the neat drug. The 5% w/w mix showed high fine particle percentages and device emptying.

Table 26. Deposition characteristics for blends of Ro 24-5913 Form A/α-lactose monohydrate emitted from the Dryhaler at 60 l min^{-1} and powder load in the DPI of 10 mg. Values of standard deviations for n=6.

	Drug Concentration [Ro 24-5913] A % w/w	Fine Particle Fraction FPD/ED %	ED/ND %	FPD/ND %
Mean	1	27.14	88.56	24.08
Std Dev.		2.62	6.87	3.38
Mean	5	33.70	73.19	24.69
Std Dev.		2.98	0.86	1.10
Mean	25	30.19	39.55	12.01
Std Dev.		1.34	2.45	1.94
Mean	50	25.87	60.18	15.46
Std Dev.		2.63	5.74	0.77

At 5% w/w drug concentration, the interaction between drug and carrier was near optimal for purposes of effective detachment of drug from carrier and also in terms of the flow properties of the drug-carrier powder blend, resulting in higher deposition characteristics when compared to the other three drug concentrations. These results are in agreement with the results obtained with a similar blend system described by Ahmed *et al.* [1994], whose study also included the effect of the carrier-to-drug ratio under two different airflow rates (30 and 60 l min^{-1}). Those authors' results showed that the fine particle percent values were constant and independent of flow rate for the 5 and 25% w/w blends.

5.2.2 Blends of Ro 24-5913 polymorph B

Aerosol testing was also conducted with blends of Ro 24-5913, polymorph B, with α-lactose monohydrate, using the same drug concentrations as for polymorph A, *i.e.*, 1, 5, 25 and 50% w/w. Table 27 shows the results obtained for emitted dose, fine particle fraction and formulation/device performance for the blends of Ro 24-5913 polymorph B.

The effect of drug concentration in blends of polymorph B, as shown in Table 27, was found to be optimal at 25% w/w. Although the device emptying was higher at the 5% drug level than at 25%, powder blends containing 5% of polymorph B produced nonetheless the lowest fine particle fraction values.

Table 27. Deposition studies for blends of Ro 24-5913 Form B/α-lactose monohydrate, emitted from the Dryhaler at 60 l min^{-1}. Values of standard deviations are for n=6.

	Drug concentration [Ro 24-5913] B % w/w	Fine Particle Fraction FPD/ED %	ED/ND %	FPD/ND %
Mean	1	28.14	47.91	15.29
Std Dev.		6.22	12.92	5.06
Mean	5	13.80	79.49	10.93
Std Dev.		1.03	4.28	0.26
Mean	25	43.35	53.94	23.36
Std Dev.		2.69	3.76	1.76
Mean	50	28.51	57.09	16.19
Std Dev.		2.69	4.19	0.70

5.2.3 Comparison of performance between polymorphs A and B of Ro 24-5913.

Figures 56, 57 and 58 show the device emptying efficiency (ED/ND), the powder formulation/device performance (FPD/ND) and fine particle dose percentage (FPD/ED), respectively, as a function of crystal form and drug concentration for the two polymorphs.

The greatest difference in device emptying between the two polymorphs was observed at 1% drug concentration, as shown in Figure 56.

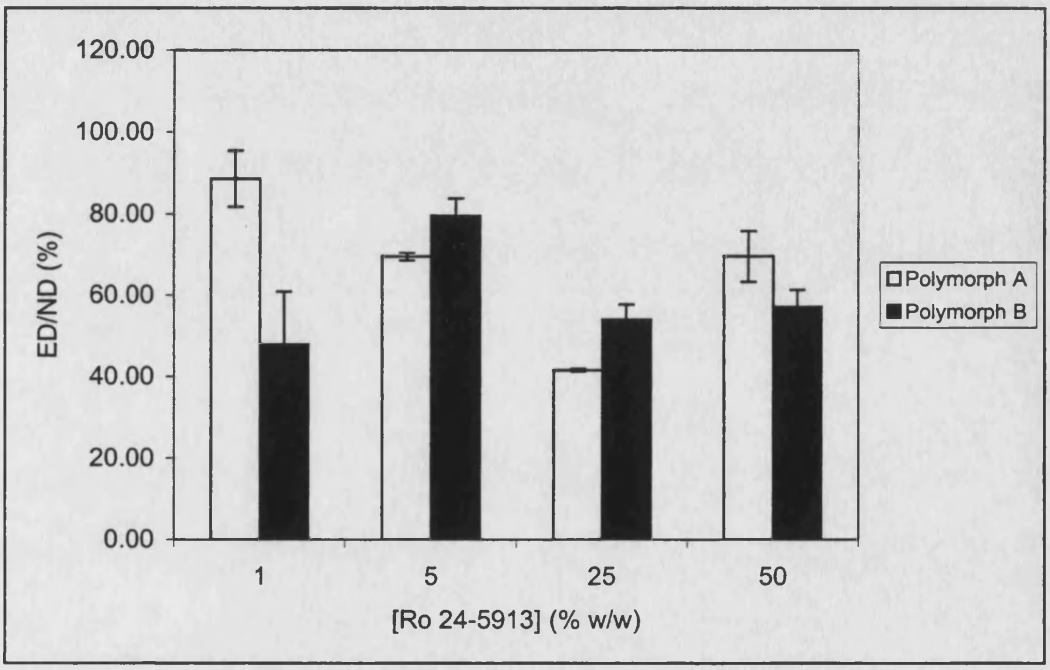

Figure 56. Device emptying represented by ED/ND for binary powder blends of Ro 24-5913 polymorphs A and B in α-lactose monohydrate (n=6).

Figure 57 shows the ratio of fine particle dose to nominal dose (FPD/ND) for blends of the two crystal forms of Ro 24-5913. The FPD/ND ratio is a measure of the amount of drug loaded into the device that was

emitted as particles of size smaller than 6.4 µm. The FPD/ND ratio can also be seen as a measure of the ability of the powder formulation/device system to produce powder in discrete particles viable for delivery into the deep lung; the higher the ratio the more effective the powder's performance. The performance of a powder formulation is dependent upon a combination of the powder's dispersion within, and its emptying from the DPI device.

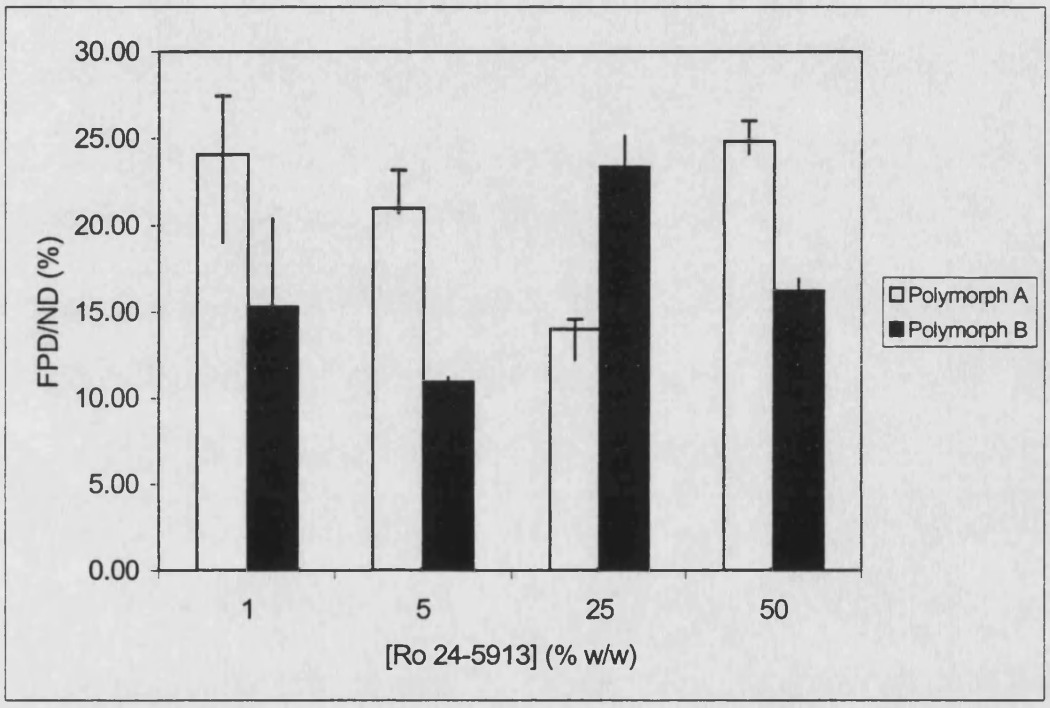

Figure 57. Formulation/Device performance (FPD/ND) for formulations of Ro 24-5913, polymorphs A and B, in α-lactose monohydrate (n=6).

Dispersion of the powder into discrete particles is achieved through the application of mechanical energy to the powder in an amount sufficiently high to overcome the cohesive forces between drug particles and adhesive forces between carrier and drug particles [Byron, 1986]. The energy applied was the same for both polymorphs, A and B, of Ro 24-5913, since the same DPI device

and airflow rate were used. Therefore, the differences in performance observed between the two crystal forms are the result of the polymorphs' different physical properties.

Figure 58 shows that the optimal dispersion of the drug into fine particles occurs at drug concentrations of 5% and 25% for polymorphs A and B, respectively. It is worth noticing that between the 5% and 25% concentrations, there is a relative reversal in optimal dispersion efficiency between the two polymorphs. At a drug concentration of 5%, polymorph A shows more efficient dispersion into fine particles than polymorph B, whereas at the 25% drug level, polymorph B shows more efficient particle dispersion. Another difference between the two polymorphs is that in the case of polymorph A, a decrease in dispersion efficiency takes place when the drug concentration is increased from 5% to 25%. Conversely, in the case of polymorph B, the same change in drug concentration results in an increase in dispersion efficiency. The 5% and 25% drug concentration levels roughly correspond to half and two-and-a-half times, respectively, the drug concentration needed for monolayer coverage of the carrier particles with the drug. Polymorph A shows optimal dispersion efficiency at a concentration below the monolayer level, that is, at drug levels where dispersion involves predominantly overcoming adhesion forces. Polymorph B in contrast shows optimal dispersion at a concentration where cohesion interactions play a very significant role in the formulation behaviour. Polymorph A produces better dispersion into fine particles at the lower concentration because of its weaker adhesive properties. These findings are consistent with the weaker adhesive

interactions of polymorph A observed in the surface probing studies of Chapter 4. Polymorph B, on the other hand produces more efficient dispersion into fine particles at the lower concentration because of its weaker cohesive properties, compared with polymorph A. These results are consistent with the stronger cohesive nature of polymorph A observed in the electrostatic studies of Chapter 3.

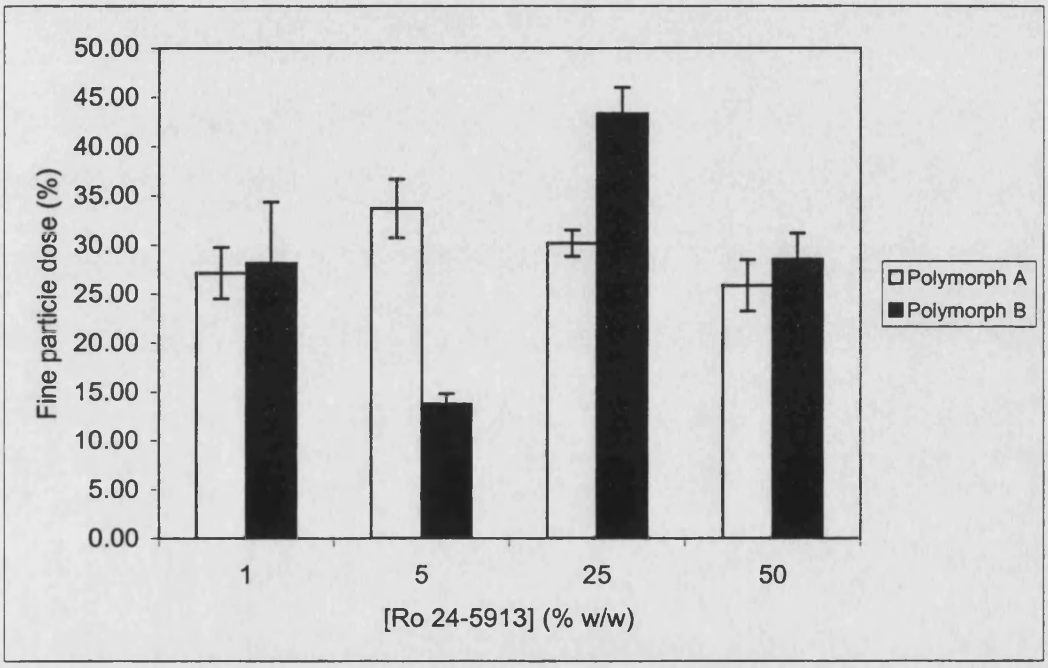

Figure 58. *In vitro* drug deposition data for binary powder blends of Ro 24-5913, polymorphs A and B, in α-lactose monohydrate (n=6).

Table 28 gives the comparison of the removal forces by centrifugation with the fine particle fraction. The table shows that there is no discernible correlation between drug detachment by centrifugation and the emitted fine particle dose for either polymorph. In each case where detachment was measured by the centrifuge method, polymorph B showed the greater value

between the two crystal forms. A plausible explanation for such a bias in the centrifuge data is the stronger cohesive nature of polymorph A. Cohesion of particles of polymorph A may produce agglomerates that are sufficiently large and stable to remain in the sample chamber of the centrifuge cell, thus accounted as undetached drug. Drug detachment in both the TSI and centrifuge methods occurs upon the application of a detachment force. But the mechanics of the applied detachment force in each case is different at least in one respect: in the centrifuge method, a mono-directional centrifugal acceleration is applied throughout the experiment, the result is a mono-directional detachment force whose magnitude depends on the mass of the particle experiencing the force. In the TSI set-up, drug detachment occurs by placing the powder blend particles into a turbulent flow. Needless to say, in the TSI experiment, the accelerations experienced by the particles vary widely, and the resulting detachment forces are anything but mono-directional.

Table 28. Comparison of the removal forces with fine particle dose.

Conditions:	Centrifugation at 5000 rpm (n=4) R.C.F= 3021.32 % Removed		TSI: fine particle percent of the emitted dose (n=6) % FPD/ED (fine particle)	
% Drug	Form A	Form B	Form A	Form B
1	1.91	4.88	27.14	22.65
5	14.87	18.40	33.70	13.80
25	17.48	21.41	30.19	43.35
50	ND	ND	25.87	28.51

The centrifuge method gives detachment values that are considerably lower than the corresponding TSI deposition values. This is most likely

explained by the unavoidable wedging of the particles in the mesh of the centrifuge cell, which combined with the mono-directional detachment, significantly restricts the amount of drug collected in the receiving chamber of the cell. Only a portion of the drug particles, those attached to the cross-sectional area facing the cell's collecting chamber can be detached. Another significant difference between the centrifuge and TSI methods is that the size of the particle plays a different role in each case. In the centrifuge method, the size of the detached particle affects the detachment force by reason of its mass. And the cut-off value of 45 μm, set by the mesh in the cell allows the collection of any detached drug powder satisfying such a dimension, whether a single particle or an agglomerate. In contrast, the basis for particle size analysis within the TSI resides in the aerodynamic diameter of the powder material that is the key particle property for characterising the respiratory deposition of airborne particles. Particle size analysis by laser light scattering of micronised drug showed that form A and B have a median volume diameter of 2.5 and 2.2 μm, respectively, with a very similar particle size distribution (Figure 17). Particle shape may also influence the deagglomeration of the powder blend during aerosolisation within the DPI, recall that particle geometry is a determining factor of the aerodynamic diameter.

Peart [1996] proposed the measurement of electrostatic detachment forces as a suitable tool for the prediction of drug deposition characteristics. The same author reported that a reduction in the detachment charge is mirrored by an increase in the emitted fine particle dose suggesting a

correlation between the two parameters. The cited exercise was undertaken with the intention of discriminating between gravitational and electrostatic effects on the performance characteristics of DPIs.

In the present work, combination of the electrostatic properties of powder blends upon detachment and TSI deposition characteristics indicated a trend based on the drug load. Table 29 and Figure 59 show the fine particle fraction from the emitted dose for both polymorphs at different drug concentrations and the correspondent electrostatic charge as measured by the airstream Faraday apparatus. The data show that in the case of polymorph A, the profile of charge as a function of drug concentration obtained very closely resembles the profile of TSI drug deposition. In the case of polymorph B, there is no similarity between electrostatic charge and drug deposition, especially at the lower drug concentrations. It is evident that polymorph B exhibited a greater fluctuation in detachment charge than polymorph A.

Table 29. Comparison between emitted fine particle dose and electrostatic detachment charge for blend of polymorphic drug with α-lactose monohydrate (n=6).

	Fine particle percent of emitted dose (%)		Detachment charge ($C \cdot g^{-1} \times 10^{9}$)	
% Drug	Form A	Form B	Form A	Form B
1	27.14	22.65	-1.275	0.351
5	33.70	13.80	0.906	8.12
25	30.19	43.35	1.193	5.023
50	25.87	28.51	0.846	1.047

Electrostatic charge data obtained with the air stream Faraday apparatus and with the capacitor interchangeable mesh (Chapter 3) indicate that polymorph A is the more electrostatic of the two forms. Because of their

greater charge, dispersed particles of polymorph A undergo rearrangement toward charge neutralisation in a shorter time scale than do particles of polymorph B. An interesting consequence of this situation, is that precisely because polymorph B is the less electrostatic of the two, the effects of its slower charge decay are more readily manifested during particle deposition as observed in Figure 59. The deposition charge of polymorph A shows a reversal in polarity when increasing the drug concentration from 1% to 5% in the blend. But the electrostatic nature of polymorph A and its fast charge decay manifest themselves in a cohesive effect on the particles, more than on an unstable deposition charge.

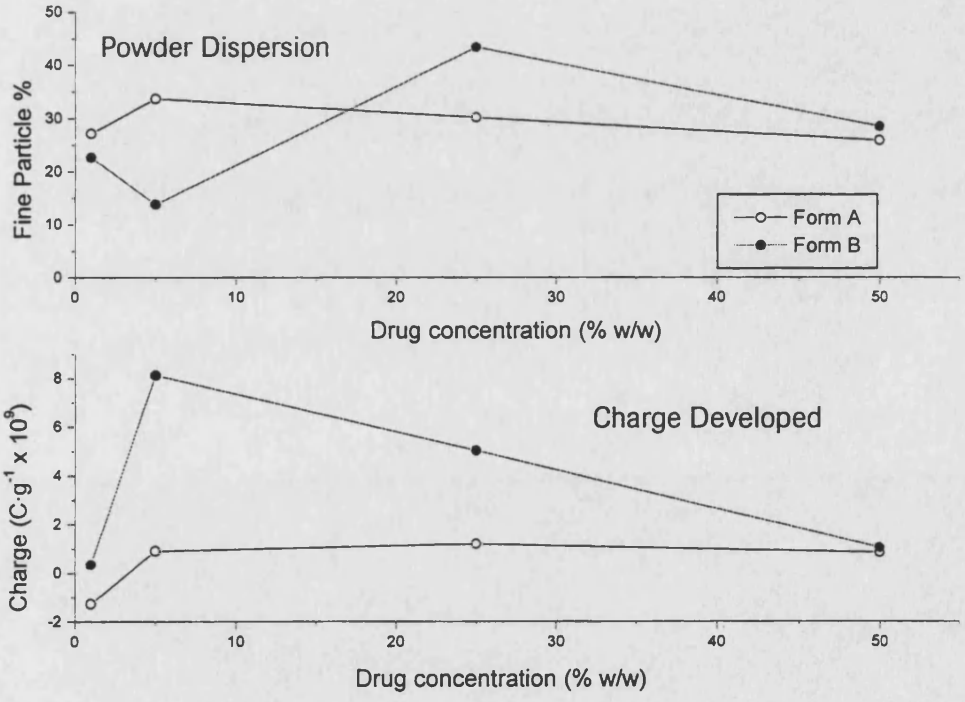

Figure 59 Comparison between emitted fine particle dose and electrostatic detachment (n=6).

The obtained results indicate that the two crystal forms of Ro 24-5913 exhibit different *in vitro* deposition behaviour, and the differences can, in turn, be attributed to differences in the adhesive and cohesive properties of the two polymorphs. Polymorph A is less adhesive but more cohesive than polymorph B. Consequently, at low drug concentrations in the blend, a case where the frequency of collisions among detached drug particles is low, form A exhibits a greater efficiency in dispersing into fine particles. Conversely, the less cohesive polymorph B exhibits greater efficiency dispersing into fine particles at higher drug concentrations, *i.e.*, in cases where drug-drug particle collisions are more frequent.

6. CONCLUSIONS

The physical and physicochemical properties of drug particles of two different crystal forms were studied in terms of their observable effects on the nature and strength of the interactive forces between the drug particles and lactose, in dry powder mixes. The relationship between physicochemical properties and particle interactions was studied from two different perspectives and scales, each requiring different instrumentation and techniques. The surface energy characteristics of the drug were determined at a microscopic level and related to macroscopic behaviour in a powder mix, such as ease of metering and dispersing.

The drug used in this study exists in two, well characterised, polymorphic forms. This type of system was chosen in order to investigate the interactive properties of two different surfaces with identical chemical composition. The basic hypothesis of this study was that two polymorphs of the same drug, will exhibit measurable differences in their interparticle cohesive/adhesive interactions. The differences in interparticle interactions between the two polymorphs, which manifest themselves macroscopically as processing performance qualities of the mix, should in turn be the result, at a molecular level, of differences between the surface energetics of the two polymorphs.

Physical characterisation of the two polymorphs was carried out on crystals with the same particle size distribution for each form. In addition, the two crystalline forms used were treated in such way that the two materials used in the study had virtually the same particle size distribution, determined

by laser light diffraction, as well as similar surface areas, as determined by BET gas adsorption measurements. These measures were taken in order to minimise, as much as possible, the potential confounding effects that size and shape may bring to the cohesive/adhesive behaviour of the drug. Physical characterisation of lactose, the material selected for use as a carrier was also performed. Drug-lactose mixes were prepared with each polymorph and characterised in terms of their deposition characteristics.

Measurement of the adhesion forces by the centrifuge method showed that the stable crystal form, polymorph B, detached more easily from the carrier than the metastable form, polymorph A, for all the drug loading levels. These results indicate stronger adhesion forces for the metastable polymorph were formed in contact with lactose than equivalent lactose bonding to the stable polymorph.

The electrostatic charges developed upon drug detachment, measured by two methods, show that both polymorphs are bipolar. The charges developed by the detachment of the drug were found to be higher in the intermediate range of drug concentration loading explored (5% w/w and 25% w/w) for each polymorph. At the low and high extremes of drug loading studied, 1% and 50%, the charges developed upon drug detachment were lower, suggesting that charge screening produced by aggregation can result in charges similar to those obtained at low loads. Even though the profiles of drug load versus charge obtained for both polymorphs are similar, form B consistently developed higher charge than form A. However, measurement of charges developed by the neat drug showed that polymorph A is more electrostatic but also exhibits faster charge decay. These results suggest

that the greater electrostatic nature of polymorph A favours the formation of agglomerates of this crystal form.

The physical reactivity of the drug surface was probed using physico-chemical methods through the adsorption of organic solvents of different polarity and different hydrogen bonding properties. Inverse gas chromatography (IGC) measurements were used to obtain adsorption coefficients, whereas microcalorimetry (TAM) provided direct measurements of the energy (*i.e.*, enthalpy) of interaction under equilibrium conditions.

Adsorption coefficients calculated from IGC experiments for different organic solvents are in most instances higher for polymorph B than for A. This is true for non-hydrogen bonding solvents, whether polarisable (toluene) or non-polarisable (hexane and heptane) as well as for hydrogen bonding solvents, whether acceptors (ethyl acetate and methyl ethyl ketone) or donor (2-propanol). IGC experiments also revealed that the surface of both polymorphs is essentially non-polar or hydrophobic, and the fact that one polymorph exhibited stronger interactions with both polar and non-polar probes is indicative of the composite nature of the surface as well as of a degree of order characteristic of crystals.

But the IGC methodology provided a key piece of information for the present study. Since IGC experiments were done under infinite dilution conditions, the obtained adsorption data correspond to the interaction of the vapour probes with the most active sites for adsorption available on the surface of either polymorph. The IGC data provided experimental evidence for the presence of molecular disorder at the surface of the two polymorphs' powders. The same methodology also revealed that the degree of such a

molecular disorder (quite possibly enhanced by the milling process) was not sufficient to mask or obliterate the crystalline character of the surfaces under investigation. Such that the differences demonstrated between the powders are due to the fact that the two materials (including their surface) are two different crystal phases.

Electrostatic interactions seem to play a significant role in the deposition behaviour of the drug. The effect, however, is a rather indirect one: Polymorph A being the more electrostatic material tends to self-neutralise the charges on its surface, creating more agglomerates, as observed by SEM. After an initial charge decay, the overall charge of the two polymorphs is approximately the same. However, the aggregation of polymorph A particles allows this material to behave as larger virtual particles of its components particles' combined mass, requiring higher forces for their removal from lactose (as measured by the centrifuge method).

The surfaces of the two polymorphs are energetically different to sufficient degree, as to allow direct and reliable measurements in terms of their interaction with a common probe such as water. These differences can in turn be related to the differences in behaviour between the two crystal forms observed in the study of drug-lactose blends studied by the centrifuge method and by electrostatic measurements. Furthermore, the discussion presented here about the differences in surface energetics between the two polymorphs also supports the explanation given above for the different deposition behaviour that these materials exhibit during the development of a DPI product.

Despite efforts to eliminate the effects of surface geometry, the results suggest that the shape of the drug particles continues to play some role,

although not necessarily dominant, in the aerosol deposition properties of powder mixes. Nevertheless, the major purpose of this study was to explore the relationship between the energetics of interaction of dry particles inhaler particles and deposition in a realistic pharmaceutical situation. The system chosen for this study is a true pharmaceutical new chemical entity for pulmonary delivery, tested in the clinic, and the results of the present study should provide a pharmaceutically relevant, representative picture of the power and limitations of the type of analysis employed.

The results obtained by TAM and IGC are in agreement showing that the surfaces of the two polymorphs are not equivalent, and these results are consistent with the original working hypothesis of this project. When the vapour probe-surface interaction involved hydrogen bonding, the two surfaces exhibited differences under nearly ideal (infinite dilution) conditions, as well as under conditions removed from ideality (TAM). For non-hydrogen bonding probes, IGC results show differences between the two polymorphic surfaces, whereas TAM results show them more or less equivalent. One important aspect regarding these techniques is that whereas IGC gives values of the adsorption (equilibrium constant) coefficient, TAM gives direct measurements of the enthalpy of interaction. The adsorption coefficient is directly related to the free energy of the process, which includes the enthalpy as one of its terms. It follows that the differences between the polymorphs detected by IGC but not by TAM for non-hydrogen bonding probes must be the result of an athermal (*i.e.*, entropic) contribution to sorption not detectable during TAM experiments. The combined results from TAM and IGC thus offer a more complete (than TAM alone) and more detailed (than IGC alone)

picture of the properties of, and differences between, the surfaces under study. When adsorption of the probe molecule is controlled by dispersion forces, the enthalpy involved is comparable for the two polymorph surfaces and differences are essentially athermal, and only observable through the measurement of an equilibrium constant. Future work aimed to test the above hypothesis can be based on the measurement of sorption isotherms of non-hydrogen bonding probes at different temperatures. Instrumentation capable of running such experiments is now commercially available. Experiments of this type will provide both the equilibrium constant and the thermal component of the process, making the athermal component obtainable by difference. When adsorption of the probe molecule involves hydrogen bonding, whether the probe is a donor of simply an acceptor, the thermal component becomes dominant, and the differences between the two polymorphic surfaces are readily measurable.

Molecules do not have sharp boundaries, and descriptions of surfaces at the molecular level cannot be meaningfully made without taking into account the nature of the probe used. The most accurate description (at a molecular level) of a surface is a description of its interactions. The interactions between water and each of the polymorphs used in this study present qualitative similarities and quantifiable differences. The heat of adsorption of the two polymorphs shows a peak at 25°C, relative to the immediate lower and higher temperatures studied. The 25°C calorimetric peak did not have a corresponding commensurate peak in microgravimetric adsorption. This additional thermal component had to be explained without adding more water. The possibility of water molecules populating stronger

(more exothermic) adsorption sites was discarded because it would require an exothermic process favoured with increasing temperature. Instead, an explanation involving the formation of water clusters and adsorption onto secondary, weaker sites was proposed. Such explanation comes from an analogy of the experimental results with the known mechanism of water adsorption on activated carbon surfaces.

Between 25°C and 35°C, the surfaces of polymorphs A and B interact with water in different fashion. Polymorph A adsorbs greater amounts of water and produces a greater heat of adsorption. But the net balance between amount of water adsorbed and the corresponding heat evolved revealed that polymorph A adsorbs water through a *greater* number of *weaker* interactions than those of polymorph B, under the same conditions. This attribute of the surface of polymorph A, relative to that of form B, was interpreted as the energetic equivalent of surface fuzziness, for lack of a better term. And the reader is kindly asked to put up with the use of such term during the present discussion. It should be stressed that the fuzziness of a surface is not a physical attribute in a conformational sense, but a manifestation of the interactive properties of that surface. Polymorph A is in fact an abrasive material; such property is always taken into account when milling the drug. The same material is nonetheless anecdotally referred to as waxy to the touch, by personnel handling it. The fuzz produced by a weakly bound layer of adsorbed water fits a qualitative explanation for reconciling these attributes of form A. The surface of polymorph A is fuzzy in its interaction with water, and also in its interaction with a richly hydrogen bonding surface such as that of lactose. Although such observations do not

necessarily imply that polymorph A will exhibit the properties of a fuzzy surface in its interaction with a non-hydrogen bonding probe or surface.

There is little doubt that Atomic Force Microscopy will prove a very powerful tool in future studies of surfaces. Danesh *et al.* [2000] have already proven that AFM can discriminate the surfaces of cimetidine polymorphs. The same authors have also shown that relative humidity produces significant changes on the AFM-determined surface of cimetidine's polymorph A, whereas the AFM-determined surface of cimetidine's form B is unaffected by relative humidity. AFM should prove to be a powerful tool in elucidating the molecular nature of the so-called surface fuzziness discussed in the present study.

It seems however, that the level of resolution obtained from AFM in pharmaceutical applications needs to be developed further, before its full potential can be achieved. Louey *et al.* [1999] have conducted adhesion force measurements on lactose surfaces using AFM. The same authors found that the detachment force from lactose of a colloidal silica probe can be described by a log-normal distribution. Let us consider the smaller, 5 μm diameter, colloidal probe used by Louey *et al.* [1999], and a scanner displacement (z distance) of 100 nm. Under these conditions, the colloidal probe will present a cross sectional interaction area of about 1.5 μm^2. Such a small area is sufficient to fit about 7.5×10^6 sites for water adsorption. Louey *et al.* [1999] scale is still too coarse to make inferences regarding active sites for sorption. But this is by no means a limitation of Atomic Force Microscopy as a technique. AFM work in non-pharmaceutical fields of research [Zambelli *et al.*,1997], have produced gas adsorption images at the

mesoscale level, with resolutions higher than 50 Å. At such resolution, individual atoms are observable. Work like that of Zambelli *et al.* [1997] has produced microphotographic evidence of gas adsorption, of adsorbate cluster formation, and of the non-random distribution of adsorption sites.

The nature, the origin, and the incidence - the existence - of surface fuzziness is a question that remains open, and one worth exploring. Surface fuzziness may be a property of the native crystal; a characteristic of one crystal phase but not the other. The work of Danesh *et al.*, [2000] showed that interaction with water vapour produces changes on the AFM-determined surface for one cimetidine polymorph, but not the other. It is also possible that the surface fuzziness observed in the present study is the manifestation of surface defects brought about by the milling process. However, in considering the latter possibility, the reader is referred to Figure 13 of the present report. The figure in question shows equiscalar microphotographs of polymorphs A and B before milling. Since the two materials were milled to the give same particle size distribution (Figure 17), it is evident from the figure that polymorph B had to undergo the more intense particle size reduction through milling. Yet it was polymorph A and not B, the form that exhibited surface fuzziness. It is also pertinent to recall that the surfaces of the two polymorphs retained their crystalline character after milling; fuzziness is thus an attribute of the crystalline surface. If fuzziness was produced by milling, it is likely that some materials (like polymorph A) have a propensity toward it, whereas others (like polymorph B) do not.

The answer to the question about fuzziness posed above is not out of reach in today's state-of-the-science. And addressing the question for

Ro 24-5913 would require to grow crystals of the two polymorphs having the particle size distribution of Figure 17, such that comparison between the two surfaces could be made on the native crystals, without the need of any milling. Such a comparison would clarify if the so-called fuzziness is a property of the crystal surface or simply a propensity of the phase toward an effect of the milling process.

Growing crystals with the extremely tight particle size distribution of Figure 17 is a proposition that would be fiercely (and understandably) opposed by the Chemical Production scientists of a company whose intention is to stay in business. Traditional schemes for crystallisation at large scale would render the pursuit of such goal prohibitively expensive and quite possibly futile. However, the work of York and his co-workers [York *et al.*, 1998a; Beach *et al.*, 1999; Yu Shekunov *et al.*, 1999] has shown that super-critical fluid technology can be successfully applied to control more than the crystal form obtained; super-critical fluid technology also allows a tight control over particle size and morphology of the particles obtained. Since super-critical fluid technology can be applied as a continuous process, the technique is suitable for small as well as industrial scale production. It should be said that even with the use of super-critical fluid technology, growing crystals of Ro 24-5913 (polymorphs A and B) with the required particle size distribution would be a major undertaking. But the use of super-critical fluid technology would bring the pursuit into the realm of feasibility. And from the results of the present investigation, this author will make a prediction that could serve as one more of the possible hypotheses to test in future investigations: the use of unmilled crystal powders, having the desired

particle size (Figure 17), would result in more pronounced differences between the powders than those observed here with micronised materials. Micronisation of the powders did not mask or obliterate the crystalline character of their surfaces, and the differences between the two crystalline surfaces are presented quantitatively in the different chapters of this work. However, as discussed in Chapter 4, micronisation is likely to have reduced the magnitude of the differences between the two polymorphs' surfaces, giving the basis for the above-stated prediction.

The present study has explored the connection between surface properties of a crystal and the macroscopic behaviour of the powder. The obtained results show that the two polymorphs used in this study are indeed different in terms of their powder processing characteristics and of the resulting product attributes. Polymorphism produced two different materials without necessarily making one polymorph a better choice than the other. At low drug concentrations, powder formulations for inhalation using polymorph A are more efficient in terms of dispersion into fine particles, due to the weaker adhesive properties of polymorph A compared with polymorph B. Conversely, at higher drug concentrations, because of its weaker cohesive properties, polymorph B in the formulation results in better dispersion into fine particles. This means that different sets of requirements for the final product could make either polymorph the material of choice for pharmaceutical development.

The impact of crystal polymorphism on pharmaceutical development is a subject that has received increasing attention in the industry. In fact, polymorphism screening is one of the standard activities in the early

development of any new chemical entity intended for a solid dosage form. It is rather unfortunate, but there seems to be a trend in the Industry by which the subject of crystal polymorphism is acquiring some sort of stigma. Crystal polymorphism is a natural phenomenon, which despite being extremely common in the pharmaceutical field, frequently triggers a "panic button"; metastable forms are often seen as potential problems, seldom as exploitable opportunities. Patent protection is perhaps the one consistently exploited venue among the potential opportunities offered by polymorphism. The results of the present investigation support the widely spread notion that crystal polymorphism can occupy a central place in Particle Engineering, a sub-discipline that has yet to materialise as a widespread programme in pharmaceutical development. The pharmaceutical industry has been the stage for some costly, highly publicised mishaps involving crystal polymorphism [see for example IAPAC's Norvir® (Abbott) Advisory of 1998]. But rather than a potential deterrent, these incidents should serve as a reminder that polymorphism presents some risks that demand due diligence, just as any other technical opportunity does. Not every polymorph is suitable for pharmaceutical development, far from it. But by the same token, not every metastable polymorph warrants being discarded as candidate for the physical form selected for product development. The criteria for selection of suitable crystal forms are based on a set of fixed and unambiguous rules. And even when at times the necessary juxtaposition of data from various instrumental techniques makes it seem more intricate, polymorph qualification is in reality more a fact-finding exercise than anything else. The key lies on observing the rules that Nature set up in advance.

7. GLOSSARIES

7.1 Glossary to Chapter 1

A	Area
A_F	Helmholtz free energy
A_H	Hamaker coefficient
B	Empirical constant. Lennard-Jones potential
C	Empirical constant. Lennard-Jones potential
D	Dipole separation distance
E	Induced dipole interaction energy
E_m	Average molar energy
F	Total adhesion force
F_e	Contact potential force
F_{im}	Coulombic interaction force
F_s	Surface tensional force
F_{vdW}	Magnitude of van der Waals force
H	Planck's constant
K	Proportionality constant
K_{eq}	Equilibrium constant
P	Partial pressure
P_F	Isothermal heat flow
P_o	Saturation vapour pressure
q, q_1, q_2	Electric charge
Q	Partition function
r	Distance: Intermolecular, interatomic, intercharge
R	Universal gas constant
r_e	Minimum radius. Lennard-Jones potential
RH	Relative Humidity
r_r	Particle radius
T	Temperature
$U(r)$	Lennard-Jones potential

X	Amount of vapour solvent sorbed
x, x_i	Mole fraction, mole fraction of species i
z	Distance between attracting plane and sphere
α	Molecular polarisability
ΔH_f	Enthalpy of melting
ΔG_s	Free energy of sorption
ΔH_s	Enthalpy of sorption
ΔS_s	Entropy of sorption
ε_o	Permitivity in vacuum
φ	Electron work function
ϕ	IGC Interaction parameter
γ	Surface/interfacial tension
G	Gibbs free energy
μ_i	Chemical potential of species i
μ_i^o	Standard chemical potential of species *i*
ν_o	Electron orbiting frequency
θ	Contact angle
atm	atmospheres
DPI	Dry powder inhaler
DSC	Differential Scanning Calorimetry
IGC	Inverse gas chromatography
TAM	Thermal Activity Monitor
vdW	van der Waals

7.2 Glossary to Chapter 2

AUC_{Std}	Chromatographic peak area of standard solution
C_p	Heat capacity
C_{Std}	Concentration of standard solution
dv_{10}	Particle diameter at the 10-percentile of the distribution
dv_{50}	Particle diameter at the 50-percentile of the distribution
dv_{90}	Particle diameter at the 90-percentile of the distribution
R	Universal gas constant
$R.F.$	Chromatographic response factor
$2\text{-}\theta$	X-ray angle of diffraction
ΔH_f	Enthalpy of melting
AFM	Atomic Force Microscopy
BET	Bennet-Emmet-Teller
DPI	Dry powder inhaler
NIST	National Institute of Standards and Technology
RPM	Revolutions per minute
XRD	X-ray diffraction

7.3 Glossary to Chapter 3

a	Centrifugal acceleration
A_s	Specific surface area
C	Capacitance
d	Inter-particle distance
D_i, D	Particle diameter – Laser diffraction
F	Force of attachment
F_{det}	Detachment force
F_g	Weight force
g	Acceleration of gravity
l	Radius of rotation
m	Mass
n_i	Number of particles of diamter D_i
P_i, P	Frequency (volume fraction)
Q	Electrical charge
Q_{sp}	Mean specific charge
RH	Relative humidity
S_ω	Centrifugal speed
T	Temperature
V_E	Applied voltage
λ	Wavelength
ω	Angular velocity
ρ	Particle density
ASFC	Air stream Faraday cage dynamic charge detector
CIMFC	Capacitor interchangeable mesh charge detector
EFM	Electrostatic field meter
rad	Radians
R.C.F.	Relative centrifugal force
RPM	Revolutions per minute
SFC	Shallow Faraday well static charge detector
TCM	Transient charge monitor

7.4 Glossary to Chapter 4

A_{sp}	Specific surface area
C	Arbitrary integration constant
C_s	Water concentration in the sorbed phase
C_v	Water concentration in the vapour phase
K	Equilibrium constant
K_D	Distribution coefficient
n	Number of moles
P	Pressure
P_μ	Heat Flow
P^o	Saturation pressure
Q_{ads}	Heat of adsorption
R	Universal gas constant
RH	Relative Humidity
T	Temperature
t_m	Interaction-free retention time
t_r	Retention time
V	Volume
V_g	Specific retention volume
V_m	Column's dead volume
V_n	Net retention volume
V_r	Retention volume
W_s	Weight of adsorbent sample
ΔH_{ads}	Enthalpy of adsorption
ΔG_s^o	Standard free energy of adsorption
ΔH_s^o	Standard enthalpy of adsorption
ΔS_s^o	Standard entropy of adsorption
ϕ	Interaction parameter
π	Surface pressure
FID	Flame ionisation detector
IGC	Inverse Gas Chromatography
PM	Peak maximum
TAM	Thermal Activity Monitor

7.5 Glossary to Chapter 5

A_D	Drug particle cross-sectional area
d_D	Drug particle diameter
d_L	Lactose carrier particle diameter
F_D	Weight percent of drug for monolayer coverage
M_D	Mass of a group of N drug particles
M_L	Mass of one lactose carrier particle
N	Number of drug particles to form a monolayer
RH	Relative Humidity
T_L	Lactose carrier specific surface area
V_D	Volume of a drug particle
ρ_D	Drug absolute density
ρ_L	Lactose carrier absolute density
ACGH	Airflow calibrated gas housing
DPI	Dry powder inhaler
ED	Emitted dose
FPD	Fine particle dose
FPF	Fine particle fraction
ND	Nominal dose
TSI	Twin stage impinger

8. REFERENCES

Adamson, A.W. Physical Chemistry of Surfaces. Fifth Edition, John Wiley & Sons, Inc., pp. 291,314,329, 406 (1990).

Aggarwal,N.D., Goldman, D., Malick, A.W. and Sethachutkul, K. Degradatiion profile and reversed-phase LC method development of the anti-inflammatory drug, Ro 24-5913. *J. Pharm. & Biomed. Anal.* **11**(10):1037-1043 (1993).

Ahfat, N.M., Buckton, G., Burrows, R. and Ticehurst, M.D. Predicting mixing performance using surface energy measurements. *Int. J. Pharm.* **156**:89-95 (1997).

Ahmed, H.A. Particle Interactions in Multicomponent Systems. Ph. D. Thesis. University of Bath, Bath U.K. (1989).

Ahmed, H.A. Pharmaceutical powder mixing from randomization to homogenization. *Personal communication. Hoffmann-LaRoche, Nutley N.J. (June 2000). American Pharmaceutical Review* submitted (June 2000).

Ahmed, H.A. Shah, D., Phillips, E.M., Tarantino, R. and Malick, A.W. Effect of Drug/carrier Ratio on the In-vitro Performance of Powders Emitted from Dura Dryhaler. *Pharm. Res.* **11**(10):S139 (1994).

Ahmed, H.A., Shah, N.H., Infeld, M.H. and Malick, A.W. Effect of electrostatic charge properties on content uniformity of pharmaceutical powder mixes. 1. The binary system. GCR No. 131604 PR&D/HLR Report (1992).

Amidon, G.E. and Houghton, M.E. The Effect of Moisture on the Mechanical Properties of Microcrystalline Cellulose. *Pharm. Res.* **12**(6):923-929 (1995).

Angberg, M., Nystrom, C. and Castensson, S. Evaluation of heat conduction microcalorimetry in pharmaceutical stability studies. *Int. J. Pharm.*, **83**:11-23 (1992).

Angell, C.A. Formation of Glasses from Liquids and Biopolymers. *Science*, **267**:1924-1935 (1995).

Apostolopoulos, D. and Gilbert, S.G. Water sorption of coffee solubles by frontal inverse gas chromatography: Thermodynamic considerations. *J. Food Sci.*, **55**:475 (1990).

Bachiller-Baeza, B; Rodriguez-Ramos, I.; Guerrero-Ruiz, A. Interaction of carbon dioxide with the surface of zirconia polymorphs. *Langmuir.* **14**: 3556-3564 (1998).

Bailey, A.G. Electrostatic phenomena during powder handlig. *Powder Technol.* **37**:71-85 (1985).

Bakri, A. A novel calorimetric approach to the study of interactions between gases and materials. 25th North American Thermal Analysis Society Conference Proceedings (NATAS) Meeting. Application for Microcalorimetry. Ovni Press. McLean, VA. Pp 1-10 (1997).

Bakri, A. Design, Testing and Pharmaceutical Applications of a Gas Pressure Controller - Device for Solid-Gas Microcalorimetric Titration. *Thermometric Application Note 22021,* Thermometric AB, Jarfalla, Sweden (1993).

Bakri, A., Wilting, J. and Jansen, L.H.M. Flow calorimetry applied to the study of chemical stability of organic compounds. *J. Thermal Analysis* **33**:1193-1199 (1988b).

Bakri, A., Wilting, J. and Jansen, L.H.M. Determination of reaction rate parameters using heat condition microcalorimetry. *J. Thermal Analysis* **33**:185-190 (1988a).

Bakri, A., Xirong, N. and Jansen, L.H.M. Effect of inclusion of benzocaine in beta-cyclodextrin upon its stability as studied by heat conduction microcalorimetry. *Minutes of the fifth International Symposium on Cyclodextrins.* Editions de Sante, 261-266 (1990).

Balanchandran,W., Ahmad,C.N. and Barton, S.A. Deposition of electrically charged drug aerosols in lungs. *Inst. Phys. Conf. Ser.*, No. **118**, Sect. 1. pp 57-63 (1991).

Beach, S., Latham, D., Sidgwick, C., Hanna, M. and York, P. Control of physical form of salmeterol xinafonate. *Org. Proc. Res. Dev.* **3**:370-376 (1999).

Berlin, E., Kliman,P.G., Anderson, B.A. and Pallansch, M.J. Calorimetric measurements of the heat of desorption of water vapor from amorphous and crystalline lactose. *Thermochim. Acta* **2**:143-152 (1971).

Bettelheim, F.A., Blook, A. and Kaufman, L.J. Heats of water vapor sorption in swelling biopolymers *Biopolymers* **9**:1531 (1970).

Blount, A.M. Chiu and L.J. Todaro X-ray Structures of Two Polymorphs of Ro 24-5913: A few Angstrons of Difference, RCR No. 133718 PChem Dept./HLR Report, December 1993).

Boerefijn, R., Ning, Z. and Ghadiri, M. Disintegration of weak lactose agglomerates for inhalation applications. *Int. J. Pharm.,* **172**:199-209 (1998).

Booth, S.W. and Newton, J.M. Experimental investigation of adhesion between powders and surfaces. *J. Pharm. Phamacol.* **39**:679-684 (1987).

Briggner, L-E., Buckton, G., Bystrom, K. and Darcy, P. The use of isothermal microcalorimetry in the study of changes in crystallinity induced during the processing of powders. *Int. J. Pharm.,* **105**:125-135 (1994).

Brittain, H.G. Perspective on polymorphism. *Pharm. Technol.* pp. 50-52 (1994).

Brunauer, S., Emmet, P.H. and Teller, E. Adsorption of gases in multimolecular layers *J. Am. Chem. Soc.* **60**:304 (1938).

Bryan, L., Rungve, Y. and Stewart, P.J. Mixing and de-mixing of microdose quantities of sodium salicylate in a direct compression vehicle. *Powder Technol.* **22**:147-151 (1979).

Bryan, W.P. The thermodynamics of water-protein interactions. *J. Theor. Biol.* **87**:639 (1980).

Buckton, G. and Beezer, A.E. Microcalorimetric study of powder surface energetics *Int. J. Pharm.,* **41**:139-145 (1988).

Buckton, G. and Newton, J.M. Liquid penetration as a method of assessing the wettability and surface energy of pharmaceutical powders *J. Pharm. Phamacol.* **38**:329-334 (1986a).

Buckton, G. and Newton, J.M. Assessment of wettability of powders by use of compressed discs. *Powder Technol.* **46**:201-208 (1986b).

Bull, H.B. Adsorption of water vapor by proteins. *J. Am. Chem. Soc.* **77**:2585 (1944).

Burger, A and Ramberger, R. On the polymorphism of pharmaceuticals and other molecular crystals. *I Mikrochimica Acta II*: 259-271 (1979).

Byron, P.R. Some future perspectives for unit-dose inhalation aerosols. *Drug. Dev. Ind. Pharm.* **12**:993-1015 (1986).

Bystrom, K. Microcalorimetric testing of physical stability of drugs in the solid state. *Thermometric Application Note 22004,* Thermometric AB, Jarfalla, Sweden (1990).

Carrillo, P.J., Gilbert, S.G. and Daun, H. Starch/solute interaction in water sorption as affected by pretreatment. *J. Food Sci.* **53**:1199 (1988).

Carvajal, M.T and Staniforth, J.N. Polymorphism and dispersibility of dry powders. *Respiratory Drug Delivery VI.* P.R. Byron, R.N. Dalby and S.J. Farr (Eds.) Interpharm Press, Buffalo Grove, IL (1998).

Carvajal, M.T., Gasior, P., Phillips, E.M., Weinrib, A., Tarantino, R. and Malick, A.W. Spray-drying optimization to produce powder for inhalation. *Pharm. Res.* **11:** S140 (1994).

Chan, H.K. and Doelker, E. Polymorphic Transformation of Some Drugs Under Compression. *Drug. Dev. Ind. Pharm.* **11**:315-322 (1985).

Chawla, A., Taylor, K.M.G., Newton, J.M. and Johnson, M.C.R. Productiion of spray dried salbutamol sulphate for use in dry powder aerosol formulation. *Int. J. Pharm.,* **108:** 233-240 (1994).

Chowhan, Z.T. Segregation of Particulate Solids, Part I and II. *Pharm. Technol.* pp.56 (1995).

Chowhan, Z.T. and Chi, L.H. Drug-excipient interactions resulting from powder mixing IV. *J. Pharm. Sci.*, **75**:534-541 (1986).

Clark, A. R. Personal Communication (2001).

Clark, A. R. Effect of powder inhaler resistance upon inspiratory profiles in health and disease. *Respiratory Drug Delivery IV.* P.R. Byron, R.N. Dalby and S.J. Farr (Eds.) Interpharm Press, Buffalo Grove, IL, pp. 117-123 (1994).

Clark, A. R. and Hollingworth, A.M. The relationship between powder inhaler resistance and peak inspiratory conditions in healthy volunteers - implications for *in-vitro* testing *J. Aerosol Sci.* **6**(2):99-110 (1993).

Coehlo, U., Miltz, J., Gilbert,, S.C. Water bindings of collagen by inverse gas chromatography: thermodynamic considerations. *Macromolecules* **12**:284 (1979).

Conder, J.R. and Purnell, J.H. Theory of frontal and elution techniques of thermodynamic measurement. *Trans. Far. Soc.* **65**:839 (1969).

Conder, J.R., Mchale, S. and Jones, M.A. Evaluation of methods for measuring gas-solid chromatographic retention on skewed peaks. *Anal. Chem.* **58**:2663 (1986).

Corn, M. The adhesion of solid particles to solid surfaces: A review *J. Air Pollut. Control Assoc.*, **11**:523-528 (1961).

Crooks, M.J. and Ho, R. Ordered mixing in direct compression tablets. *Powder Technol.* **14**:161-167 (1976).

Cross, J.A. Electrostatic principles, problems and applications Adam Hilger:Bristol (1987).

Dalby, R. The effect of time delays between inhaler actuation and onset of inhalatoin on the dose of albuterol exiting Optihaler, Aerochamber and aerosol cloud enhancer (ACE) sparcers *Respiratory Drug Delivery V.* P.R. Byron, R.N. Dalby and S.J. Farr (Eds.) Interpharm Press, Buffalo Grove, IL, pp. 324-326 (1996).

Danesh, A.; Chen, X.; Davies, M.C.; Roberts, C.J.; Sanders, G.H.W.; Tendler, S.J.B.; Williams, P.M. Polymorphic discrimination using Atomic Force Microscopy: Distinguishing between two polymorphs of the drug cimetidine. *Langmuir.* **16**: 866-870 (2000).

De Boer, J.H. The Dynamic Character of Adsorption. Second Edition, Clarendon Press, Oxford (1968).

De Villiers, M.M., Van Der Watt, J.G. and Lotter, A.P. Deaggregation of cohesive particle agglomerates through interactive mixing: Defining a degree of dispersion. *Pharm. Res.* **11**(10):S241 (1994).

Derjaguin, B.V., Krotova, N.A. and Smiga, V.P. Adhesion of solids. Consultant Bureau:New York, pp 26, 234 (1978).

Donald, D.K. Electrostatic contribution to powder-particle adhesion *J. Appl. Phys.* **40**(7):3013-3019 (1969).

Donald, D.K. and Watson, P.K. The influence of electric fields on particle adhesion in xerographic developer mixtures. *Photographic Science and Engineering,* **14**:36-41 (1970).

Egawa, H., Maeda,S., Yonemochi,E., Oguchi, T., Yamamoto, K. and Nakai, Y. Solubility parameter and dissolution behavior of Cefalexin powders with different crystallinity. *Chem. Pharm. Bull.* **40**:819-820 (1992).

Esposito, P., Colombo, I. and Lovrecich, M. Investigation of surface properties of some polymers by a thermodynamic and mechanical approach: possibility of predicting mucoadhesion and biocompatibility. *Biomaterials* **15**(3):177-182 (1994).

Fairbrother, J.E. & Grant, D.J.W. . The crystal habit modification of a tablet lubricant, adipic acid. *J. Pharm. Pharmacol.* **30 Suppl**:19P (1978).

Feeley, J.C., York, P., Sumby,B.S. and Dicks, H. Determination of surface properties and flow characteristics of salbutamol sulphate, before and after micronization. *Int. J. Pharm.,* **172**:89-96 (1998).

Fowkes, F.M. Attractive forces at interfaces. *Ind. Eng. Chem.* **56**:40 (1964).

Fowkes, F.M. Surface effects of anisotropic London dispersion forces in n-Alkanes. *J. Phys. Chem.* **84**:510-512 (1980).

Fuchs, N.A. The mechanics of aerosols. Pergammon Press, Oxford, 1964.

Fults, K., Cyr,T.D. and Hickey,A.J. The influence of sampling chamber dimensions on aerosol particle size measurement by cascade impactor and twin impinger. *J. Pharm. Pharmacol.* **43**:726-728 (1991).

Gal, S. Recent advances in techniques for determination of sorption isotherms. *Water Relations of Foods.* R.B. Duckworth (Ed.) Academic Press, New York (1975).

Gale, R.L. and Beebe, R.A. Determination of heats of adsorption on carbon blacks and bone mineral by chromatography using the eluted pulse technique. *J. Phys. Chem.* **68**:555 (1964).

Gallo, C.F. and Lama, W.L. Some charge exchange phenomena explained by classical model of the work function *J. Electrostatics* **2**: 145-150 (1976).

Ganderton, D. The generation of respirable clouds from coarse powder aggregates *J. Biopharmac. Sci.* **3**:101-105 (1992).

Ganderton, D. and Kaseem, N.M. Dry powder inhalers *Advances in Pharmaceutical Sciences,* **6**:165-191 (1992).

Gerrity, T.R. Pathophysiological and disease constraints on aerosol delivery. *Respiratory Drug Delivery II.* P.R. Byron (Ed.) CRC Press Inc.: Florida pp. 1-38 (1990).

Gilbert, S.G and Rosdhy, T.H. The use of inverse gas chromatography in food science research. Flavors and off-flavors. Proceedings of 6th International Flavor Conference. Ed. Charalambous, G. Elsevier Science Publishers, Amsterdam, Netherlands (1989).

Gilbert, S.G. Inverse Gas Chromatography *Advances in Chromatography* **v. 23** Giddings, J.C., Grushka,E., Cazes, J. and Brown,P.R., Marcel Dekker, New York (1984).

Girafalco, L.A. and Good R.J. A theory for the estimation of surface and interfacial energies. I. Derivation and application to interfacial tension. *J. Phys. Chem.* **61**: 904-909 (1957).

Giron, D. Le polymorphisme des excipients. *S. T. P. Pharma* **6**:87-98 (1990).

Gonda, I. and Chan, H.K. Aerodynamic properties of elongated particles of cromoglycic acid. *J. Aerosol Sci.*, **20**:157-168 (1989).

Gregg, S.J. and Sing,K.S.W. Adsorption, surface area and porosity Academic Press, Inc., New York (1982).

Hallworth, G.W. Improved design of powder inhaler. *British J. Clin. Pharmacol.* **4**:689-690 (1977).

Hallworth, G.W. and Westmoreland, D.G. The twin impinger: a simple device for assessing the delivery of drugs from metered dose pressurized aerosol inhalers. *J. Pharm. Pharmacol.* **39**:966-972 (1987).

Hancock, B.C., York, P. and Rowe, R.C. The use of solubility parameters in pharmaceutical dosage form design. *Int. J. Pharm.* **148**:1-21 (1997).

Handbook of Pharmaceutical Excipients American Pharmaceutical Assocoiation and The Pharmaceutical Society of Great Britain. The Pharmaceutical Press: London (1986).

Hansford, D.T., Grant, D.J.W. and Newton, J.M. Surface Energetics of the Wetting of a Hydrophobic Powder. *J. Chem. Soc., Faraday I*, **76**:2417-2431 (1980).

Hashish, A.H., Bailey, A.G. and Williams, T.J. Selective deposition of pulsed charged aerosols in the human lung *J. Aerosols Medicine* **7**(2):167-171 (1994).

Hatzidimitriu, E.P. Polyamide interactions with organic solutes: Effect of structure and water. Ph.D. Thesis, Rutgers University, New Brunswick, NJ. (1987).

Hawkins, A.E. The shape of powder-particle outlines John Wiley & Sons, Inc. First Edition. New York, pp. 26 (1993).

Hegedus, C.R. and Kamel, I.L. A review of inverse gas chromatography theory used in the thermodynamic analysis of pigment and polymer surfaces. *J. Coatings Technol.* **65(820)**:23-30 (1993).

Hendricks, C.D. Charging macroscopic particles *Electrostatics and Applications.* A.D. Moore (Ed.). pp 57-85 Wiley Interscience, New York (1973).

Hendrisken, B.A., Preston, M.S. and York, P. Processing effect on crystallinity on cephalexin:characterisation by vacuum microbalance. *Int. J. Pharm.,* **118**:1-10 (1995).

Hersey, J.A. Ordered powder mixing: a new concept in powder mixing practice *Powder Technol.* **11:** 41-44 (1975).

Heywood, H. Particle shape coefficients *J. Imperial College Chem. Eng. Soc.* **8**:25-33 (1954).

Hickey, A.J. and Martonen, T.B. Behavior of hygroscopic pharmaceutical aerosols and the influence of hydrophobic additives. *Pharm. Res.* **10**:1-7 (1993).

Hickey, A.J., Concessio, N.M., Van Oort, M. and Plarz, R.M. Factors influencing the dispersion of dry powders as aerosols *Pharm. Technol.* **18**(8), 58-64,82 (1994).

Hickey, A.J., Fults, K.A. and Pillai, R.S.. Use of particle morphology to influence the delivery of drugs from dry powder aerosols. *J. Biopharmac. Sci.* **3**(1/2):107-113 (1992).

Hickey, A.J., Gonda, I., Irwin, W.J. and Fildes, F.J.T. Effect of hydrophobic coating on the behavior of hygroscopic aerosol powder in an environment of controlled temperature and relative humidity. *J. Pharm. Sci.,* **79**:1009-1014 (1990).

Hiemenz, P.C. Principles of Colloid and Surface Chemistry. Second Edition, Marcel Dekker, Inc., pp.339, 489 (1986).

Hill, M. Characteristics of an active, multiple dose dry powder inhaler *Respiratory Drug Delivery IV.* P.R. Byron, R.N. Dalby and S.J. Farr (Eds.) Interpharm Press, Buffalo Grove, IL, pp. 109116 (1994).

Hill, T.L. Statistical mechanics of adsorption. IX. Adsorption thermodynamicsand solution thermodynamics *J. Chem. Phys.* **18**:3 (1950).

Hindle, M. and Byron, P.R. Dose emissions from marketed dry powder inhalers. *Int. J. Pharm.,* **116**:169-177 (1995).

Hindle, M., Byron, P.R. and Miller, N.C. Cascade impaction methods for dry powder inhalers using the high flow rate Marple-Miller impactor, *Int. J. Pharm.,* **134**:137-146 (1996).

Hindle, M., Jashnani,R.N. and Byron, P.R. Dose emissions from marketed inhalers:influence of low volume and environment. *Respiratory Drug Delivery IV.* P.R. Byron, R.N. Dalby and S.J. Farr (Eds.) Interpharm Press, Buffalo Grove, IL, pp. 137-142 (1994).

Holden, A. The nature of solids Dover Publications, Inc. New York, pp165-180 (1992).

Holzner, P.M. and Muller, B.W. Particle size determination of metered dose inhalers with inertial separation methods:Apparatus A and B (B.P.), four stagge impinger and Andersen Mark II cascade impactor. *Int. J. Pharm.,* **116:**11-18 (1995).

Hughes, J.F. Powder coating technology. *J. Electrostatics* **23**:3-23 (1989).

Huu-Phouc, N., Luu,R.P.T., Munafo, A., Ruelle, P., Nam-Tran, H., Buchmann, M. and Kesselring, U.W. Experimentally optimized determination of partial and total cohesion parameters of an insoluble polymer (microcrystalline cellulose) by inverse gas chromatography. *Int. J. Pharm.,* **34**:217-223 (1987).

Huu-Phouc, N., Luu,R.P.T., Munafo, A., Ruelle, P., Nam-Tran, H., Buchmann, M. and Kesselring, U.W. Determination of partial solubility parameters of lactose by gas-solid chromatography. *J. Pharm. Sci.* **75**:68-72 (1986).

IAPAC Norvir Advisory. International Association of Physicians in AIDS Care. September 1, 1998.

Iglesias, H.A., Chirife, J. and Viollaz, P. Thermodynamics of water vapor sorption by sugar beet root. *J. Food Technol.,* **11**:91 (1976).

Israelachvili, J.N. Intermolecular & Surfaces Forces. Second Edition. Academic Press pp. 83, 114, 122, 152 (1992).

Jager, P.D., De Stefano, G.A and McNamara, D.P. Particle size measurement using right-angle light scattering *Pharm. Technol.* pp. 102-110 (1993).

Kaiser, M.A. Physicochemical measurements by gas chromatography. In "Modern Practice in Gas Chromatography". Ed. Grob, R.L., John Wiley & Sons, Inc., Mew York (1977).

Kassem, N.M. and Ganderton, D. The influence of carrier surface on the characteristics of inspirable powder aerosols. *J. Pharm. Pharmacol.* **42** (Suppl):11P (1990).

Kassem,N.M., Ho, K.K.L. and Ganderton, D. The effect of air flow and carrier size on the characteristics of an inspirable cloud *J. Pharm. Pharmacol.,* **42** (Suppl):14P (1989).

Kauzman, W. Some factors in the interpretation of protein denaturation. *Adv. Protein Chem.,* **14**:1-63 (1959).

Kawashima, Y., Serigano, T., Hino, T.,Yamamoto, H. and Takeuchi, H. Effect of surface morphology of carrier lactose on dry powder inhalation property of pranlukast hydrate. *Int. J. Pharm.,* **172**:179-188 (1998).

Kawashima, Y.; Takagi,H. and Takenaka, H. Wet spherical agglomeration of binary mixtures. Part 2. Mechanism and kinetics of agglomeration and the crushing strength of agglomerates *Chem. Pharm. Bull.* **29**:1403-1409 (1981).

Kemball, C. and Rideal, E.K. The adsorption of vapors on mercury. I. Nonpolar substances. *Proc. Roy. Soc.,* **A187**:53 (1946).

Kitaigorodskiy, A.I. Order and disorder in the world of atoms. Edited by S. Chomet, King's College, London. Springer-Verlag New York Inc. (1967).

Kontominas, M.G., Demertzis, P.G. and Gilbert, S.G. Sorption of vinylchloride onto polyvinylchloride by inverse gas chromatography. *J. Food Proc. Pres.* **9**:223 (1985).

Krupp, H. Particle adhesion, theory and practice. *Adv. Colloid & Int. Sci.*, **1**:111-239 (1967).

Kubelka, R. and Munk, F. New contributions to the optics of intensely light-scattering materials. Original:*Z. Tech. Phys. 12:593 (1931). J. Opt. Sci. Am.* **38**:448-457 (1948).

Kulkarni, A. and Robinson, R, Polymorphism of Ro 24-5913 RCR 300592 HLR (1994).

Kulvanich , P. Characterization of Particle Adhesion in Drug-Carrier Interactive Systems. Ph.D. Dissertation (1986).

Kulvanich, P. and Stewart, P.J. Fundamental considerations in the measurement of adhesional forces between particles using the centrifuge method. *Int. J. Pharm.*, **35:**111-120 (1987c).

Kulvanich, P. and Stewart, P.J. Influence of relative humidity on the adhesive properties of a model interactive system *J. Pharm. Pharmacol.* **40**:453-458 (1988).

Kulvanich, P. and Stewart,P.J. An evaluation of the air stream Faraday cage in the electrostatic charge measurement of interactive drug systems. *Int. J. Pharm.*, **36:** 243-252 (1987a).

Kulvanich, P. and Stewart,P.J. Effect of particle size and concentration on the adhesive characteristics of a model-drug carrier interactive system. *J. Pharm. Pharmacol.*, **39**:673-678 (1987b).

Labuza, T.P., Kaanane, A. and Chen, J.Y. Effect of temperature on the moisture sorption isotherms and water activity shift of two dehydrated foods. *J. Food Sci.*, **50**:385 (1985).

Landin, M., Martinez-Pacheco, R., Gomez-Amosa, J.L., Souto, C., Concheiro, A. and Rowe, R.C. Effect of country of origin on the propertuies of microcrystalline cellulose. *Int. J. Pharm.*, **91**:123-131 (1993).

Lanyi, M and Toome, V. Determination of Polymorphic Content of Ro 24-5913/003 by Fourier Transform Raman Spectroscopy RCR No. 134564 PChem Dept./HLR Report Nov. 1993).

Laycock, S and Staniforth, J.N. A method for determining interparticulate forces in ordered mixes. *Labo. Pharma Probl. Technol.* **32:**185-189 (1984).

Leusen, F.J.J. ab initio prediction of possible crystal structures, *Zeitschrift für Kristallographie, Suppl.* **8**:161 (1994).

Lin, Hsien-Yiing. Water sorption properties of corn meal extrudates. Thermodynamic approach by the methods of inverse gas chromatography and water sorption isotherms. Ph.D. Dissertation, Rutgers University, New Brunswick, NJ (1993).

Lipson, J.E.G. and Guillet, J.E. Study of structure and interactions in polymers by inverse gas chromatography. Developments in polymer characterization-3 Drawkins, J.V. (Ed.), Applied Science, New Jersey (1982).

Littlewood, A.B. Gas Chromatography: Principles, Techniques and Applications. Academic Press, Inc., New York (1970).

Lord, J.D. Particle interactions in dry powder inhalations. Ph.D. Dissertation. University of Bath, Bath U.K. (1993).

Lord, J.D. and Staniforth, J.N. Particle size effects on packing and dispersion of powders *Respiratory Drug Delivery V.* P.R. Byron, R.N. Dalby and S.J. Farr (Eds.) Interpharm Press, Buffalo Grove, IL, pp. (1996).

Louey, M.D. and Stewart, P.J. Fine particle effects on drug deposition from dry powder inhalers. *Pharm. Res.* **1**(4):S545 (1999).

Louey, M.D., Mulvaney,P. and Stewart, P.J. Distributions in adhesion force of lactose carriers by atomic force microscopy. *Pharm. Res.* **1**(4):S540 (1999).

Machowski, W. Transient Charge Monitoring (TCM) *Personal communication.* Brunel, The University of West London (1996).

Marple, V.A., Olson, B.A. and Miller, N.C. A low-loss cascade impactor with stage collection cups: calibration and pharmaceutical inhaler applications. *Aerosol Sci. Technology* **22**:124-134 (1995).

Marshall, P.V. and York, P. Crystallization solvent induced solid-state and particulate modifications of nitrofurantoin *Int. J. Pharm.,* **55**:257-263 (1989).

Martin, A. Physical Pharmacy. Physical Chemical Principles in the Pharmaceutical Sciences Lea & Febiger, Malvern, PA., USA (1993).

Martin, B. R. Relative Humidity. *J. Chem. Educ.* **76**(8):1081-1082 (1999).

Martin, G.P., Onyechi, J.O. and Marrioitt, C. Future prospects for pulmonary delivery of drugs *S. T. P. Pharma* **4**:5-10 (1994).

Masters, K. Spray Drying. An introduction to principles, operational and applications. Second Edition pp. 583, 592, 608. (1976).

McNair, H.M. and Bonelli, E.J. Basic Gas Chromatography Varian Instrument Division Office, Palo Alto, CA (1969).

Meakin, B.J., Cainey, J.M. and Woodcock,P.M. Drug delivery characteristics of Bricanyl TurbohalerTM dry powder inhalers. *Int. J. Pharm.,* **119**:91-102 (1995).

Meakin, P. Fractal aggregates and their fractal measure. *Phase Transition and Critical Phenomena.* C. Domb and J.L. Lebowitz (Eds.) Vol. 12 Academic Press, New York (1988).

Meyer, E.F. On thermodynamics of adsorption using gas-solid chromatography *J. Chem. Educ.* **57(2)**:120-124 (1980).

Meyer, E.F., Stec, K.S. and Holz, R.D. A thermodynamic study of solute-solvent interactions using inverse gas-liquid chromatography. *J. Phys. Chem.,* **77**:2140 (1973).

Miller, N.C., Marple, V.A,; Schultz,R.K. and Poon,W.S. Assessment of the twin stage impinger for size measurement of metered-dose inhaler sprays. *Pharm. Res.* **9**(9):1123-1127 (1992).

Miller,J.M. Chromatography:Concepts and Contrasts John Wiley & Sons, Inc. New York (1988).

Mosharraf, M. and Nystrom, C. The effect of particle size and shape on the surface specific dissolution rate of micronized practically insoluble drugs. *Int. J. Pharm.,* **122**:35-47 (1995).

Niven, R.W. Development and use of an *in vitro* system to evaluate inhaler devices *Int. J. Pharm.,* **101**:81-87 (1994).

Niven, R.W. Aerodynamic particle size testing using a time-of-flight aerosol beam spectrometer *Pharm. Technol.* Pp. 72-78 (1993).

Noggle, J.H. Physical Chemistry Little Brown and Company, Boston pp. 171 (1985).
O'Byrne, P.M. Clinical comparisons of inhaler systems:what are the important aspects? *J. Aerosols Medicine* **8**:S39-S47 (1995).

Olsson, B., Aiache, J-M., Bull, H., Ganderton, D., Haywood, P., Meakin, B.J., Schorn, P.J. and Wright, P. The use of inertial impactors to measure the fine particle dose generated by inhalers. *Pharmaeuropa,* **8**:291-298 (1996a).

Olsson, B., Borgstrom, L., Asking, L. and Bondesson, E. Effect of inlet throat on the correlation between measured fine particle dose and lung deposition *Respiratory Drug Delivery V.* P.R. Byron, R.N. Dalby and S.J. Farr (Eds.) Interpharm Press, Buffalo Grove, IL, pp. 273-281 (1996b).

Otsuka, A., Lida, K., Danjo, K. and Sunada, H. Measurements of the adhesive force between particles of powdered organic substances and glass substrate by means of the impact separation method. I. Effect of particle shape and surface asperity. *Chem Pharm. Bull.* **36**:741-749 (1988).

Peart, J. Electrostatic charge interactions in pharmaceutical dry powder aerosols Ph.D. Dissertation. University of Bath, Bath U.K. (1996).

Peart, J., Staniforth, J.N., Byron, P.R. and Meakin, B.J. Electrostatic charge interactions in dry powder aerosols *Respiratory Drug Delivery V.* P.R. Byron, R.N. Dalby and S.J. Farr (Eds.). Interpharm Press, Deerfield IL pp 85-93 (1996).

Pennell, K.D., Rhue, R.D., Rao, P.S.C. and Johnston, C.T. Vapor-Phase Sorption of p-Xylene and Water on Solids and Clay Minerals. *Environ. Sci. Technol.* **26**(4):756-763 (1992).

Phillips, E.M., Byron, P.K., Fults, K. and Hickey, A.J. Optimized inhalation aerosols. II. Inertial testing methods for particle size analysis of pressurized inhalers. *Pharm. Res.* **7**(12):1228-1233 (1990).

Phuapradit, W., Shah, N.H., Sethachutkul, K., Rana, J., Munroe, M.and Infeld, M.H. Compaction, dissolution and stability of Ro 24-5913 polymorphs RCR No. 134527 PR&D/HLR Report (1993).

Podczeck, F. The relationship between physical properties of lactose monohydrate and the aerodynamic behaviour of adhered drug particles. *Int. J. Pharm.,* **160**:119-130 (1998).

Podczeck, F., Newton, J.M. and James, M.B. Adhesion and friction between powders and polymer or aluminiium surfaces determined by a centrifuge technique *Powder Technology* **83**:201-209 (1995).

Prixton, S.W. and Warburton, S. The relationship between moisture content and equilibrium relative humidity of dry figs *J. Stored Product Res.* **12**:87 (1976).

Purnell, H. Gas Chromatography John Wiley & Sons, Inc. New York (1962).

Randall, C.S., DiNenno, B.K., Schultz, R.K., Dayter, L. Konieczny, M. and Wunder, S.L. Solid-state transformation of a leukotriene antagonist. *Int. J. Pharm.,* **120**:235-245 (1995).

Rhue, R.D and Rao, P.S.C. Application of gas chromatographic techniques for characterizing vapor sorption on soils: A review. *Chemosphere* **21**:537-556 (1990).

Ridgway, K. and Rupp, R. The effect of particle shape on powder properties. *J. Pharm. Pharmacol.* **21**:S30-S39 (1990).

Rizvi, S.S.H. and Benado, A.L. Thermodynamic properties of dehydrated foods. *Food Tec.* **38**(3):83 (1984).

Robertson, D.L.N. Effect of carrier shape and texture on drug availability of aerosolised particles Ph.D. Dissertation. University of Bath, Bath U.K. (1997).

Rowe, R.C., Parker, M.D. and Mckillop, A.G. The effect of particle size on the heat of immersion of Microcrystalline Cellulose. *Int. J. Pharm.,* **91**:247-250 (1993).

Salame, I. and Bandosz, T. Experimental study in water adsorption on activated carbons. *Langmuir.* **15**: 587-593 (1999).

Salari, A. and Young, R.E. Application of attenuated total reflectance FTIR spectroscopy to the analysis of mixtures of pharmaceutical polymorphs. *Int. J. Pharm.,* **163**:157-166 (1998).

Saleki-Gerhardt, A., Ahlneck, C. and Zografi, G. Assessment of disorder in crystalline solids. *Int. J. Pharm.,* **101**:237-247 (1994).

Schaefer, D.M., Carpenter, M., Gady, B., Reifenberger, R., Demejo,L.P. and Rimai, D.S. Surface roughness and its influence on particle adhesion using atomic force techniques *J. Adhesion Sci. and Technol.* **9**(8):1049-1062 (1995).

Schein, L.B. The theory of toner charging *J. Imaging Sci, & Technol.* **37**:1-4 (1993).

Schein, L.B. and Cranch, J. The static electrification of mixtures of insulating powders *J. Appl. Phys.* **46:** 5140-5149 (1975).

Schultz, J., Lavielle, L. and Martin, C. Interfacial properties of carbon-fibers epoxy matrix composites *J. Adhesion* **23**:45 (1987).

Sebbatu, T., Angberg, M., Ahlneck, C. Assessment of degree of disorder in crystalline solids by isothermal microcalorimetry. *Int. J. Pharm.,* **104**:135-144 (1994a).

Sebhatu, T., Elamin, A.A. and Ahlneck, C. Effect of moisture sorption on tableting characteristics on spray dried (15% amorphous) lactose *Pharm. Res.,* (1994b).

Shah, N.H., Phuapradit, W., Bachynsky, M. Infeld, M.H., Iqbal, K. and Malick, A.W. High energy ordered mixture for improving the dissolution rate of sparingly soluble compounds. *Drug Dev. Ind. Pharm.* **20**(5):873-888 (1994).

Shaw, D. Introduction to colloid and surface chemistry Fourth Edition. Butterworth Heinemann Ltd. Oxford, Great Britain (1992).

Silverstein, R.M., Bassler, G.C. and Morril, T.C. Spectrometric identification of organic compounds. Third Edition. John Willey and Sons, Inc. 1974.

Smith, D.S., Mannheim, C.H. and Gilbert, S.G. Water sorption isotherms of sucrose and glucose by IGC *J. Food Sci.,* **46**:1051 (1981).

Staniforth, J.N. The effect of frictional charge on flow properties of direct compression tableting excipients. *Int. J. Pharm.,***11**:109-117 (1982b).

Staniforth, J.N. Order out of Chaos *J. Pharm. Pharmacol.,* **39:** 329-334 (1987).

Staniforth, J.N. Ordered mixing of drugs with particulate excipients. Ph.D Dissertation, Aston University, Birmingham, U.K. (1980).

Staniforth, J.N. Ordered mixing or spontaneous granulation? *Powder Technol.* **45:** 73-77 (1985).

Staniforth, J.N. Relationship between vibration produced during powder handling and segregation of pharmaceutical powder mixes. *Int. J. Pharm.,* **12**:199-207 (1982a).

Staniforth, J.N. Performance-Modifying Influences in Dry Powder Inhalation Systems. Presented at the American Association for Aerosol Research Meeting. Chicago, IL. October (1993).

Staniforth, J.N. The importance of electrostatic measurements in aerosol formulation and preforformulation", *Respiratory Drug Delivery IV.* P.R. Byron, R.N. Dalby and S.J. Farr (Eds.) Interpharm Press, Buffalo Grove, IL, pp. 303-311 (1994).

Staniforth, J.N. and Thacker, C.J. Ordered unit segregation in a tumbling blender. *Pharm. Acta Helv.* **59**:158-161 (1984).

Staniforth, J.N. and Rees, J.E. Electrostatic charge interactions in ordered powder mixes. *J. Pharm. Pharmacol.* **34**:69-76 (1982a).

Staniforth, J.N., Rees, J.E., Lai, F.K. and Hersey, J.A. Determination of interparticulate forces in ordered powder mixes. *J. Pharm. Pharmacol.*, **33**:485-490 (1981a).

Staniforth, J.N., Rees, J.E., Lai, F.K. and Hersey, J.A. Interparticle forces in binary and ternary powder mixes *J. Pharm. Pharmacol.*, **34**:141-145 (1982b).

Staniforth, J.N., Rees, J.F., Kayes, J.B., Priest, R.C. and Cotterill, N.J. The design of a direct compression tablet excipient. *Drug Dev. Ind. Pharm.* **7**: 179-190 (1981b).

Steckel, H. and Muller, B.W *In-vitro* evaluation of dry powder inhalers II: influence of carrier particle size and concentration on *in-vitro* deposition. *Int. J. Pharm.*, **154**:31-37 (1997).

Stephenson, P.L. and Thiel, W.J. The effect of humidity on the production of ordered mixtures *Powder Technology* **25**:115 (1980).

Stewart, P.J. Particle interaction in pharmaceutical systems. *Pharmacy International*, June 146-149 (1986).

Stubberud, L., Arwidsson, H.G. and Graffner, C. Water-solid interaction: I. A technique for studying moisture sorption/desorption. *Int. J. Pharm.*, **114**:55-64 (1995).

Sumby, B.S., Cooper, S.M. and Smith, I.J. A comparison of the inspiratory effort required to operate the Diskhaler and Turbohaler inhalers in the administration of powder drug formulations. *British J. Clin. Res.* **3**:117-123 (1992).

Tanford, C. The hydrophobic effect. Wiley, New York 1980.

Ticehurst, M.D., Rowe, R.C. and York, P. Determination of the surface properties of two batches of salbutamol sulphate by inverse gas chromatography. *Int. J. Pharm.*, **111**:241-249 (1994).

Ticehurst, M.D.,York, P., Rowe, R.C. and Dwivedi, S.K. Characterisation of the surface properties of alpha-lactose monohydrate with inverse gas chromatography, used to detect batch variation. *Int. J. Pharm.*, **141**:93-99 (1996).

Timsina, M.P., Martin, G.P., Marriott, C., Ganderton, D. and Yianneskis, M. Drug delivery to the respiratory tract using dry powder inhalers. *Int. J. Pharm.,* **101**:1-13 (1994).

Travers, D.N. Some observations in the ordered mixing of micronised sodium bicarbonate with sucrose *Powder Technol.,* **12**:189-190 (1975).

Troller, J.A. and Christian, J.H.B. Water activity and foods. Academic Press, Inc., New York (1978).

Tuladhar, M.D., Carless, J.E. and Summers, M.P. Thermal behavior and dissolution properties of phenylbutazone polymorphs. *J. Pharm. Phamacol.* **35**:208-214 (1983).

USP23-NF18 <905> Content Uniformity of Dosage Units The United States Pharmacopeia (USP23) - The National Formulary (NF 18), (1995).

van den Berg, C. Vapor sorption equilibria and other water-starch interactions: A physico-chemical approach. Ph.D Dissertation, Agricultural University, Wageningen, The Netherlands (1981).

Varsano, J.L. and Gilbert, S.G. Evaluation of interactions between polymers and low molecular weight compounds by GLC. I. Methodology and interaction evaluation. *J. Pharm. Sciences* **62**:87-91 (1973).

Vaughan, N.P. The Andersen impactor:calibration, wall losses and numerical simulation. *J. Aerosol Sci.* **20**(1):67-90 (1989).

Vemulapalli, G.K. Physical Chemistry Prentice Hall, New Jersey, pp. 169, 799, 823 (1993).

Vidgren, M.T., Vidgren, P.A. and Paronen, T.P. Comparison of physical and inhalation properties of spray-dried and mechanically micronised disodium cromoglycate. *Int. J. Pharm.,* **35**:139-144 (1987).

Vilan, A.; Ussyshkin, R.; Gartsman, K.; Cahen, D.; Naaman, R.; Shanzer, A. Real-time electronic monitoring of adsorption kinetics: Evidence for two-site adsorption mechanism of dicarboxylic acids on GaAs(100). *J. Phys. Chem. B.* **102**: 3307-3309 (1998).

Visser, J. Colloid and other forces in particle adhesion and particle removal (A review) *Deposition Filtr. Part. Gases Liq. Symp. Soc. Chem. Ind.,* p 121-141 (1978).

Visser, J. An Invited Review: van der Waals and other cohessive forces affecting powder fluidization. *Powder Technol.* **58:** 1-10 (1989).

Williams, D.R. Chromatography and Analysis. Feb., 9-11 (1991)

Wong, L.W. and Pilpel, N. The effect of particle shape on the mechanical properties of powders. *Int. J. Pharm.* **59:** 145-154 (1990b).

Wong, L.W. and Pilpel, N. Effect of particle shape on the mixing of powders. *J. Pharm. Pharmacol.* **42**:1-6 (1990a).

Wong, L.W. and Pilpel, N. The effect of shape of fine particles on the formation of ordered mixtures. *J. Pharm. Pharmacol.* **40:** 567-568 (1988).

Wong, L.W., Kassem,N.M. and Ganderton, D. The effect of the shape of fine particles on the inhalation properties of powder mixtures *J. Pharm. Pharmacol.,* **41** (Suppl):24P (1989).

Yip, C.W. and Hersey, J.A. Segregation of ordered powder mixtures. *Powder Technol.* **16**:149-150 (1977).

York, P. Powdered Raw Materials: Characterizing Batch Uniformity. *Respiratory Drug Delivery IV*, P.R. Byron, R.N. Dalby and S.J. Farr, Eds. Interpharm Press, Buffalo Grove, IL, pp.83-91, (1994).

York, P. Solid-state properties of powders in the formulation and processing of solid dosage forms. *Int. J. Pharm.,* **14**: 1-28 (1983).

York, P., Ticehurst, M.D., Osborn, J.C., Roberts, R.J. and Rowe, R.C. Characterisation of the surface energetics of milled dl-propanolol hydrochloride using inverse gas chromatography and molecular modelling. *Int. J. Pharm.,* **174**:179-186 (1998).

York, P., Hanna, M., Yu Shekunov, B. and Humphreys, G.O. Microfine particle formation by SEDS (Solution Enhanced Dispersion by Supercritical fluids): scale up by design. Respiratory Drug Delivery VI, Hilton Head, SC, 1998a.

Young, C.L. The use of gas-liquid chromatography for the determination of thermodynamic properties. *Chromatographic Reviews* **10**:129-158 (1968).

Yu Shekunov, B., Hanna, M. and York, P. Crystallization process in turbulent supercritical flows. *J. Cryst. Growth* **198/199**:1345-1351 (1999).

Zambelli, T.; Barth, J.V.; Wintterlin, J.; Ertl, G. Complex pathways in dissociative adsorption of oxygen on platinum. *Nature*, **390**: 495-497 (1997).

Zanen, P. van Spiegel, P.I. van der Kolk, H., Tushuizen, E. and Enthoven, R. The effect of the inhalation flow on the performance of a dry powder system. *Int. J. Pharm.,* **81**:199-203 (1992).

Zimon, A.D. Adhesion of solid particles to a plane surface. 2. Influence of air humidity on adhesion. *Coll. J. USSR.,* **25**:265-268 (1963).

Zimon, A.D. Adhesion of dust and powder. Second Edition. Consultant Bureau: New York (1982).

Zografi, G. and Tam, S. Wettability of pharmaceutical solids:estimates of solid surface polarity *J. Pharm. Sci.* **65**:1145-1149 (1976).

9. APPENDIX

9. APPENDIX A

Table A1 Percentage of drug detached from the carrier as function of the spin rate for the two polymorphs (n=4).

Form A									
rpm	**1000**			**3000**			**5000**		
Drug concn.	1%	5%	25%	1%	5%	25%	1%	5%	25%
run #									
1	ND	2.857	7.143	ND	3.448	12.500	2.353	12.121	16.902
2	ND	3.448	6.780	ND	2.439	11.111	1.408	13.953	17.464
3	ND	2.778	5.128	ND	3.226	12.647	1.587	18.519	17.397
4	ND	3.030	5.263	ND	3.448	11.111	2.273	14.894	18.155
average	ND	3.028	6.078	ND	3.140	11.842	1.905	14.872	17.479
s.d.	ND	0.299	1.032	ND	0.479	0.846	0.477	2.690	0.515
Form B									
rpm	**1000**			**3000**			**5000**		
Drug concn.	1%	5%	25%	1%	5%	25%	1%	5%	25%
run #									
1	ND	5.263	9.667	ND	7.692	15.667	5.333	17.857	21.729
2	ND	5.000	10.286	ND	5.882	13.771	6.122	18.647	19.931
3	ND	4.167	10.000	ND	7.143	15.979	4.082	18.286	23.000
4	ND	4.545	9.222	ND	4.762	14.568	4.000	18.810	21.000
average	ND	4.744	9.794	ND	6.370	14.996	4.884	18.400	21.415
s.d.	ND	0.486	0.457	ND	1.313	1.016	1.026	0.423	1.289

Table A2 Electrostatic charge measurements of powders on Air Stream Faraday Cage (ASFC, n=5).
Conditions: ~ 21 °C/30%RH; air flow rate = 60 l min^{-1}

System	n	Charge to mass ratio Cg^{-1} 10^9	avg.	s.d.	c.v %
Lactose monohydrate (45-106 µm)	4	0.602			
		0.830			
		0.738			
		0.887			
			0.764	0.124	16.27
1% Form A/Lactose monohydrate	5	1.200			
		1.210			
		1.437			
		1.008			
		1.518			
			1.275	0.204	16.00
1% Form B/Lactose monohydrate	5	0.302			
		0.250			
		0.371			
		0.491			
		0.343			
			0.351	0.090	25.72

System	n	Charge to mass ratio $Cg^{-1}\ 10^{9}$	avg.	s.d.	c.v %
5% Form A/Lactose monohydrate	5	1.123			
		1.021			
		0.808			
		0.812			
		0.765			
			0.906	0.157	17.34
5% Form B/Lactose monohydrate	5	7.367			
		9.003			
		8.489			
		7.039			
		8.696			
			8.120	0.864	10.64
25% Form A/Lactose monohydrate	5	1.089			
		1.183			
		1.418			
		1.105			
		1.204			
			1.193	0.135	10.96
25% Form B/Lactose monohydrate	5	4.890			
		5.225			
		4.706			
		4.363			
		5.964			
			5.023	0.608	12.09

System	n	Charge to mass ratio $Cg^{-1}\ 10^9$	avg.	s.d.	c.v %
50% Form A/Lactose monohydrate	5	0.973			
		0.995			
		0.777			
		0.784			
		0.702			
			0.846	0.130	15.390
50% Form B/Lactose monohydrate	5	1.020			
		0.830			
		1.083			
		1.069			
		1.232			
			1.047	0.145	13.83

Table A3 **Pure components.** Electrostatic charge measurements of powders on Capacitor Interchangeable Mesh Faraday Cage (CIMFC, n=7).
Conditions: ~ 20 °C/26%RH; air flow rate = 60 l min^{-1}

	Form A (unmicronized)		Form B (unmicronized)		Form A (micronized)		Form B (micronized)	
	Polarity	Charge C x 10^9	Polarity	Charge C x 10^9	Polarity	Charge C x 10^9	Polarity	Charge C x 10^9
	-	1.78	-	1.32	-	3.87	-	2.58
	-	1.62	-	1.37	-	3.79	-	2.58
	-	1.55	-	1.05	-	4.20	-	2.40
	-	1.52	-	1.50	-	4.00	-	2.40
	-	1.92	-	0.92	-	3.95	-	2.62
	-	2.28	-	0.86	-	5.19	-	2.85
	-	1.86	-	1.22	-	3.43	-	2.96
n=	-	7	-	7	-	7	-	7
avg=		1.79		1.18		4.06		2.63
s.d.=		0.26		0.24		0.55		0.21
rsd =		14.78		20.30		13.59		7.99

Table A4 **Ro 24-5913 – Lactose monohydrate blends.** Electrostatic charge measurements of powders on Capacitor Interchangeable Mesh Faraday Cage (CIMFC, n=6).
Conditions: ~ 20 °C/26%RH; air flow rate = 60 l min^{-1}

	1% Ro 24-5913 in lactose monohydrate				5% Ro 24-5913 in lactose monohydrate				25% Ro 24-5913 in lactose monohydrate				50% Ro 24-5913 in lactose monohydrate			
	A		B		A		B		A		B		A		B	
	Polarity	Charge C x 10^9	Polarity	Charge C x 10^9	Polarity	Charge C x 10^9	Polarity	Charge C x 10^9	Polarity	Charge C x 10^9	Polarity	Charge C x 10^9	Polarity	Charge C x 10^9	Polarity	Charge C x 10^9
	+	3.177	-	1.052	-	2.725	-	9.836	-	3.398	-	6.569	-	4.80	-/+	3.80
	+	2.800	-	1.000	-	1.616	-	9.000	-	3.518	-	6.590	-	4.80	+	5.20
	+	3.529	-	1.270	-	2.781	-	7.947	-	3.750	-	5.364	-	5.60	-/+	3.40
	+	3.320	-	1.032	-	2.626	-	10.265	-	2.980	-	5.255	-	4.00	-/+	3.80
	+	2.911	-	1.430	-	2.630	-	10.423	-	2.557	-	5.248	-	3.20	-/+	3.70
	+	3.618	-	1.176	-	1.480	-	10.774	-	2.392	-	6.159	+	5.00	+	4.90
n=		6		6		6		6		6		6		6		6
avg=	+	3.226	-	1.160	-	2.310	-	9.708	-	3.099	-	5.864	-	4.57	-	4.13
s.d.=		0.328		0.167		0.594		1.056		0.547		0.650		0.84		0.73
rsd =		10.17		14.37		25.73		10.88		17.65		11.08		18.46		17.69

Table A5 Electrostatic properties of aerosolised lactose monohydrate, 25 mg powder in a gelatin capsule measured using TCM after actuation of the rotahaler (n=4).
Conditions: ~ 22 °C/60%RH; air flow rate = 60 l min^{-1}

Electrode Number	Shot 1			Shot 2			Shot 3			Shot 4			Electrode Potential	
	U pos	U neg [V]	U net	U pos	U neg [V]	U net	U pos	U neg [V]	U net	U pos	U neg [V]	U net	U net avg [V]	s.d.
1	2.00	0.00	2.00	2.80	0.00	2.80	2.10	0.00	2.10	2.80	0.00	2.80	2.43	0.43
2	1.20	0.00	1.20	1.20	0.00	1.20	1.20	0.00	1.20	1.80	0.00	1.80	1.35	0.30
3	0.40	0.00	0.40	0.60	0.00	0.60	0.60	0.00	0.60	0.80	0.00	0.80	0.60	0.16
4	0.30	0.00	0.30	0.30	0.00	0.30	0.50	0.00	0.50	0.50	0.00	0.50	0.40	0.12
5	0.20	0.00	0.20	0.20	0.00	0.20	0.05	0.00	0.05	0.10	0.00	0.10	0.14	0.08
6	0.10	0.00	0.10	0.05	0.00	0.05	0.00	0.00	0.00	0.00	0.00	0.00	0.04	0.05
7	0.00	0.00	0.00	0.00	0.00	0.00	0.00	0.00	0.00	0.00	0.00	0.00	0.00	0.00
8	0.00	0.00	0.00	0.00	0.00	0.00	0.00	0.00	0.00	0.00	0.00	0.00	0.00	0.00
V sum [V]	4.20	0.00	4.20	5.15	0.00	5.15	4.45	0.00	4.45	6.00	0.00	6.00	4.95	0.81

Table A6 Electrostatic properties of aerosolised 5% Ro 24-5913 form A in lactose monohydrate, 25 mg powder in a gelatin capsule measured using TCM after actuation of the rotahaler (n=3). Conditions: ~ 22 °C/60%RH; air flow rate = 60 l min^{-1}

Electrode Number	Shot 1			Shot 2			Shot 3			Electrode Potential	
	U pos	U neg [V]	U net	U pos	U neg [V]	U net	U pos	U neg [V]	U net	U net avg [V]	s.d.
1	3	-0.4	2.60	4	-0.8	3.20	4.2	-0.4	3.80	3.20	1.20
2	1.8	-0.6	1.20	2.8	-0.8	2.00	3	-0.8	2.20	1.80	0.44
3	1.2	-1.6	-0.40	2	-1.8	0.20	2	-1.6	0.40	0.07	1.51
4	1	-1.6	-0.60	1.5	-2	-0.50	1.8	-1.6	0.20	-0.30	2.18
5	1	-1.8	-0.80	1.2	-2.4	-1.20	1.6	-2	-0.40	-0.80	2.92
6	0.8	-1.6	-0.80	1.1	-2.2	-1.10	1.4	-1.8	-0.40	-0.77	3.40
7	0.8	-1.6	-0.80	1	-2.2	-1.20	1.4	-1.8	-0.40	-0.80	3.91
8	0.8	-1.4	-0.60	1	-2	-1.00	1.4	-1.6	-0.20	-0.60	4.31
V sum [V]	10.40	-10.60	-0.20	14.60	-14.20	0.40	16.80	-11.60	5.20	1.80	2.96

Table A7 Electrostatic properties of aerosolised 5% Ro 24-5913 form B in lactose monohydrate, 25 mg powder in a gelatin capsule measured using TCM after actuation of the rotahaler (n=3). Conditions: ~ 22 °C/60%RH; air flow rate = 60 l min^{-1}

Electrode Number	Shot 1			Shot 2			Shot 3			Electrode Potential	
	U pos	U neg [V]	U net	U pos	U neg [V]	U net	U pos	U neg [V]	U net	U net avg [V]	s.d.
1	10.00	-2.00	8.00	3.00	-1.50	1.50	7.50	-2.50	5.00	3.25	3.25
2	7.00	-6.00	1.00	2.50	-3.00	-0.50	6.00	-5.50	0.50	0.00	0.76
3	5.00	-8.50	-3.50	1.00	-4.00	-3.00	4.00	-6.50	-2.50	-2.75	0.50
4	4.00	-8.00	-4.00	0.50	-4.00	-3.50	3.00	-6.00	-3.00	-3.25	0.50
5	3.00	-8.50	-5.50	0.25	-4.00	-3.75	2.50	-6.00	-3.50	-3.63	1.09
6	2.00	-8.00	-6.00	0.00	-4.00	-4.00	2.00	-5.50	-3.50	-3.75	1.32
7	2.00	-7.50	-5.50	0.00	-4.00	-4.00	2.00	-5.50	-3.50	-3.75	1.04
8	2.00	-7.00	-5.00	0.00	-3.50	-3.50	2.00	-5.00	-3.00	-3.25	1.04
V sum [V]	35.00	-55.50	-20.50	7.25	-28.00	-20.75	29.00	-42.50	-13.50	-17.13	4.12

Table A8 Electrostatic properties of aerosolised 5% Ro 24-5913 form A in lactose monohydrate, 25 mg powder in a gelatin capsule measured using TCM after actuation of the dryhaler (n=3). Conditions: ~ 22 °C/60%RH; air flow rate = 60 l min^{-1}

Electrode Number	Shot 1			Shot 2			Shot 3			Electrode Potential	
	U pos	U neg [V]	U net	U pos	U neg [V]	U net	U pos	U neg [V]	U net	U net avg [V]	s.d.
1	11.50	-5.00	6.50	12.00	-2.50	9.50	12.00	-5.00	7.00	7.67	1.61
2	4.00	-10.00	-6.00	3.50	-6.00	-2.50	4.75	-8.50	-3.75	-4.08	1.77
3	5.00	-9.00	-4.00	4.00	-5.50	-1.50	5.00	-8.00	-3.00	-2.83	1.26
4	3.50	-8.00	-4.50	2.50	-5.00	-2.50	3.50	-7.00	-3.50	-3.50	1.00
5	3.00	-8.00	-5.00	2.25	-5.00	-2.75	3.00	-7.00	-4.00	-3.92	1.13
6	2.75	-7.00	-4.25	2.00	-4.75	-2.75	2.75	-6.50	-3.75	-3.58	0.76
7	2.75	-6.50	-3.75	2.00	-4.50	-2.50	2.75	-6.00	-3.25	-3.17	0.63
8	2.75	-6.00	-3.25	2.00	-4.25	-2.25	2.50	-5.50	-3.00	-2.83	0.52
V sum [V]	35.25	-59.50	-24.25	30.25	-37.50	-7.25	36.25	-53.50	-17.25	-16.25	8.54

Table A9 Electrostatic properties of aerosolised 5% Ro 24-5913 form B in lactose monohydrate, 25 mg powder in a gelatin capsule measured using TCM after actuation of the dryhaler (n=3). Conditions: ~ 22 °C/60%RH; air flow rate = 60 l min^{-1}

Electrode Number	Shot 1			Shot 2			Shot 3			Electrode Potential	
	U pos	U neg [V]	U net	U pos	U neg [V]	U net	U pos	U neg [V]	U net	U net avg	s.d.
1	10.00	-8.50	1.50	10.00	-11.00	-1.00	10.00	-11.50	-1.50	-0.33	1.47
2	4.00	-8.50	-4.50	3.00	-13.00	-10.00	3.50	-13.00	-9.50	-8.00	5.58
3	4.00	-8.50	-4.50	4.00	-12.50	-8.50	4.00	-11.50	-7.50	-6.83	5.20
4	3.00	-7.00	-4.00	2.50	-10.50	-8.00	2.50	-10.00	-7.50	-6.50	5.54
5	2.50	-7.00	-4.50	2.25	-10.50	-8.25	2.00	-10.00	-8.00	-6.92	6.20
6	2.00	-5.25	-3.25	2.00	-9.50	-7.50	1.50	-9.00	-7.50	-6.08	6.37
7	2.00	-4.50	-2.50	2.00	-9.00	-7.00	1.50	-8.00	-6.50	-5.33	6.49
8	2.00	-4.50	-2.50	2.00	-9.00	-7.00	1.50	-8.00	-6.50	-5.33	6.96
V sum [V]	29.50	-53.75	-24.25	27.75	-85.00	-57.25	26.50	-81.00	-54.50	-45.33	18.31

Table A10 Values used in IGC calculations

Pi, Pressure at column inlet = 1.5 atm = 22.04 psi				
Pi = mm Hg	**1140**			
Po, Pressure at column outlet = 1 atm = 14.696 psi				
Po = mm Hg	**760**			
j = 3/2 [(Pi/Po)^2-1/(Pi/Po)^3-1]		0.789473684		
j = Martin-James compressibility factor				
j =	**0.7895**			
k', capacity factor				
K, partition coefficient				
beta, V_N/Vs				
Fc, corrected flow rate				
(average flow rate along the column)				
Fo, measured flow rate at the outlet			30	ml/min
Tc, column temperature (°K)			298.15	°K
Ta, ambient temperature (25°C = °K)			298.15	°K
P, atmospheric pressure at Ta = 1 atm			760	mm Hg
Pw, vapor pressure of water at Ta = mmHg			23.756	mm Hg
Fc = Fo [(Tc/Ta)*((P-Pw)/P)]			29.0623	ml/min
F_c =	**29.0623**	**ml/min**		
Standard states as per deBoer, 1953				
Standard vapor state (pg)		1.01325	x 10^5 N m^{-2} 1 atm	
			=	
Standard surface pressure (ps)		3.38000	x 10^{-4} N m^{-1}	
	p_g/p_s, r=	**0.29978**	x 10^9 m^{-1}	
		299.7781	x10^6 m^{-1}	
	R =	**8.314**	**J mol^{-1} °K^{-1}**	
	Column Temp.=	**°C**	**°K**	
		25	298.15	
		35	308.15	
		45	318.15	

Table A11 Average of specific retention volume for polar and non-polar probes on drug polymorphs A and B at different temperatures (n=18).

Probes	°C	Polymorph A VgT Vn/W ml g^{-1}	s.d.	Polymorph B VgT Vn/W ml g^{-1}	s.d.
Hexane	25	21.644	0.561	34.280	0.523
Hexane	35	21.449	0.124	35.095	0.228
Hexane	45	24.512	0.409	32.277	0.221
Heptane	25	36.384	0.185	54.209	0.397
Heptane	35	36.596	0.056	48.728	0.098
Heptane	45	38.639	0.561	39.466	0.513
Toulene	25	37.358	0.301	64.266	0.127
Toulene	35	28.690	0.063	52.176	0.496
Toulene	45	27.129	0.152	42.962	0.308
MEK	25	38.698	0.210	40.194	0.169
MEK	35	26.092	0.170	39.941	0.185
MEK	45	24.381	0.225	32.514	0.275
EA	25	30.503	0.313	41.928	0.206
EA	35	26.671	0.188	33.605	0.113
EA	45	22.709	0.225	32.922	0.246
2-Propyl OH	25	47.059	0.245	39.113	0.128
2-Propyl OH	35	30.213	0.135	35.743	0.266
2-Propyl OH	45	25.616	0.317	28.673	0.251

Table A12 Deposition characteristics for micronised Ro 24-5913 polymorph A blended with 45-106 µm lactose monohydrate. Powder hand loaded into the Dura device (~ 10 mg). Conditions: 21°C and 50% RH; Q=60 l min^{-1}.

		STD H = 52.88 ug/ml STD L = 11.11 ug/ml									
Sample ID	Theor.	[Ro 24-5913] Exp.		Gravimetric Load wt.	[Ro 24-5913] Nominal (ND) Theoretical	Stage I	Stage II	Emitted Dose	RD/ED Resp	ED/ND	RD/ND
		% w/w		mg	ug	ug	ug	ug	%	%	%
1A-1		1	0.97	10.9	105.73	69.47	28.37	97.84	28.99	92.53	26.83
1A-1				10.9	105.73	68.50	22.64	91.14	24.84	86.20	21.42
1A-2				11.0	106.70	72.20	27.25	99.44	27.40	93.20	25.54
1A-3				11.9	115.43	79.53	32.53	112.05	29.03	97.07	28.18
1A-4				10.0	97.00	53.86	22.52	76.38	29.49	78.74	23.22
1A-4				10.0	97.00	62.39	18.73	81.12	23.09	83.63	19.31
	Mean								**27.14**	**88.56**	**24.08**
	Std Dev.								**2.62**	**6.87**	**3.38**
5A-1		5	5.03	10.6	533.18	264.99	128.08	393.07	32.58	73.72	24.02
				10.6	533.18	262.79	127.43	390.22	32.66	73.19	23.90
5A-2				9.7	487.91	231.03	125.88	356.91	35.27	73.15	25.80
				9.7	487.91	220.24	128.81	349.04	36.90	71.54	26.40
5A-3				10.3	518.09	256.72	124.48	381.20	32.65	73.58	24.03
				10.3	518.09	258.88	124.21	383.09	32.42	73.94	23.97
									33.75	**73.19**	**24.69**
									1.88	**0.86**	**1.11**

Table A12 continued

Sample ID	Theor.	[Ro 24-5913] Exp.	Gravimetric Load wt.	[Ro 24-5913] Nominal (ND) Theoretical	Stage I	Stage II	Emitted Dose	RD/ED Resp	ED/ND	RD/ND
	% w/w		mg	µg	µg	µg	µg	%	%	%
25A-1	25	25.05	10.3	2580.15	685.58	266.78	952.36	28.01	36.91	10.34
			10.3	2580.15	713.32	284.87	998.19	28.54	38.69	11.04
25A-2			10.7	2680.35	764.43	383.43	1147.85	33.40	42.82	14.31
			10.7	2680.35	743.48	392.63	1136.11	34.56	42.39	14.65
25A-3			10.1	2530.05	690.53	267.63	958.16	27.93	37.87	10.58
			10.1	2530.05	697.11	280.62	977.72	28.70	38.64	11.09
	n	6								
	Average							**30.19**	**39.55**	**12.00**
	Std Dev.							**2.97**	**2.45**	**1.94**
50A-1	50	49.97	10.00	4997.00	1761.21	602.45	2363.66	25.49	47.30	12.06
			10.00	4997.00	1772.08	613.74	2385.82	25.72	47.74	12.28
50A-2			10.00	4997.00	1909.29	484.63	2393.92	20.24	47.91	9.70
			10.00	4997.00	1903.73	492.13	2395.86	20.54	47.95	9.85
50A-3			11.10	5546.67	2068.29	845.78	2914.06	29.02	52.54	15.25
			11.10	5546.67	2092.35	851.03	2943.38	28.91	53.07	15.34
50A-4			11.20	5596.64	2669.76	912.39	3582.14	25.47	64.01	16.30
			11.20	5596.64	2680.36	921.77	3602.13	25.59	64.36	16.47
50A-5			10.10	5046.97	2445.49	741.75	3187.24	23.27	63.15	14.70
			10.10	5046.97	2487.97	741.50	3229.46	22.96	63.99	14.69
	n	10								
	Average							**25.87**	**60.18**	**15.46**
	Std Dev.							**2.63**	**5.74**	**0.77**

Table A13 Deposition characteristics for micronised Ro 24-5913 polymorph B blended with 45-106 µm lactose monohydrate. Powder hand loaded into the Dura device (~ 10 mg). Conditions: 21°C and 50% RH; Q=60 l min^{-1}.

Sample ID	Theor.	[Ro 24-5913] Exp.	Gravimetric Load wt.	[Ro 24-5913] Nominal (ND) Theoretical	Stage I	Stage II	Emitted Dose	RD/ED Resp	ED/ND	RD/ND
		% w/w	mg	µg	µg	µg	µg	%	%	%
1B-1	1	1.020	10.9	111.13	42.37	24.38	67.75	35.99	60.96	21.94
			10.9	111.13	42.25	23.92	66.16	36.15	59.53	21.52
1B-2			11.0	112.15	41.13	14.19	55.32	25.64	49.32	12.65
			11.1	113.17	44.06	14.15	58.21	24.31	51.44	12.51
1B-3			10.9	111.13	43.89	14.06	57.95	24.27	52.15	12.65
			11.2	114.19	41.28	11.97	53.25	22.48	46.63	10.48
	n	6								
	Average						6.00	**28.14**	**47.91**	**15.29**
	Std Dev.							**6.22**	**12.92**	**5.06**
5B-1	5	4.98	11.8	587.64	368.25	65.43	433.68	15.09	73.80	11.13
			11.8	587.64	375.66	65.75	441.40	14.90	75.11	11.19
5B-2			11.1	552.78	379.76	60.03	439.79	13.65	79.56	10.86
			11.1	552.78	385.29	61.57	446.86	13.78	80.84	11.14
5B-3			11.0	547.80	397.40	58.02	455.41	12.74	83.13	10.59
			11.0	547.80	404.41	58.51	462.92	12.64	84.51	10.68
	n	6								
	Average							**13.80**	**79.49**	**10.93**
	Std Dev.							**1.03**	**4.28**	**0.26**

Table A13 continued

Sample ID	Theor.	[Ro 24-5913] Exp.	Gravimetric Load wt.	[Ro 24-5913] Nominal (ND) Theoretical	Stage I	Stage II	Emitted Dose	RD/ED Resp	ED/ND	RD/ND
		% w/w	mg	µg	µg	µg	µg	%	%	%
25B-1	25	25.05	12.0	3006.00	858.11	733.49	1591.60	46.09	52.95	24.40
			12.0	3006.00	832.13	631.89	1464.02	43.16	48.70	21.02
25B-2			11.5	2880.75	992.64	652.75	1645.39	39.67	57.12	22.66
			11.6	2905.80	998.43	713.35	1711.78	41.67	58.91	24.55
25B-3			11.7	2930.85	853.16	750.22	1603.37	46.79	54.71	25.60
			11.7	2930.85	860.82	642.32	1503.14	42.73	51.29	21.92
	n	6								
	Average							**43.35**	**53.94**	**23.36**
	Std Dev.							**2.69**	**3.76**	**1.76**
50B-1	50	50.215	11.6	5824.92	2061.96	948.10	3010.06	31.50	51.68	16.28
			11.6	5824.92	2064.03	950.03	3014.06	31.52	51.74	16.31
50B-2			10.0	5021.48	2130.13	848.99	2979.12	28.50	59.33	16.91
			10.0	5021.48	2127.59	850.49	2978.08	28.56	59.31	16.94
50B-3			10.4	5222.34	2343.77	801.90	3145.67	25.49	60.23	15.36
			10.4	5222.34	2343.48	802.47	3145.94	25.51	60.24	15.37
	n	6								
	Average							**28.51**	**57.09**	**16.19**
	Std Dev.							**2.69**	**4.19**	**0.70**